The Importance of Endoglin for Cardiac Structure and Function

Benjamin John Davison

Institute of Genetic Medicine

Faculty of Medical Sciences

Thesis submitted for the degree of

Doctor of Philosophy

Newcastle University

December 2013

Abstract

Endoglin is an accessory receptor for the transforming growth factor beta family. Patients carrying mutations in the endoglin gene develop the inherited vascular dysplasia, Hereditary Haemorrhagic Telangiectasia (HHT). However, it is becoming apparent that endoglin may also be important in acquired cardiovascular diseases such as hypertension, atherosclerosis and heart failure. The work in this thesis investigates the role of endoglin in the structure and function of the adult cardiovascular system by utilising a conditional endoglin knockout model and murine cardiac magnetic resonance imaging (CMR).

I established and validated murine CMR at Newcastle University allowing accurate quantification of *in vivo* cardiac structure and function in a number of mouse models of cardiac disease either at single time points or in longitudinal studies. Immunohistochemical analysis confirmed that endoglin is expressed in the endocardium and vasculature of the adult mouse heart. Following myocardial infarction there was increased endoglin expression which co-localised with endothelial cells and myofibroblasts. Cre-lox genetics was then used to ubiquitously knockdown endoglin in the adult mouse. This resulted in significant ventricular remodelling within three weeks, with ventricular dilatation associated with cardiomyocyte hypertrophy. These changes gradually progressed over three months following endoglin knockdown; however, overt heart failure was not seen within this time frame. Invasive measurement of ventricular function suggested an impairment of vasomotor control and reduced contractile reserve following endoglin knockdown. Also, using an endothelial-specific endoglin knockdown mouse I demonstrated that these novel cardiac changes were due to endoglin depletion in endothelial cells. Together these data suggests that the alterations in cardiac structure and function are secondary to alterations in the wider cardiovascular system. This is supported by evidence of eNOS uncoupling following endoglin knockdown.

The results reported in this thesis describe a novel phenotype and highlight the importance of endoglin in the maintenance of cardiac structure and function. Further work will clarify the mechanism behind these alterations.

Declaration

This thesis describes work undertaken in the laboratory of Professor Helen Arthur, at the Institute of Human Genetics, in fulfilment of the requirements for the degree of Doctor of Philosophy, at the University of Newcastle. This thesis is the result of my own work and contains nothing that is the outcome of work done in collaboration, except where specified in the text.

The work described here has not been submitted for a degree or diploma or any other qualification at any other University or Institution. This thesis does not exceed the word limit prescribed by the Faculty of Medical Sciences.

Benjamin John Davison
December 2013

Acknowledgements

This work was funded by a British Heart Foundation Clinical Research Training Fellowship.

I would like to thank my supervisor Professor Helen Arthur for allowing me the opportunity to undertake my PhD in her laboratory and for her help and guidance in completing my studies. My second supervisor Professor Andrew Blamire, along with Dr Ross Maxwell and Mr Ian Wilson, have provided me with a good grounding in the theory and practice of magnetic resonance imaging. Their help was invaluable when setting up murine cardiac MRI. I would also like to thank Dr Jurgen Schneider for providing me with the opportunity to visit his lab and pre-clinical MRI scanner at the University of Oxford. Thanks to all the staff at the Institute of Human Genetics who have made my three years there enjoyable. My special thanks to Dr Rachael Redgrave for her help with the infarct model and to Dr Alison Blain for her assistance with the cardiac conductance catheterisation experiments. In particular I would like to thank Miss Elizabeth Greally whom I worked closely with to set up the preclinical cardiac MRI.

I dedicate this thesis to Emma for her love, understanding and support throughout my career and to my children, Isabel and Oliver, who will be over the moon now "Daddy's finished his book!"

Table of Contents

List of Figures

List of Tables

List of Abbreviations

4-OHT	4-hydroxytamoxifen
ALK	activin receptor-like kinase
ANOVA	analysis of variance
αSMA	α smooth muscle actin
AT	angiotensin
bp	base pair
bpm	beats per minute
CDCs	cardiosphere derived cells
cDNA	complementary DNA
CF	cardiac fibroblasts
CI	cardiac index
cm	centimetres
CMR	cardiac magnetic resonance
CO	cardiac output
Co-SMAD	common mediator SMAD
CTGF	connective tissue growth factor
DAB	3-3'-diaminobenzidine tetrahydrochloride
DBP	diastolic blood pressure
DMEM	Dulbeccos' modified Eagles medium
DMSO	Dimethylsulphoxide
DNA	deoxyribonucleic acid
dP/dt_{max}	maximum rate of pressure rise
dP/dt_{min}	maximum rate of pressure decline
dsDNA	double stranded DNA
Ea	arterial elastance
EDP	end diastolic pressure
EDTA	ethylenediaminetetraacetic acid
EDV	end diastolic volume
EDVI	end diastolic volume index
Ees	end-systolic elastance
EF	ejection fraction

Eng	endoglin
eNOS	endothelial nitric oxide synthase
ESP	end systolic pressure
ESV	end systolic volume
ESVI	end systolic volume index
FCS	foetal calf serum
fl	floxed
FLASH	fast low angle shot
FOV	field of view
fsp	fibroblast specific protein
g	gram
Gapdh	glyceraldehyde-3-phosphate dehydrogenase
H&E	haematoxylin and eosin
HHT	Hereditary Haemorrhagic Telangiestasia
Hprt	hypoxanthine-guanine phosphoribosyltransferase
ID	inhibitor of DNA binding
ip	intra-peritoneal
I-SMAD	inhibitory SMAD
kb	kilobase
kDa	kilo Dalton
kg	kilogram
LAD	left anterior descending
loxP	locus of X-over P1
LV	left ventricle
LVAD	left ventricular assist device
MAP	Mean arterial pressure
MEMRI	manganese enhanced MRI
mg	milligram
MI	myocardial infarction
min	minute
ml	millilitre
mm	millimetre
mmHg	millimetres of mercury

MMP	matrix metalloproteinase
MRI	magnetic resonance imaging
mRNA	messenger RNA
ms	millisecond
MTT	methylthiazolyldiphenyl-tetrazolium bromide
NA	number of averages
ng	nanogram
NMV	net magnetisation vector
PAGE	polyacrylamide gel electrophoresis
PAI-1	plasminogen activator inhibitor 1
PBS	phosphate buffered saline
PCI	percutaneous coronary intervention
PCR	polymerase chain reaction
PRSW	Preload recruited stroke work,
pSMAD	phosphorylated Smad
qPCR	quantative PCR
R26R	Rosa26R
RAAS	renin angiotensin aldosterone system
RF	radio frequency
RNA	ribonucleic acid
ROI	region of interest
ROS	reactive oxygen species
rpm	revolutions per minute
R-SMAD	receptor-regulated SMAD
RT-PCR	reverse transcription PCR
RV	right ventricle
SBP	systolic blood pressure
SDS	sodium dodecyl sulphate
sEng	soluble endoglin
siRNA	small interference RNA
STEMI	ST elevation myocardial infarction
SV	stroke volume
SVI	stroke volume index

SVR	systemic vascular resistance
T	tesla
TAE	tris-acetate EDTA
Tau	isovolumetric relaxation time constant
TBS	tris buffered saline
TBST	tris buffered saline Tween
TE	echo time
TGFβ	transforming growth factor beta
Tgfbr2	TGFβ type II receptor
TIMP	tissue inhibitor of metalloproteinase
TNFα	tumour necrosis factor alpha
TR	repetition time
μg	microgram
μl	microlitre
μM	micromolar
μm	micrometre
X-gal	5-bromo-4-chloro-3-indolyl-beta-D-galactopyranoside

Chapter 1 Introduction

In the UK approximately 146,000 people suffer an acute myocardial infarction (MI) each year (Allender *et al.*, 2008). ST elevation myocardial infarction (STEMI) results from thrombotic occlusion of an epicardial coronary artery. The time from onset of STEMI to reperfusion (total ischaemic time) is of paramount importance as longer times result in larger area of infarction and increased mortality (Reimer and Jennings, 1979; Gersh *et al.*, 2005). For this reason emergency restoration of antegrade flow in the infarct related artery, with either primary percutaneous coronary intervention (PCI) or fibrinolysis, improves outcome following acute MI (Fibrinolytic Therapy Trialists' Collaborative Group, 1994; Keeley *et al.*, 2003; Keeley and Hillis, 2007). In the UK, 95% of patients with STEMI receive primary PCI as the initial reperfusion therapy (Gavalova and Weston, 2012). However, in addition to ischemic myocardial injury a further insult to the myocardium occurs at the time of reperfusion. There are a number of pathological mechanisms that result in reperfusion injury which include oxygen free radical formation, resulting in myocyte and endothelial injury, and dysfunctional intracellular calcium homeostasis, resulting in mitochondrial injury and cell death (Sharma *et al.*, 2012). Potential therapeutic options to ameliorate reperfusion injury include ischemic preconditioning (Murry *et al.*, 1986), ischemic postconditioning (Tsang *et al.*, 2005) and a number of pharmacological agents (Sharma *et al.*, 2012). The consequence of ischemic and reperfusion injury is myocyte necrosis and myocardial dysfunction resulting in neurohormonal activation and adverse ventricular remodelling resulting in a further decline in cardiac function (McKay *et al.*, 1986; J. M. Pfeffer *et al.*, 1991; Cohn *et al.*, 2000). Pharmacological therapy with inhibitors of the renin-angiotensin-aldosterone and sympathetic nervous system, aimed at reducing adverse cardiac remodelling, have also lead to significant improvements in morbidity and mortality following MI (Flather *et al.*, 2000; Packer *et al.*, 2001; Pitt *et al.*, 2003). Despite these improvements, ischaemic heart disease still remains the leading cause of heart failure and new strategies are needed to further improve long term prognosis following MI.

1.1 Infarct Healing

Myocardial infarction usually results following rupture of an unstable coronary atherosclerotic plaque, subsequent thrombus formation and coronary occlusion. The resultant myocardial ischaemia causes cardiomyocyte necrosis and leads to a series of events that culminates in a 'wound' healing process and the formation of a mature scar. This healing process has three overlapping phases: the inflammatory phase, the proliferative phase and the maturation phase (figure 1.1). Infarct healing is closely intertwined with the structural and functional changes seen in the infarcted and non-infarcted myocardium following MI, a process called ventricular remodelling (Frangogiannis, 2008).

Following myocardial infarction there is a rapid and robust inflammatory response. Cardiomyocyte ischaemia and cell death leads to activation of the complement cascade, free radical release and activation of Toll Like receptors and Nuclear Factor κB (NF κB) signalling pathways (Frangogiannis, 2008). There is increased synthesis of chemokines and cytokines with up regulation of adhesion molecule expression in endothelial cells and leukocytes. The infarcted myocardium is rapidly infiltrated by neutrophils and macrophages, which are involved in phagocytosis of dead cells and extracellular matrix debris, synthesis of cytokines and growth factors and regulation of matrix metalloproteinase activity (Dewald *et al.*, 2004).

The transition from the inflammatory phase to proliferative phase is marked by the suppression of pro-inflammatory mediators by cytokines such as interleukin-10 and transforming growth factor-β (Dobaczewski *et al.*, 2010). Granulation tissue consisting of fibroblasts and endothelial cells infiltrate and proliferate in the wound. Within the healing infarct, fibroblasts undergo a phenotypic change to become myofibroblasts, with features of smooth muscle cells including expression of α-smooth muscle actin (Willems *et al.*, 1994; Gabbiani, 1998). Cardiac fibroblasts play an important role in healing post MI by regulating the degradation and synthesis of extracellular matrix proteins (Porter and Turner, 2009). Myofibroblasts orientate themselves parallel to adjacent surviving cardiomyocytes (Willems *et al.*, 1994) and the contractile properties of myofibroblasts contribute to the tensile strength of the

infarct (Blanjesteijn *et al.*, 2001). During this phase vascular cells also proliferate to form an extensive microvascular network in the infarcted region.

During the maturation phase there is loss of cellularity within the healing infarct with apoptosis of cardiac fibroblasts and endothelial cells. The collagen secreted by the myofibroblasts forms cross linked bundles resulting in the formation of a mature scar. Myofibroblasts have been shown to have a persistent presence within the infarct scar (Willems *et al.*, 1994).

1.2 Ventricular Remodelling

Following myocardial infarction there are changes to ventricular architecture that initially may be an adaptive response to the sudden decrease in cardiac function but may ultimately result in deterioration of cardiac function and is associated with an adverse prognosis (M. A. Pfeffer and Braunwald, 1990; J. M. Pfeffer *et al.*, 1991). This process affects both the infarcted and non-infarcted myocardium and is termed ventricular remodelling (McKay *et al.*, 1986; White *et al.*, 1987; M. A. Pfeffer and Braunwald, 1990) and begins within the first few hours post MI (Cohn *et al.*, 2000). Ventricular remodelling can be divided into two phases; early (within 3 days) and late (after 3 days) remodelling.

Following the breakdown of the extracellular matrix, but before there is extensive collagen deposition and an increase in tensile strength, the infarct region can thin and elongate, this is called infarct expansion (Hutchins and Bulkley, 1978). It has been shown to be the result of slippage between muscle bundles leading to a reduced number of cardiomyocytes across the left ventricular (LV) wall in the infarct region (Weisman *et al.*, 1988) and is defined as ‘acute dilatation of the area of infarction not explained by additional myocardial necrosis’ (Hutchins and Bulkley, 1978). This is the predominant cause of early infarct remodelling. The extent of infarct expansion is proportional to the size and transmurality of MI (Hutchins and Bulkley, 1978; J. M. Pfeffer *et al.*, 1991) and can range from clinically unapparent to ventricular rupture.

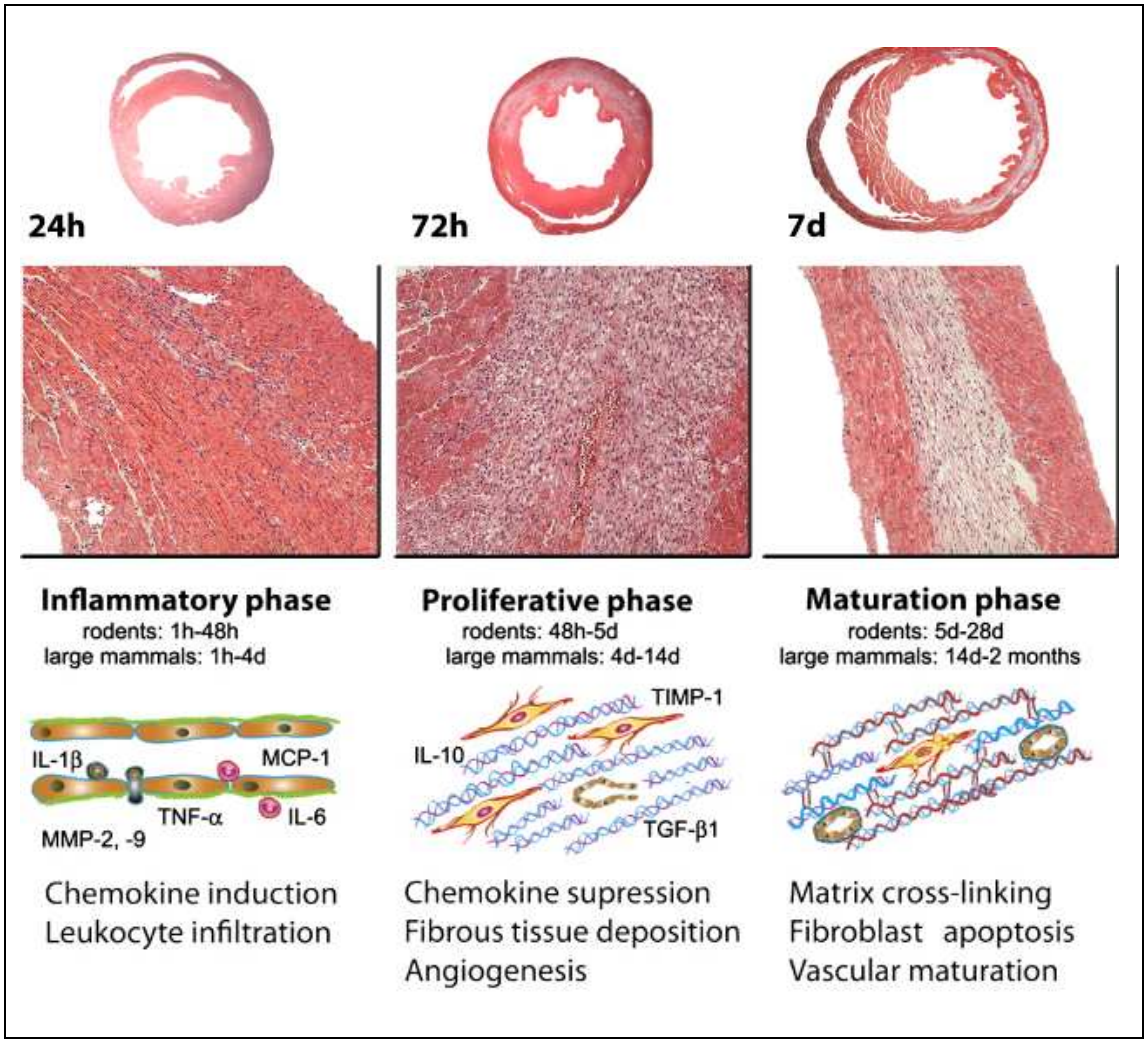

Figure 1.1 The phases of cardiac healing following myocardial infarction.

Adapted from Frangogiannis N.G. Pharmacological Research, 2008;58(2):88-111 (Frangogiannis, 2008) and Dobaczewski et al Journal of Molecular and Cellular Cardiology (2010) (Dobaczewski *et al.*, 2010).

Ventricular remodelling also affects healthy, remote myocardium in a process that begins immediately following MI and can last for several months. The increase in volume load leads to volume overload hypertrophy with lengthening and hypertrophy of the non-infarcted cardiomyocytes (McKay *et al.*, 1986). This further increases left ventricular dimensions, resulting in a more spherical left ventricle (McKay *et al.*, 1986; Mitchell *et al.*, 1992).

Cardiac remodelling is influenced by haemodynamic loading conditions and by neurohormonal activation via the sympathetic nervous system and renin angiotensin aldosterone system (Cohn *et al.*, 2000). Activation of the sympathetic nervous system

initially results in increased myocardial contractility and heart rate, thereby increasing cardiac output. Its activation also results in increased sodium and water retention, peripheral vasoconstriction, increased electrical instability and activation of the renin angiotensin aldosterone system (RAAS). RAAS activation results in augmented production of angiotensin II, an important mediator of adverse ventricular remodelling. Increased angiotensin II levels leads to sodium and water retention and peripheral vasoconstriction. It also mediates myocyte hypertrophy and interstitial fibrosis. Its actions are mediated via angiotensin type I (ATI) receptors. Initially these alterations in the sympathetic and renal angiotensin aldosterone systems are adaptive responses to maintain cardiac function post MI and may be beneficial but have deleterious long term haemodynamic consequences (Opie *et al.*, 2006). Inhibition of both these systems has lead to an improvement in mortality in patients with heart failure (Flather *et al.*, 2000; Packer *et al.*, 2001; Pitt *et al.*, 2003).

1.3 Cardiac fibroblasts

The cardiac extracellular matrix is comprised of interstitial collagens (predominantly type 1 and type 3), proteoglycans, glycoproteins, matrix metalloproteinases (MMPs) and their inhibitors (tissue inhibitor of matrix metalloproteinases, TIMPS) (Porter and Turner, 2009). Cardiac fibroblasts play a key role in the normal maintenance of the cardiac extracellular matrix which in turn regulates cardiac structure and hence mechanical, chemical and electrical function. The adult human heart comprises 30% cardiomyocytes and 70% non-myocytes, the majority of which are cardiac fibroblasts (Jugdutt, 2003). They are arranged parallel to muscle fibres and help to maintain normal cardiac function by maintaining the continuity between cells and the structural integrity in the myocardium (Weber, 2004; Brown *et al.*, 2005; Camelliti *et al.*, 2005; Kohl *et al.*, 2005; Banerjee *et al.*, 2006). During infarct healing cardiac fibroblasts undergo phenotypic modulation to myofibroblasts (Weber, 2004; Brown *et al.*, 2005; Camelliti *et al.*, 2005). This phenotypic change can be induced by TFG-β (Eghbali *et al.*, 1991b). These differentiated myofibroblasts secrete collagen and other extracellular matrix proteins, activate and regulate MMPs and TIMPs (table 1.1), thus playing a key role in ventricular remodelling (Brown *et al.*, 2005; Vanhoutte *et al.*, 2006; Porter and Turner, 2009). Cardiac fibroblasts play an important role in infarct healing and left ventricular remodelling and their regulation, particularly in response

to TGFβ, may represent a potential therapeutic target for promoting efficient cardiac repair.

Table 1.1 The temporal and spatial expression of MMPs and TIMPs following myocardial infarction.

Reproduced from Vanhoutte et al. Cardiovascular Research 2006:69(3);604-613 (Vanhoutte *et al.*, 2006).

Class	**Temporal and spatial window**								
	Early wound healing: 0-7 days			**Granulatory - early remodelling: 7-21 days**			**Late remodelling phase: 8 weeks**		
	Remote	**Border**	**Infarct**	**Remote**	**Border**	**Infarct**	**Remote**	**Border**	**Infarct**
Collagenases									
MMP1	↑*	↑*	↑*	ND	ND	ND	≈	↓	↓:UD
MMP8	≈	≈	≈	↑*	↑*	↑*	≈	↑	↑
MMP13	↑*	↑*	↑*	↑*	↑*	↑*	≈	↑	↑
Gelatinases									
MMP2	↑	↑	↑	↑	↑	↑	≈	↑	↑
MMP9	↑	↑	↑	↑	↑	↑	↑	↓	UD
Stromelysins									
MMP3	ND	ND	↑	↑	↑	↑	≈	≈	↓
MMP7	ND	ND	ND	ND	ND	ND	≈	↓	↓
MT1-MMP	≈	≈	≈	≈	≈	≈	≈	↑	↑
TIMPs									
TIMP1	≈	≈	≈	↑*	↑*	↑*	≈	↓	↓:UD
TIMP2	≈	≈	≈	↑*	↑*	↑*	↓	↓	↓:UD
TIMP3	ND	ND	ND	ND	ND	ND	↓	↓	↓:UD
TIMP4	≈	↓*	↓*	ND	ND	ND	≈	↓	↓:50%

MMP: matrix metalloproteinase; TIMP: tissue inhibitor of MMPs; UD: undetectable; ND: not determined; ↑increase; ↓: decrease; ≈: remains at basal level; ∗: activity levels were measured without distinction between indicated areas.

1.4 Transforming Growth Factor Beta

Transforming growth factor β1 (TGFβ1) regulates many of the cardiac repair processes outlined above. It is the archetypical member of the TGFβ superfamily, a group of evolutionarily conserved, pleiotropic cytokines that regulate many cellular functions, including cell growth, adhesion, migration, cell fate determination and differentiation, and apoptosis (Schmierer and Hill, 2007). Several human diseases, such as cancer, organ fibrosis, atherosclerosis, hereditary haemorrhagic telangiectasia and pulmonary artery hypertension, are associated with disordered signalling of TGFβ superfamily members (Blobe *et al.*, 2000; ten Dijke and Arthur, 2007).

TGFβ1 is synthesised as a dimeric pre-proprotein and is secreted in latent form being non-covalently attached to the latent binding protein. This latent complex is found mainly as a component of the extracellular matrix. It requires further activation to liberate active TGFβ1 ligand (Annes *et al.*, 2003; Gordon and Blobe, 2008).

TGFβ1 ligand mediates its action by binding to high affinity homodimeric complexes of type I and II receptors (Shi and Massagué, 2003). The constitutively active type II receptor then phosphorylates the type I receptor leading to its activation. This allows recruitment and subsequent phosphorylation of receptor regulated SMADs (R-SMADs), which then forms a complex with the common mediator SMAD (co-SMAD: SMAD 4). SMAD complexes are then shuttled to the nucleus where they directly regulate gene transcription (Shi and Massagué, 2003; Schmierer and Hill, 2007). There are also inhibitory SMADs (I-SMADs: SMAD 6 and SMAD 7), that can antagonise TGFβ signalling by inhibiting the activation of R-SMADs (figure 1.2) (ten Dijke and Arthur, 2007). TGFβ1 can also signal through non-canonical signalling pathways. These include MAP kinase, JNK and phosphatidylinositol-3-kinase pathways (Derynck and Zhang, 2003).

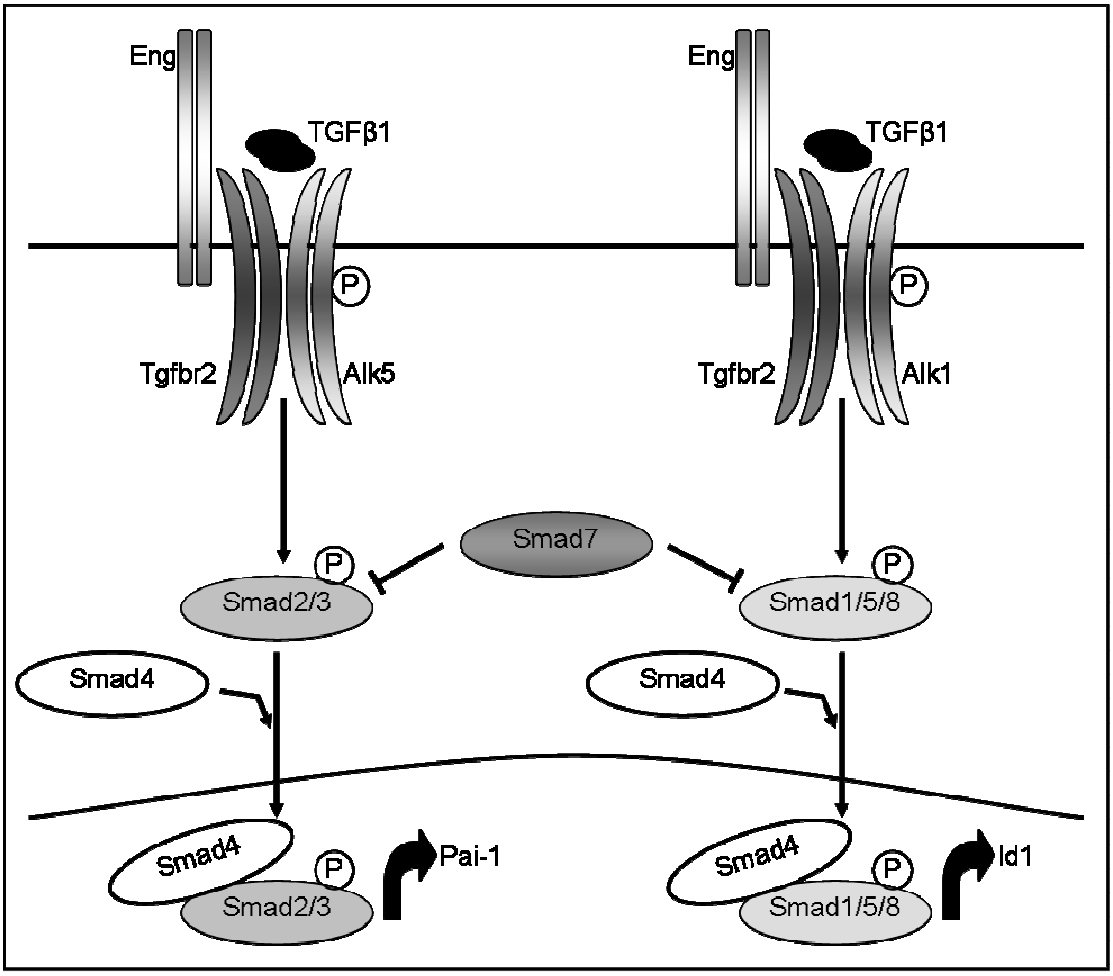

Figure 1.2 TGFβ family signalling pathways.

TGFβ1 normally signals via Tgfbr2/Alk5 receptor complex whereby binding of TGFβ1 results in phosphorylation of Smad2/3, this then associates with Smad 4 (the common Smad (Co-Smad)) and this complex then translocates to the nucleus where it results in transcription of effecter genes such as Pai-1. In endothelial cells (as depicted here) TGFβ1 can also signal via the Tgfbr2/Alk1 receptor complex, with the resulting transcription of genes such as Id1. Inhibitor Smads (Smad 7 is depicted here) inhibit both Smad2/3 and Smad1/5/8 signalling in response to TGFβ1. Adapted from ten Dijke et al Angiogenesis 2008:11(1): 79-89 (ten Dijke *et al.*, 2008).

1.5 Endoglin

Endoglin (CD105) is an 180kDa type I integral membrane glycoprotein expressed as a homodimer with each subunit consisting of a 561 amino acid extracellular domain, a hydrophobic transmembrane domain and a short cytoplasmic tail (figure 1.3) (Gougos and Letarte, 1990; Mahmoud *et al.*, 2011). The extra cellular domain of human endoglin contains a tripeptide arginine-glycine-aspartic acid (RGD) domain which is a key recognition structure for cellular adhesion (Gougos and Letarte, 1990). However, murine endoglin lacks this structure (Duff *et al.*, 2003). There are two isoforms of human endoglin which differ in the length of the intracellular domain. L-endoglin has a cytoplasmic tail of 47 amino acids and in S-endoglin it is 14 amino acids (figure 1.3) (Bellón *et al.*, 1993). Endoglin is primarily expressed in vascular endothelial cells (Gougos and Letarte, 1990) but is also expressed in fibroblasts (Leask *et al.*, 2002; K. Chen *et al.*, 2004), myofibroblasts (Torsney *et al.*, 2002), vascular smooth muscle cells (Adam *et al.*, 1998), monocytes (Pedro *et al.*, 1992) macrophages (Lastres *et al.*, 1992), and adult mesenchymal stem cells (Barry *et al.*, 1999; Smith *et al.*, 2007).

Endoglin is a TGFβ accessory receptor which is structurally similar to betaglycan (López-Casillas *et al.*, 1991; Cheifetz *et al.*, 1992). Endoglin is not directly involved in cell signalling but modulates the response to several TGFβ superfamily ligands (Lastres *et al.*, 1996). In endothelial cells TGFβ is able to signal via two type I receptor pathways, ALK1, which stimulates endothelial cell proliferation and migration, and ALK5, which inhibits these responses through activation of different R-SMADS (figure 1.2) (Goumans *et al.*, 2002). Subsequent experiments demonstrated that endoglin is responsible for modulating this response to TGFβ. Lebrin and colleagues demonstrated that endoglin is necessary for TGFβ/ALK1 signalling and indirectly inhibits TGFβ/ALK5 signalling (Lebrin *et al.*, 2004). The different isoforms of endoglin may also play a role in this differential regulation of TGFβ. For example, in endoglin deficient L_6E_9 myoblasts ectopic expression of L-endoglin results in enhanced signalling via the TGFβ/ALK1 pathway whereas S-endoglin promoted the TGFβ/ALK5 pathway (Velasco *et al.*, 2008). These effects of the different endoglin isoforms may be significant in age related vascular disorders as the expression of S-endoglin is associated with endothelial senescence (Blanco *et al.*, 2008).

The extracellular domain of endoglin can be cleaved from the surface of cells and circulates in the blood as a 65kDa protein, termed soluble endoglin. Soluble endoglin is found at increased levels in patients with pre-eclampsia (Venkatesha *et al.*, 2006), atherosclerosis (Blann *et al.*, 1996), familial hypercholesterolaemia (Blaha *et al.*, 2008) and heart failure (Kapur *et al.*, 2010; Kapur *et al.*, 2012). It is cleaved from the cell surface by MMP14 (Hawinkels *et al.*, 2010) and its levels are increased by TNFα *in vitro* (Cudmore *et al.*, 2007; Ikemoto *et al.*, 2012). Its exact function in the cardiovascular system is unknown but it has been shown to bind to and inhibit TGFβ (Venkatesha *et al.*, 2006; Walshe *et al.*, 2009). The role of soluble endoglin in the cardiovascular system will be discussed in further detail below.

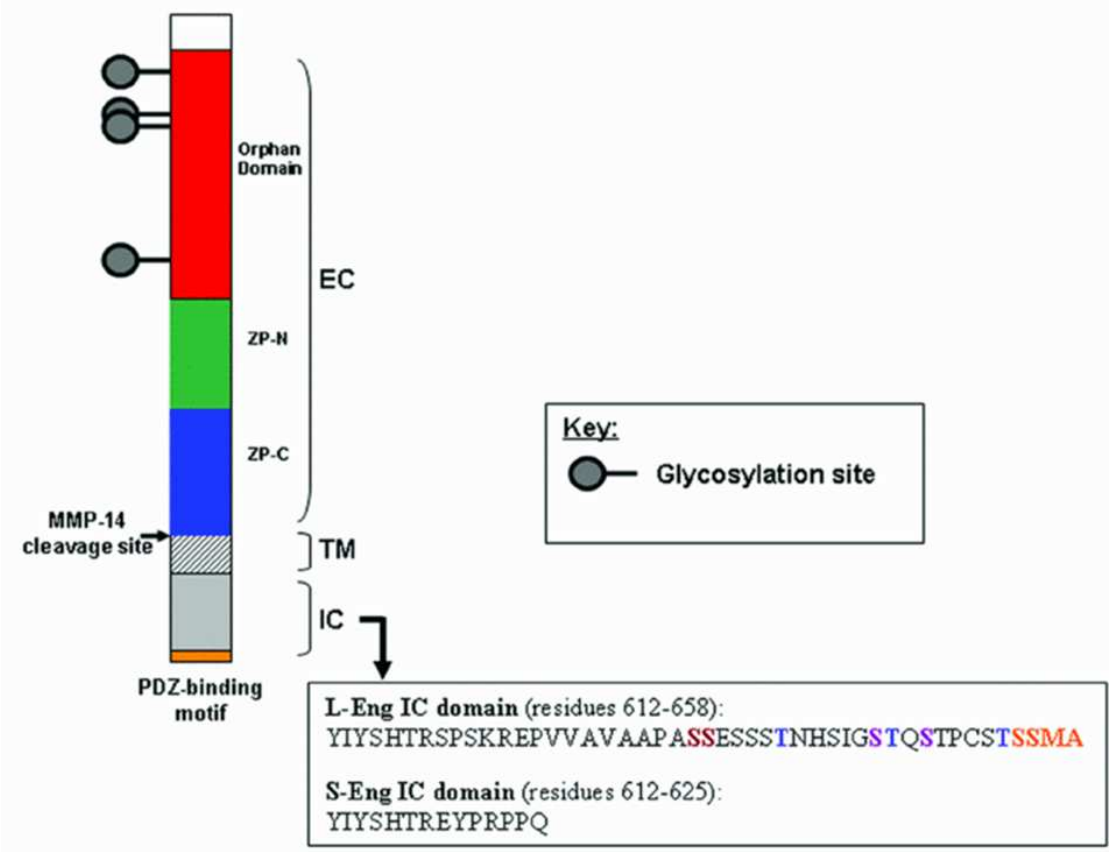

Figure 1.3 Structure of Endoglin.

Endoglin is divided into 3 distinct regions: the extracellular (EC) domain, important for ligand binding, the transmembrane (TM) and intracellular (IC) domain. Alternative splicing generates two different IC domains for endoglin (L-Eng and S-Eng). Adapted from (Mahmoud *et al.*, 2011).

1.6 Endoglin in cardiovascular disease

Haplo-insufficiency for endoglin has been shown to be responsible for hereditary haemorrhagic telangiectases (HHT) type 1, a rare familial vascular disorder characterised by cutaneous telangiectasia and arteriovenous malformations (McAllister *et al.*, 1994). The clinical phenotype of fragile vessels, haemorrhage and vascular malformations in these patients points to the importance of endoglin in the development and maintenance of the vasculature. However, ongoing research suggests that endoglin is also important in more common cardiovascular diseases.

1.6.1 Endoglin in atherosclerosis

In addition to being expressed in vascular endothelium endoglin is also expressed in smooth muscle cells and macrophages in human atherosclerotic plaques (Adam *et al.*, 1998; Conley *et al.*, 2000; Ma *et al.*, 2000; Piao and Tokunaga, 2006). It is predominantly the L isoform of endoglin that is expressed in atherosclerotic plaques (Conley *et al.*, 2000). Increased endoglin expression is also associated with more advanced lesions (Piao and Tokunaga, 2006). *In vitro* vascular smooth muscle cells express endoglin and its expression is increased by TGFβ1 and reduced by TNFα (Conley *et al.*, 2000). Endoglin has also been shown to be up regulated following balloon injury to porcine coronary arteries (Ma *et al.*, 2000). Inhibition of endoglin antagonised the TGFβ1 mediated inhibition of smooth muscle cell migration (Ma *et al.*, 2000). This may be of importance in arterial healing following percutaneous coronary intervention; particularly given that immunosuppressant drugs, similar to those used to reduce neointimal hyperplasia following PCI, have been shown to enhance endoglin expression (Albinana *et al.*, 2011; Giordano *et al.*, 2012).

In addition to endoglin expression in vascular smooth muscle cells and macrophages of atherosclerotic plaques, its microvascular expression also appears to be important in the stability of the plaque. In a study examining the expression of endoglin in coronary atherosclerosis in autopsy specimens, microvascular endoglin was correlated with plaque haemorrhage and deep seated inflammation. Both of which are features associated with plaque vulnerability (Xiaofei Li *et al.*, 2012).

One group in particular has examined the effects of dyslipidaemia and its treatment on endoglin expression using the ApoE/LDL receptor double knockout mouse. They demonstrated that the HMG-CoA-reductase inhibitor atorvastatin, used in the management of dyslipidaemia and secondary prevention in coronary artery disease, enhanced the expression of endoglin and resulted in an increase in Smad2, pSmad2/3 and endothelial nitric oxide synthase (eNos) (Nachtigal *et al.*, 2009). Subsequently they have shown that a high cholesterol diet led to a reduction in endoglin expression in atherosclerotic plaques along with a reduction in Alk1 and pSmad2, with soluble endoglin being increased in the serum of these mice (Strasky *et al.*, 2011). In another paper they then demonstrated that treatment of these mice, fed a high cholesterol diet, with atorvastatin led to a reduction in atherosclerotic lesion size and reduced levels of soluble endoglin (Rathouska *et al.*, 2011). Finally they confirmed that treatment with atorvastatin reduced cholesterol levels and plaque size and this was associated with an increase in plaque endoglin, Alk1, pSmad1, pSmad2, Vegf and eNos expression (Vecerova *et al.*, 2012). The effect of hypercholesterolaemia on soluble endoglin was also seen patients with Familial Hypercholesterolaemia. Blaha and colleagues demonstrate that soluble endoglin was elevated in these patients and that cholesterol reduction, using extracorporeal elimination therapy, resulted in a reduction of soluble endoglin levels. They demonstrated that this effect was not due to the capture of soluble endoglin in adsorption and filtration columns used in this therapy (Blaha *et al.*, 2008). The authors suggest that this reduction in soluble endoglin may be due to removal of atherogenic elements resulting in a reduction in endothelial activation and hence reduced release of soluble endoglin (Blaha *et al.*, 2008).

In patients with stable coronary artery disease following percutaneous coronary intervention, levels of circulating soluble endoglin was an independent risk factor for the development of major adverse cardiac events (Ikemoto *et al.*, 2012). In addition increased circulating soluble endoglin is associated with diabetes and hypertension, both of which are risk factors for the development of atherosclerosis. The level of soluble endoglin positively correlated with HbA1c (a measure of glycaemic control, with higher levels showing poor control) and systolic blood pressure (Blazquez-Medela *et al.*, 2010). Although not commented on in the study, the absolute levels of soluble endoglin were higher in the healthy controls, suggesting that there was a modifying influence in the diabetic and hypertensive groups. Statin therapy is widely

used in both these groups and may have resulted in lower soluble endoglin levels in these patients.

1.6.2 Endoglin in heart failure

Endoglin expression is increased in the left ventricles of patients with end-stage heart failure referred for mechanical left ventricular assist devices (LVAD) (Kapur *et al.*, 2012). Off loading of the left ventricle with these devices was associated with a reduction in tissue endoglin expression back to the levels in patients without heart failure, suggesting an association of endoglin levels and pressure overload in the failing heart (Kapur *et al.*, 2012). A previous study has demonstrated that circulating soluble endoglin levels are also increased in patients with heart failure compared to controls (Kapur *et al.*, 2010). Serum levels of soluble endoglin were inversely correlated with left ventricular ejection fraction and positively correlated with left ventricular end diastolic pressure and cardiac functional class (Kapur *et al.*, 2010). In a smaller group of patients (n=10) who were admitted for in-patient management of their heart failure, a reduction in soluble endoglin levels was seen following treatment and was associated with a reduction in pulmonary capillary wedge pressure (a measurement of left ventricular filling pressures) (Kapur *et al.*, 2010). Furthermore, circulating soluble endoglin levels are lower in smokers with heart failure compared to non-smokers with heart failure. There was also greater flow mediated dilatation (a measure of endothelial function) in smokers with heart failure. However there was no difference in soluble endoglin between smokers and non-smokers without heart failure (Heffernan *et al.*, 2011). This study suggests that reduced soluble endoglin levels are associated with improved endothelial function in heart failure.

However, alterations in soluble endoglin appear to be more complex as demonstrated by the effect of myocardial infarction on soluble endoglin levels. Levels of soluble endoglin in patients presenting with MI were significantly lower than in healthy controls and these levels fell further in the first 48 hours after admission (Cruz-Gonzalez *et al.*, 2008). There was no correlation between soluble endoglin level at admission and clinical outcome but a greater reduction in soluble endoglin over 48 hours was associated with increased mortality. In fact the percentage reduction in soluble endoglin levels was an independent predictor of post MI mortality (Cruz-

Gonzalez *et al.*, 2008). This reduction in serum soluble endoglin following a major vascular event was also seen in patients presenting with subarachnoid haemorrhage (SAH) (Dietmann *et al.*, 2012). This study also demonstrated that both lower serum levels of soluble endoglin and higher plasma levels of TGFβ1 were associated with complications following SAH and low mean soluble endoglin levels over the study period were associated with a poor, long term functional outcome (Dietmann *et al.*, 2012).

1.6.3 Endoglin in the regulation of vascular tone and oxidative stress

One of the pathological manifestations of HHT are cutaneous telangectases, which are post capillary venule dilatations connecting directly to dilated arterioles (Braverman *et al.*, 1990). This suggested that endoglin may be involved in regulation of vascular homeostasis and led Jerkic and colleagues to investigate the effect of endoglin on vascular tone. They demonstrated that in endoglin heterozygous mice mean arterial pressure was slightly (6mmHg) higher than in controls. There was also an attenuated hypotensive response to the endothelium dependent vasodilators bradykinin and acetylcholine (Jerkic *et al.*, 2004). In an isolated hind limb perfusion model they determined that this attenuated response was due to impaired vasodilatation in endoglin heterozygous mice. This was consistent with reduced levels of endothelial nitric oxide synthase (eNOS) in endoglin heterozygous mice and the authors showed that levels of eNOS were related to endoglin expression *in vitro* (Jerkic *et al.*, 2004).

This reduction in eNos levels in endoglin heterozygous mice has been confirmed by others (Toporsian *et al.*, 2005). They demonstrated that this reduction in eNOS was due to a reduction in the stability of eNOS protein in endoglin deficient mice where it has a significantly reduced half life. In addition, they demonstrated that endoglin resides in the caveolae where it is associated with eNOS suggesting a mechanism for its stabilising function. However, in isolated, pre-constricted mesenteric arterioles from endoglin heterozygous mice Toporsian and colleagues demonstrated an enhanced vasodilator response to acetylcholine compared to controls. This was due to eNOS uncoupling and increased production of reactive oxygen species (ROS) (Toporsian *et al.*, 2005).

The same group subsequently showed that, compared to control mice, endoglin heterozygous mice have dilated pulmonary arteries and there is an enhanced vasorelaxant response to acetylcholine in pre-constricted pulmonary artery ring segments *ex-vivo*, a response that was inhibited by L-NAME (an NO inhibitor) suggesting eNOS dependence (Belik *et al.*, 2009). They also demonstrated increased ROS production and eNOS uncoupling in the lungs of endoglin heterozygous mice compared to controls (Belik *et al.*, 2009). This suggests that the increased pulmonary vasorelaxation seen in endoglin heterozygous mice is due to increased eNOS dependent ROS production (Belik *et al.,* 2009).

1.6.4 Transforming growth factor β and endoglin in cardiac repair

Following surgically induced myocardial infarction in animal models TGFβ expression is upregulated. However, the different TGFβ isoforms display different temporal and spatial expression patterns. TGFβ1 and TGFβ2 mRNA follow a similar time course with their expression increasing 6 hours post infarction, reaching a peak after 3 days (Deten *et al.*, 2001; Dewald *et al.*, 2004). Thereafter, they decrease but remained elevated 2 to 3 fold, with TGFβ2 having a second peak after 21 days (Deten *et al.*, 2001). In the same study, TGFβ2 expression was much more pronounced in the non-infarcted versus the infarcted LV in the first day following MI (Deten *et al.*, 2001). TGFβ3 demonstrated quite a different time course. TGFβ3 mRNA levels were not significantly increased until 6 days post MI, reaching a peak on day 32 and remaining elevated for the length of the study which was 82 days (Deten *et al.*, 2001). In addition to increased TGFβ1 expression in the infarct scar, there is also an increase in Smad 2, 3 and 4 in both infarcted and non-infarcted myocardium following experimental MI (Hao *et al.*, 1999). In a study by Bujak et al, levels of phosphorylated Smad2 (pSmad2) were significantly elevated in infarcted mouse hearts within the first 24 hours, suggesting activation of the Smad 2/3 pathway (Bujak *et al.*, 2007). This western blot data was supported by immunohistochemical staining for pSmad2, which identified immunoreactive cells in the granulation tissue of the infarct border zone (Bujak *et al.*, 2007). The western blot analysis also showed an increase in pSmad1 at 24 and 72 hours post MI, and a corresponding decrease in inhibitory Smad 7 (Bujak *et al.*, 2007). This study also showed the importance of Smad3 in the cardiac fibrosis response. Smad3 knock out mice demonstrated a similar

density of macrophages to controls but reduced neutrophil infiltration and reduced chemokine and proinflammatory cytokine expression (Bujak *et al.*, 2007). There was no difference in the time taken for the inflammatory infiltrate to resolve. However, there was an increase in myofibroblast density but a reduction in collagen synthesis and interstitial fibrosis, which resulted in an improvement in diastolic function in Smad 3 null mice (Bujak *et al.*, 2007).

Due to its pleiotropic nature, TGFβ1 plays a complex role in infarct healing. It affects multiple cell types involved in the healing response (figure 1.4). TGFβ1 is a potent chemo-attractant of monocytes and it regulates cytokine and chemokine expression by monocytes and macrophages. Its primary effect on macrophages is the suppression of chemokine and proinflammatory cytokine synthesis (Bujak and Frangogiannis, 2007). TGFβ1 appears to have a cardioprotective effect in the early phase post MI. Lefer and colleagues demonstrated that administration of TGFβ1 at the time of experimental MI reduced levels of TNF-α and attenuated neutrophil adhesion to vascular endothelium (Lefer *et al.*, 1990; Lefer *et al.*, 1993). Similarly inhibition of TGFβ1 at the time of MI resulted in increased infiltration of neutrophils into infarcted tissue and an increase in the synthesis of proinflammatory cytokines and chemokines. This exacerbated LV dilatation and increased mortality (Ikeuchi *et al.*, 2004). Thus all three studies show that the immunosuppressive action of TGFβ1 around the time of MI is cardio-protective.

TGF-β stimulation also has a pro-fibrotic effect. It induces synthesis of the major extracellular proteins, fibronectin and collagen (Ignotz and Massague, 1986). In cardiac fibroblasts, TGFβ has been shown to increase type I and III collagen *in vitro* (Eghbali *et al.*, 1991a), and induce the transformation of cardiac fibroblasts to a myofibroblast phenotype (Eghbali *et al.*, 1991b), suggesting that TGFβ is important in the development of cardiac fibrosis. In contrast to inhibition of TGFβ at the time of MI, delayed inhibition of TGF resulted in reduced LV volumes and improved function combined with reduced interstitial fibrosis. This suggests that TGFβ inhibition post MI exacerbates early cardiac dysfunction but prevents late adverse remodelling (Ikeuchi *et al.*, 2004; Okada *et al.*, 2005). Angiotensin II, an important mediator of adverse ventricular remodelling, induces TGFβ both *in vivo,* following experimental MI, and *in vitro,* in cardiac fibroblasts, leading to increased collagen

synthesis (Sun *et al.*, 1998; Gao *et al.*, 2009). Angiotensin type 1 (AT1) receptor antagonism resulted in an attenuation of both TGFβ and collagen synthesis (Sun *et al.*, 1998; Yu *et al.*, 2001).

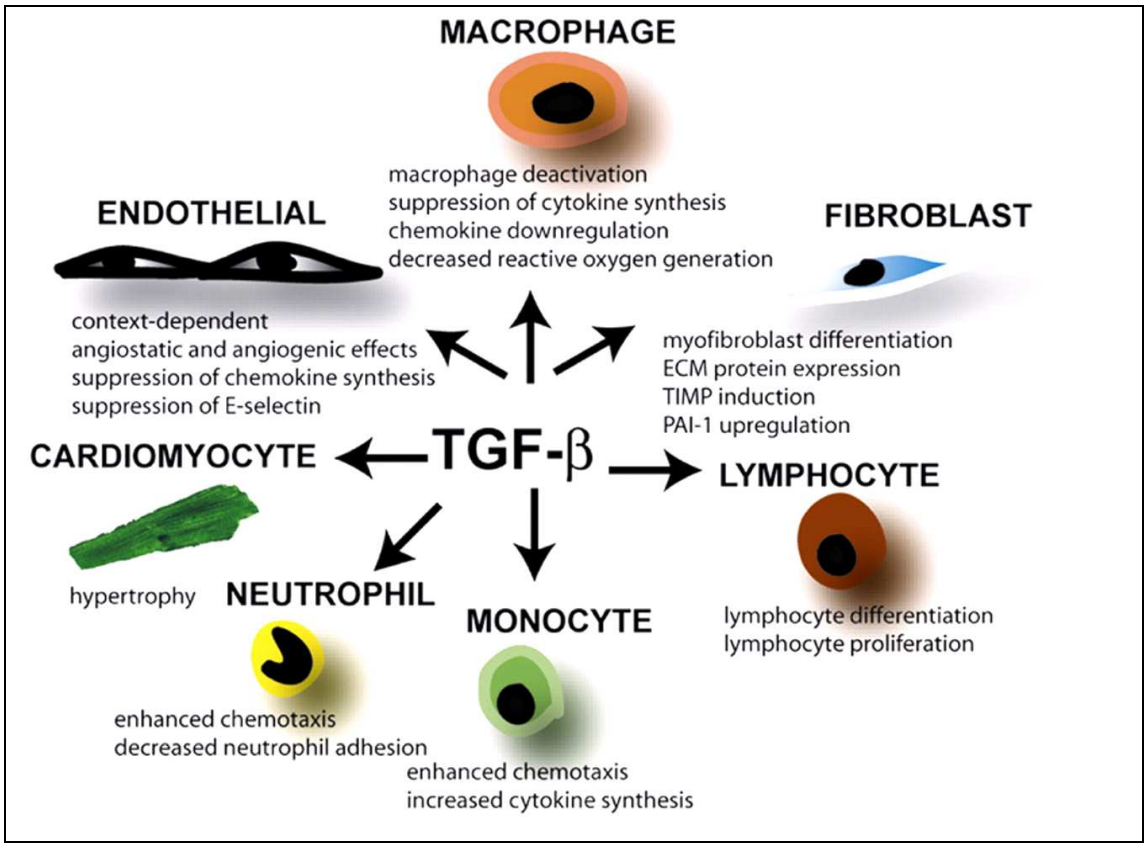

Figure 1.4 The diverse, multifunctional, and pleiotropic effects of TGF-β on cell types involved in infarct healing.

From Bujak, M. et al. Cardiovasc Res 2007 74:184-195 (Bujak *et al.*, 2007).

Endoglin has an important role in blood cell mediated vascular repair (van Laake *et al.*, 2006). It is strongly expressed in the infarct area 1 week following MI and the data from this study suggested that endoglin expression was confined to endothelial cells (van Laake *et al.*, 2006). However, the temporal and spatial expression of endoglin in the heart following MI has not been studied in detail and will be addressed in this thesis. Following surgical MI, endoglin heterozygous mice have significantly reduced cardiac function compared to control mice. They also exhibited impaired angiogenesis in the infarct region suggesting that this may result in greater adverse remodelling following myocardial infarction. Intravenous injection of bone marrow mononuclear cells from healthy human donors significantly improved cardiac function but cells from donors with HHT1 (i.e. patients who were heterozygous for

endoglin mutations) did not (van Laake *et al.*, 2006). This impaired ability, of bone marrow mononuclear cells from HHT1 patients, to augment cardiac repair appears to be due to impaired homing of these cells to the infarcted heart and a disruption of the SDF1-CXCR4 axis (Post *et al.*, 2010). This clearly shows a role for endoglin in infarct healing and cardiac repair *de novo* as well as following adult stem cell transplantation. One of the goals of this thesis was to investigate the role of endoglin in cardiac repair in more detail. Interestingly, during the course of this study, endoglin heterozygous mice were shown to have improved survival and cardiac function in a pressure overload model of heart failure (Kapur *et al.*, 2012), and is discussed further below.

1.6.5 Endoglin in fibrogenesis

Studies have shown that endoglin is expressed in cardiac fibroblasts either freshly isolated or in culture (K. Chen *et al.*, 2004; Shyu *et al.*, 2010; Kapur *et al.*, 2012). Endoglin has also been shown to be expressed in other cell types involved in extracellular matrix regulation in other organs. For example, cutaneous fibroblasts (Leask *et al.*, 2002), intestinal fibroblasts (Burke *et al.*, 2010), hepatic stellate cells and portal fibroblasts (Meurer *et al.*, 2010), mesangial cells (Diez-Marques *et al.*, 2002) and chondrocytes (Finnson *et al.*, 2010).

Angiotensin II stimulation of rat cardiac fibroblasts has been shown to result in increase expression of endoglin which was mediated via the AT1 receptor and the MAP kinase pathway (K. Chen *et al.*, 2004). In this study the induction of collagen 1 and suppression of MMP1 by angiotensin II was antagonised by an endoglin specific antibody (K. Chen *et al.*, 2004). TGFβ1 stimulation of rat cardiac fibroblasts also results in induction of endoglin and collagen 1. However, this induction was mediated via the PI3 kinase, Akt and Smad3 pathways but not the MAP kinase pathway. Inhibition of endoglin by siRNA resulted in a significant reduction in collagen 1 synthesis in response to TGFβ1, suggesting that endoglin may play a role in fibrosis. Interestingly, suppression of TGFβ1-induced collagen 1 synthesis by atorvastatin occurred independently of the presence or absence of endoglin (Shyu *et al.*, 2010). Both these studies confirm that the profibrotic cytokines angiotensin II and TGFβ1,

induce endoglin expression in cardiac fibroblasts and that endoglin is a positive regulator of collagen production.

The effect of endoglin on models of fibrosis in other organ systems has also been studied. Hepatic stellate cells are pericytes found in the perisinusoidal space of the liver and are an important cell type in hepatic fibrosis. A study by Meurer and colleagues demonstrated that endoglin expression is increased in rat models of experimental liver fibrogenesis and confirmed that endoglin is expressed in rat hepatic stellate cells. This expression of endoglin is up regulated by TGFβ1 (Meurer *et al.*, 2010). In these cells, TGFβ1 stimulation results in Alk5 dependent, phosphorylation of Smad1/5, Smad2 and Smad3. Transient over expression of endoglin enhanced Smad1/5 phosphorylation and resulted in an increase in expression of alpha smooth muscle actin (αSMA, also known as Acta1) (Meurer *et al.*, 2010). These data also suggest that endoglin is a positive regulator of fibrogenesis.

Human mesangial cells, present in the kidney and important in glomerulosclerosis, also express endoglin in culture. TGFβ1 stimulation of these cells results in increased expression of endoglin, TGFBR2 and TGFβ1 along with the extracellular matrix proteins collagen I, collagen IV and fibronectin (Diez-Marques *et al.*, 2002). This study also demonstrated that the composition of the extracellular matrix influences the expression of endoglin, with increased expression in mesangial cells cultured on collagen coated plates (Diez-Marques *et al.*, 2002). Finally, they investigated the effect of over expression of endoglin in a mouse fibroblast cell line. In endoglin transfected cells the levels of collagen I was lower in both untreated and TGFβ1 treated cells (Diez-Marques *et al.*, 2002). From this they concluded that endoglin is a negative regulator of collagen synthesis. This finding is in contradiction to those discussed above that indicated endoglin was a positive regulator of collagen synthesis. However, a number of other studies, where endoglin is over-expressed, also suggest that over-expression of endoglin is a negative regulator of the TGFβ1 induced fibrotic response. For example in an intestinal fibroblast cell line over-expression of endoglin resulted in an abrogation of the increased expression of connective tissure growth factor (CTGF) seen in control fibroblasts following TGFβ1 stimulation (Burke *et al.*, 2010). In the same study they also knocked down endoglin in primary intestinal fibroblasts with siRNA. This resulted in a small non-significant increase in CTGF

protein expression following TGFβ1 stimulation in endoglin depleted fibroblasts compared to control. However, there was a significant increase in collagen gel contraction (an *in vitro* model of connective tissue remodelling) by endoglin depleted fibroblast under basal conditions and following TGFβ1 stimulation (Burke *et al.*, 2010).

Scleroderma (systemic sclerosis) is a chronic autoimmune disease characterised by progressive fibrosis of the skin, blood vessels, muscles and other internal organs. It has been found that endoglin is over-expressed in dermal fibroblasts cultured from patients with scleroderma and the expression of endoglin increases with progression of the disease (Leask *et al.*, 2002). However, over expression of endoglin in dermal and NIH3T3 fibroblasts blocked the TGFβ1 induction of CTGF (Leask *et al.*, 2002). Another study by the same group confirmed the overexpression of endoglin in dermal fibroblasts from patients with scleroderma and that betaglycan (another TGFβ type III receptor) expression was also increased (Holmes *et al.*, 2011). Similarly, basal transcription of CTGF and collagen I was increased in sclerodermal fibroblasts but these cells showed a decreased responsiveness to TGFβ1 when compared to control fibroblasts. Once again, over-expression of endoglin inhibited TGFβ1 induced CTGF activity. However, over expression of betaglycan enhanced basal and TGFβ1 induced activity. The same response was seen when endoglin and betaglycan were co-transfected (Holmes *et al.*, 2011). These data support endoglin as a negative regulator of the fibrotic response in scleroderma but suggest that the different type III receptors may have antagonistic roles in this response.

However, a recent study by Morris et al. (Morris *et al.*, 2011) casts doubt on endoglin as negative regulator of the fibrotic response in scleroderma. In this study they knocked down endoglin, using siRNA, in dermal fibroblasts from patients with scleroderma and normal controls. They found no effect of endoglin knock down on CTGF or collagen I gene expression. However, in fibroblasts from patients with scleroderma they found that endoglin knockdown resulted in down regulation of both CTGF and collagen I. These results suggest that endoglin is a positive regulator of extracellular matrix production in scleroderma (Morris *et al.*, 2011).

These studies all examine the effects of endoglin *in vitro* and the precise culture and experimental conditions may explain the contradictory results. It may therefore be more informative to investigate the role of endoglin on the fibrotic response *in vivo*. In the heart the role of endoglin has been studied in two *in vivo* models of heart failure; myocardial infarction (van Laake *et al.*, 2006) and pressure overload following transverse aortic constriction (Kapur *et al.*, 2012). The study by van Laake and colleagues has been discussed above and demonstrated that cardiac function following surgically induced myocardial infarction is significantly reduced in endoglin heterozygous mice compared to controls (van Laake *et al.*, 2006). In a study using pressure overload as a model of heart failure, Kapur and colleagues demonstrated that there is improved cardiac function and reduced fibrosis in endoglin heterozygous mice compared to controls. They noted that there was no difference in the LV hypertrophy induced by aortic constriction between endoglin heterozygous mice and controls. However, there was an increase in myocardial capillarity in endoglin heterozygous mice compared to controls. Their study suggested that reduced endoglin limits fibrosis by limiting TGFβ1 signalling via the SMAD2/3 and ERK1/2 pathways (Kapur *et al.*, 2012). They also investigated the effects of endoglin on human cardiac fibroblasts *in vitro*. They found that inhibiting endoglin resulted in reduced type 1 collagen production. Interestingly, they found a paradoxical attenuation of type 1 collage production when they over expressed endoglin in these fibroblasts, similar to some of the scleroderma data discussed above. Kapur et al demonstrated that soluble endoglin antagonised TGFβ1 signalling and confirmed that there was increased soluble endoglin in the conditioned media of cardiac fibroblasts over expressing endoglin (Kapur *et al.*, 2012). This suggests that it is increased soluble endoglin, not the over-expression of endoglin, which is responsible for this paradoxical response and potentially explains the differing result previously seen in scleroderma fibroblasts.

In the kidney endoglin haploinsufficiency also results in reduced fibrosis following irradiation compared to controls (Scharpfenecker *et al.*, 2009). Further research by the same group demonstrated that this reduction in fibrosis was associated with a reduced macrophage infiltration and cytokine production (interleukin 1 beta and interleukin 6) in the endoglin heterozygous mice (Scharpfenecker *et al.*, 2012). This role of endoglin in modulating the inflammatory response has been demonstrated by other groups. In a

renal infarct reperfusion injury model, endoglin heterozygosity is protective against infarct reperfusion injury and is also associated with reduced macrophage infiltration (Docherty *et al.*, 2006). This may be due to the effect of endoglin on leucocyte adhesion and endothelial transmigration. Transendothelial transmigration of leucocytes during inflammation has been shown to be impaired in endoglin deficient mice (Elisa Rossi *et al.*, 2013). *In vitro* studies suggest that the RGD motif of endoglin is responsible for this adhesion and transmigration (Elisa Rossi *et al.*, 2013), which is interesting as murine endoglin does not possess this motif (Duff *et al.*, 2003). Also soluble endoglin was demonstrated to abolish this endoglin dependent leucocyte adhesion (Elisa Rossi *et al.*, 2013).

Clearly endoglin plays an important role in regulation of fibrosis but it is unclear from these studies if these effects are due to the effect of endoglin directly regulating TGFβ collagen production or indirectly by its effects on inflammation or indeed both. Therefore one of the goals of this thesis was to investigate the role of endoglin in collagen production by cardiac fibroblasts.

1.7 Mouse models

Significant advances in mouse genetics have provided powerful *in vivo* models with which to study gene function. In the case of endoglin, null embryos show embryonic lethality due to defects in angiogenesis (Arthur *et al.*, 2000). However, mice heterozygous for the endoglin gene develop normally with no effect on survival. They show reduced levels of endoglin and serve as a model of HHT type 1 in the 129/Ola background (Arthur *et al.*, 2000). In order to study the effects of this essential gene in adult life a different approach is needed, using conditional knockout mice. This allows the tissue specific inactivation of a target gene at a specific point in time. Our group has developed an inducible endoglin knockout model (Allinson *et al.*, 2007). This is achieved by flanking specific exons of the target gene (in this case, exons 5 and 6) by loxP sites. In the presence of the enzyme Cre-recombinase, these exons are excised to inactivate the gene. In the case of the inducible endoglin knockout mouse an inducible version of Cre (Cre^{ERT2}) is used and is activated by tamoxifen (figure 4.5). Within our group we have two inducible Cre lines, *Cdh5(PAC)-*Cre^{ERT2} (an endothelial specific Cre line) and *Rosa26-*Cre^{ERT2} (in which Cre is ubiquitously expressed). Both lines

were used in the work described in this thesis to investigate the roles of endoglin in cardiac function. The different *in vivo* and *in vitro* experimental approaches that were used are introduced in the relevant chapters.

1.8 Magnetic resonance imaging to assess cardiac structure and function in mice

In parallel with the increased use of genetically modified mouse models in the study of cardiovascular development and disease, improved techniques to analyse their cardiac function have evolved. Magnetic resonance imaging (MRI) allows for an accurate and reproducible, non-invasive assessment of cardiac structure and function (Florentine *et al.*, 1986; Shapiro *et al.*, 1989; Ruff *et al.*, 1998). Although, given the small size of the mouse heart and high physiological heart rates, this assessment remains technically challenging. Each aspect of the experimental process requires careful consideration to optimise image quality and to ensure accurate and reproducible data collection (Johnson, 2008). Important factors include choice of hardware, anaesthetic agent and gating strategy used. Here I will initially discuss the physics of nuclear magnetic resonance to explain how magnetic resonance images are obtained. I will then discuss the experimental factors that influence image quality. Finally, I will discuss the use of MRI for the assessment of cardiac function in mice.

1.8.1 Nuclear magnetic resonance

In order to understand how MRI images are generated it is important to understand the basic structure of atoms. An atom consists of a central nucleus, made up of protons and neutrons, and orbiting electrons. Within the atom there are three kinds of motion, electrons spinning on their own axis, electrons orbiting the nucleus and the nucleus spinning on its own axis. Nuclei with an odd mass number (total number of protons and neutrons) have net spin or angular momentum and are MR active nuclei. It is the spinning of specific nuclei present in biological tissue that underpins the principles of MRI. The hydrogen nucleus consists of a solitary proton which gives it a relatively large magnetic moment. It is the most abundant atom in biological tissue. Both these facts make hydrogen the ideal MR active nuclei for magnetic resonance imaging (Westbrook *et al.*, 2005).

The fundamental laws of electromagnetism state that a magnetic field is created when a charged particle moves. Thus the spinning of a positively charged hydrogen nucleus induces a magnetic field around it. It is easiest to conceptualise these protons as tiny magnets or "spins". Normally these protons are randomly orientated but the application of a strong external magnetic field (B_0) causes them to align with the magnetic field. Some will align parallel (in the same direction) and some will align anti-parallel (in the opposite direction) to the magnetic field. There is a small excess of protons aligned parallel to the magnetic field resulting in a net magnetic moment called the net magnetisation vector (NMV) and this magnetisation within a subject allows the generation of the MR image (see below) (Westbrook *et al.*, 2005).

The influence of the strong magnetic field also produces an additional spin or wobble of the magnetic moments of hydrogen nuclei around B_0. This is called precession. The circular path they follow around B_0 is called the precessional path and the speed at which they move around this path is called the precessional frequency. The precessional frequency is governed by the Larmor equation. The Larmor equation states that:

$\boldsymbol{\omega_0 = B_0 \times \gamma}$

where:

$\boldsymbol{\omega_0}$ is the precessional frequency (measured in megahertz (MHz))

$\mathbf{B_0}$ is the magnetic field strength of the magnet (measured in tesla, T)

$\boldsymbol{\gamma}$ is the gyromagnetic ratio (unit is megahertz per tesla (MHz/T)). The gyromagnetic ratio for hydrogen is 42.57 MHz/T (Westbrook *et al.*, 2005).

If a radiofrequency (RF) pulse is then applied at the same frequency as the precessional (Larmor) frequency for hydrogen then the hydrogen nuclei gain energy and resonate. The result is that the NMV rotates away from the longitudinal plane (which is in the same direction of the magnetic field) towards the transverse plane, which is at 90° to the longitudinal plane. This is a process called "excitation." The magnitude of this rotation (terned the "flip angle") is dependent on the magnitude and duration of the RF pulse. The other result of resonance is that the magnetic moments of the individual hydrogen nuclei move into phase with each other (Westbrook *et al.*, 2005). When the RF pulse is switched off then the hydrogen nuclei lose the energy

and the NMV realigns with the magnetic field. At the same time but independently the magnetic moments of hydrogen nuclei lose coherency due to dephasing. Together, these processes are called relaxation. Relaxation results in the decay of transverse magnetisation, due to nuclei exchanging energy with their neighbouring nuclei, called T2 decay and the recovery of longitudinal magnetisation, due to the nuclei giving up energy to their surrounding environment, termed T1 recovery (Westbrook *et al.*, 2005).

If a radiofrequency receiver coil is placed in the transverse plane then an electrical current is produced when in-phase magnetisation cuts across it. This current constitutes the MR signal. The time between the applications of RF pulses, during which relaxation occurs, is called the repetition time (TR). The time from the application of the RF pulse to the peak signal induced in the receiving coil is called the echo time (TE). Both are measured in milliseconds.

Tissue contrast is produced due to the fact that molecules in biological tissues relax at different rates. The useful example is to compare fat and water. Fat molecules contain atoms of hydrogen, carbon and oxygen where the hydrogen atoms are closely packed and relatively immobile relative to one another. Water is comprised of two hydrogen atoms with one oxygen atom and its molecules are widely spaced. These differences in structure influence the time for which individual protons can interact with each other and other atoms in their local environment. Consequently relaxation in fat is quicker than in water. This results in fat having a short T2 (fast signal decay) and short T1 (fast recovery of longitudinal NMV). The opposite is true for water. Selection of appropriate MRI scan parameters are used to sensitise the image to these differences and create contrast between different tissues. For example, in T1 weighted images, where fat appears bright and water dark, the TR and TE are both short. Whereas, in T2 weighted images, where fat appears dark and water appears bright, the TR and TE are both long. The use of MR contrast agents can significantly alter the local T1 and/or T2 resulting in an increased or decreased signal intensity and hence positive or negative tissue contrast. Examples of such agents include gadolinium, manganese and iron (Westbrook *et al.*, 2005).

1.8.2 Experimental Factors

1.8.2.1 Hardware

Given the small size of the mouse's heart an optimised hardware setup is required (Schneider *et al.,* 2006). Cine MRI of mice hearts has been described using magnetic field strengths between 1.5T (Gilson and Kraitchman, 2007) and 11.4T (Schneider *et al.,* 2003). However, increasing magnetic field strengths benefits the signal to noise ratio (SNR) allowing improved spatial resolution and can reduce time required to collect MR images (Schneider *et al.*, 2006). Most magnets used for murine CMR have a horizontal bore. However, some older experimental high field magnets (≥11T) were built with vertical bores (Wiesmann *et al.*, 2001a; Schneider *et al.,* 2003). This potentially poses a problem as mice have to be imaged with an upright body position which is not physiological. Wiesmann et al. (Wiesmann *et al.,* 2001a) showed that following a transient drop in left ventricular (LV) systolic pressure on vertical tilting, which returns to baseline by six minutes, a vertical body position did not affect invasive hemodynamic parameters over a follow up period of 60 minutes. When applied to a high field, vertical bore MR system, a vertical body position did not affect measured cardiac function parameters when compared to a horizontal bore system (Schneider *et al.*, 2003). The pre-clinical magnet at Newcastle University and used in the work described in this thesis has a horizontal bore so the animals are placed prone, which is a more physiological position for mice.

1.8.2.2 Gating

The imaged generated is built up using a number of signal excitations, with the duration of the scan (from milliseconds to minutes) being dependent on the type of scan and the contrast required. The MRI process assumes that the object being imaged is not moving and so any uncontrolled movement results in image blurring. As the heart is constantly beating and moving with respiration, cardiac MR is severely affected by both cardiac and respiratory motion artefacts. This is exacerbated by the high mouse heart rate (400-600 beats per minute (bpm)) and fast respiratory rates. These are minimised by the use of physiological gating to trigger the start of a scan and synchronise the image sequence to the beating heart. Cardiac gating is essential and image quality is improved with respiratory gating, which becomes more important at higher field strengths (> 7T) (Schneider *et al.*, 2003; Cassidy *et al.*, 2004).

The maintenance of a steady state level of magnetisation during respiration without acquiring image data has also been shown to improve image quality (Cassidy *et al.*, 2004). Although initial experiments were performed using only cardiac gating the majority of the work described in this thesis used both respiratory and cardiac gating.

1.8.2.3 Anaesthetic

Mice need to be anaesthetised for the duration of an MRI scan. The choice of anaesthetic influences the quality of data depending on the duration of action and the effects on cardiac function. An echocardiographic study comparing inhaled halothane to a ketamine and xylazine combination showed that ketamine/xylazine produced significant reductions in heart rate, left ventricular fractional shortening and cardiac output (Chaves *et al.*, 2001). Anaesthesia was induced with the ketamine/xylazine combination (80/10 mg/kg i.p.) within 5 to 20 minutes of injection with duration of action between 30 and 60 minutes. Whereas, halothane (0.25-0.75% in 95% O2) induced anaesthesia in less than 5 minutes of inhalation, maintained an adequate depth throughout and mice recovered to ambulatory activity within 2 minutes of halothane withdrawal (Chaves *et al.*, 2001). Further studies have confirmed the myocardial depressive nature of ketamine/xylazine (Roth *et al.*, 2002; Kober *et al.*, 2004). Roth et al. (Roth *et al.*, 2002) compared a range of anaesthetic agents. They found that inhaled isoflurane produced higher initial heart rates of about 550 beats per minute but gradually declined over the 20 minute study period to about 400 beats per minute. Isoflurane provided the most stable cardiac function over this time and was the most reproducible in repeat studies. The concentration of isoflurane (1.25% versus 2.00%) was found to affect respiration rate in a concentration dependent manner but did not affect cardiac function (Kober *et al.*, 2004). Mouse cardiac MR scans normally take between 45 and 60 minutes and cardiac function needs to remain stable during this time. As a result of its ease of use and cardiac stability, isoflurane is commonly used in murine MRI experiments (Ruff *et al.*, 1998; Wiesmann *et al.*, 2001a; Wiesmann *et al.*, 2002; Schneider *et al.*, 2003; Cassidy *et al.*, 2004).

1.8.3 Assessment of cardiac function with MRI

Cardiac magnetic resonance imaging (CMR) provides three dimensional images of the heart with high spatial and temporal resolution. It has been used to accurately and reliably assess cardiac function in both humans (Sechtem *et al.*, 1987; Cranney *et al.*,

1990) and large animal models (Florentine *et al.*, 1986; Shapiro *et al.*, 1989). The small size of the mouse heart and its high physiological heart rate provide additional challenges for the study of murine cardiac function. However, Ruff and colleagues (Ruff *et al.*, 1998) demonstrated that small volumes could be accurately measured with high resolution magnetic resonance imaging. They also found that there was precise agreement between left ventricular mass calculated by MRI and at autopsy. Finally, they were able to show that the assessment of cardiac function by MRI was highly reproducible with low inter-observer and intra-observer variability. Echocardiography is an alternate imaging modality that has been validated for assessing LV mass and function (Manning *et al.*, 1994; Gardin *et al.*, 1995). However, echocardiography relies on geometric assumptions which may limit its accuracy in hearts with abnormally shaped left ventricles that may result from disease (Dulce *et al.*, 1993 125). The development of three dimensional echocardiography, which does not rely on geometric models, may reduce this limitation (Dawson *et al.*, 2004). The complex geometry of the right ventricle (RV) makes assessment of its function more difficult. Nevertheless, assessment of RV size and function can be accurately made using CMR in humans (Sechtem *et al.*, 1987) and mice (Wiesmann *et al.*, 2002). MRI allows accurate assessment of cardiac function without relying on geometric models and provides valuable three dimensional structural information.

Magnetic resonance imaging has been successfully applied to several mouse models of cardiac disease. Siri et al (Siri *et al.*, 1997) were able to show that MRI could be used to assess changes in LV mass, geometry and function in a mouse model of left ventricular hypertrophy. Following myocardial infarction (MI) cardiomyocyte loss, fibrosis and neurohormonal changes lead to LV wall thinning, LV dilatation and impaired regional function. These changes in structure and function have been serially assessed in a mouse model of reperfused myocardial infarction using MRI (Ross *et al.*, 2002). They demonstrated that at 1 day following MI the LV function had declined by greater than 50% and remained depressed for the duration of the study. Over the course of the next 4 weeks the left ventricle progressively dilates. They also showed a transient reduction in contractile function in regions remote from the infarcted myocardium. This resolved by 7 days post infarct, but was followed by a late phase of myocardial dysfunction that became fully manifest by 28 days. This reduction in contractile function in non-infarcted regions was also demonstrated by Yang et al.

(Yang *et al.*, 2004). However, their study only assessed LV function at a single time point (24 hours post MI) and therefore did not demonstrate an early and late phase of contractile dysfunction. Together these studies demonstrate that ventricular remodelling is a dynamic process and highlights the value of MRI to serially evaluate cardiac function in the same animal, at different time points post MI. In addition to global myocardial function, regional function can be assessed by measuring myocardial torsion with magnetic resonance tagging (Henson *et al.*, 2000) or myocardial velocity mapping using phase contrast MRI (Nahrendorf *et al.*, 2006).

Magnetic resonance contrast agents can be used to assess myocardial perfusion, infarct size and myocardial viability. In clinical studies gadolinium based agents are used as these increase the intensity of T1 weighted images. The principles underlying this technique are that the first pass of gadolinium through the heart demonstrates myocardial perfusion since the contrast agent is essentially only within the vasculature at this time. The gadolinium then accumulates in the abnormal interstitium of the infarcted region. This results in increased T1 weighted image intensity in the area of infarct after a delay of 5 to 20 minutes. This technique is called late gadolinium enhancement. In a mouse infarct model, there was good agreement between infarct size as assessed by late gadolinium contrast enhancement and histological staining with 2,3,5-triphenyl tetrazolium chloride (TCC) (Yang *et al.*, 2004). Manganese is another MR contrast agent used in preclinical models and Manganese-Enhanced Magnetic Resonance Imaging (MEMRI) can indirectly assess myocardial calcium influx (Hu *et al.*, 2001). To image calcium influx MEMRI exploits 2 properties of the manganese ion: one is that the ion is divalent and so enters the cardiac myocyte through the L-type calcium channel (or potentially other routes of abnormal calcium cell entry), and secondly, that it is a contrast agent on T1 weighted images. These 2 properties allow us to non-invasively monitor myocyte calcium uptake in-vivo. Hu et al, demonstrated that manganese enhanced MRI (MEMRI) can be used to assess calcium influx and inotropic state of the heart (Hu *et al.*, 2001). The same group showed that MEMRI was able to accurately assess infarct size in vivo as measured by TCC staining post mortem. It also allowed the simultaneous evaluation of LV function and viability (Hu *et al.*, 2004).

In conclusion magnetic resonance is a versatile tool for the accurate and reproducible assessment of cardiac function *in vivo*. It has been used in several models of cardiovascular disease to assess the effects of gene mutations, response to pharmaceutical therapies and response to cell therapies (Akki *et al.*, 2013). However, it is expensive and requires careful optimisation to achieve these results. At the time of starting my PhD studies, cardiac MRI of mouse models had not yet been established in Newcastle and this was therefore one of the first aims of my project.

1.9 Aims

1. To establish and validate murine cardiac MRI at Newcastle University using a 7T Varian magnet.
2. To evaluate applications of cardiac MRI in three mouse models of cardiac disease.
3. To investigate the role of endoglin in endogenous cardiac repair.
    a. To establish the temporal and spatial expression of endoglin in the heart following myocardial infarction.
    b. To establish a ubiquitous endoglin knockdown mouse model using tamoxifen treated *Eng*$^{fl/fl}$*;Rosa26-Cre*^{ERT2} mice.
    c. To use this mouse model to investigate the effects of endoglin depletion on infarct size and myocardial function *in vivo* using cardiac MRI.
4. To investigate the role of endoglin in primary cardiac fibroblasts *in vitro* during the pro-fibrotic response to TGF-β stimulation.

Chapter 2 Materials and methods.

2.1 Suppliers.

All chemicals and reagents were purchased from VWR International, Sigma-Aldrich, Vector Laboratories, Thermo Scientific, GE Healthcare, Pierce Biotechnology, Qiagen, Roche or Invitrogen.

All plastic ware and apparatus for Western blotting and general laboratory use was purchased from BioRad Laboratories, Iwaki, Greiner, RA Lamb, or Scientific Laboratory Supplies.

Oligonucleotides were purchased from Integrated DNA Technologies.

2.2 Mice strains and genotyping.

All animal experiments were performed under Home Office personal and project licences in accordance with the Animals (Scientific Procedures) Act 1986 and had local ethical approval.

2.2.1 Mouse strains.

For the MRI validation experiments and the myocardial infarction model C57Bl/6 mice were used. For the manganese enhanced MRI experiments delta-sarcoglycan deficient (*Scgd-/-) mice*, a model for limb girdle muscular dystrophy type 2 (Nonaka, 1998), were used with age matched C57Bl/10 mice used as controls. The $Eng^{fl/fl}$ mice were developed in my host laboratory (Allinson *et al.*, 2007) and were homozygous for the floxed endoglin allele, with loxP sites flanking exons 5 and 6 (figure 4.5). To achieve ubiquitous or endothelial specific endoglin knockdown the $Eng^{fl/fl}$ mice were crossed with the tamoxifen inducible *Rosa26-*Cre^{ERT2} (generated in Dr A. Joyner's lab, New York, and were obtained from Dr C Guo, University of Connecticut) or *Cdh5(PAC)-*Cre^{ERT2} mice (Dr Ralf Adams, CRUK, London).

2.2.2 DNA extraction.

The solutions needed were made up from stock solutions as follows:

Lysis buffer 1 (25mM NaOH/0.2mM EDTA).

2.5ml of 0.5M NaOH + 0.02ml 0.5M EDTA in 50ml sterile double distilled H_2O, adjusted to pH12.

Lysis Buffer 2 (40mM Tris-HCl).

4ml of 0.5M Tris-HCl in 50ml sterile double distilled H_2O adjusted to pH 5 with HCl.

Ear clips of adult mice were incubated with 100µl of lysis buffer 1 in a thermomixer at 95°C, 350 rpm for 60 minutes. Following a quick vortex, 100µl of lysis buffer 2 was then added. This solution was then quickly vortexed and centrifuged for 5 minutes at 13,000g. The resultant supernatant contained the DNA, 2µl of which was then used in the subsequent PCR reaction, with the majority of undigested tissue and impurities remaining at the bottom of the tube.

2.2.3 Genotyping.

All genotyping was carried out using polymerase chain reaction (PCR). To genotype the *Eng$^{fl/fl}$;Rosa26-Cre^{ERT2}* and *Eng $^{fl/f}$;Cdh5(PAC)-Cre^{ERT2}* mice a four primer mix (table 2.1) was used to amplify part of the *endoglin* gene and part of the *Cre* gene. Each PCR reaction was carried out in 0.2ml thin walled PCR tubes. Individual reaction mixes consisted of 2µl of extracted DNA, 1µl of 20µM primer mix, 2.5µl of 25mM $MgCl_2$, 2.5µl 10x Reaction Buffer IV, 0.2µl Red Hot *Taq* DNA Polymerase (all purchased from ABgene, Thermo Scientific), 0.5µl of 10mM dNTPs (New England Biolabs) and 16.8µl dH_2O to make a reaction volume of 25µl

.

Table 2.1 Primers used for genotyping *Eng$^{fl/fl}$;Rosa26-Cre^{ERT2}* and *Eng$^{fl/fl}$;Cdh5(PAC)-Cre^{ERT2}* mice.

Primer	Sequence (5'-3')	Product size
engF6	GACGCCATTCTCATCCTGC	500bp
engR7	CCACGCCTTTGTCCTTGC	
Cre5F	TGCCACCAGCCAGCTATCAACT	191bp
Cre5R	AGCCACCAGCTTGCATGATCTC	

PCR reactions were carried out using the GeneAmp® PCR System 2400 (Applied Biosystems). The PCR cycle program used was as follows:

Initial denaturing step:	95°C	-	2 minutes	
Denaturing step:	95°C	-	15 seconds	x35 cycles
Annealing step:	58°C	-	30 seconds	
Extension step:	74°C	-	1 minute	
Final extension step:	74°C	-	7 minutes	

PCR products were then resolved on 1.5% agarose gels. These were made by heating, in a microwave, 1.5g DNA agar (Seakem®LE Agarose for gel electrophoresis) in 100ml of 1xTAE buffer (40mM tris base-acetate and 1mM EDTA) to generate a clear solution. This was allowed to partially cool before 10µl of 10,000x GelRed™ (Biotum Inc) was added. The gel was then poured in to horizontal gel tray with combs. Once cooled and fully set the gel was fully submerged in a gel electrophoresis tank containing 1xTAE buffer and the comb carefully removed. Prior to loading the DNA samples into the gel they were mixed with a DNA loading dye (0.25% bromophenol blue, 0.25% xylene cyanol FF and 40% sucrose in dH_2O) allowing the DNA to sink to the bottom of the wells and visualisation of DNA migration during electrophoresis. A 1kb DNA ladder (Invitrogen) was loaded alongside the samples to enable accurate sizing of the DNA product. Following electrophoresis the DNA bands were visualised by exposure to UV light and the image captured using a GeneGnome System and GeneSnap Software (Syngene Bio Imaging).

2.3 Magnetic resonance imaging.

Magnetic resonance images were acquired on a horizontal bore 7.0T Varian microimaging system (Varian Inc, Paulo Alto, CA, USA) equipped with a 12-cm microimaging gradient insert (40 gauss/cm). Animals were anaesthetised with isoflurane (5% with 1l/min oxygen for induction followed by 1-2% with 1l/min oxygen for maintenance) via a facemask and positioned on a custom built sled (Dazai Research Instruments, Toronto, Canada), with integrated electrocardiographic (via electrodes in contact with the shaved chest with conductive hydro-gel), respiratory (via a pneumatic pillow) and cutaneous temperature monitoring. An SA Instruments

Inc. (Edison, NJ, USA) small animal system was used for physiological monitoring and gating. A 30mm or 39mm quadrature birdcage coil (Rapid Biomedical, GmbH) was used to transmit/receive the MR signal. Global cardiac function was measured using an ECG triggered, respiratory gated gradient echo (FLASH) cine MR sequence. The sequence was triggered by the R wave of the ECG, which was end diastole. Scout images were obtained and orientated to the short axis and 2 long axes (horizontal and vertical) of the heart (see chapter 3 for further details). T1 weighted scans from 8 to 10 contiguous short axis slices were obtained covering the whole left ventricle. Single horizontal and vertical long axis slices were also obtained. The following imaging parameters were used: TE 1.42ms, TR 5ms, flip angle 15°, matrix 128x128 (zero filled to 256x256), field of view 25.6x25.6mm, slice thickness 1mm, number of averages 4.

2.3.1 MRI based measurement of myocardial mass and cardiac function.

Myocardial mass.

1. Using the Image J (NIH) software package, the area between the epicardial and endocardial borders were measured in all slices at end diastole and end systole (figure 2.1).
2. Left ventricular (LV) myocardial area is the area between the epicardial (yellow) and endocardial (red) borders and was calculated for each slice using:

   Myocardial area per slice = epicardial area – endocardial area
3. LV myocardial volume for each slice was calculated using:

   Myocardial volume per slice = area × slice thickness
4. The total myocardial volume was calculated using:

   $$\textit{Total myocardial volume} = \sum \textit{myocardial volume per slice}$$
5. LV mass was calculated using:

   $$\textit{LV mass (mg)} = \textit{Total myocardial volume} \times \textit{myocardial specific gravity (1.05g/cm}^3\textit{)}$$
6. The mean myocardial mass was calculated from the myocardial mass at end diastole and end systole.
7. To ensure accurate measurement of myocardial mass was made, there should be no more than a 5% difference in the myocardial mass calculated at end diastole and end systole.

Global systolic function.

1. The measurements from the endocardial border for each slice (figure 2.1) at end diastole and end systole were taken. The LV chamber area is that within the endocardial border.
2. The LV chamber volume for each slice at end diastole and end systole was calculated using:

   $$LV\ volume\ per\ slice = LV\ area \times slice\ thickness$$

3. The LV end diastolic volume was calculated using:

   $$LVEDV\ (\mu l) = \sum LV\ volume\ per\ slice\ at\ end\ diastole$$

4. The LV end systolic volume was calculated using:

   $$LVESV\ (\mu l) = \sum LV\ volume\ per\ slice\ at\ end\ systole$$

5. Various function parameters were calculated from these volumes as follows:

   $$Stroke\ volume\ (SV)\ (\mu l) = LVEDV - LVESV$$

   $$Ejection\ fraction\ (EF)\ (\%) = {}^{(SV}/_{LVEDV)} \times 100$$

   $$Cardiac\ output\ (CO)\ (ml/min) = {}^{(SV \times heart\ rate)}/_{1000}$$

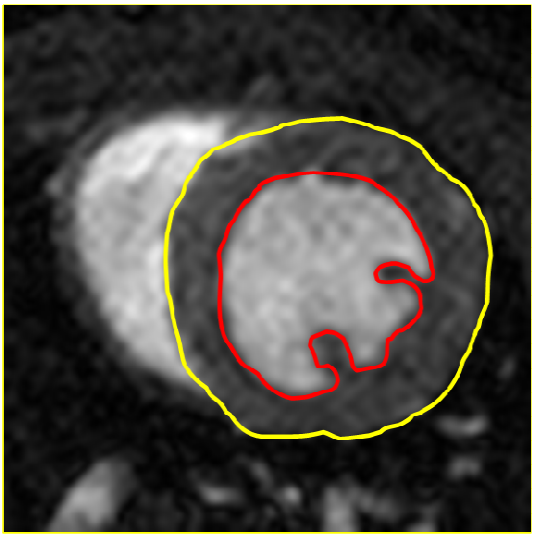

Figure 2.1 Mid-ventricular short axis slice showing epicardial (yellow) and endocardial (red) borders of the left ventricle.

Border lines were manually traced using ImageJ software.

2.3.2 Reproducibility of MRI measurements.

To assess reproducibility of MRI measurements I performed all measurements on two separate occasions. Intra-observer variability was calculated for each subject as the standard deviation of the measurements divided by the mean of the measurements multiplied by 100. The mean value and standard deviation for all subjects was used as a summary measure for each variable.

2.3.3 Measuring size of myocardial infarct.

The infarcted myocardium is characterised by thinned, akinetic area of myocardium. The infarct size, as a percentage of the left ventricular myocardium can be calculated by measuring the left ventricular epicardial (Tep) and endocardial (Ten) circumference as well as the infarct length (Iep and Ien) at end-diastole (figure 2.2) (Schneider *et al.*, 2006). The infarct size can then be calculated by:

$$Infarct\ size = {}^{1}/_{NSLICES} \sum {}^{1}/_{2}\left({}^{Iep}/_{Tep} + {}^{Ien}/_{Ten}\right).100\%$$

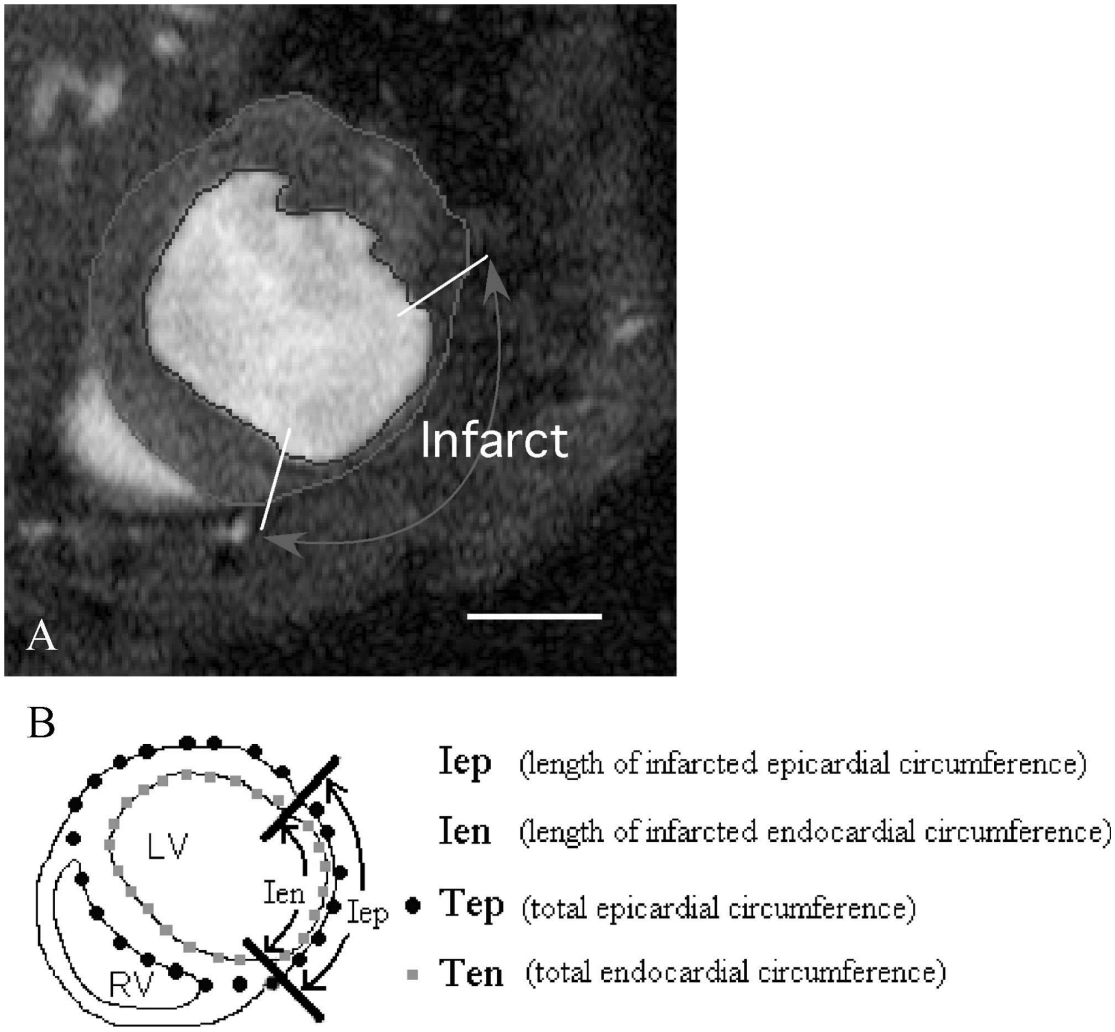

Figure 2.2 Mid-ventricular short axis slice demonstrating how infarct size is measured.
A. Traces of left ventricular endocardial (dark grey) and epicardial (light grey) circumferences. The area of myocardial infarction is indicated. **B.** Cartoon indicating the measurements needed to calculate infarct size. Taken from (Schneider *et al.*, 2006)

2.4 Coronary artery ligation.

Myocardial infarction was induced by permanent coronary artery ligation. Mice were anaesthetised with isoflurane. They were then intubated and ventilated (Harvard Minivent 230Vac) with anaesthesia maintained with 2% isoflurane/98% oxygen. Body temperature was maintained by means of a heated blanket. A left thoracotomy was performed, the heart exposed and the left anterior descending artery identified. This was then permanently ligated using 7-0 prolene suture 1 to 2 mm from the inferior border of the left auricle. The area of infarction can be visualised as it quickly blanches (figure 2.3). The wound was then closed in layers using 5-0 vicryl suture. The mice were then allowed to recover in a temperature controlled incubator at 33°C.

Analgesia was provided by an intraoperative, subcutaneous injection of buprenorphine. A soaked diet was used post operatively. The operative mortality for all surgery performed during these experiments was 20%.

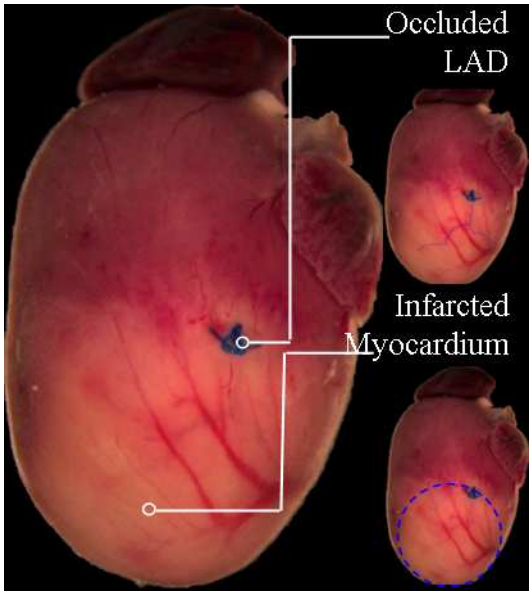

Figure 2.3 Macroscopic image of a mouse heart following LAD ligation.
The suture can be seen with the faint outline of the LAD below (indicated by the branched blue line in upper inset). The infarcted myocardium can be easily seen by the blanching of the myocardium (indicated by the dotted blue line in lower inset). Image courtesy of Dr Rachael Redgrave.

2.5 Invasive measurement of cardiac function.

These experiments were performed under terminal anaesthesia. Measurements were made in closed chest, spontaneously breathing mice as follows. The mice were anaesthetised using isoflurane as for the MRI experiments. Body temperature was maintained by means of a homoeothermic blanket (Harvard Apparatus). Following an inverted T shaped, mid-neck incision the left internal jugular vein was isolated, ligated cranially and, following venotomy, the vein was canulated with p10 plastic tubing. Then the right common carotid artery was isolated, ligated cranially and, following arteriotomy a 1.4F conductance catheter (Millar) was introduced. Baseline aortic pressure measurements were made. Then the catheter was advanced retrogradely, through the aortic valve into the left ventricle. After stabilization, measurements at steady-state, during transient occlusion of the inferior vena cava and during infusion of dobutamine (5 and 10 μg/kg/min), were recorded using Powerlab® Chart 5 software (ADInstruments®, Colorado Springs) and analysed using PVAN

pressure–volume data analysis software package (Millar, Houston, TX). Volume was calculated using the Relative Volume Units/Cuvette method and parallel conductance was estimated by the hypersaline method (Pacher *et al.*, 2008; Cingolani and Kass). Measurements made are described in table 2.2.

Table 2.2 Haemodynamic indices obtained from cardiac conductance catheter experiments.

Parameter	**Definition**
Aortic SBP (mmHg)	Aortic systolic blood pressure
Aortic DBP (mmHg)	Aortic diastolic blood pressure
MAP (mmHg)	Mean arterial pressure
Heart rate (bpm)	Heart rate
LV EDV (μl)	Left ventricular end diastolic volume
LV ESV (μl)	Left ventricular end systolic volume
LV SV (μl)	Left ventricular stroke volume
CO (ml/min)	Cardiac output
EF (%)	Ejection fraction
LV EDP (mmHg)	Left ventricular end diastolic pressure
LV ESP (mmHg)	Left ventricular end systolic pressure
Stroke work (mmHg.μl)	Work performed by left ventricle
Ea (mmHg/μl)	Arterial elastance, a measure of ventricular afterload
dP/dt_{max} (mmHg/s)	Peak rate of pressure rise
dP/dt_{min} (mmHg/s)	Peak rate of pressure decline
Tau (ms)	Isovolumetric relaxation time constant
Total SVR (mmHg/ml/min)	Total systemic vascular resistance
PRSW (mmHg)	Preload recruited stroke work, a measure of cardiac contractility
Ees (mmHg/μl)	End-systolic elastance, an index of myocardial contractility
dP/dt_{max}-EDV (mmHg/s/μl)	maximum rate of left ventricular pressure rise-end-diastolic volume relation, a measure of cardiac contractility.

2.6 Primary cardiac fibroblast culture.

2.6.1 Reagents.

Phosphate Buffered Saline (PBS) pH 7.4 stored at 4°C (Gibco® #10010-023).
Dulbecco's Modified Eagle Medium (DMEM), stored at 4°C (Gibco® #41965-039).
Foetal Calf Serum (FCS) (Gibco® #10106-169). This was heat inactivated by incubating at 56°C for 1 hour and stored in 50ml aliquots at -20°C.
Penicillin-Streptomycin (P/S) (Gibco® #15070-063). This was stored in 10ml aliquots at-20°C
0.25% Trypsin/EDTA (Gibco® #25200-056). This was stored at -20°C in 5 ml aliquots.
Type 2 Collagenase (Worthington Biochemical #CLS-2). A fresh 1mg/ml solution was obtained by diluting 50mg type 2 collagenase in 50ml DMEM and was kept on ice during the isolation procedure.
4-hydroxytamoxifen (4-OHT) (Sigma #H7904).
Recombinant Human TGFβ1 (PeproTech #100-21).
Methylthiazolyldiphenyl-tetrazolium bromide (MTT) (Sigma #M2128). A 5mg/ml solution was obtained by dissolving 5mg MTT in 1 ml of filter sterilised dH_2O.
Dimethylsulphoxide (DMSO) spectrophotometric grade (Sigma #154938)

2.6.2 Isolation of primary cardiac fibroblasts.

Three mice were used for each isolation. Following humane euthanasia by cervical dislocation, hearts were rapidly dissected by lifting at the apex and cutting across the base of the heart thus removing atrial and great vessels and leaving left and right ventricle only. The hearts were then washed in sterile, ice cold PBS and transported to a tissue culture hood in sterile PBS on ice. Hearts were further washed in 5 changes of ice cold sterile PBS. They then transferred to a 35mm petri dish and 2mls of type 2 collagenase (1mg/ml) was added and the hearts quickly minced into small pieces. A further 4 ml of collagenase was added and the minced hearts in collagenase were transferred to a 7ml bijous tube. This was then incubated in a shaking waterbath set at 37°C and 100rpm for 10 minutes. The supernatant was removed and discarded. 5mls of fresh collagenase was added and a further incubation at 37°C and 100rpm for 15

minutes was performed. 2mls of supernatant was then removed and placed in a 50ml tube containing 5ml DMEM + 20% FCS. The remaining suspension was gently pipetted 5 to 6 times to release cells attached to the tissue fragments. The tissue fragments were allowed to settle and the supernatant removed and placed in the DMEM + 20% FCS. This was then centrifuged at 1200rpm for 8minutes. The media was then removed and the cells resuspended in 5-10ml pre-warmed DMEM + 10% FCS + 1% P/S and kept at 37°C, 5% CO_2. Meanwhile, a further 5ml collagenase was added to the tissue fragments and digestion repeated. The above steps, pooling all the cells together, were repeated until all the tissue had been digested (about 5 digestions in total). The pooled cell suspension was centrifuged at 1200rpm for 10 minutes and the cells were resuspended in DMEM + 10% FCS + 1% P/S and placed in a T75 tissue culture flask. The fibroblasts were allowed to adhere for 90minutes. After this period the media was removed and cells washed very gently with warm, sterile PBS and fresh culture media added (DMEM + 10% FCS + 1% P/S). The cells were grown for 4 days after which they were ready to passage. All experiments were performed after the second passage.

2.6.3 Cre^{ERT2} activation *in vitro*.

To activate the Cre^{ERT2} and enable endoglin knockdown, 4-hydroxytamoxifen was added to the culture media at the first passage and was refreshed in subsequent media changes.

2.6.4 Transforming Growth Factor β1 stimulation.

Primary cardiac fibroblasts were plated in 2ml of DMEM +10% FCS + 1% P/S onto 6 well tissue culture plates (100,000 cells per well). They were allowed to adhere overnight. The media was removed and the cells gently washed in warm sterile PBS. 2mls fresh, warmed culture media was then added and the cells stimulated with 5-10ng/ml of TGFβ1. They were incubated at 37°C, 5% CO_2 for a variable period of time depending on the experimental conditions. After this the culture media was removed, the cells washed in warm, sterile PBS. For protein analysis cells were harvested by the addition of 1ml Trypsin/EDTA and incubated for 3 minutes at 37°C, 5%CO_2. Once the fibroblasts had detached from the culture dish the trypsin/EDTA

was neutralised with 1 ml of culture medium. The detached cells were then transferred to a 2ml microcentrifuge tube. They were then spun down in a microcentrifuge at 13,000rpm for 5 minutes at 4°C. The media was removed and the cell pellet was gently rinsed in ice cold sterile PBS. They were then centrifuged for at further 5 minutes at the same speed settings before the PBS was completely removed and the cell pellets were either used directly or frozen and stored at -80°C until used for protein analysis. For RNA analysis the cells were harvested by the addition of 350µl RLT buffer (RNeasy Mini Kit, Qiagen) and then used directly or frozen and stored at -80°C until used for RNA analysis.

2.6.5 MTT assay.

Primary cardiac fibroblasts were seeded in 96 well, flat-bottomed tissue culture plates (5000 cells per well) at passage 1 and subjected to various culture conditions as described in chapter 4. Following treatment, 10µl MTT (5mg/ml) was added to each well and incubated at 37°C, 5% CO_2 for 5 hours. The media was then removed and 100µl DMSO was added to solubilise the formazan crystals. The absorbance was measured at 570nm on a spectrophotometric plate reader (Thermo Scientific).

2.7 Histological procedures.

2.7.1 General solutions.

10 x Phosphate Buffered Saline (PBS).

80g NaCl, 2g KCl, 14.4g Na2HPO4 and 2.4g KH2PO4 dissolved in 800ml of dH2O. pH adjusted to 7.4 with HCl then dH2O added to make volume up to 1 litre. Sterilized by autoclaving at 121°C for 30mins.

LacZ Detergent Rinse.

120ml of 0.5M Phosphate Buffer (pH7.2), 1.2ml of 1M MgCl2, 6ml of 1% NaDeoxycholate, 1.2ml of 10%NP40, made up to 600ml with dH2O.

LacZ Staining Solution.

6ml of 0.5M K3 Ferricyanide, 6ml of 0.5M K4 Ferrocyanide, 120ml of 0.5M Phosphate Buffer (pH7.2), 1.2ml of 1M MgCl2, 6ml of 1%NaDeoxycholate, 1.2ml of 10% NP40, made up to 600ml with dH2O. This staining solution should be stored in

the dark at 4°C. 400µl of 25mg/ml XGAL solution was added to every 10ml of pre-warmed (37oC) LacZ staining solution immediately before use.

X-gal (25mg/ml).

0.25g of X-gal dissolved in 10ml of dimethylformamide. Stored in the dark at -20°C.

2.7.2 Tissue sampling, processing and sectioning.

Hearts were dissected from euthanised mice and washed to ensure removal of excess blood. For the LV mass experiments the atria and right ventricle was dissected away from the left ventricle. The hearts were briefly blotted dry using filter paper and the left ventricular mass was measured. Hearts to be used for immunofluorescence were fixed overnight in 0.2% paraformaldehyde in phosphate buffered saline (PBS) at 4°C. They were than washed twice in PBS at 4°C followed by a further overnight incubation in 30% sucrose at 4°C. Following further washes in PBS hearts were embedded in OCT (RA Lamb) and frozen in liquid nitrogen. They were stored at -80°C until needed for sectioning. 10µm cryosections were taken onto Histobond slides and allowed to air dry. These were then stored at -80°C until needed for histological staining. Prior to staining all tissue sections were removed from -80°C and allowed to reach room temperature inside their slide mailers to reduce condensation. They were then allowed to air dry at room temperature before being stained.

2.7.3 Haematoxylin and Eosin histological staining.

Sections were post fixed in cold AnalaR acetone for 10 minutes then allowed to air dry for 20 minutes. Sections were then rinsed in dH2O and incubated in Mayer's haematoxylin (RA Lamb) for 2-3 minutes followed by a long rinse under running tap water. Sections were quickly immersed in Eosin (1% aqueous, RA Lamb) for a few seconds followed by a quick rinse in tap water. Sections were dehydrated in a graded alcohol series of 50%, 70%, 100% ethanol by immersing for 1 minute in each, followed by clearing in Histoclear (National Diagnostics, 2x5 minutes) and mounting under cover slips with HistoMount (Vector Laboratories).

2.7.4 Immunohistochemistry using Vecastain® ABC kit.

Anti-CD105 (Clone: MJ7/18, stock concentration: 0.5mg/ml, eBiosciences #14-1051) a rat anti-mouse monoclonal antibody was used to detect endoglin. All incubations were carried out in a humidified chamber.

Endogenous peroxidise activity was blocked by incubating sections in 0.3% hydrogen peroxide in dH_2O for 10 minutes. Cryosections were then washed in PBS for 5 minutes then blocked with 5% rabbit serum (Vector Laboratories) in PBS for 30 minutes. Endogenous biotin activity was then blocked using an Avidin/Biotin blocking kit (Vector Laboratories) according to manufacturer's instructions; sections were incubated with Avidin D solution for 15 minutes then rinsed briefly in PBS followed by 15 minutes incubation with the Biotin solution. This was followed by 2x5 minute washes with PBS. Sections were then incubated with anti-CD105 (1:200 dilution in serum blocking solution) overnight at 4°C. Following this the sections were washed in PBS, 3x5 minutes. They were then incubated with biotinylated rabbit anti-rat secondary antibody (Vector Laboratories, BA-4001) at 1:200 dilution in serum blocking solution for 30 minutes. The Vectastain® ABC reagent (Vector Laboratories) was prepared as per manufacturer's instructions 30 minutes prior to use. Following 3 further 5 minute washes in PBS, tissue sections were incubated in the Vectastain® ABC reagent for 30 minutes. After 3x5 minute washes, antibody binding was visualised using the liquid DAB substrate kit (Biogenex). Sections were counter stained with Mayer's haematoxylin (RA Lamb) followed by rinsing in water. Finally the sections were dehydrated in a graded alcohol series of 50%, 70%, 100% ethanol by immersing for 1 minute in each, followed by clearing in Histoclear (National Diagnostics, 2x5 minutes) and mounting under cover slips with HistoMount (Vector Laboratories).

2.7.5 Immunofluorescence.

All incubations were performed in a humidified chamber which was protected from light. For double staining antibody combinations were limited due to the species in which the primary antibody was raised, and the anti-endoglin primary antibody was always used first (table 2.3). Cryosections were washed for 5 minutes in PBS

followed by incubation in the appropriate blocking solution for 2 hours (table 2.4). They were then incubated with the first primary antibody diluted in appropriate blocking solution overnight at 4°C (table 2.3). Following incubation, sections were washed for 3x5 minutes in PBS. They were then incubated in the appropriate secondary antibody (table 2.4), 1:200 dilution, in blocking solution. Following 3 further 5 minute washes in PBS sections were blocked again in the blocking solution appropriate for the second primary antibody for 2 hours (table 2.4). They were then incubated with the second primary antibody diluted in appropriate blocking solution overnight at 4°C (table 2.3). Sections were then washed 3x5 minutes in PBS. They were then incubated in the appropriate secondary antibody for 2 hours (table 2.4). Finally, after 3x5 minute washes in PBS the sections were mounted under cover slips in hard set Vectashield® with DAPI. Slides were left to dry at 4°C in the dark.

Table 2.3 Order and combinations of primary antibodies used in double immunofluorescent staining.

Antibody 1	Antibody 2
Polyclonal goat anti-mouse CD105	Monoclonal rat anti-mouse CD31
Polyclonal goat anti-mouse CD105	Monoclonal rat anti-mouse CD11b
Monoclonal rat anti-mouse CD105	Polyclonal rabbit anti-mouse Fsp1
Monoclonal rat anti-mouse CD105	Monoclonal mouse anti-SMA-Cy3

Table 2.4 Antibodies and conditions used in immunofluorescent staining of cryosections.

Primary antibody	Primary antibody supplier	Working dilution	Blocking solution	Secondary antibody
Polyclonal goat anti-mouse CD105	R&D Systems #AF1320	1:25	5% donkey serum, 1% BSA, 0.1% Tween	Donkey anti-goat IgG-alexa 595 conjugate
Monoclonal rat anti-mouse CD105	eBioscience #14-1051	1:100	5% goat serum, 1% BSA, 0.1% Tween	Goat anti-rat IgG-alexa 594 conjugate
Monoclonal rat anti-mouse CD31	BD Biosciences Pharmingen #550274	1:100	5% goat serum, 1% BSA, 0.1% Tween	Goat anti-rat IgG-alexa 488 conjugate
Monoclonal rat anti-mouse CD11b	BD Biosciences Pharmingen #550282	1:100	5% goat serum, 1% BSA, 0.1% Tween	Goat anti-rat IgG-alexa 488 conjugate
Polyclonal rabbit anti-mouse Fsp1	Millipore #07-2274	1:100	5% donkey serum, 1% BSA, 0.1% Tween	Donkey anti-rabbit IgG-alexa 488 conjugate
Monoclonal mouse anti-SMA-Cy3 conjugate	Sigma #6198	1:100	5% donkey serum, 1% BSA, 0.1% Tween	

2.7.6 Measurement of cardiomyocyte cross sectional area.

Cryosections of the mouse heart were washed in PBS for 5 minutes. They were then incubated with Fluorescein conjugated Wheat Germ Agglutinin (20μg/ml in PBS, Vector Laboratories, #FL-1021) for 1 hour at room temperature. Sections were then washed 3x5 minutes in PBS and mounted under cover slips in hard set Vectashield® with DAPI. Slides were left to dry at 4°C in the dark. Digital images were captured using epifluorescent microscopy (see below) and cardiomyocyte area was measured using ImageJ (NIH) by tracing around cardiomyocytes in short axis. Approximately 70 to 100 cardiomyocytes were traced for each ventricle and the average cardiomyocyte area calculated.

2.7.7 Immunocytochemistry.

Cells (e.g. fibroblasts) were seeded into wells of an 8-well slide (Lab Tek II, Nunc) and cultured for 48 hours at 37°C and 5% CO_2. Cells were gently washed in PBS followed by fixing in ice cold acetone for 5 minutes. They were then washed in twice in PBS. They were then blocked in serum-free protein block (Dako) for 20 minutes. Following this the cells were incubated with appropriate primary antibody (table 2.5), diluted in blocking solution, overnight at 4°C. Slides were washed 3x5 minutes in PBS. They were then incubated with the appropriate secondary antibody (table 2.5), 1:200 dilution, in blocking solution for 1 hour. 3 further 5 minute washes in PBS were performed prior to mounting the slides under cover slips with hard set Vectashield® with DAPI. Slides were allowed to dry at 4°C in the dark.

2.7.8 LacZ staining.

Tissue sections were post fixed in 0.2% paraformaldehyde for 30 minutes at room temperature followed by a 10 minute wash in PBS containing 2mM $MgCl_2$. They were then placed in lacZ detergent rinse on ice for 10 minutes. Sections were immersed in pre-warmed (37°C) LacZ staining solution () and incubated at 37°C for 3 hours. Following this sections were washed in PBS with 2mM $MgCl_2$ for 2x5 minutes. They were then rinsed in dH_2O prior to counterstaining with Eosin (1% aqueous, RA Lamb). 3 further 5 minute washes in dH_2O were performed prior to dehydration in a

graded alcohol series of 50%, 70%, 100% ethanol by immersing for 1 minute in each, followed by clearing in Histoclear (National Diagnostics, 2x5 minutes) and mounting under cover slips with HistoMount (Vector Laboratories).

Table 2.5 Primary and secondary antibodies used for immunofluorescent staining.

Primary antibody	Primary antibody supplier	Dilution	Secondary antibody
Monoclonal rat anti-mouse CD105	eBioscience #14-1051	1:100	Goat anti-rat IgG-alexa 594 conjugate
Monoclonal rat anti-mouse CD31	BD Biosciences Pharmingen #550274	1:100	Goat anti-rat IgG-alexa 594 conjugate
Polyclonal goat anti-human vimentin	Millpore #AT1620	1:100	Donkey anti-goat IgG-alexa 595 conjugate
Monoclonal mouse anti-SMA-Cy3 conjugate	Sigma #6198	1:100	

2.7.9 Microscopy.

For light microscopy, sections were viewed using a Ziess Axioplan microscope For fluorescent microscopy tissue sections were imaged using either a Zeiss Axioimager or a Nikon A1Rconfocal microscope. Digital images were captured using an Axiocam camera and analysed using Axiovision or ImageJ software.

2.8 Protein analysis.

2.8.1 General solutions.

Lysis Buffer.

10mM Tris-HCl pH7.4, 1% Triton X-100, 1/100 dilution of protease inhibitors (Sigma), 1/20 dilution of 10x phosphatase inhibitor (PhosSTOP tablets, Roche).

2x Protein Gel Loading Buffer.

12.5ml 0.5M Tris (pH6.8), 10ml glycerol, 20ml 10% SDS, 7ml dH_2O, 0.5% β-mercaptoethanol, 20mg bromophenol blue.

10x Gel Running Buffer.

30g Tris base, 144g Glycine, 10g Sodium Dodecyl Sulphate (SDS), made up to 1L with dH_2O.

10x Western Transfer Buffer.

144g glycine, 30g Tris base.

10 x Tris Buffered Saline (TBS).

24.2g Trizma® base (C4H11NO3) and 80g NaCl dissolved in 1 litre of dH2O. Adjust pH to 7.6 with concentrated HCl.

TBST Wash Buffer.

1x TBS/0.1% Tween-20. To prepare add 100ml of 10xTBS to 900ml of dH2O then add 1ml Tween-20 and mix.

Strip Buffer.

0.1M glycine in H2O, pH<2, adjusted with HCl.

2.8.2 Sample preparation.

For primary cardiac fibroblasts 50µl of lysis buffer was added to the cell pellets (prepared as described in section 2.6.4). For protein analysis of whole hearts, the hearts were rapidly dissected and rinsed in sterile PBS to remove blood following humane euthanasia. They were then homogenised in lysis buffer with QIAGEN Tissue Ruptor with disposable probes. Following homogenisation, the samples were briefly vortexed, total protein estimated using Pierce BCA protein assay (Thermo Scientific #23227) and stored at -80°C. 20µg of total protein was added to each well for SDS-PAGE.

2.8.3 SDS-PAGE.

A volume of 2xGel loading buffer was added to the protein sample to achieve a 1:1 2xGel loading buffer to sample volume ratio. The samples were then heated at 95°C for 10 minutes in a thermomixer. This denatures the proteins, facilitates loading of samples onto the gels and allows tracking of the samples during gel electrophoresis.

The samples were allowed to reach room temperature then spun down briefly in a centrifuge for 10-15 seconds before loading onto a precast 10% polyacrylamide gel (Mini-PROTEAN® TGX™ precast gels, BioRad # 456-1039) along with a prestained protein marker (Precision Plus Protein Dual Coloured Standards, BioRad # 161-0374). Gels were run in running buffer for 1 hour at 150 volts.

For the identification of eNOS dimmer and monomers a "cold" SDS-PAGE was performed by modifying the above protocol as follows: β-mercaptoethanol was omitted from 2xGel loading buffer and samples were not heated to 95°C. After loading the samples and protein marker the gel was run in ice cold running buffer for 1 hour at 150 volts. To maintain the temperature of the running buffer a frozen ice pack was placed in the gel tank and the whole tank placed in ice

.

2.8.4 Western Blotting.

Following protein separation by SDS-PAGE, the proteins were transferred to a Hybond ECL (GE Healthcare) membrane at 4°C in transfer buffer for 1 hour at 100 volts. Membranes were then blocked in appropriate blocking solution (table 2.6) for 1 hour at room temperature. They were then incubated with appropriate primary antibody (table 2.6) in blocking solution overnight at 4°C with gentle rocking. Following this the membranes were washed in TBST, 3x10 minutes. They were then incubated in HRP conjugated secondary antibody directed against the species of origin of the primary antibody for 1 hour at room temperature. Secondary antibodies were also diluted in blocking solution. Membranes were then washed in TBST, 3x10 minutes. The protein-antibody complex was visualised by chemiluminescence using the SuperSignal West Pico Chemiluminescent Substrate (Pierce Biotechnology). Band signals were detected after exposure of the Western blot membranes to X-ray film (GE Healthcare) and processing in a Xograph Compact X4 automatic X-ray film processor (Xograph Imaging Systems Ltd.).

To strip the membrane of the bound antibodies, the membrane was incubated with strip buffer for 15 minutes at room temperature followed by 3 x 5 minute washes in TBST before the membrane was used again for another Western blot.

2.8.5 Band Intensity Quantitation.

Western blot band intensity measurements were made by scanning the x-ray film using an ImageScanner III scanner (GE Healthcare). The images were saved as tiff files and opened in ImageJ (NIH), where band intensity was measured using the gel analysis tool.

Table 2.6 Antibodies and conditions used for Western blotting.

BSA=bovine serum albumin.

Primary antibody	Primary antibody supplier	Concentration	Blocking solution	Secondary antibody
Smad 1 Polyclonal rabbit IgG	Cell Signalling Technology #9743	1:1000	5% BSA/TBST	Anti-rabbit IgG, HRP-linked antibody (Dako, #P0399)
Phospho-Smad 1,5,8 Polyclonal rabbit IgG	Cell Signalling Technology #9511	1:1000	5% BSA/TBST	Anti-rabbit IgG, HRP-linked antibody (Dako, #P0399)
Smad 2 (L16D3) Mouse monoclonal IgG	Cell Signalling Technology #3103	1:1000	5% Marvel/TBST	Anti-mouse IgG, HRP-linked antibody (Dako, #P0447)
Phospho-Smad 2 Polyclonal rabbit IgG	Cell Signalling Technology #3101	1:1000	5% Marvel/TBST	Anti-rabbit IgG, HRP-linked antibody (Dako, #P0399)
eNOS Mouse monoclonal IgG	BD Transduction Laboratories #610296	1:1000	5% Marvel/TBST	Anti-mouse IgG, HRP-linked antibody (Dako, #P0447)
Type 1 collagen Polyclonal goat IgG	Santa Cruz Biotechnology #sc-8784	1:100	5% Marvel/TBST	Anti-goat IgG, HRP-linked antibody (Dako, #P0449)

2.9 Quantative RT-PCR.

2.9.1 RNA extraction.

Primary cardiac fibroblasts were dissociated from the tissue culture plates by the addition of 350µl of RLT buffer (RNeasy Mini kit, Qiagen) and stored at -80°C until the sample was processed. For RNA analysis of heart tissue the experimental animals were euthanised and the hearts rapidly dissected under sterile conditions to reduce the risk of contamination. The hearts were rinsed in sterile PBS for tissue culture and the left ventricular apex was stored in RNAlater (Qiagen) at -80°C until the sample was processed. Following thawing the cardiac tissue was homogenised in 600µl RLT buffer (RNeasy Mini Kit, Qiagen) with a TissueRuptor® with disposable probes (Qiagen). The RNeasy Mini kit (Qiagen) with on-column DNase digestion was used as per manufacturer's instructions to generate RNA from both primary cardiac fibroblasts and cardiac tissue. The concentration and quality of RNA was measured using a NanoDrop spectrophotometer (Thermo Scientific).

2.9.2 Generation of cDNA by reverse transcription.

RNA (0.5µg of RNA from primary cardiac fibroblasts or 1µg of RNA from cardiac tissue) was converted to cDNA using a high capacity cDNA reverse transcription kit (Applied Biosystems) as per manufacturer's instructions. .Quantative RT-PCR was performed immediately after cDNA generation or the cDNA was stored at -20°C until needed for quantative PCR.

2.9.3 Quantative PCR (qPCR).

The relative gene expression of experimental samples was measured using quantative PCR with the DNA binding, fluorescence dye SYBR® green. In these experiments all primers, except TGFβ1, were already in use in our laboratory and are summarised in table 2.7. The primers for amplifying TGFβ1 cDNA were previously published (Davidson *et al.*, 2006). In order to measure the relative concentrations of each gene of interest, three internal reference genes (Gapdh, Hrpt and β Actin) were used. SYBR® Green JumpStart™ Taq ReadyMix™ (Sigma #S4438) was used in all experiments and reagents were mixed in the following amounts:

SYBR® Green	5µl
Forward Primer	0.5µl
Reverse Primer	0.5µl
Reference dye	0.1µl
Sterile dH_2O	2.9µl

The 9µl reaction mix was then dispensed into one well of a 384 well plate. 1µl cDNA was then added each well. Each gene for every cDNA sample was run in triplicate. No template controls were included by the substitution of cDNA with 1µl for sterile water. The plate was then covered with an optical adhesive cover and placed in an Applied Biosystems 7900HT Fast Real-Time PCR system. Quantative PCR was then performed using the following thermal cycling protocol:

Initial denaturing step	95°C	10 minutes	
Denaturing step	95°C	15 seconds	40 cycles
Annealing step	60°C	1 minute	
Extension step	70°C	30 seconds	

For all reactions a thermal dissociation curve was generated at the end of the qPCR reaction to ensure that a single PCR product was produced, see chapter 4.

Table 2.7 Primer pairs used for quantative RT-PCR experiments.

calculated by LinReg.

Gene	Accession No	Forward primer (5'-3')	Exon	Reverse Primer (5'-3')	Exon	Amplicon size (bp)	PCR efficiency#
Gapdh	NM_008084	AACTTTGGCATTGTGGAAGG	4	GGATGCAGGGATGATGTTCT	5	132	1.8
Hprt	NM_013556	TCAGTCAACGGGGGACATAAA	4	GGGGCTGTACTGCTTAACCAG	6	124	1.8
β Actin	NM_007393	GGCTGTATTCCCCTCCATCG	2	CCAGTTGGTAACAATGCCATGT	3	154	1.8
Alk1	NM_009612	GGGCCTTTTGATGCTGTCG	3	TGGCAGAATGGTCTCTTGCAG	4	114	1.9
Alk5	NM_009370	TCCCAACTACAGACCTTTTTCA	2/3	GCAGTGGTAAACCTGATCCAGA	3/4	266	1.7
Tgfbr2	NM_029575	CCGCTGCATATCGTCCTGTG	1	AGTGGATGGATGGTCCTATTACA	2	131	1.9
Endoglin	NM_007932	CTGCCAATGCTGTGCGTGAA	3	GCTGGAGTCGTAGGCCAAGT	4/5	191	1.8
TGFβ1	NM_011577	GCAGTGGCTGAACCAAGGA	3	AAGAGCAGTGAGCGCTGAATC	4	59	1.8
Id1	NM_010495	CCTAGCTGTTCGCTGAAGGC	1	CTTTGCTCCGACAGACCAAGTACCAC	2	65	1.9
Id2	NM_010496	ACTCGCATCCCACTATCGTCAG	1	TGCTATCATTCGACATAAGCTCAGA	2	150	1.9
Pai-1	NM_008871	AGTCTTTCCGACCAAGAGCA	6/7	ATCACTTGGCCCATGAAGAG	9	209	1.9
Col1A1	NM_007742	GCTCCTCTTAGGGGCCACT	1	CCACGTCTCACCATTGGGG	2	103	1.9
Col3A1	NM_009930	ACGTAGATGAATTGGGATGCAG	1/2	GGGTTGGGGCAGTCTAGTG	2	154	1.8
Ctgf	NM_010217	CCGCCAACCGCAAGATC	2	ACCGACCCACCGAAGACA	3	67	1.8
αSMA	NM_007392	GTCCCAGACATCAGGGAGTAA	2/3	TCGGATACTTCAGCGTCAGGA	3	102	1.9
Mmp2	NM_008610	CAAGTTCCCCGGCGATGTC	1	TTCTGGTCAAGGTCACCTGTC	2	171	1.8
Mmp9	NM_013599	TGCCCATTTCGACGACGAC	4	GTGCAGGCCGAATAGGAGC	5	132	1.9
Timp1	NM_011593	TACACCCCAGTCATGGAAAGC	4	CGGCCCGTGATGAGAAACT	4/5	74	1.9
Timp2	NM_011594	TCAGAGCCAAAGCAGTGAGC	2	GCCGTGTAGATAAACTCGATGTC	3	114	1.8

2.9.4 Data analysis.

Raw data generated from the qPCR reaction was loaded into LinReg (Ramakers *et al.*, 2003) and the cycle threshold (Ct) was calculated for each gene of interest. As samples were run in triplicate the mean Ct for each sample was used. Mean PCR efficiency of each primer pair was determined from the slopes of the qPCR amplification curve using the LinReg method (Ramakers *et al.*, 2003; Karlen *et al.*, 2007).

To calculate the relative gene expression the comparative Ct method was used (Schmittgen and Livak, 2008). Briefly the mean Ct of the three internal reference genes was calculated. The difference between the Ct of the gene of interest and the reference gene was calculated by:

$$\Delta Ct = Ct_{(\text{gene of interest})} - \text{mean } Ct_{(\text{reference genes})}$$

In experiments were there was a direct biological comparator, for example in the TGFβ1 stimulated primary cardiac fibroblasts where the same cells acted as controls, then the relative gene expression between the control and treated sample was calculated by:

$$\text{Relative gene expression} = 2^{-\Delta\Delta Ct}$$

$$\text{where } \Delta\Delta Ct = \Delta Ct_{(\text{treated sample})} - \Delta Ct_{(\text{control sample})}$$

In experiments where there was an indirect biological comparator, for example the *in vivo* endoglin knockdown experiments then the gene expression relative to the internal reference genes was calculated by:

$$\text{Relative gene expression} = 2^{-\Delta Ct}$$

2.10 Statistical analysis.

Statistical analysis was performed using Minitab 15 statistical software. All graphs were drawn either in Minitab or using Microsoft Excel. For direct comparison between two experimental conditions an unpaired student's t-test was performed. For comparison of three or more groups, analysis of variance (ANOVA) was performed. For multiple comparisons over time, repeat measure ANOVA was used and post hoc comparisons were made using Tukey-Kramer method. Agreement between methods

of measuring left ventricular mass was assessed using a Bland Altman analysis (Bland and Altman, 1999).

Chapter 3 Establishing mouse cardiac magnetic resonance imaging

3.1 Introduction

Advances in transgenic techniques have led to the increased use of genetically modified mouse models in the study of cardiovascular disease. Integral to this study is the assessment of myocardial structure and function. *In vivo* cardiac magnetic resonance imaging (MRI) is ideal for this assessment as it is non-invasive, has good spatial and temporal resolution and allows for longitudinal study. This spatial and temporal resolution allows for accurate assessment of cardiac function (Ruff *et al.*, 1998) and means that, compared to other methods for assessing cardiac function, fewer animals are required to provide adequate statistical power (Stuckey *et al.*, 2008; Winter *et al.*, 2008). This is in keeping with the need to reduce the numbers of animals used in research. Additionally, by altering tissue characteristics with contrast agents or using different pulse sequences further information about cardiac physiology and function can be gained. For example the T1 contrast agent gadolinium can be used to assess myocardial perfusion and infarct size (Chapon *et al.*, 2008; Protti *et al.*, 2010). Manganese enhanced MRI (MEMRI) can be used to investigate alterations in calcium homeostasis *in vivo* (Hu *et al.*, 2001; Waghorn *et al.*, 2008; Blain *et al.*, 2013; Greally *et al.*, 2013). The application of myocardial tag lines during cardiac MRI can reveal information about regional cardiac function and myocardial strain (Epstein *et al.*, 2002; Liu *et al.*, 2006; Alistair A. Young *et al.*, 2006; Zhong *et al.*, 2008).

The acquisition of a 7T horizontal bore magnetic resonance system gave the ideal opportunity to introduce and develop preclinical CMR. The aims of these experiments were to set up preclinical mouse cardiac MRI at Newcastle University, to demonstrate that we could reliably obtain images with good spatial and temporal resolution, to demonstrate that we could use these images to accurately and reproducibly measure cardiac mass and function and finally to use this technique to investigate changes in cardiac function in mouse models of heart disease. This work was done in collaboration with Miss Elizabeth Greally, a research technician within the Institute of Genetic Medicine, and also involved a series of short visits to the laboratory of Dr

Jurgen Schneider at the University of Oxford, who has considerable expertise in this technique.

In this chapter I will discuss the rationale of the approach we took to optimise the acquisition of cine cardiac images. Secondly, I will present the experimental validation of cardiac MRI. Finally, I will demonstrate the use of cardiac MRI to measure cardiac function in three different experimental models of heart disease. The work done in developing mouse CMR has led to a number of publications using this technique (Jorgensen *et al.*, 2011; Blain *et al.*, 2013; Greally *et al.*, 2013).

3.2 Methods and Results

3.2.1 Optimising mouse cardiac MRI

The aim of optimising mouse cardiac MRI was to produce reproducible, good quality images that could be manually segmented to provide accurate measurements of cardiac mass and function in mouse models of cardiovascular disease. So when establishing this technique there were several factors we needed to take into consideration to achieve this.

3.2.1.1 Anaesthetic

Mice were to be anaesthetised for the duration of the MRI scan using isoflurane (the choice of anaesthetic agent is discussed in section 1.8.2.3) using a facemask (as described in section 2.3). During MRI experiments, which took approximately 45 minutes, I observed no significant variability in heart rate over the course of the scans (ANOVA p=0.98), figure 3.1.

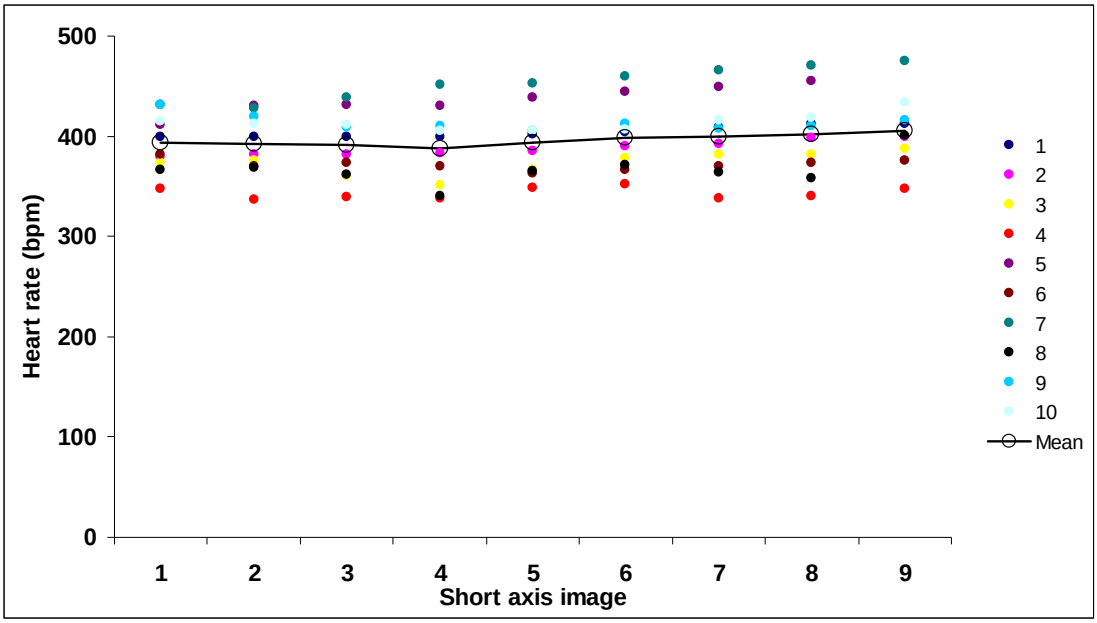

Figure 3.1 Heart rate variability during cardiac MRI.

The heart rate for each mouse (n=10) under isoflurane anaesthesia was recorded at the start of acquisition of each short axis image taken. Typically 9 short axis images were obtained to cover the whole left ventricle. Each short axis image took approximately 2 minutes to aquire and so the data represents the heart rate stability over 18 minutes. There was no significant difference in mean heart rate over the duration of the scan (ANOVA p=0.98). Data expressed as individual value plots with mean value (○).

3.2.1.2 Image planning

To be able to accurately assess cardiac function using MRI the imaging planes need to correspond to the axes of the heart. These axes are short axis (figure 3.2D), horizontal long axis (also known as 4 chamber view, figure 3.2E) and vertical long axis (also known as 2 chamber view, figure 3.2F). However, these planes lie at a double oblique angle to the normal scanner coordinate system (axial, coronal and sagittal). In order to correctly plan these planes we followed the method described by Schneider et al. (Schneider *et al.*, 2006) as shown in figure 3.2. An axial scout scan is taken (figure 3.2A) followed by a single, longitudinal slice (s1, figure 3.2B) orientated through both ventricles as shown in figure 3.2A. A second, single slice scan (s2, figure 3.2C), perpendicular to s1 and orientated through the apex of the left ventricle (figure 3.2B), is obtained. By orientating a slice (s3) perpendicular to both s1 and s2 a true short axis image can be obtained (figure 3.2D). The horizontal long axis (s4, figure 3.2D) is planned by orientating a slice through the left and right ventricle, as shown in figure 3.2D, and orthogonal to s3 (figure 3.2C). Finally, the vertical long axis (s5, figure 3.2F) is planned by an image plane which is orthogonal to both the short and horizontal long axes (figure 3.2D and E). Figure 3.3 shows these image planes in both diastole (A-C) and systole (D-F). To calculate left ventricular mass and function a series of multi frame (cine) images are obtained covering the whole of the left ventricle from base to apex (figure 3.4).

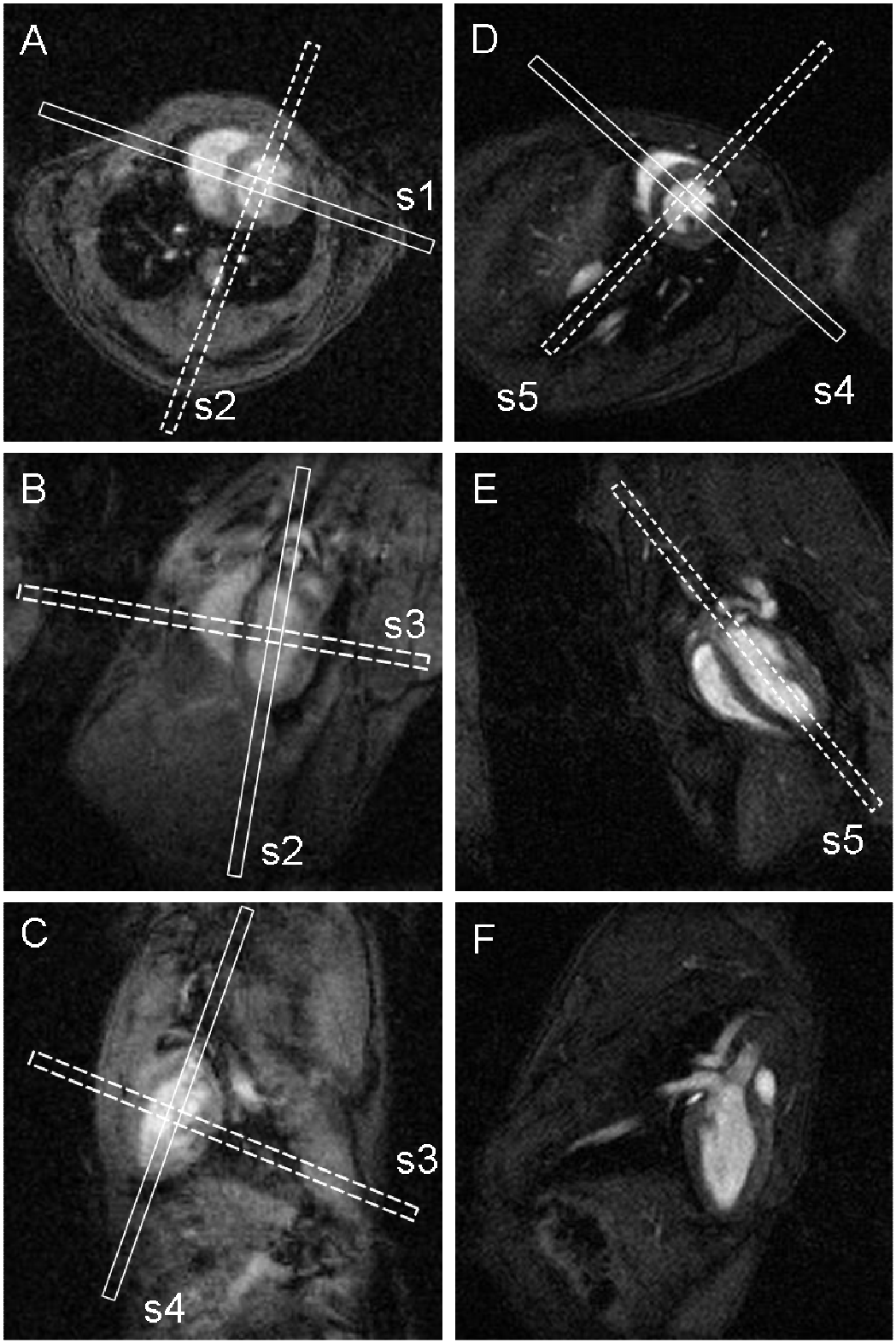

Figure 3.2 Planning the cardiac planes.

As described in Schneider at al I took an axial scout image **(A)**. Then a single, longitudinal slice (s1) orthogonal to the axial image and orientated through both ventricles was obtained **(B)**. A second longitudinal slice (s2) orthogonal to s1 and orientated through the apex of the left ventricle was acquired **(C)**. Finally, the cardiac short axis (s3, D), horizontal long axis (s4, E) and vertical long axis (s5, F) were generated (Schneider *et al.*, 2006).

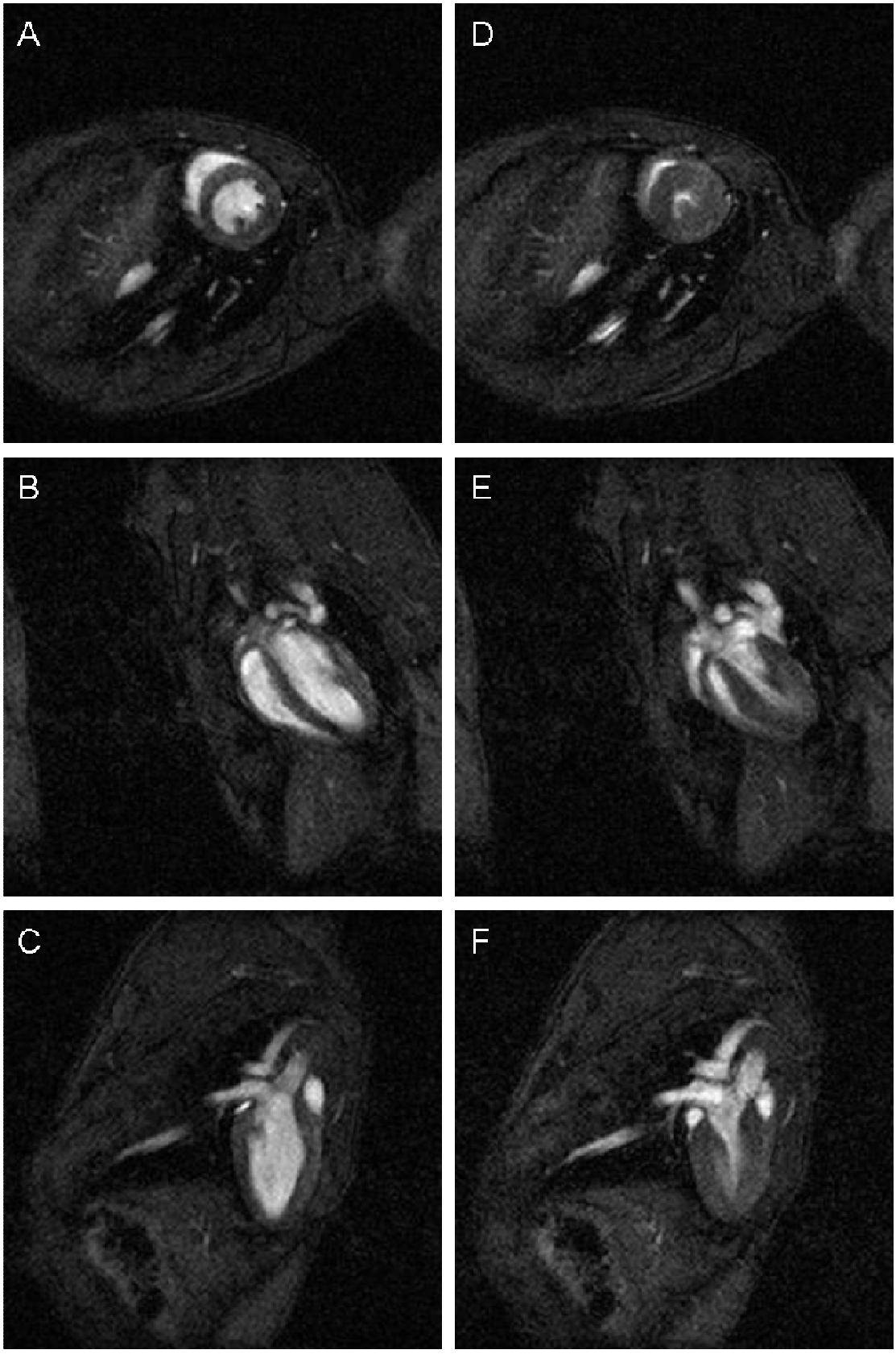

Figure 3.3 The cardiac axes.

Representative cardiac MRI images of the mouse heart in short axis (A, D), horizontal long axis (B, E) and vertical long axis (C, F) in both diastole (A-C) and systole (D-F).

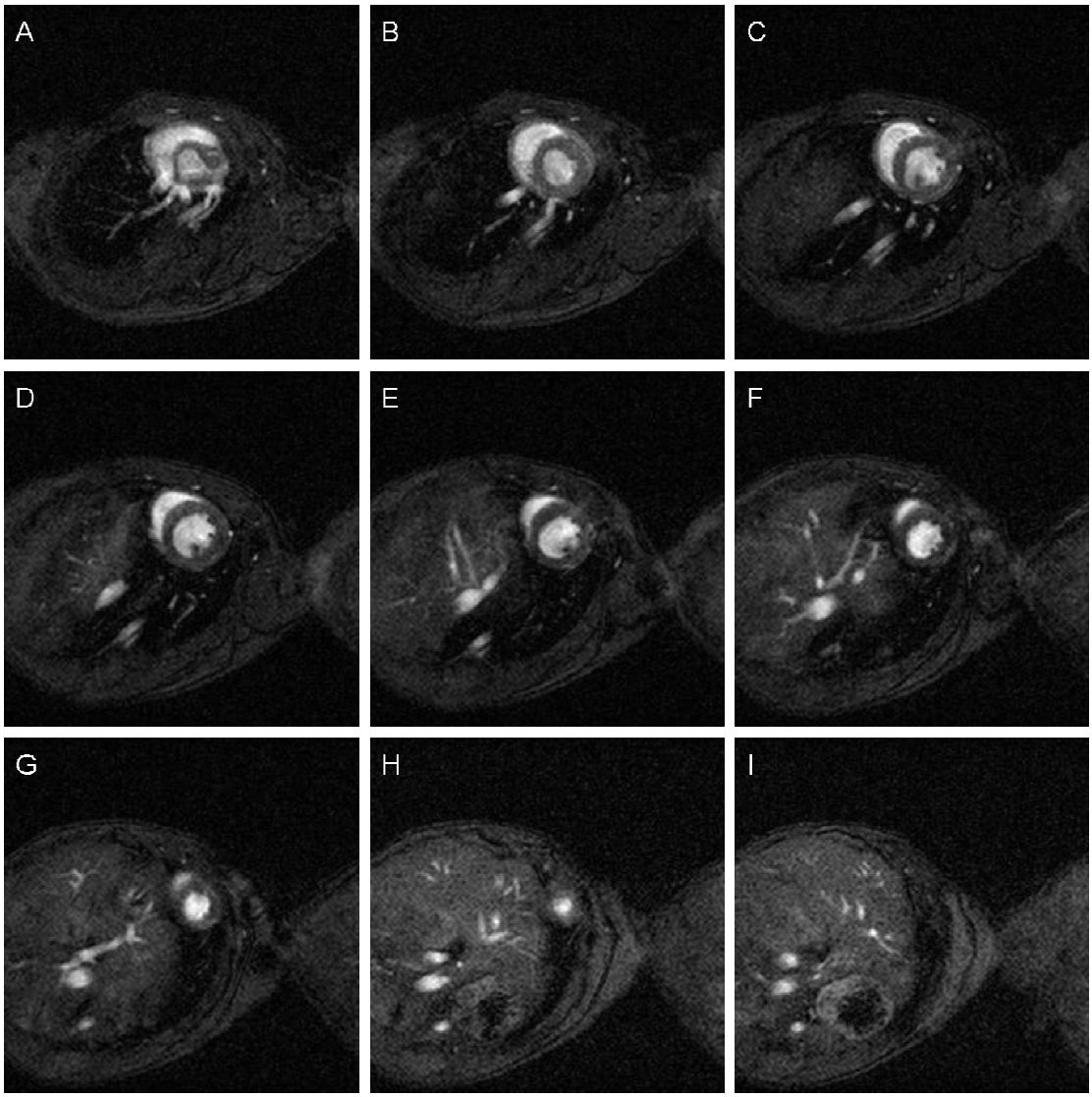

Figure 3.4 Cardiac MRI of the mouse heart from base to apex.

A contiguous stack of 1mm short axis slices in end diastole from the base (A) to apex (I) of the mouse heart.

3.2.1.3 Image parameters

When performing mouse cine cardiac MRI using a FLASH pulse sequence it is recommended that the echo time is short, approximately 1-2ms and the repetition time is 5ms or less (Schneider *et al.*, 2006), as this allows good temporal resolution of the moving myocardium. We chose the minimum echo time possible, which was 1.43ms, and a repetition time of 5ms. However, there are no such recommendations for other imaging parameters such as the field of view, the size of the data matrix or the use of signal averaging. When deciding on these parameters it is important to balance the quality of the image against the time taken to acquire the image. For example, increasing the data matrix from 128x128 to 256x256 will increase the resolution of the image but it will reduce the signal to noise ratio by a factor of 4 and take twice as long to acquire. To improve the image signal averaging can also be used but again this increases the acquisition time and the signal is only increased by the square root of the number of averages. So four signal averages will increase the scan time four fold but will only improve the signal to noise ratio two fold. So the decision as to which image parameters to use is a compromise between image resolution, signal to noise ratio and total scan time.

I took a heuristic approach to investigate what these parameters should be. As the accuracy of LV measurements was dependent on the image resolution, the criteria I chose were that the images should demonstrate sufficient endocardial and epicardial definition to enable manual segmentation of the left ventricular myocardium. The same short axis slice, at the level of the mid left ventricle, was obtained with varying parameters as shown in figure 3.5. There is improved resolution in the images using the 256x256 matrix but there is also the expected reduction in signal to noise ratio (figure 3.5B&D). The use of four signal averages improves the image quality (figure 3.5 C, D) with both these images having good endocardial and epicardial definition, equally enabling left ventricular segmentation. However, the times taken to obtain these images were approximately 1minute (figure 3.1A), 2 minutes (figure 3.1B & C) and 4 minutes (figure 3.1D). So, using a 128x128 data matrix and 4 signal averages (figure 3.5C), the time taken to acquire a stack of short axis slices would be about 20 minutes. Whereas, using a 256x256 data matrix and four signal averages (figure 3.5D), would double the total scan time. Therefore, I chose a data matrix of 128x128 with

four signal averages (figure 3.5C) as the best compromise between image resolution, signal to noise and total imaging time. To enhance the ease of manual segmentation of the left ventricle the data was zero filled by a factor of 2 to give a final matrix size of 256 x 256 and an in plane reconstructed pixel resolution of 100 x 100 μm^2.

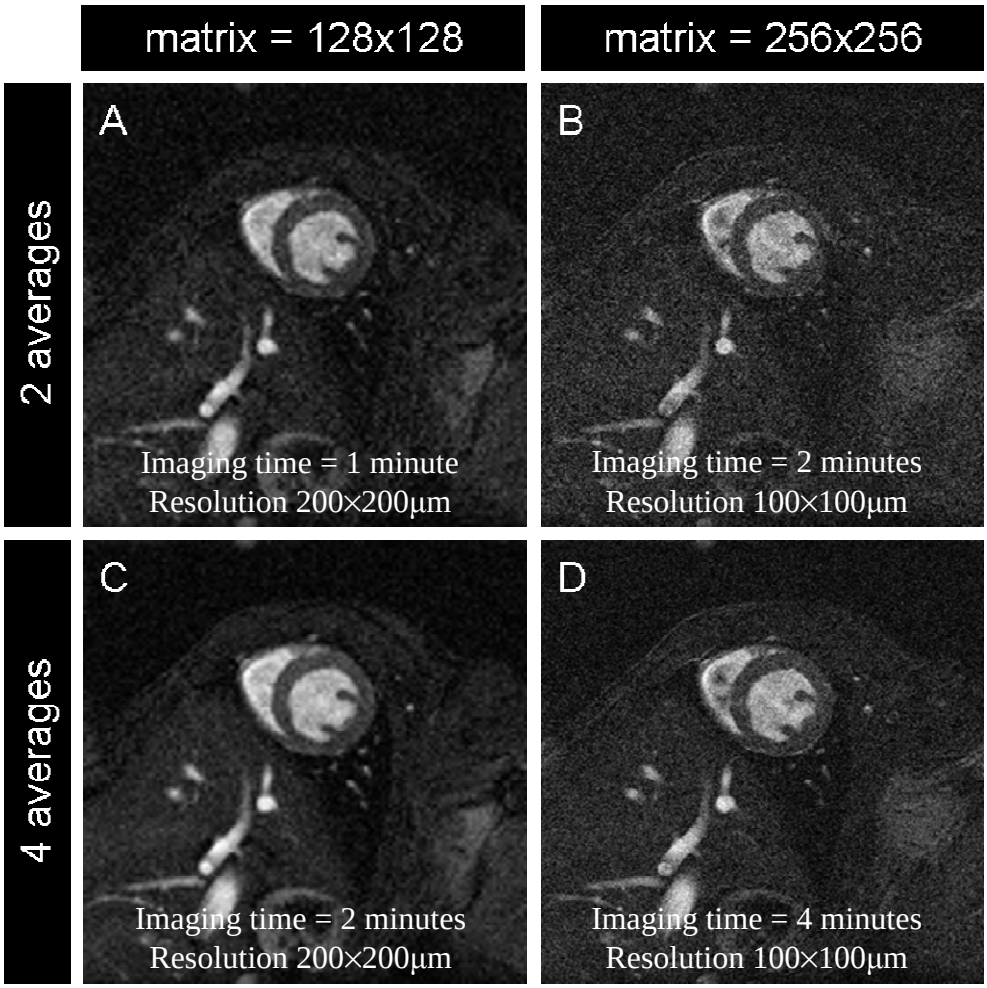

Figure 3.5 The effect of data matrix size and signal averaging on image quality.
Increasing the matrix size (B and D) increases the resolution of the image but at the expense of signal to noise ratio and increased scan time. Increasing the number of signal averages (C and D) improves the signal to noise ratio but at the expense of increased scan time. I chose a data matrix of 128x128 with four signal averages (C) as the best compromise between image resolution, signal to noise and total imaging time. FOV=25.6×25.6 mm.

3.2.1.4 Physiological gating

Cardiac MR is severely affected by cardiac and respiratory motion artefacts. I used prospective cardiac gating which is needed to synchronise the pulse sequence to the cardiac cycle and at 7T respiratory gating improves image quality. The maintenance of a steady state level of magnetisation during respiration without acquiring image data has also been shown to improve image quality (Cassidy *et al.*, 2004).

With our hardware set up we had the following options:

1. No gating.
2. Cardiac gating alone.
3. Cardiac and conventional respiratory gating whereby the pulse sequence is not triggered during respiration. The result of this is a stop/start acquisition and can lead to modulation of signal strength affecting contrast and image clarity (Cassidy *et al.*, 2004). The cause of this modulation is T1 recovery of magnetisation during respiration and can be improved by the maintenance of a steady state of magnetisation (Cassidy *et al.*, 2004).
4. Cardiac and respiratory gating with maintenance of a steady state level of magnetisation, whereby the pulse sequence is triggered by every heart beat but the data is not collected during respiration.

In order to determine the preferred gating strategy I first acquired a single frame short axis image, using each of the 4 strategies in turn. To ensure that the effects of image quality were only due to the gating strategy, the images were acquired without any signal averaging. The imaging parameters used were: field of view 25.6 x 25.6mm, data matrix 128 x 128, echo time = 1.43ms, repetition time = R-R interval (approximately 140ms), flip angle 60° and number of averages = 1. Then to demonstrate the effects on the cine images I acquired multi frame, short axis images using my standard cine imaging parameters: field of view 25.6 x 25.6mm, data matrix 128 x 128, echo time = 1.43ms, repetition time = 5ms, flip angle = 15° and number of averages = 4. Figure 3.6 confirms that cardiac gating (option 2) is essential to generate quality images and demonstrates that, at 7T, respiratory gating (option 3) improves the image quality with further improvements following maintenance of a steady state of magnetisation (option 4). This improvement appears to be less obvious in cine

images most likely due to the use of signal averaging in the acquisition of these images.

In summary, the experiments described in this section demonstrated that I was able to orientate the imaging plane to the correct axes of the heart and obtain cine images of the heart. For all experiments described in this thesis I used cardiac and respiratory gating and the following parameters: echo time 1.43ms, repetition time 5ms, flip angle 15°, number of signal averages 4, field of view 25.6 x 25.6mm, data matrix 128 x 128 (zerofilled to 256 x 256, giving an in plane resolution of 100 x 100μm^2), slice thickness 1mm. Once I had established this setup I proceeded to validate the data obtained from cardiac MRI.

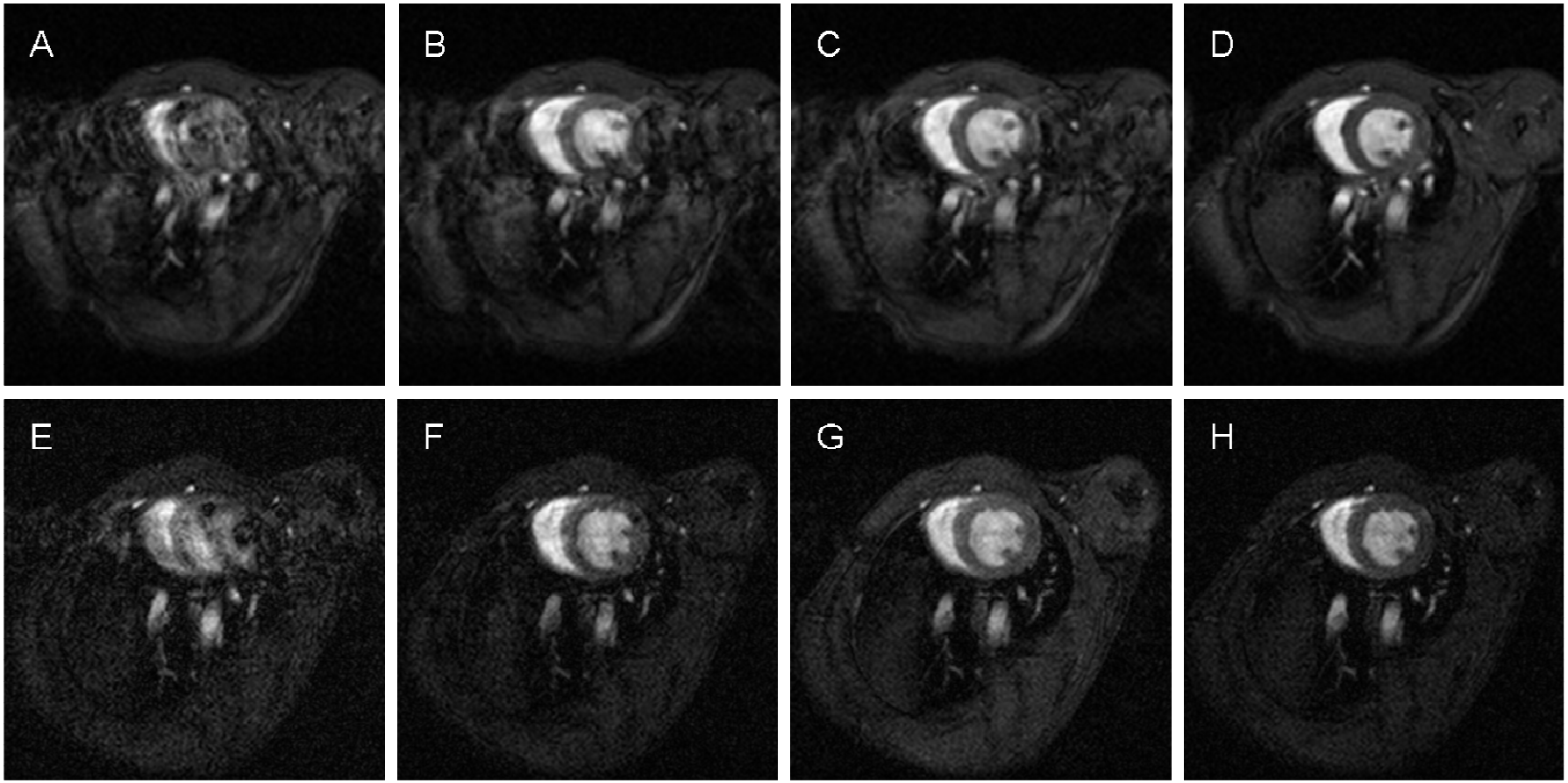

Figure 3.6 The effect of physiological gating on image quality.

A-D. A single frame short axis image was acquired at the level of the papillary muscles with no gating (A), cardiac gating only (B), cardiac and conventional respiratory gating (C) and cardiac and respiratory gating with steady state (D). The imaging parameters were TE = 1.43ms, TR = one heart beat (approx 140ms), flip angle = 60° and number of averages = 1. **E-F.** Multi frame (cine) short axis images were obtained at the level of the papillary muscle. End diastolic frames are shown with no gating (E), cardiac gating only (F), cardiac and conventional respiratory gating (G) and cardiac and respiratory gating with steady state (H Imaging parameters: FOV 25.6x2 5.6mm, matrix 128x128 (zerofilled to 256x256), TE = 1.43ms, TR = 5ms, flip angle 15°, NA= 4.

3.2.2 Validation of MRI for the measurement of cardiac mass and function.

To validate cardiac MRI it was necessary to show that I could accurately and reproducibly measure left ventricular mass and function. To achieve this I repeated an experiment performed by Ruff et al. (Ruff *et al.*, 1998). Cine cardiac MRI was performed on nine *C57BL/6* (7 male, 2 female) mice between 8 and 12 weeks old. A stack of short axis cine images covering the whole left ventricle was obtained. Following acquisition of the images the mice were euthanized, the hearts were dissected and the left ventricle isolated, washed in PBS to remove excess blood and blotted dry. The autopsy left ventricular mass was then recorded. Analysis of the MRI images was performed using ImageJ software. The parameters measured were left ventricular myocardial volumes in diastole and systole, end diastolic volume (EDV) and end systolic volume (ESV). From these measurements left ventricular mass, stroke volume (SV), ejection fraction (EF) and cardiac output (CO) were calculated. To compare the agreement between the LV mass measured at autopsy and by MRI, a Bland Altman analysis was performed (Bland and Altman, 1986). Intra-observer variability was assessed by analysing the MRI images on two separate occasions.

The autopsy and MRI results are shown in table 3.1. They reveal no significant differences between autopsy mass (90.4 ± 5.7mg) and either MRI mass calculated at end diastole (88.7 ± 5.0mg, p=0.50) or MRI mass calculated at end systole (89.3 ± 7.1mg, p=0.73). There was significant correlation between autopsy mass and MRI mass calculated at end diastole ($r=0.92$ $p<0.001$) and end systole ($r=0.91$, $p=0.001$). Bland Altman analysis demonstrated good agreement between autopsy and MRI myocardial mass with a mean difference (autopsy minus MRI) of 1.4 ± 2.6mg with limits of agreement -3.7mg to 6.5mg (figure 3.7). The left ventricular functional parameters (mean ± SD) were heart rate 504 ± 55 beats per minute, end diastolic volume 48.3 ± 4.8μl, end systolic volume 12.5 ± 4.5μl, stroke volume 35.8 ± 5.0μl, ejection fraction 74 ± 8%, and cardiac output 18 ± 2.8ml/min. The results demonstrated low intra-observer variability with an intra-observer variability for LV mass of 2.5 ± 1.8% at end diastole and 2.9 ± 1.9% at end systole. Intra-observer variability for functional parameters were: end diastolic volume 2.5 ± 1.0%, end systolic volume 6.4 ± 3.5%, stroke volume 3.8 ± 2.0%, ejection fraction was 2.2 ± 1.7% and cardiac output 3.8 ± 2.0% (table 3.2).

These results demonstrate that I was able to accurately measure left ventricular mass and function using cardiac MRI. This provides a powerful, *in vivo* tool to accurately phenotype heart structure and function in cardiac disease models.

Table 3.1 Autopsy and MRI analysis of left ventricular mass, volumes and function in normal *C57Bl/6* mice.

(LV=left ventricle, bpm=beats per minute, EDV=end diastolic volume, ESV=end systolic volume, SV=stroke volume, EF=ejection fraction and CO=cardiac output)

Mouse (gender)	Age (weeks)	LV mass (autopsy) (mg)	LV mass (diastole) (mg)	LV mass (systole) (mg)	Heart rate (bpm)	EDV (µl)	ESV (µl)	SV (µl)	EF (%)	CO (ml/min)
1 (M)	10	100	97.5	98.9	590	44.7	10.5	34.2	76	20.2
2 (M)	10	92.3	86.7	86.6	550	47	14.9	32.1	68	17.6
3 (M)	10	95.5	93.7	97.6	470	46.2	15.2	31.0	67	14.6
4 (F)	9	86.3	83.9	84.4	490	52.8	21.2	31.7	60	15.5
5 (F)	9	83.0	84.1	78	560	41.2	8.0	33.2	80	18.6
6 (M)	10	86.7	85.4	88.6	515	45.3	6.3	39.0	86	20.1
7 (M)	10	94.0	93.6	96.7	490	57.0	10.1	46.9	82	23.0
8 (M)	11	92.0	88.1	89.1	420	50.1	14.1	36.0	71	15.1
9 (M)	13	84.0	85.2	84.2	450	50.5	12.1	38.4	76	17.3
Mean ± SD	**10 ± 1.2**	**90.4 ± 5.7**	**88.7 ± 5.0**	**89.3 ± 7.1**	**504 ± 55**	**48.3 ± 4.8**	**12.5 ± 4.5**	**35.8 ± 5.0**	**74 ± 8**	**18.0 ± 2.8**

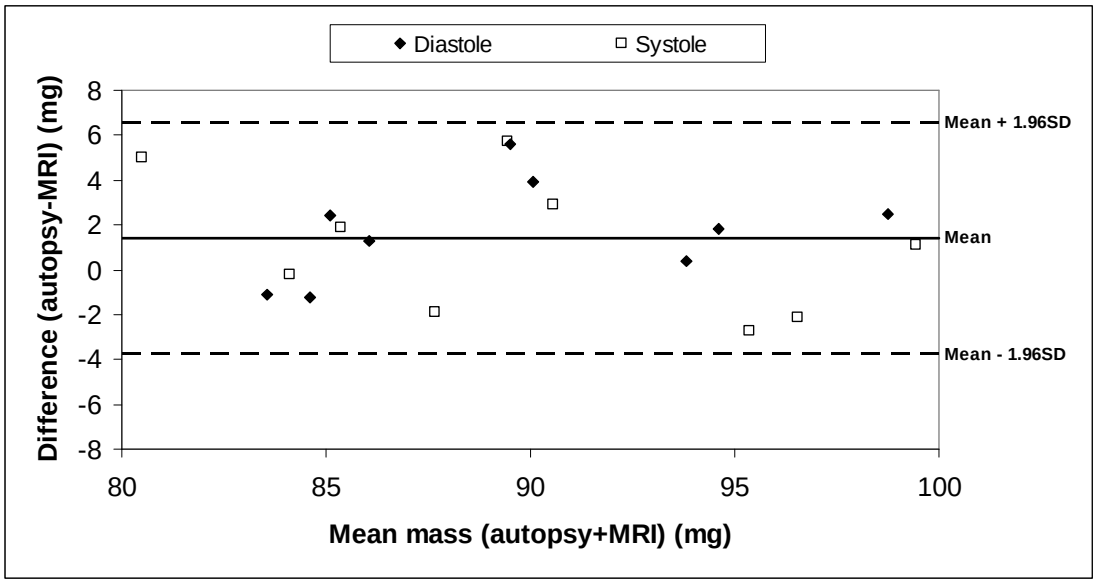

Figure 3.7 Bland-Altman plot (difference versus mean) of left ventricular mass at autopsy compared to MRI (n=9).

The mean difference between these two methods was 1.4mg and the limits of agreement -3.7 to 6.5mg, demonstrating good agreement between these methods.

Table 3.2 Intra-observer variability in measurements of left ventricular volumes and mass.

I analysed the raw MRI data from 9 hearts on 2 independent occasions to determine the reproducibility of the calculated measurements. Data expressed as mean ± SD.

Measurement	Intra-observer variability (%)
Diastolic mass	2.5 ± 1.8
Systolic mass	3.0 ± 1.9
End diastolic volume	2.5 ± 1.0
End systolic volume	6.3 ± 3.5
Stroke volume	3.8 ± 2.0
Ejection fraction	2.2 ± 1.7
Cardiac output	3.8 ± 2.0

3.2.3 Cardiac MRI in mouse models of cardiac disease

To test whether we could use MRI to investigate differences in cardiac structure and function in models of cardiac disease I performed cardiac MRI in three mouse models:

1. Myocardial infarction model.
2. Adult stem cell mediated cardiac repair post MI model.
3. Muscular dystrophy related cardiomyopathy in the delta sarcoglycan deficient mouse (a model of limb girdle muscular dystrophy type 2F).

3.2.3.1 Mouse myocardial infarction model

To evaluate the use of MRI as a means of tracking heart function following myocardial infarction, I performed cardiac MRI 4 weeks following permanent LAD ligation (as described in chapter 2). Controls were mice that had undergone a sham operation (a thoracotomy without LAD ligation). The surgical operations for this experiment were performed by Dr Rachael Redgrave.

The MRI images in figure 3.8 clearly demonstrate increased sphericity of the left ventricle with myocardial wall thinning and akinesis in the anterolateral and apical walls of the infarcted left ventricle. Comparison of cardiac function can be seen in table 3.3. These data reveal that compared to sham operated mice there are significant increases in myocardial mass (122.29 ± 9.18mg vs. 111.93 ± 4.87mg, p =0.01), end diastolic volume (116.65 ± 36.24µl vs. 66.35 ± 5.51µl, p=0.001) and end systolic volume (85.08 ± 39.62µl vs. 21.79 ± 2.41µl, p<0.001) in the mice that had undergone LAD ligation. In addition, there are also significant reductions in stroke volume (30.39 ± 4.12µl vs. 44.55 ± 4.12 µl, p<0.001), ejection fraction (26.63 ± 8.84% vs. 67.14 ± 2.59%, p<0.001) and cardiac output (12.57 ± 2.27ml/min vs. 18.22 ± 2.25ml/min, p<0.001) following LAD ligation. There were no significant differences in mean heart rate (416 ± 38bpm vs. 409 ± 27bpm, p=0.6).

There is a significant difference in pre surgery weights between the groups (25.46 ± 2.73 in the infarct group vs. 29.01 ± 3.56 in the sham group, p=0.03). This is most likely due to the different numbers of each sex in this experiment. There were 5 males and 3 females in the sham group and 3 males and 7 females in the infarct group. To

account for this difference I indexed the measurements made to the body weight of the animal (table 3.3). I chose the pre-operative weight of the animal to index the measurement to in order to eliminate any effect of the operative procedure or subsequent heart failure on body weight. In agreement with the non-indexed measurement there was a significant increase in myocardial mass index (4.95 ± 0.65mg/g vs. 3.89 ± 0.51mg/g, p=0.002), end diastolic volume index (4.79 ± 1.75 µl/g vs. 2.32 ± 0.43µl/g, p=0.001) and end systolic volume index (3.52 ± 1.80µl/g vs. 0.76 ± 0.15µl/g, p< 0.001) in the mice with LAD ligation compared to sham controls. There was also a significant reduction in stroke volume index (1.27 ± 0.16µl/g vs. 1.56 ± 0.30µl/g, p=0.02) and a trend towards a reduction in cardiac index (0.53 ± 0.08ml/min/g vs. 0.64 ± 0.15ml/min/g, p=0.06) in the LAD ligation group.

The mean infarct size in the LAD ligation group was 34.29 ± 7.94%. There was an inverse linear relationship (slope = -1.296) and strong inverse correlation between infarct size and ejection fraction (figure 3.9, r=-0.96, p<0.001). This confirms that the larger myocardial infarction the greater reduction in left ventricular systolic function.

These data confirm left ventricular hypertrophy with dilatation and a reduction in systolic function occurred in mice by 4 weeks following permanent LAD ligation, and agrees with expected outcomes (Wiesmann *et al.*, 2001b; Ross *et al.*, 2002; Yang *et al.*, 2004).

Table 3.3 Cardiac function post MI.

Cardiac functional parameters in mice 4 weeks following coronary artery ligation (n=10) or sham operation (n=8). Data expressed as mean ± standard deviation, statistical comparisons made using unpaired Student's ttest.

	Sham	**Infarct**	**p value**
Sex	**5M 3F**	**3M 7F**	**n/a**
Body weight – pre surgery (g)	29.20 ± 4.07	24.96 ± 2.83	**0.02**
Body weight – pre MRI (g)	29.01 ± 3.6	25.03 ± 2.91	**0.02**
Age at infarct (wks)	12.38 ± 1.33	12.00 ± 1.27	0.55
Time to MRI (days)	26 ± 2.45	27.70 ± 3.89	0.3
Mean heart rate (bpm)	409 ± 27	416 ± 38	0.6
Mean myocardial mass (mg)	111.93 ± 4.87	122.29 ± 9.18	**0.01**
Myocardial mass index (mg/g)	3.89 ± 0.51	4.95 ± 0.65	**0.002**
End diastolic volume (µl)	66.35 ± 5.51	116.65 ± 36.24	**0.001**
End diastolic volume index (µl/g)	2.32 ± 0.43	4.79 ± 1.75	**0.001**
End systolic volume (µl)	21.79 ± 2.41	85.08 ± 39.62	**<0.001**
End systolic volume index (µl/g)	0.76 ± 0.15	3.52 ± 1.80	**<0.001**
Stroke volume (µl)	44.55 ± 4.12	30.39 ± 4.12	**<0.001**
Stroke volume index (µl/g)	1.56 ± 0.30	1.27 ± 0.16	**0.02**
Ejection fraction (%)	67.14 ± 2.59	26.63 ± 8.84	**<0.001**
Cardiac output (ml/min)	18.22 ± 2.25	12.57 ± 2.27	**<0.001**
Cardiac index (ml/min/g)	0.64 ± 0.15	0.53 ± 0.08	0.06
Infarct size (%LV)	n/a	34.29 ± 7.94	n/a

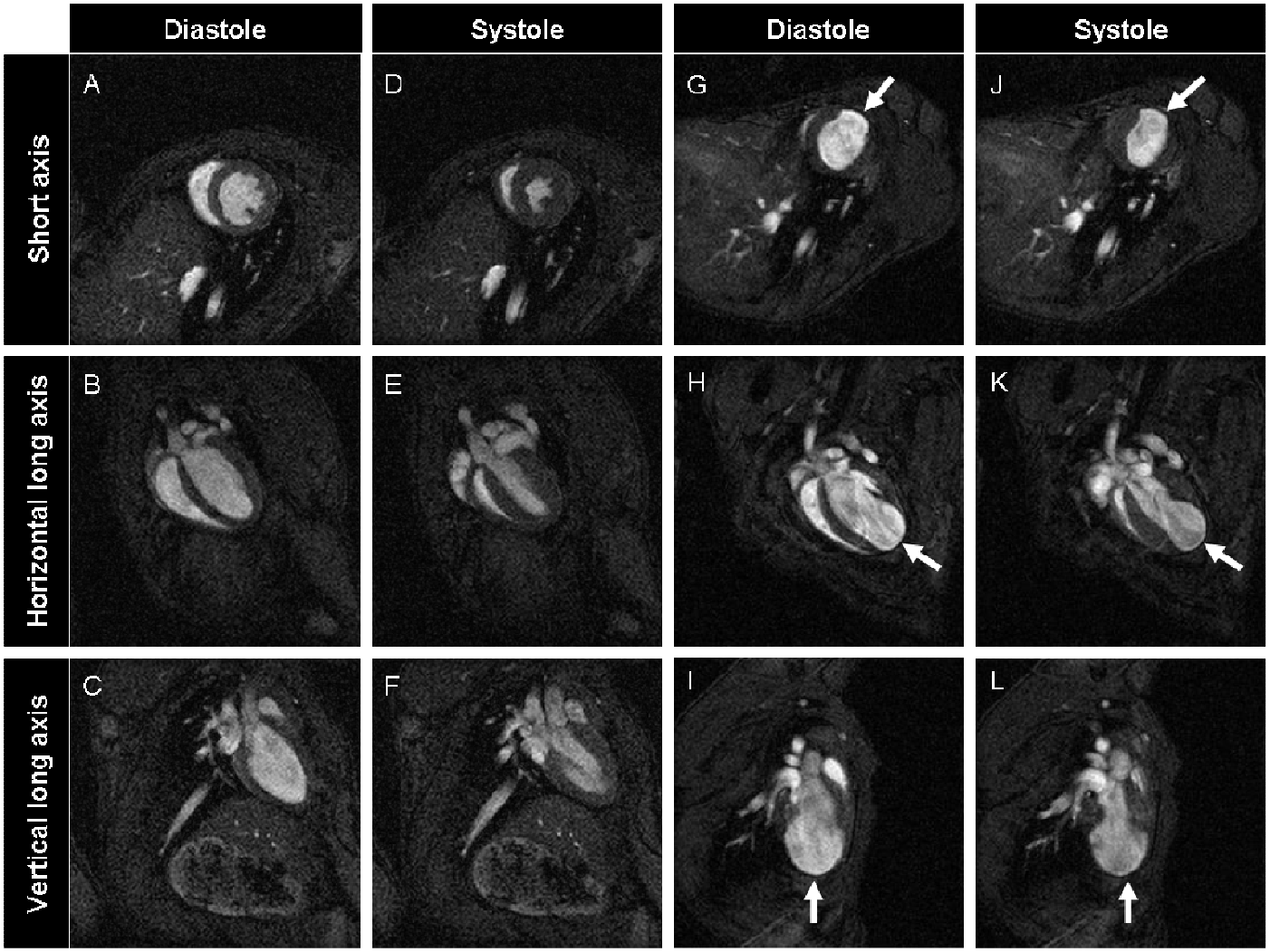

Figure 3.8 MRI images of a representative mouse hearts 4 weeks following sham operation (A-F) or LAD ligation (G-L).

The arrows identify the thinned, akinetic area of the myocardial infarct. Imaging parameters: FOV 25.6x2 5.6mm, matrix 128x128 (zerofilled to 256x256), TE = 1.43ms, TR = 5ms, flip angle 15°, NA= 4.

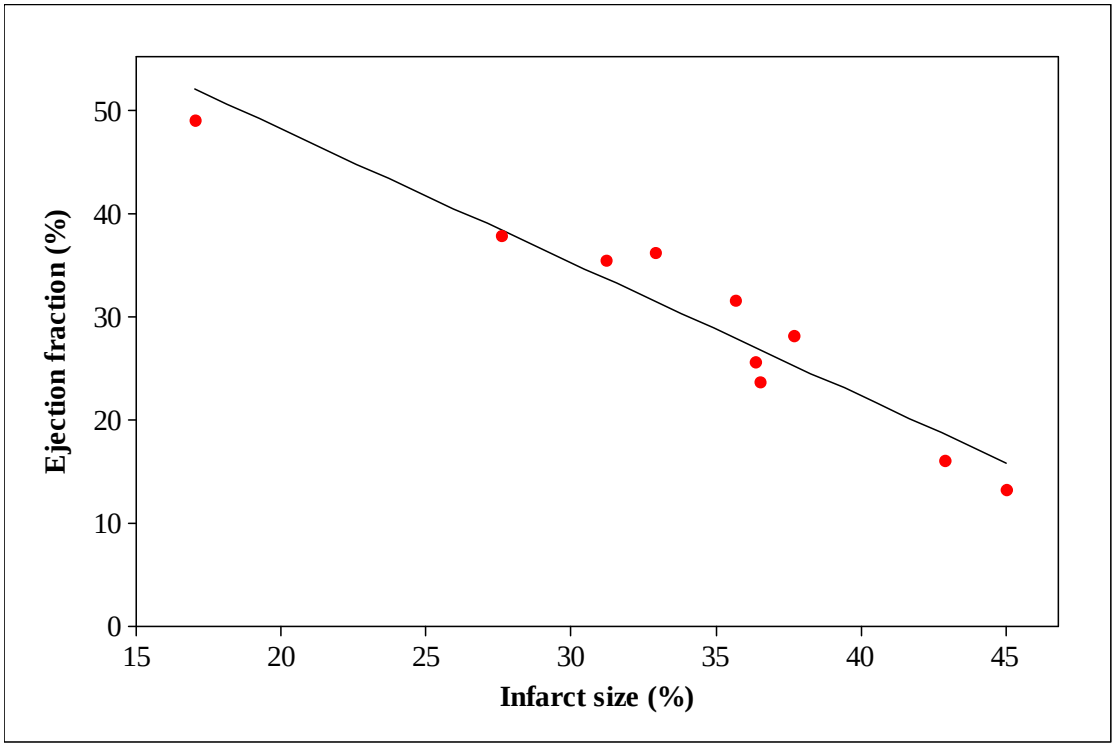

Figure 3.9 Relationship between infarct size and ejection fraction.

There is an inverse linear relationship between infarct size and ejection fraction (slope = -1.296) and a strong inverse correlation ($r=-0.96$, $p<0.001$).

3.2.3.2 Adult stem cell mediated cardiac repair model

The aim of this project was to investigate the effect of endoglin depletion on the ability of an adult stem cell to mediate cardiac repair following myocardial infarction. Cardiosphere derived cells (CDCs) are grown from myocardial tissue and have been shown to have stem cell properties, are able to mediate cardiac repair following myocardial infarction and express endoglin (Messina *et al.*, 2004; Smith *et al.*, 2007). CDCs were isolated and expanded from murine hearts. Cre-lox technology (see chapter 4 for further information) was used to knockdown endoglin in these cells. Following permanent LAD ligation, CDCs (with or without endoglin knockdown) or sterile PBS was injected in the peri-infarct myocardium. They were then imaged by cardiac MRI at 1 and 4 weeks following LAD ligation. The CDC culture and surgical procedures were performed by Dr Rachael Redgrave in my host laboratory. I performed and analysed the cardiac MRI.

Representative short and long axis cardiac MR images for sham operated, infarct alone group, infarct with CDCs group and infarct with endoglin knockdown (*Eng iKO*^{u}) CDCs 4 weeks following surgery are shown in figure 3.10 A to D respectively. These images clearly demonstrate that there is left ventricular enlargement following myocardial infarction but that this is attenuated by cell transplantation. The results of analysis of the cardiac MRI data are shown in table 3.4 and figure 3.11. These demonstrate a difference between the sham operated and all infarct groups and that the mean left ventricular volumes were smaller in the CDC treated groups compared to the infarct only group but this difference is not statistically significant. The main effect of cell transplantation is the significant attenuation adverse remodelling compared to the infarct alone group table 3.5 (ANOVA $p<0.05$). These results demonstrate that CDC transplantation have a beneficial effect on cardiac function. However, both CDCs with and without endoglin appear to be equally beneficial in reducing the adverse remodelling seen following myocardial infarction.

This study demonstrates that cardiac MRI is able to longitudinally measure ventricular function and assess the effects of different therapies on cardiac function.

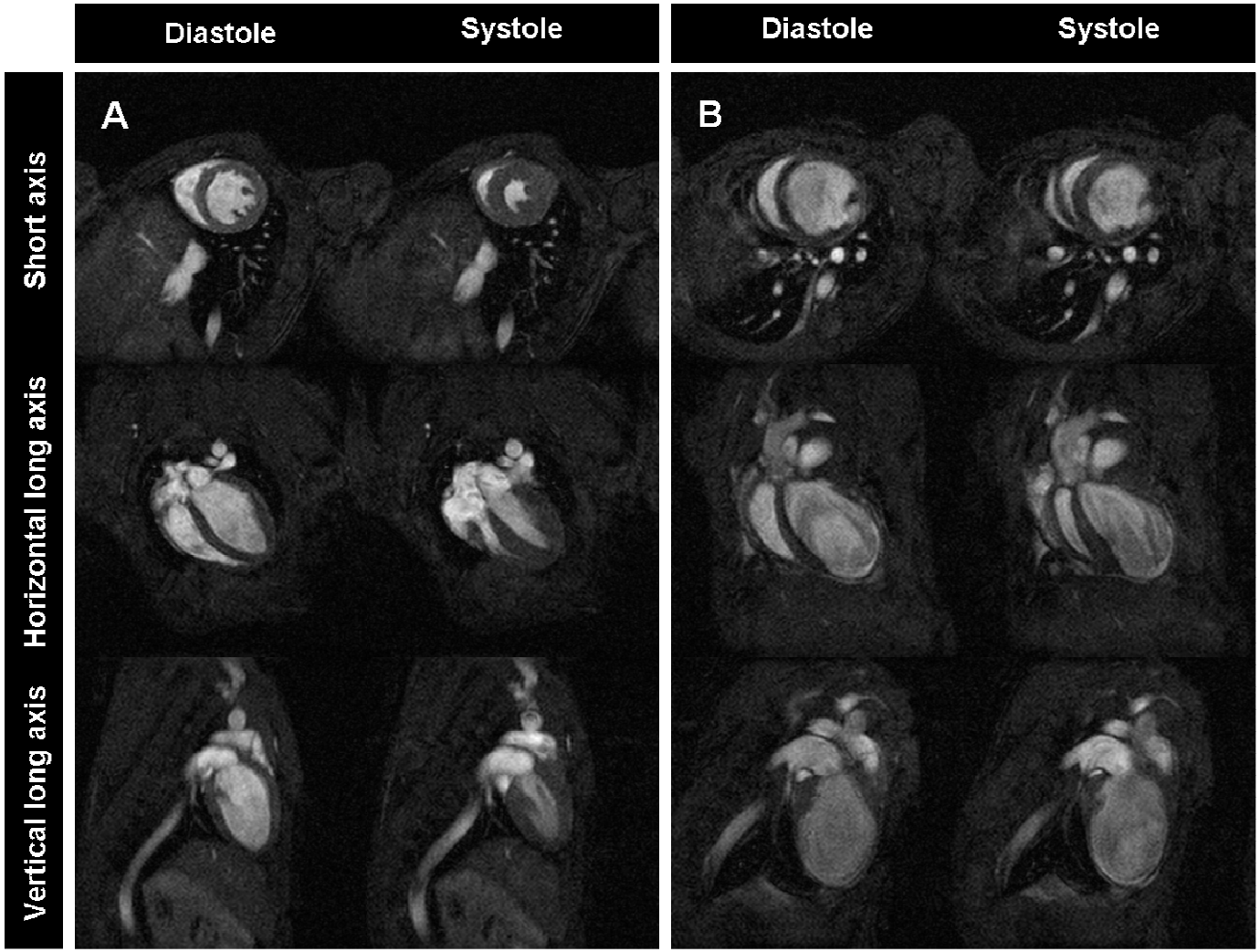
Diastole
Systole
Diastole
Systole
A
B
Short axis
Horizontal long axis
Vertical long axis

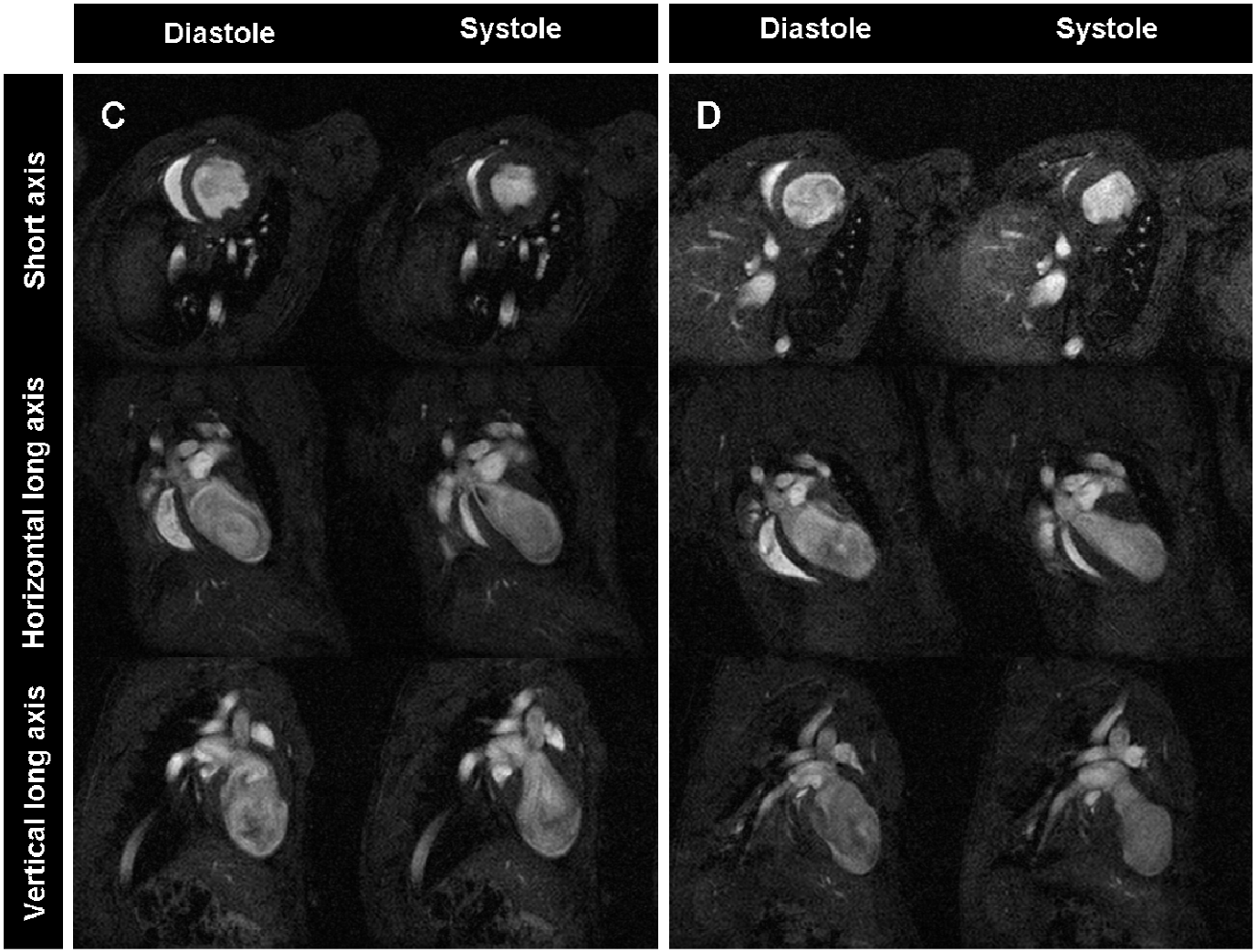

Figure 3.10 Cardiac MRI of representative mice 4 weeks following coronary artery ligation and cell therapy.

A. sham operated control. **B.** Coronary artery ligation alone. **C.** Coronary artery ligation with endoglin positive CDCs. **D.** Coronary artery ligation with endoglin knockdown CDCs. Imaging parameters: FOV 25.6x2 5.6mm, matrix 128x128 (zerofilled to 256x256), TE = 1.43ms, TR = 5ms, flip angle 15°, NA= 4.

Table 3.4 Cardiac function 1 and 4 weeks following coronary artery ligation with or without cell therapy.

Left ventricular volumes were smaller and ejection fraction greater in the infarct with CDC transplantation groups compared to the infarct and PBS treated group but these differences were not significant using parametric ANOVA. Data expressed as mean ± SE.

	1 week				4 weeks			
	Sham operation (n=4)	**MI + PBS (n=3)**	**MI + CDCs (n=6)**	**MI + Eng iKO^{u} CDCs (n=4)**	**Sham operation (n=4)**	**MI + saline (n=3)**	**MI + CDCs (n=6)**	**MI + Eng iKO^{u} CDCs (n=4)**
Weight (g)	23.8 ± 2.3	23.2 ± 1.5	25.5 ± 0.9	25.5 ± 3.2	26.3 ± 2.4	25.5 ± 2.0	28.3 ± 1	28.9 ± 2.8
Mean HR (bpm)	423 ± 15	429 ± 28	448 ± 24	432 ± 9	425 ± 11	420 ± 7.9	456 ± 15	440 ± 15
Mean mass (mg)	113 ± 6.1	146 ± 18	136 ± 4.3	146 ± 7.5	121 ± 8.7	167 ± 22	144 ± 4.7	159 ± 9.3
Mass index (mg/g)	4.4 ± 0.2	5.8 ± 0.6	4.6 ± 0.2	5.18 ± 0.6	4.7 ± 0.3	6.6 ± 0.9	4.9 ± 0.2	5.7 ± 0.8
EDV (µl)	66.3 ± 3.6	146.3 ± 24.6	125.8 ± 14.8	124.9 ± 20.8	72.9 ± 4.1	210.5 ±27.3	153.1 ± 17.2	153.9 ± 30.1
EDVI (µl/g)	2.6 ± 0.2	5.8 ± 0.9	4.2 ± 0.5	4.6 ± 1.2	2.9 ± 0.2	8.4 ± 1.1	5.2 ± 0.6	5.7 ± 1.6
ESV (µl)	20.5 ± 1.5	119.4 ± 20.7	87.7 ±15.4	87.4 ± 25.6	23.3 ± 2.2	171.3 ± 20.4	110.6 ± 20.7	111.7 ± 37.7
ESVI (µl/g)	0.81 ± 0.08	4.7 ± 0.7	3.0 ± 0.5	3.3 ± 1.3	0.9 ± 0.04	6.8 ± 0.9	3.9 ± 0.7	4.28 ± 1.8
SV (µl)	45.7 ± 2.3	26.9 ± 4.0	36.7 ± 4.2	37.5 ± 6.6	44.7 ± 6.1	39.2 ± 7.6	41.2 ± 4.9	42.2 ± 8.0
SVI (µl/g)	1.79 ± 0.1	1.1 ± 0.1	1.2 ± 0.1	1.3 ± 0.1	1.97 ± 0.2	1.6 ± 0.3	1.43 ± 0.1	1.4 ± 0.2
EF (%)	69.1 ± 1.0	18.6 ± 0.8	32.0 ± 6.3	33.4 ± 7.9	67.9 ± 3.0	18.4 ± 1.7	30.8 ± 6.1	35.1 ± 10.6
CO (ml/min)	19.4 ± 1.3	11.7 ± 2.2	16.1 ± 1.4	16.1 ± 2.6	21.2 ± 2.2	16.5 ± 3.3	19.2 ± 1.9	18.3 ± 3.2
CI (ml/min/g)	0.76 ± 0.03	0.5 ± 0.08	0.5 ± 0.04	0.5 ± 0.04	0.84 ± 0.1	0.7 ± 0.1	0.7 ± 0.06	0.6 ± 0.07
Infarct size (%)	n/a	50.2 ± 4.73	40.1 ± 3.69	38.2 ± 6.5	n/a	51.8 ± 1.9	42.1 ± 4.7	38.3 ± 6.8

Table 3.5 Change in cardiac functional parameters between 1 and 4 weeks following coronary artery ligation with or without cell therapy.

Using ANOVA there was a significant attenuation in the increase in EDV (and EDVI) between the groups. The difference was significant between the MI+PBS and endoglin positive CDC groups, but not between MI+PBS and endoglin knockdown CDC groups (this was likely due to smaller numbers in the endoglin knockdown CDC group). Data expressed as mean ± SE, *p<0.05 compared to MI+PBS

	Sham operation (n=4)	**MI + PBS (n=3)**	**MI + CDCs (n=6)**	**MI + Eng iKO^{u} CDCs (n=4)**	**p value (ANOVA)**
ΔMean HR (bpm)	1.5 ± 25	-8.3 ± 32	8.5 ± 19.7	7.8 ± 13.7	0.9
ΔMean mass (mg)	7.9 ± 2.7	21.7 ± 7.0	8.5 ± 1.7	12.8 ± 4.5	0.1
ΔMass index (mg/g)	0.3 ± 0.1	0.9 ± 0.3	0.3 ± 0.05	0.5 ± 0.2	0.1
ΔEDV (µl)	6.7 ± 1.1	64.2 ± 12.8	27.3 ± 5.5*	29.0 ± 11.2	**0.041**
ΔEDVI (µl/g)	0.3 ± 0.06	2.6 ± 0.6	1.0 ± 0.2*	1.1 ± 0.5	**0.048**
ΔESV (µl)	2.7 ± 2.7	51.9 ± 12.0	23.0 ± 7.6	24.3 ± 12.8	0.2
ΔESVI (µl/g)	0.1 ± 0.1	2.1 ± 0.6	0.9 ± 0.3	1.0 ± 0.6	0.17
ΔSV (µl)	-1.3 ± 6.8	12.4 ± 3.9	4.5 ± 4.8	4.7 ± 0.1	0.5
ΔSVI (µl/g)	0.2 ± 0.2	0.5 ± 0.2	0.2 ± 0.2	0.2 ± 0.08	0.3
ΔEF (%)	-1.2 ± 7.8	-0.2 ± 2.1	-1.26 ± 3.4	1.8 ± 3.8	0.8
ΔCO (ml/min)	1.9 ± 2.2	4.86 ± 1.1	3.1 ± 2.4	2.3 ± 1.1	0.7
ΔCI (ml/min/g)	-0.004 ± 0.07	0.2 ± 0.04	0.1 ± 0.08	0.08 ± 0.04	0.6
ΔInfarct size (%)	n/a	1.6 ± 3.5	2.1 ± 1.7	0.08 ± 0.9	0.2

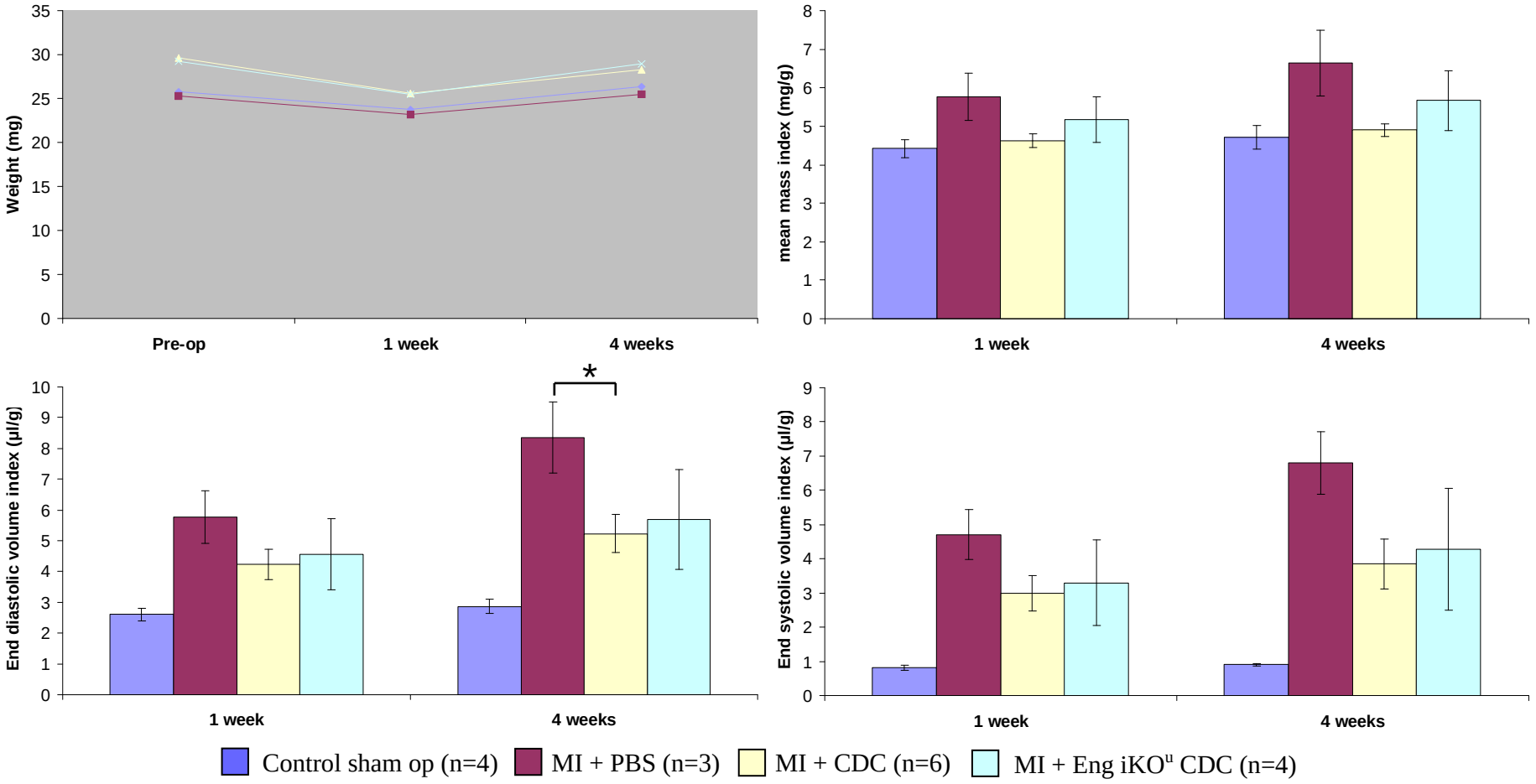
Weight (mg)
Pre-op
1 week
4 weeks
mean mass index (mg/g)
1 week
4 weeks
End diastolic volume index (µl/g)
*
1 week
4 weeks
End systolic volume index (µl/g)
1 week
4 weeks
Control sham op (n=4)
MI + PBS (n=3)
MI + CDC (n=6)
MI + Eng iKO^{u} CDC (n=4)

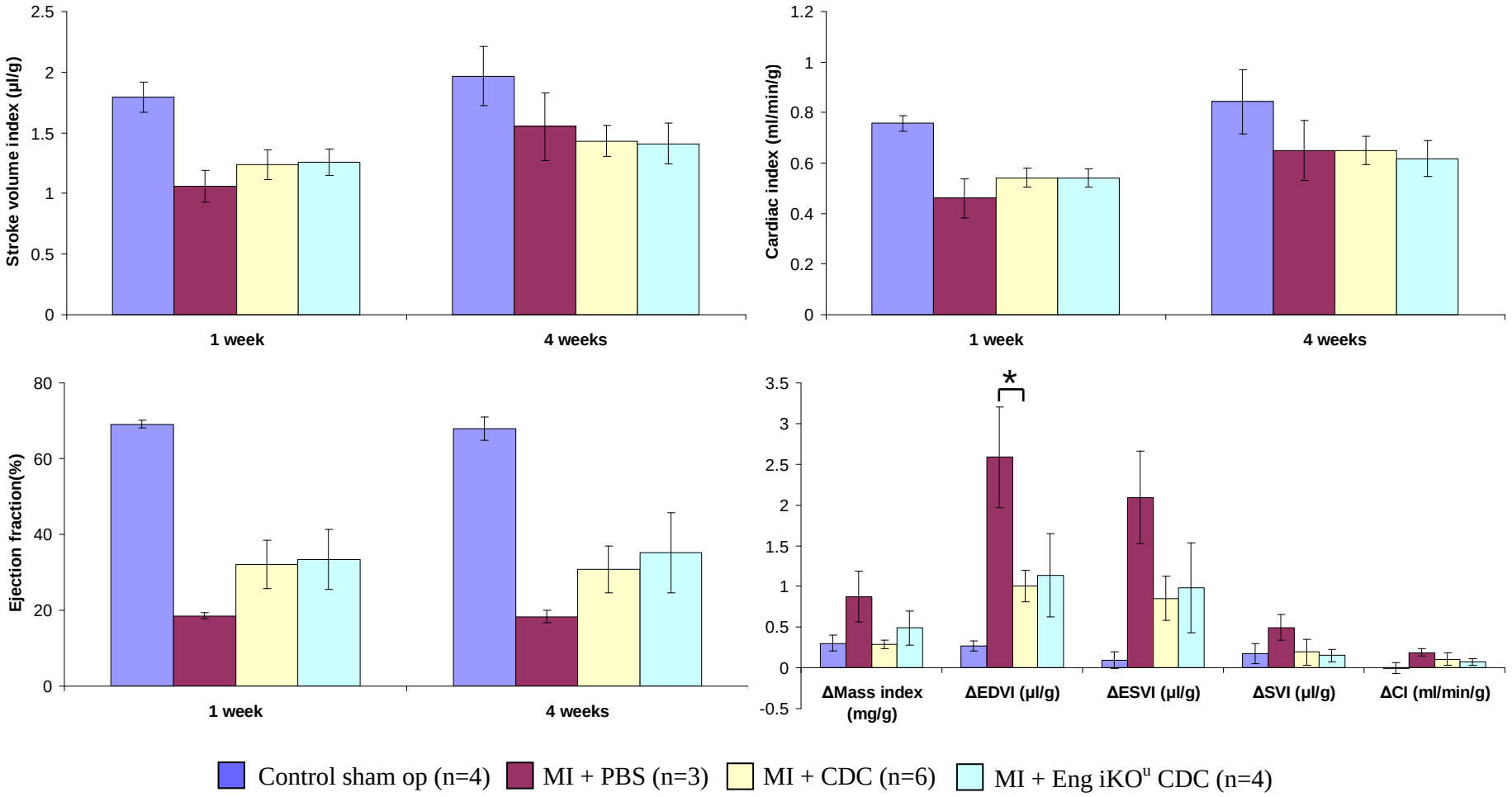

Figure 3.11 Cardiac volumes and function 1 and 4 weeks following coronary artery ligation with or without cell therapy.

*p<0.05.

3.2.3.3 Muscular dystrophy related cardiomyopathy.

In order to evaluate another independent mouse model of cardiomyopathy by cardiac MRI, I turned to a model of muscular dystrophy that was being used for studies within my host Institute. Muscular dystrophies are frequently associated with cardiomyopathies (Bushby *et al.*, 2003). The δ-sarcoglycan deficient mouse (*Scgd*-/-) is a model for limb girdle muscular dystrophy type 2F. Patients with this type of muscular dystrophy can develop a progressive and potentially fatal cardiomyopathy (Politano *et al.*, 2001). The *Scgd*-/- mouse develops cardiac pathology from about 16 weeks of age (Coral-Vazquez *et al.*, 1999) and *in vivo* studies have demonstrated alterations in cardiac function at 16 (Bauer *et al.*, 2008) and 32 (Wansapura *et al.*, 2011) weeks of age. The effects of a number of treatments used clinically for the treatment of both muscular dystrophies and heart failure have been assessed by colleagues in my host Institute (Bauer *et al.*, 2008; Bauer *et al.*, 2010a; Bauer *et al.*, 2010b). However, longitudinal studies using cardiac MRI in these mice would enable investigation of the onset and progression of the cardiomyopathy, as well as gaining understanding into alterations in calcium homeostasis by using manganese enhanced MRI, as discussed in chapter 1 (Hu *et al.*, 2001).

32 week old, male *Sgcd*-/- and 40 week old, control male C57BL/10 mice underwent cine cardiac MRI (n=16 and 9 respectively) as described in section 2.3. The results (table 3.6) show that the *Sgcd*-/- mice had higher heart rates (487 ± 30bpm vs. 385 ± 41 bpm, $p<0.001$) and an increased left ventricular mass (126.19 ± 11.62mg vs. 112 ± 8.37mg, $p=0.004$) than the control mice. However, there is a trend towards a reduced left ventricular end diastolic volume (63.25 ± 14.46μl vs. 74.11 ± 9.18μl, $p=0.055$) and a significantly smaller end systolic volume (21.25 ± 7.16μl vs. 27.67 ± 5.34μl, $p=0.028$) in the *Sgcd*-/- mice. There is no significant difference in stroke volume (42.06 ± 8.49μl vs. 46.46 ± 5.77μl, $p=0.17$), ejection fraction (67.19 ± 5.91% vs. 63.00 ± 4.97%, $p=0.086$) or cardiac output (20.39 ± 4.17ml/min vs. 17.79 ± 2.53ml/min, $p=0.10$). These data suggest that at this age *Sgcd*-/- mice had developed left ventricular hypertrophy but had preserved systolic function.

Table 3.6 Cardiac function in *Sgcd*-/- mice.

Cardiac functional parameters in 32 week old male *Sgcd*-/- mice (n=16) and 40 week old, male C57Bl/10 mice (n=9). Data expressed as mean ± standard deviation, statistical com parison was made using unpaired Student's ttest.

	C57BL/10	***Sgcd*-/-**	**p value**
Mean heart rate (bpm)	385 ± 41	487 ± 30	**<0.001**
Mean myocardial mass (mg)	112.00 ± 8.37	126.19 ± 11.62	**0.004**
End diastolic volume (µl)	74.11 ± 9.18	63.25 ± 14.46	0.055
End systolic volume (µl)	27.67 ± 5.34	21.25 ± 7.16	**0.028**
Stroke volume (µl)	46.46 ± 5.77	42.06 ± 8.49	0.17
Ejection fraction (%)	63.00 ± 4.97	67.19 ± 5.91	0.086
Cardiac output (ml/min)	17.79 ± 2.53	20.39 ± 4.17	0.10

3.3 Discussion

The ability to measure *in vivo* cardiac function is important in cardiovascular research. Cine cardiac MRI is a widely used technique to do this. The aim of this study was to establish cardiac MRI to allow its use in the study of models of cardiac disease. Using a heuristic approach I was able to quickly define optimal imaging parameters. These parameters are similar to previously published studies that used a gradient echo FLASH pulse sequence (table 3.7). I validated this technique and demonstrated that I was able to accurately and reproducibly measure myocardial mass and cardiac function in mice.

Table 3.7 Summary of MRI imaging parameters in a selection of studies using a FLASH pulse sequence in murine cardiac MRI.

(TE – echo time, TR – repetition time, FOV – field of view, NA – number of signal averages, ns – not stated)

Study	TE (ms)	TR (ms)	Flip angle (°)	FOV (mm)	Matrix size	NA	Field strength (T)
This thesis	1.43	5	15	25.6 x 25.6	128 x 128	4	7
(Ruff *et al.*, 1998)	1.6	4-11	40	30 x 30	256 x 256	2	7
(Schneider *et al.*, 2003)	1.43	4.6	15	25.6 x 25.6	256 x 256	2	11.7
(Hu *et al.*, 2004)	2.3	11.0	ns	25 x 25	128 x 128	4	9.4
(Winter *et al.*, 2008)	1.9	7	15	25.6 x 25.6	256 x 256	4	9.4
(Wansapura *et al.*, 2011)	3	5.2	20	25.6 x 25.6	256 x 256	ns	ns
(Amundsen *et al.*, 2011)	3	6	15	35 x 35	128 x 128	ns	7
(Smart *et al.*, 2011)	1.18	4.5	20	25.6 x 25.6	128 x 128	2	9.4

The earliest described multi-frame cardiac MRI used a spin echo pulse sequence and was able to achieve an in plane resolution of 117 x117 μm^2 and a temporal resolution of approximately 24ms resulting in 8 frames being acquired to cover the cardiac cycle (Kubota *et al.*, 1997). They demonstrated that LV mass measured gravimetrically and by MRI were linearly related with a mean error between the methods of 0.28±2.70 mg (Kubota *et al.*, 1997). However, the nature of their spin echo pulse sequence meant they had to rotate the acquisition order of their multi-slice set in order to obtain multi-frame images. The limiting factor with this method is the R-R interval as this determines how many slices can be obtained within one heart beat. They used sodium phenobarbital as the anaesthetic agent, which resulted in markedly lower heart rates (~ 220 beats per minute, R-R interval ~270ms) in their mice (Kubota *et al.*, 1997). Higher heart rates, such as those in our study (~500 beats per minute, R-R interval ~120ms), would reduce the number of slices and time frames that could be obtained.

The use of fast gradient echo pulse sequences (FLASH) enabled the use of shorter TE and TR without sacrificing special resolution (Haase *et al.*, 1986). Initial experiments, in mice, using a FLASH pulse sequence on a clinical MRI scanner at 1.5T had an in plane resolution of 195 x 195 μm^2 and a temporal resolution of 39ms (Franco *et al.*, 1998). However, they used a slice thickness of 1.6mm, which would have been required to increase the signal as their magnetic field strength is lower. However, they still reported strong correlation and good agreement between gravimetric mass and MRI mass (Franco *et al.*, 1998). At high field strength (7T), Ruff et al. were able to achieve an in plane resolution of 117 x117 μm^2 (slice thickness 1mm) and a temporal resolution of between 4 and 11 ms. They altered the TR, depending on the heart rate, to achieve 12 frames per cardiac cycle, which resulted in the variable temporal resolution (Ruff *et al.*, 1998). They validated their ability to measure small volumes with a water filled, glass phantom. However, it was 190µl, which is 4 times the mean end diastolic volume (45.2 ± 9.3µl). They demonstrate good agreement between gravimetric and MRI mass. Measurements of myocardial mass and function were reproducible (Ruff *et al.*, 1998). Schneider et al. also demonstrated good agreement (mean difference 0.04mg and coefficient of variation ± 7.2) and reproducibility between cardiac mass and function using an 11.5T vertical magnet. They also demonstrate that the use of respiratory gating improved image quality (Schneider *et al.*, 2003).

The results of my validation experiment are comparable to these previously published studies. However, the intra-observer variability for end systolic volume was higher in my study. This is likely due to my use of manual, rather than automatic (Ruff *et al.*, 1998; Schneider *et al.*, 2003), segmentation to measure ventricular volumes. Interestingly, in the work described in this chapter the mean difference between the 2 independent measurements of end diastolic and end systolic volumes were similar (1.7 ± 0.7μl vs. 1.1 ± 0.8μl respectively). However, as the end systolic volume is very small (12.5 ± 4.5μl) a small difference in volume results in greater percentage variability. Consequently, it is essential to ensure careful, accurate segmentation of the left ventricular cavity, particularly at end systole. To ensure this I routinely calculated the left ventricular mass in both systole and diastole and only accepted the measurements if there was less than 5% difference between the two measurements.

Following myocardial infarction, cardiac function is impaired and left ventricular remodelling occurs. In mice undergoing infarct reperfusion injury there is a significant increase in ventricular volumes and reduced function by the first day following surgery (Yang *et al.*, 2004). This reduction in function was not simply due to the size of the infarct as it was not strongly correlated with ejection fraction (r=0.53). Also Yang et al were able to demonstrate a reduction in regional function in myocardium remote from the infarct. This suggests that the early reduction in cardiac function is due to loss of viable myocardium and contractile dysfunction in non-infarcted regions (Yang *et al.*, 2004). In another study, Wiesmann et al. (Wiesmann *et al.*, 2001b) demonstrated a reduction in cardiac function in mice two weeks following permanent LAD ligation but no difference in LV mass. A longitudinal study investigating left ventricular remodelling in mice following infarct reperfusion injury documented that most LV remodelling occurs in the first 4 weeks following injury (Ross *et al.*, 2002). They also documented a 50% increase in LV mass 1 day following infarction with a trend towards further increases at later time points (Ross *et al.*, 2002). However, inspection of their data gives the impression that there may be an increase in LV mass, peaking at one week post infarct followed by a slight reduction at two and four weeks post MI before an increased mass from six weeks onwards. This may reflect the resolution of initial myocardial oedema along side the left ventricular hypertrophy seen in ventricular remodelling. This might also account for the fact that Wiesmann did not see a difference in LV mass at 2 weeks post infarction.

The data presented in this chapter is consistent with these studies as I saw significant increases in ventricular volumes and myocardial mass and a significant reduction in cardiac function four weeks following permanent LAD ligation when compared to sham operated controls (summarised in table 5.8). In contrast to Yang et al. (Yang *et al.*, 2004), at four weeks post infarct I demonstrated a significant correlation between infarct size and ejection fraction ($r=-0.96$, $p<0.001$). This is in agreement with a study by Schneider et al. which demonstrated significant correlation between infarct size and ejection fraction in their data ($r=-0.91$, $p<0.01$) and in that of Wiesmann et al (Wiesmann *et al.*, 2001b) following a retrospective analysis ($r=-0.95$, $p<0.01$) (Schneider *et al.*, 2003).

One of the challenges of assessing cardiac function following myocardial infarction is the fact that the infarction results in myocardial deformation. An advantage of MRI is that it does not rely on geometric assumption when calculating myocardial mass and ventricular volumes and is considered to be the gold standard for these measurements (Siri *et al.*, 1997; Ruff *et al.*, 1998). However, other techniques such as echocardiography and cardiac conductance catheters are commonly used in published studies and are vulnerable to misinterpretation. Two-dimensional echocardiography depends on geometric assumptions which may not be valid following myocardial infarction given the alterations in left ventricular geometry. A study comparing two-dimensional echocardiography with MRI in both normal and chronically infarcted rat hearts demonstrated that measurements made by the two methods were correlated. However, cine-MRI measurements of ejection fraction were $12 \pm 6\%$ higher when compared to 2D echocardiography, which they attributed to the differences in temporal resolution (4.6ms for MRI and 8.3ms for echocardiography). A higher temporal resolution results in more images obtained per cardiac cycle meaning you would be more likely to image true end diastole and end systole. They also found that MRI was more reproducible in repeated studies (Stuckey *et al.*, 2008). This study was performed in rats and it is not known how these two techniques compare in mice. However, given that mice have smaller hearts and faster heart rates, the higher spatial and temporal resolutions of cine MRI are likely to be in its favour. Unlike two-dimensional echocardiography, three-dimensional echocardiography does not rely on geometric assumptions and has been used to try to overcome this limitation (Dawson *et al.*, 2004). That study demonstrated excellent correlations for measurements of

ventricular volumes, function, mass and infarct size. They also found good agreement in myocardial mass and infarct size when measured using three-dimensional echocardiography and at necropsy. The advantage of the three dimensional echocardiography in this study was that it took 4 minutes to obtain the three dimensional data set with the whole study taking 10 minutes in contrast to MRI which took 40 to 60 minutes (Dawson *et al.*, 2004). However, they used a bespoke imaging platform and data reconstruction software for the three-dimensional echocardiography study which would limit transferability to other research groups.

Following peri-infarct transplantation of human CDCs into immunodeficient mice, Smith and colleagues demonstrated a significant decline in LV function within 2 days. Moreover, the further decline in LV function seen in control mice at 3 weeks was not seen in CDC treated mice (Smith *et al.*, 2007). This suggests that the main action of CDCs is in the prevention of adverse left ventricular remodelling. The results described in this chapter are in agreement and also demonstrate that there is a reduction in adverse remodelling following delivery of CDCs. This beneficial effect was also seen in endoglin depleted CDCs suggesting that endoglin plays no role in this process. However, the numbers of animals per group was low (n=4) and this experiment is being repeated to validate this finding.

The *in vivo* cardiac function in the δ-sarcoglycan deficient mouse (*Sgcd-/-*) was first described in our institution by Bauer et al. using cardiac conductance catheters. He demonstrated that at 16 weeks of age there was no difference in ventricular volumes, but there were significant differences in systolic and contractile function in these mice compared to controls. However, due to alterations on preload and afterload these mice maintained their stroke volume and cardiac output, resulting in a compensated cardiomyopathy (Bauer *et al.*, 2008). At the time of our initial experiments MRI had not been used to measure cardiac structure and function in the *Sgcd-/-* mouse. However, Wansapura et al. have subsequently used MRI to assess these mice at 32 weeks of age. They demonstrated that these mice have an increased left ventricular mass. There was no difference in left ventricular end diastolic volume but right ventricular end diastolic volume was significantly increased. Also both left and right ventricular ejection fractions were significantly reduced (Wansapura *et al.*, 2011). We measured left ventricular mass, volumes and function at 32 weeks. In agreement with

Wansapura we also demonstrated an increased LV mass with no difference in left ventricular end diastolic volume. In contrast to their results we did not demonstrate any change in left ventricular ejection fraction. The reasons for this difference are unclear but I used only male mice and Wansapura do not comment on gender in their paper, so it is possible that there are gender difference in the *Sgcd-/-* mouse but this has not been investigated.

In conclusion, the work described in this chapter demonstrates that cardiac MRI can be used as an accurate, non-invasive method of measuring cardiac structure and function in various mouse models of cardiac disease, with methods and data being comparable to those in the published literature. Establishing this valuable technique has enabled me to use cardiac MRI in my studies investigating the role of endoglin in the cells of the heart in vivo as will be described in chapter 5. However, I first evaluated the role of endoglin in the cardiac fibroblast using an *in vitro* approach and this is described in the next chapter.

Chapter 4 The effect of endoglin depletion on primary mouse cardiac fibroblasts.

4.1 Introduction

In contrast to the human heart, cardiac fibroblasts compromise approximately 30% of the adult murine heart (Banerjee *et al.*, 2007). As discussed in chapter 1, cardiac fibroblasts play an integral part in the structure and function of the heart. However, they also play an important role in cardiac diseases with fibrosis an important factor in the development and progression of cardiac disease (Leask, 2007; Krenning *et al.*, 2010; Leask, 2010). Endoglin appears to be involved in the regulation of fibrosis in a number of organ systems. However, studies examining the role of endogen in the fibrotic response *in vitro* suggest a conflicting role for endoglin, with some studies suggesting it negatively regulates fibrosis (Diez-Marques *et al.*, 2002; Leask *et al.*, 2002; Burke *et al.*, 2010; Holmes *et al.*, 2011), whereas others suggest it is a positive regulator (K. Chen *et al.*, 2004; Meurer *et al.*, 2010; Shyu *et al.*, 2010; Morris *et al.*, 2011; Kapur *et al.*, 2012). A number of methods were used in these studies, including over expression of endoglin (Leask *et al.*, 2002; Holmes *et al.*, 2011), inhibition of endoglin with siRNA (Burke *et al.*, 2010) or antibodies directed against endoglin (K. Chen *et al.*, 2004). However, *in vivo* data from endoglin heterozygous mice demonstrate that endoglin haploinsufficiency results in reduced fibrosis following tissue injury, suggesting that endoglin positively regulates the fibrotic response (Docherty *et al.*, 2006; Scharpfenecker *et al.*, 2009; Kapur *et al.*, 2012).

My hypothesis was that endoglin was a regulator of cardiac fibrosis, most likely a positive regulator, and that a novel approach was needed to elucidate its role. Therefore, I chose to develop an *in vitro,* inducible endoglin knockdown model to further investigate the role of endoglin in the regulation of cardiac fibrosis.

The aims of these experiments was to establish primary cultures of mouse cardiac fibroblasts, identify whether these cells express endoglin, establish the conditional knockdown of endoglin and to investigate the effect of endoglin knockdown on the fibroblast response to TGFβ1.

4.2 Results

4.2.1 Establishing mouse primary cardiac fibroblast culture

To achieve the aims of this study I first needed to establish primary cultures of murine cardiac fibroblasts. One of the commonest methods in the literature is enzymatic digestion of the heart, followed by a short period of attachment, after which the non-adherent cells are discarded. The majority of these adherent cells are fibroblasts and are cultured until confluent and then passaged (Eghbali *et al.*, 1991b; Peng Li *et al.*, 2008; Y. Chen *et al.*, 2009; Shyu *et al.*, 2010). In fact a similar method was used in our laboratory to deplete fibroblasts from primary rat cardiomyocyte cultures. I adapted these methods to develop the final protocol described in chapter 2. In initial experiments I used a single heart to obtain fibroblasts. However, although these cells attached to the culture dish they were sparsely distributed and did not proliferate. In order to increase the seeding density I pooled 3 hearts during the digestion period. Again these cells rapidly adhered to the culture dish (figure 4.1A) and reached confluence after 4 days (figure 4.1E). Figure 4.1 shows these fibroblasts in the first 4 days of culture. It demonstrates how the small round cells that adhere to the culture dish develop the morphological characteristics of fibroblasts, which are a flat, spindle shaped cell with multiple processes emanating from the cell body (Souders *et al.*, 2009).

It is necessary to characterise these cells to ensure that they are fibroblasts and there is minimal contamination with other cell types. Cardiac fibroblasts are of mesenchymal origin, so in order to confirm that the isolated cells are indeed fibroblasts I performed immunocytochemistry with an antibody against vimentin. Vimentin is a type III intermediate filament protein expressed in mesenchymal cells. Figure 4.2 demonstrates that on the first day after isolation (figure 4.2A), the majority of cells express vimentin confirming them as fibroblasts. The number of cells expressing vimentin remains high at passage 2 (figure 4.2E). The vimentin staining pattern seen in figure 4.2E clearly demonstrates the morphological characteristics of fibroblasts. These cells do not express the endothelial cell marker CD31 (figure 4.2B&F) and nor do they express α-smooth muscle actin immediately after isolation (figure 4.2C).

However, by passage 2 some cells do express α-smooth muscle actin suggesting conversion from a fibroblast to a myofibroblast phenotype (figure 4.2G).

As two previous studies demonstrating that endoglin is expressed in cardiac fibroblasts used rat primary cardiac fibroblasts (K. Chen *et al.*, 2004; Shyu *et al.*, 2010), it was important to demonstrate that endoglin is also expressed on mouse primary cardiac fibroblasts in culture. To do this I performed immunocytochemistry using an antibody against endoglin. Figure 4.3 demonstrates that mouse primary cardiac fibroblasts express endoglin at passage 1 and 2.

Now that I had established the culture of mouse primary cardiac fibroblasts it was necessary to develop an *in vitro* model to investigate the effects of endoglin knockdown on these fibroblasts.

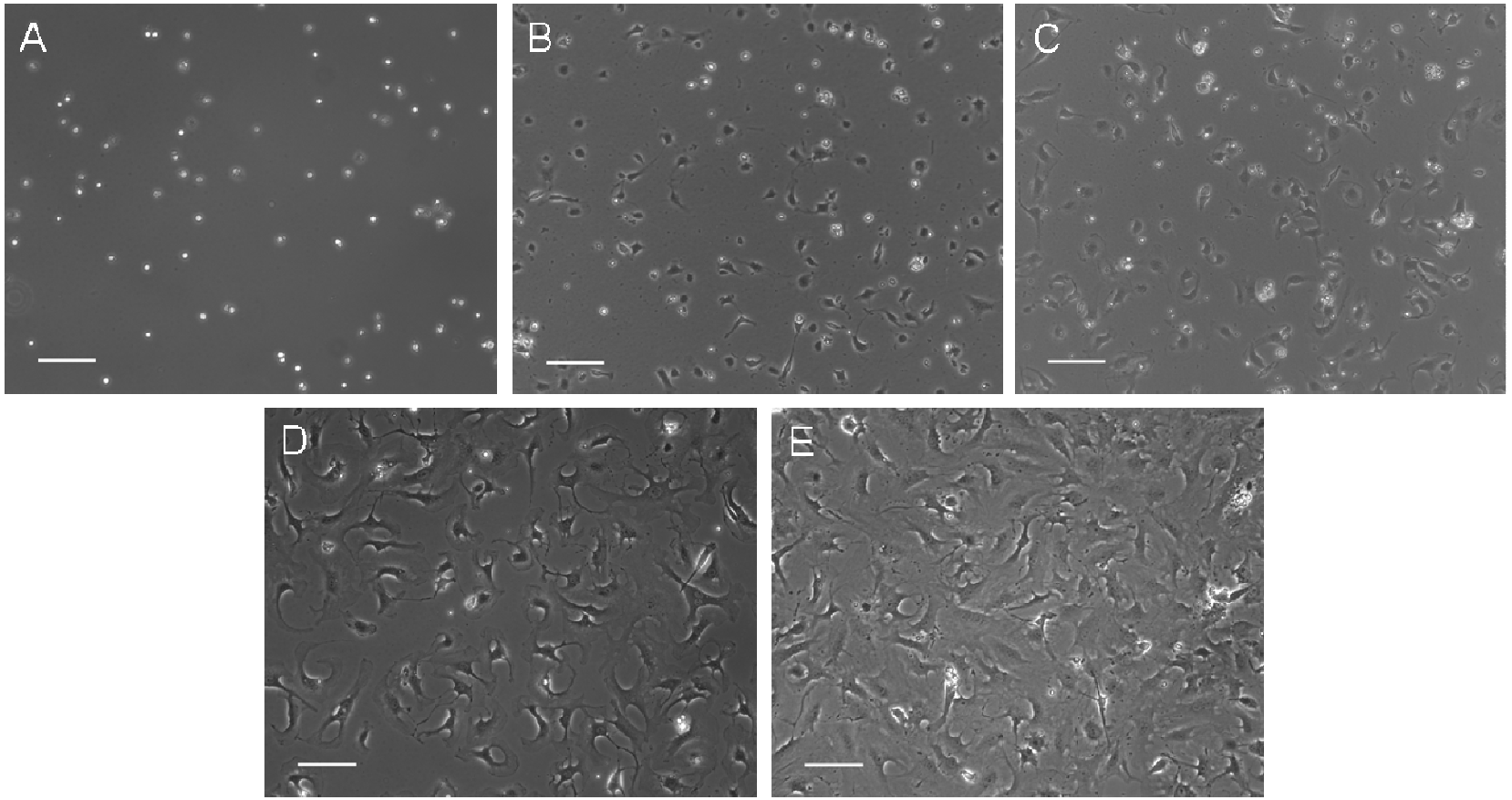

Figure 4.1 Primary mouse cardiac fibroblasts in culture.

Following enzymatic digestion of adult heart tissue, the digested cells were plated into a T75 flask. Following 90 minutes the flasks were rinsed with PBS to remove non-adherent cells. Adherent cells (A) were then cultured in DMEM with 10% FCS and 1% penicillin/streptomycin. The cells were then cultured for 4 days (B-E) until confluent (E). They were then passaged and fibroblasts from passage 2 were used for subsequent experiments.

(A=day 0, B=day1, C=day 2, D=day 3 and E=day 4. Scale bar=100μm).

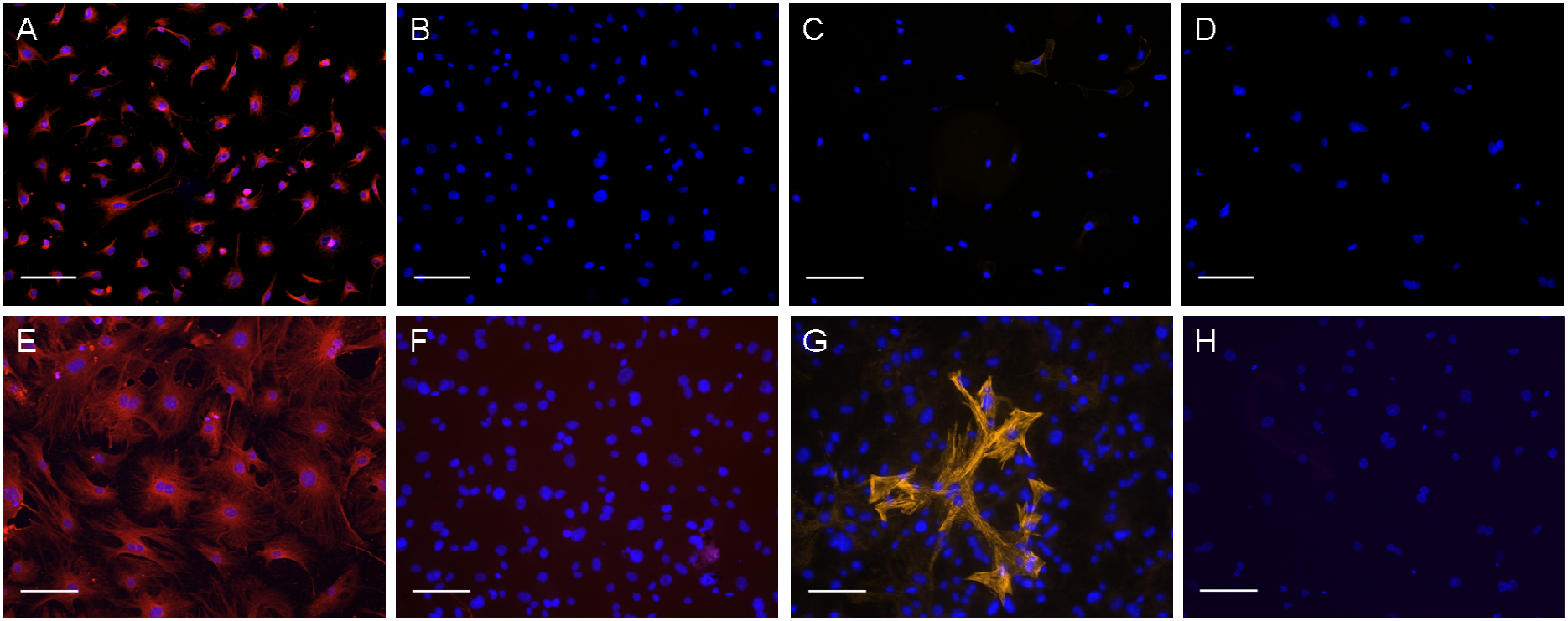

Figure 4.2 Characterisation of primary cardiac fibroblasts in culture.

Primary cardiac fibroblasts at passage 0 (A-D) and passage 2 (E-H) were immunostained with antibodies to vimentin (A & E), CD31 (B & F) and α smooth muscle actin (C & G). Representative no primary controls are shown in D & H. (Scale bar 100μm).

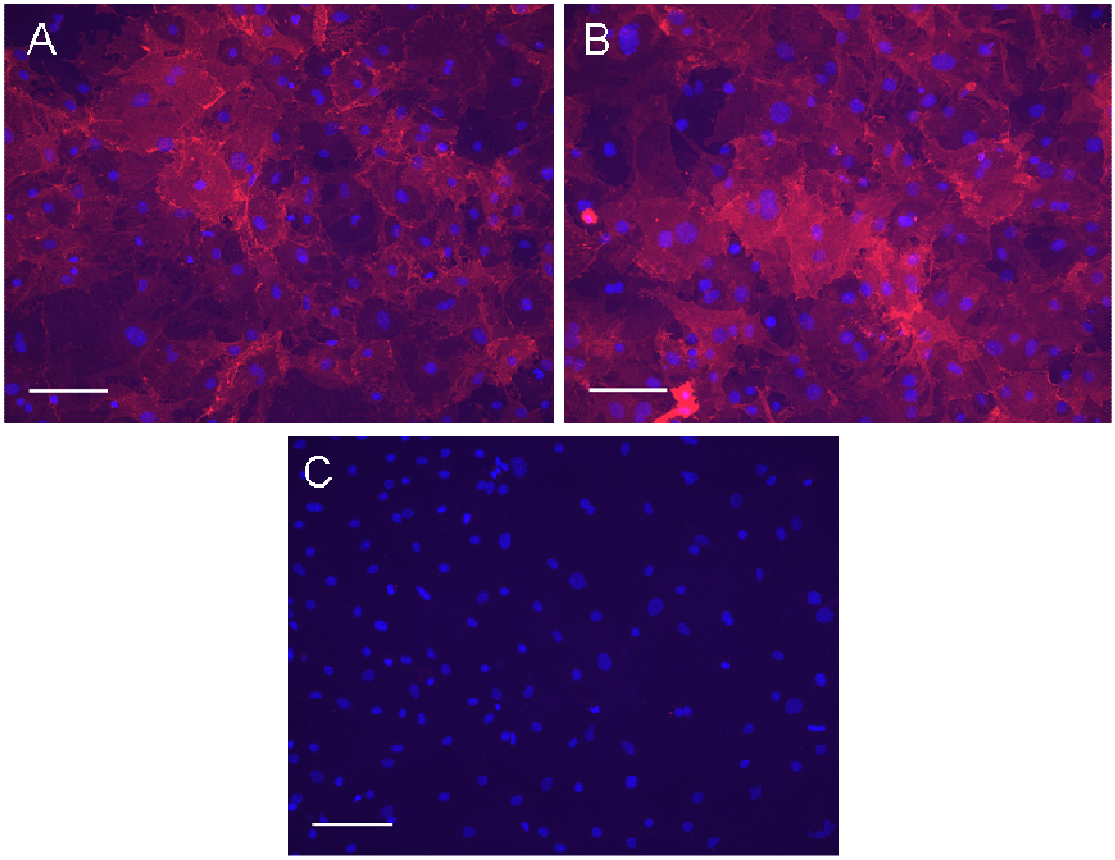

Figure 4.3 Endoglin expression in mouse primary cardiac fibroblasts.

Endoglin is expressed in mouse primary cardiac fibroblasts at passage 1 (A) and passage 2(B). No primary control, C. Scale bar 100 μm.

4.2.2 Endoglin depletion in mouse primary cardiac fibroblasts.

I next aimed to generate cardiac fibroblasts in which knockdown of endoglin could be achieved in a time specific manner using Cre-Lox genetics. As we did not have a fibroblast specific inducible Cre recombinase at this time I chose to use the ubiquitously expressed, tamoxifen inducible *Rosa26-Cre^{ERT2}* transgenic mouse line (Cheng *et al.*). This line drives expression of a mutated oestrogen receptor (ER^{T2}) fused to Cre recombinase in most cell types. Binding of 4-hydroxytamoxifen to the receptor results in activation of the Cre recombinase (Feil *et al.*, 1997). This mouse line was crossed with our floxed endoglin line to give *Eng$^{fl/fl}$;Rosa26-Cre^{ERT2}* mice enabling temporal regulation of endoglin knockdown *in vitro* using 4-hydroxytamoxifen.

4.2.2.1 *Rosa26-Cre^{ERT2}* is expressed in primary cardiac fibroblasts

Although the Rosa26 promoter drives ubiquitous gene expression and therefore *Rosa26-Cre^{ERT2}* should express *Cre^{ERT2}* in all cell types it was important to demonstrate that it was expressed in my cultured fibroblasts. To investigate this I used the Rosa26R reporter, which monitors Cre expression (Soriano, 1999). In this line, the *lacZ* gene is inserted into the ubiquitously expressed Rosa26 locus. However, a PGK neo cassette flanked by loxP sites is present that blocks transcription of the *lacZ* gene (figure 4.4A). In the presence of Cre recombinase this PGK neo cassette is excised following Cre/lox recombination and allows the transcription of the *lacZ* gene(Soriano, 1999). When stained with X-gal the beta galactosidase enzyme encoded by *lacZ* converts the colourless X-gal to a blue precipitate that is easily visible in white light. So those cells in which the Cre recombinase was activated, and hence the *lac Z* gene expressed, will appear blue.

Eng$^{fl/fl}$; Rosa26-Cre^{ERT2} mice were crossed with *Rosa26R* mice to produce *Eng$^{fl/fl}$;Rosa26-Cre^{ERT2};R26R* mice. Cardiac fibroblasts were isolated and cultured from the hearts of these mice. Culture medium containing various concentrations of 4-hydroxytamoxifen (1, 2 and 5 μM) was added to the cardiac fibroblasts at passage 1 or 2 to activate the Cre recombinase. They were then cultured for a further 72 hours following which they were fixed and stained with X-gal. Figure 4.4 demonstrates

widespread blue staining of fibroblasts at all concentrations of 4-hydroxytamoxifen used. There are a small number of unstained cells and these represent cell that don't express either *Rosa26-Cre^{ERT2}* or the Rosa26 reporter, demonstrating that the Rosa locus is not 100% ubiquitous.

These data clearly demonstrate that *Rosa26-Cre^{ERT2}* is expressed in primary cardiac fibroblasts. However, the efficiency of endoglin knockdown in these cells is of greater importance for this study and this was tested as follows.

4.2.2.2 Endoglin is efficiently depleted in *Eng$^{fl/fl}$; Rosa26-Cre^{ERT2}* primary cardiac fibroblasts.

Although Cre activation is required for Cre/lox recombination and the knockdown of endoglin (figure 4.5A), it is essential to demonstrate efficient knockdown and identify the concentration of 4-hydroxytamoxifen needed to achieve this. Primary cardiac fibroblasts isolated from *Eng$^{fl/f}$;Rosa26-Cre^{ERT2};R26R* mice were exposed to 4-hydroxytamoxifen at varying concentrations as described above. First, I confirmed that exons 5 and 6 of the endoglin gene had been deleted using genomic PCR (figure 4.5B). Second, I performed immunocytochemistry using an antibody against endoglin to confirm endoglin protein had also been depleted. Figure 4.6 demonstrates that at all concentrations of 4-hydroxytamoxifen used, endoglin is efficiently depleted from the primary cardiac fibroblasts. In order to quantify the efficiency of endoglin knockdown, four random fields of view were obtained and the total number of cells and the number of cells expressing endoglin were counted. Efficiency of knockdown was then calculated which demonstrates that in cells at passage 1 and 2, and all concentrations of 4-hydroxytamoxifen used, there is greater than 95% depletion of endoglin (figure 4.6I). These cells will be termed endoglin knockdown (*Eng-IKO^{u}*) fibroblasts for the remainder of this chapter.

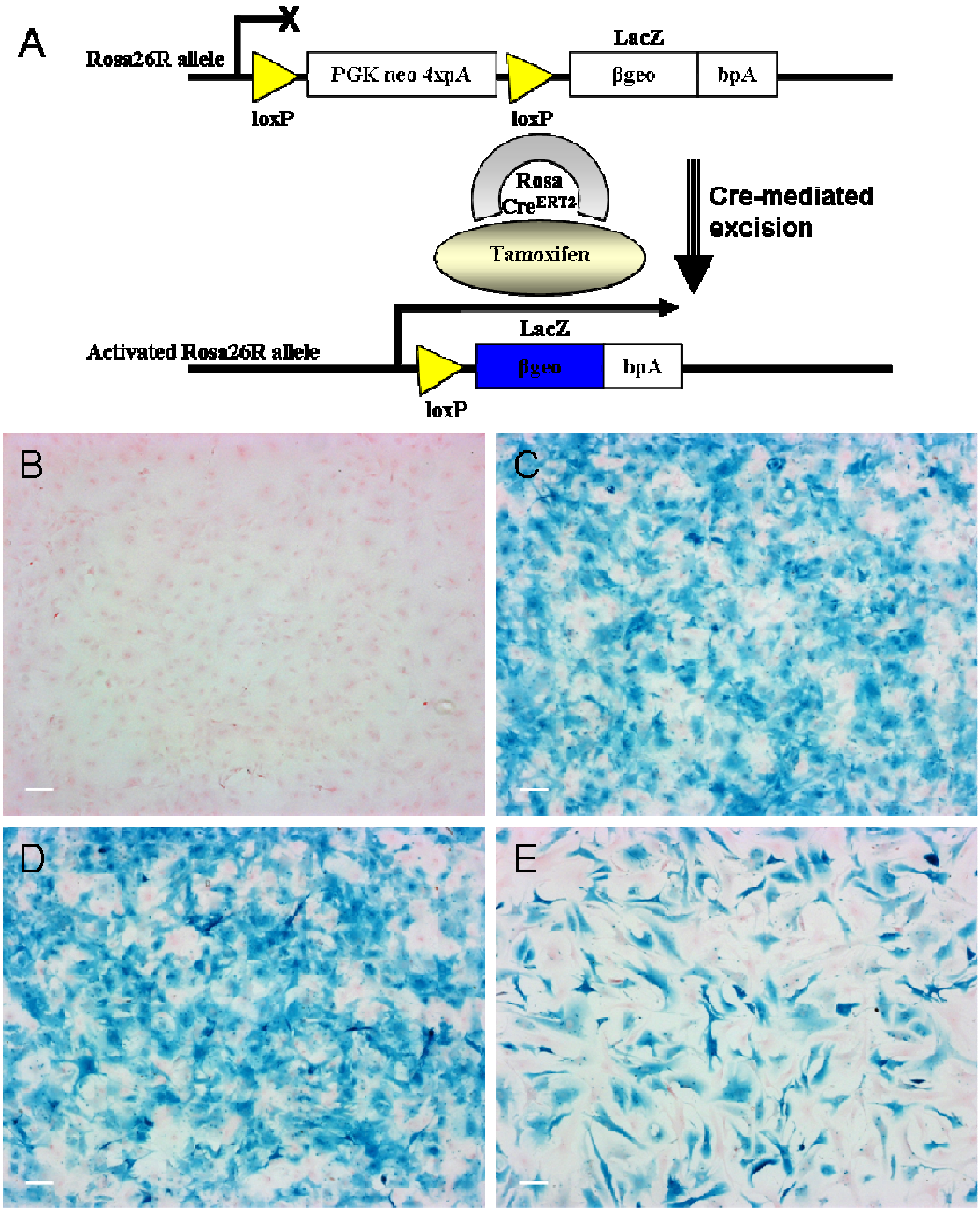

Figure 4.4 Cre activation in primary cardiac fibroblasts isolated from *Eng$^{fl/fl}$;Rosa26-Cre^{ERT};Rosa26R* mice.

A, schematic showing Cre/lox recombination of the *Rosa26R* allele in the presence a tamoxifen inducible Cre recombinase resulting in the expression of β-galactocidase. **B – E**, X-gal staining, for β-galactosidase, demonstrating Cre activation in primary cardiac fibroblasts isolated from *Eng$^{fl/fl}$;Rosa26-Cre^{ERT};Rosa26R* mice following incubation with various concentrations of 4-hydroxytamoxifen. (**B** = no 4-hydroxytamoxifen, **C** = 1μM 4-hydroxytamoxifen, **D** = 2μM 4-hydroxytamoxifen and **E** = 5μM 4-hydroxytamoxifen). Cells were counterstained with eosin. Scale bar = 100 μm.

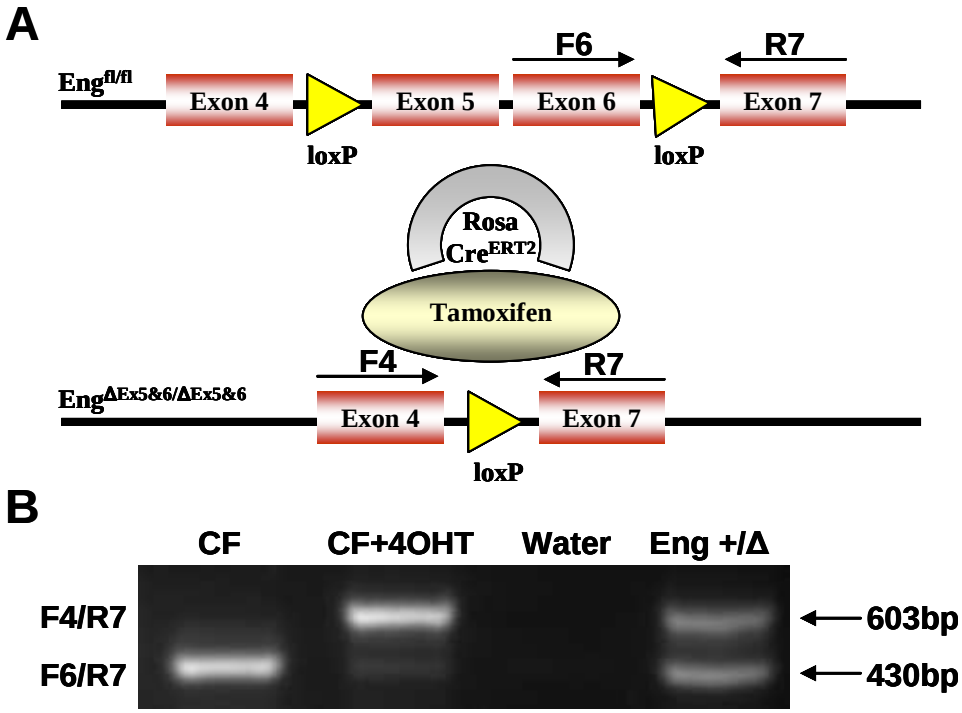

Figure 4.5 Treatment of *Eng$^{fl/fl}$; Rosa26-Cre^{ERT2}* primary cardiac fibroblast with 4-hydroxytamoxifen resulted in excision of exons 5 and 6.

A. Schematic showing the position of the primers in the endoglin gene before and after Cre mediated excision of exons 5 and 6. **B.** Agarose gel showing the PCR products amplified from genomic DNA isolated from *Eng$^{fl/fl}$;Rosa26-Cre^{ERT2}* cardiac fibroblasts (CF) with and without treatment with 1μM 4-hydroxytamoxifen (4-OHT) for 72 hours. The gain of the 603bp F4/R7 PCR product and loss of the 430bp F6/R7 PCR product demonstrates the presence of the endoglin deleted allele in fibroblast cells only after exposure to 4-OHT. (Note that the size of the F4/R7 PCR product from the floxed endoglin allele prior to recombination is too large to be amplified by standard PCR methods.)

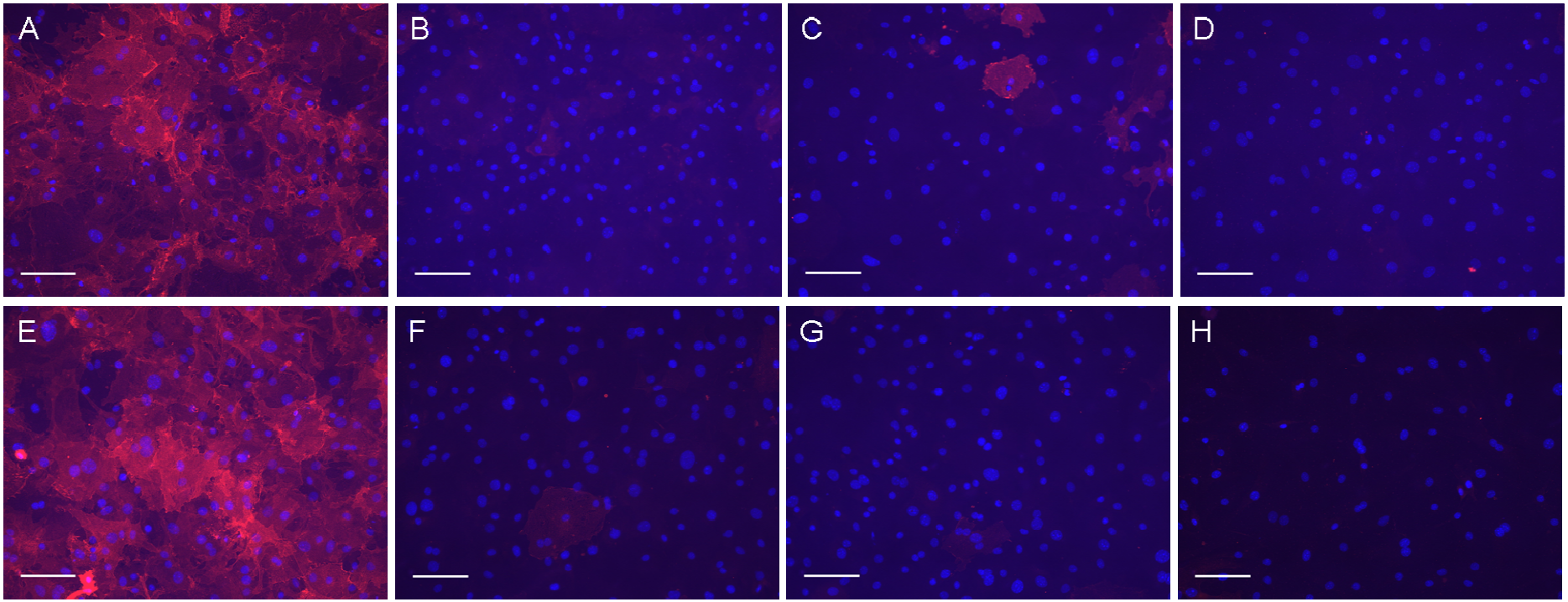

I

	1uM	2uM	5uM
Passage 1	96%	94%	97%
Passage 2	97%	99%	98%

Figure 4.6 Endoglin expression in *Eng$^{fl/fl}$; Rosa26-Cre^{ERT2}* primary cardiac fibroblasts is depleted following treatment with 4-hydroxytamoxifen.

Primary cardiac fibroblasts at passage 1 (A-D) and passage 2(E-H) were treated with different concentrations of 4-hydroxytamoxifen for 72 hours. A & E – no 4-hydroxytamoxifen, B & F, 1µM, C & G, 2µM and D &H, 5µM. The table in I shows the efficiency of endoglin knock down in passage 1 and 2 fibroblasts with the different concentrations of 4-hydroxytamoxifen. Scale bars 100µm.

4.2.2.3 4-hydroxytamoxifen has no effect on the viability of primary cardiac fibroblasts.

In order to knockdown endoglin *in vitro*, 4-hydroxytamoxifen needs to be added to the cells. Consequently I needed to ensure that it is not toxic to the fibroblasts at the concentration required to knockdown endoglin. I addressed this by performing a MTT assay on my primary cardiac fibroblasts prepared from $Eng^{fl/fl}$ mice.

MTT (3-(4,5-Dimethylthiazol-2-yl)-2,5-diphenyltetrazolium bromide) is a yellow tetrazole, that enters the cell and passes into the mitochondria. Once there it is reduced by mitochondrial succinate dehydrogenase to a water-insoluble, purple formazan product. Following incubation with MTT, an organic solvent (dimethyl sulphoxide, DMSO) is added to the cells to dissolve the formazan and produce a purple coloured solution. The absorbance of this solution can be measured spectrophotometrically. As the reduction reaction can only occur in metabolically active cells the absorbance is proportional to the viability of the cells (Mosmann, 1983).

In this experiment primary cardiac fibroblasts at passage 1 were seeded into a 96 well plate (5000 cells per well) and incubated with 4-hydroxytamoxifen (0, 1, 2, 5 μM, using 3 technical replicates at each concentration) for 4 days. The MTT assay was then performed as described in chapter 2. Figure 4.7 confirms that 4-hydroxytamoxifen has no effect on primary cardiac fibroblast viability at any of the concentrations examined (ANOVA, p=0.642)

As a result of these experiments I chose to use 1μM 4-hydroxytamoxifen in all subsequent experiments as it efficiently knocks down endoglin and is not toxic to the fibroblasts.

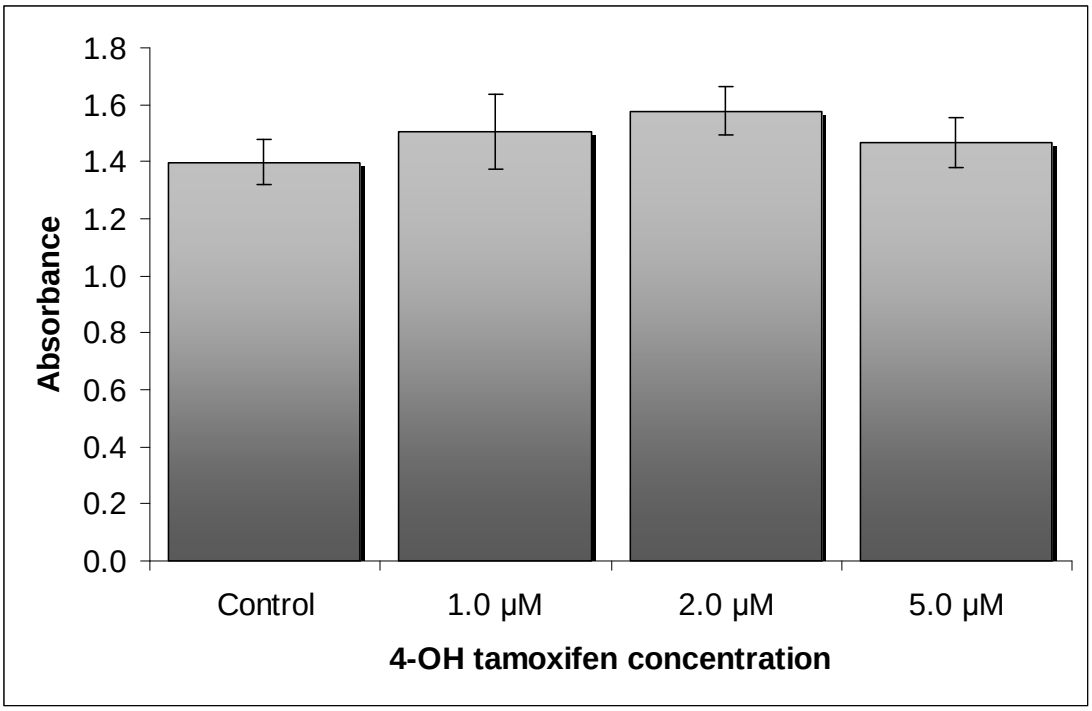

Figure 4.7 MTT assay of primary cardiac fibroblasts from *Eng*$^{fl/fl}$ mice following incubation with various concentrations of 4-hydroxytamoxifen.

Absorbance of the solubilised formazan product was measured at 570nM. There was no significant difference in absorbance at any of the concentrations used (ANOVA, p=0.642) demonstrating that 4-hydroxytamoxifen does not effect cell viability. Data expressed as mean ± SE.

4.2.3 The effect of endoglin knockdown on TGFβ signalling pathways in response to TGFβ1 stimulation

The aim of these experiments was to investigate the effect endoglin knockdown had on components of the TGFβ signalling pathway, including Smad phosphorylation and of selected downstream genes that were related to the cardiac fibrotic response.

4.2.3.1 TGFβ1 stimulation of primary cardiac fibroblasts results in Smad2 phosphorylation.

The initial aim of this experiment was to establish whether serum starvation was necessary for the Smad phosphorylation experiments, to determine the optimum dose of TGFβ1 required and the duration of stimulation.

It is common to serum starve fibroblasts prior to TGFβ1 stimulation experiments, because TGFβ1 and related growth factors are present in the serum used in complete growth media (Goustin *et al.*, 1986). However, when the fibroblasts are serum starved there can be cell death (Leicht *et al.*, 2001). This is dependent on the conditions used so it was important to assess the viability of these cells over the potential time course of the experiment. This was achieved using the MTT assay to monitor cell viability, as described above. Again primary cardiac fibroblasts from $Eng^{fl/fl}$ mice, at passage 1, were seeded into 96 well plates (5000 cells per well, 8 replicates per time point) and allowed to adhere overnight before serum starvation (0.2% foetal calf serum) for 16, 24 and 40 hours. Following this period of starvation an MTT assay was performed. For the control sample the MTT assay was performed after overnight adherence only and represents the viability of the cells prior to serum starvation. Figure 4.8 shows the absorbance of the solubilised formazan product at the different time points. It demonstrates a significant reduction in absorbance with the serum starved cells compared to control (ANOVA, $p<0.001$). This likely represents a reduction in both cell viability and metabolic activity as the MTT assay does not distinguish between the two. However, there is no difference between absorbance over the course of serum starvation (ANOVA, $p=0.318$) suggesting that no further cell death occurs but the cells remain quiescent.

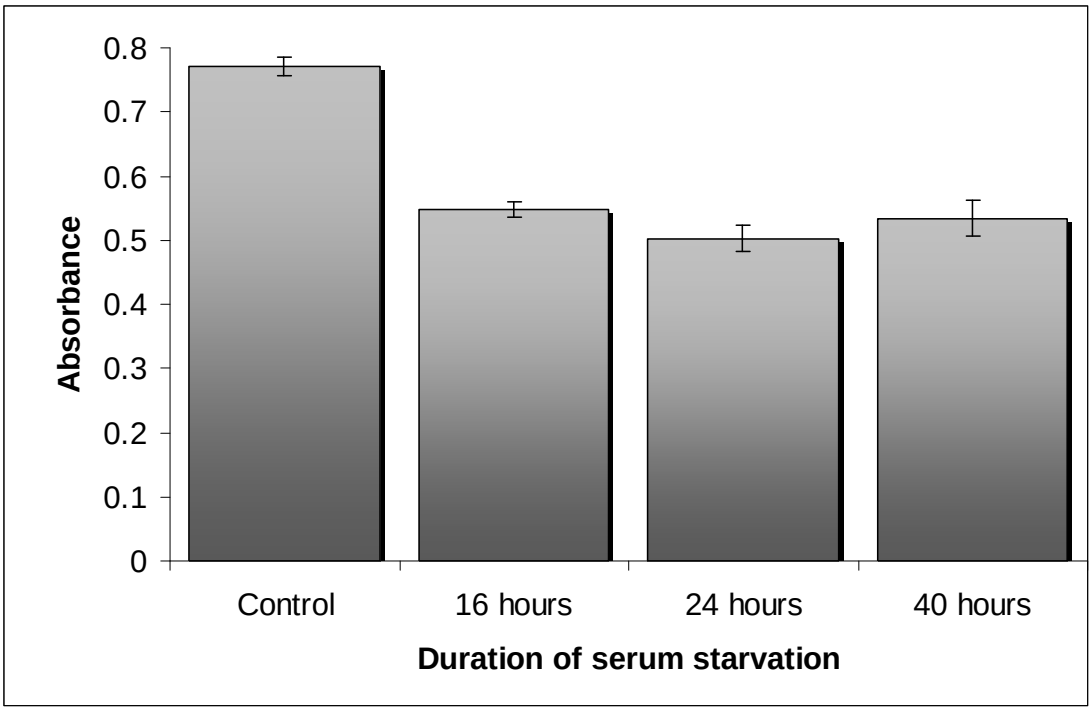

Figure 4.8 MTT assay of primary cardiac fibroblasts from *Eng*$^{fl/fl}$ mice following serum starvation.

Absorbance of the solubilised formazan product was measured at 570nM. There was a significant reduction in absorbance of the control sample compared to the serum starved samples at all time points (ANOVA, $p<0.001$) but no difference between the different durations of serum starvation (ANOVA, $p=0.318$). This demonstrates that there is a reduction in cell viability/metabolic activity by 16 hours following serum starvation, but the cells remained quiescent without a reduction in viability for the duration of the experiment. Data expressed as mean ± SE.

To determine the optimal dose and incubation time to investigate the effect of endoglin depletion on Smad phosphorylation following TGFβ1 stimulation I performed 2 experiments. The first addressed the effect of serum starvation and concentration of TGFβ1 on the primary cardiac fibroblasts. In this experiment primary cardiac fibroblasts were seeded onto 6 well plates (100,000 cells per well). Following overnight adherence the cells were cultured for a further 24 hours in either normal media or low serum media (0.2% FCS). The cells were then stimulated with TGFβ1, at concentrations of 0, 5 and 10ng/ml, for 30 minutes. Following this the cells were collected for western blot analysis using antibodies to phospho-Smad2 and total Smad2. Figure 4.9A demonstrates that in the absence of TGFβ1 there is minimal phosphorylation of Smad2. Following stimulation with both doses of TGFβ1 Smad2

becomes phosphorylated. This phosphorylation appears to be greater in the cells that were serum starved prior to stimulation.

The second experiment aimed to establish the optimal duration of TGFβ1 stimulation. In this experiment following seeding and adherence in 6 well plates the primary cardiac fibroblasts were serum starved for 24 hours followed by stimulation with 5ng/ml of TGFβ1 for 15, 30 and 60 minutes. Again the cells were collected for western blot analysis as described above. Figure 4.9B demonstrates that Smad 2 phosphorylation occurs with in 15 minutes and remains for at least 60 minutes.

Following these results I decided that in all subsequent western blot experiments, the primary cardiac fibroblasts would be serum starved in 0.2% FCS for 24 hours prior to stimulation with 5ng/ml $TGF\beta_1$ for 30 minutes.

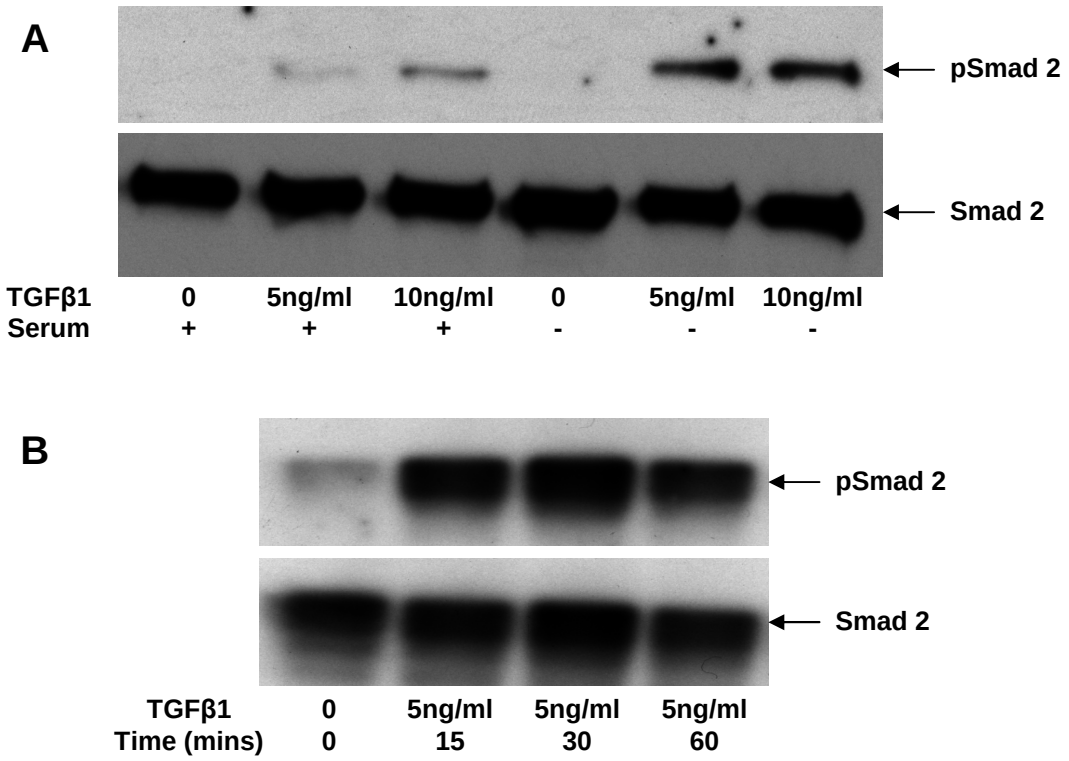

Figure 4.9 Phosphorylation of Smad2 following TGFβ1 stimulation of primary cardiac fibroblasts from *Eng*$^{fl/fl}$ mice.

A, phosphorylation of Smad2 in primary cardiac fibroblasts with and without serum starvation (0.2% FCE for 24 hours), in response to TGFβ1 at 5 and 10ng/ml. B, phosphorylation of Smad2 over time following stimulation with 5ng/ml TGFβ1 in serum starved primary cardiac fibroblasts. Total Smad2 levels were similar in all samples. These experiments were repeated 3 times with similar results.

4.2.3.2 Endoglin knockdown in primary cardiac fibroblasts does not affect Smad phosphorylation following TGFβ1 stimulation.

To investigate the effect of endoglin knockdown on Smad phosphorylation in response to $TGF\beta_{1,}$ primary cardiac fibroblasts from *Eng*$^{fl/fl}$*;Rosa26-Cre*^{ERT2} and *Eng*$^{fl/fl}$ mice were cultured. All cells were treated with 4-hydroxytamoxifen and cardiac fibroblasts from *Eng*$^{fl/fl}$ mice were used as controls. The primary cardiac fibroblasts were treated with 4-hydroxytamoxifen at passage 1 and grown to confluence. They were then passaged and seeded to 6 well plates (100,000 cells per well). Following overnight adherence, they were serum starved for 24 hours followed by stimulation with 5ng/ml TGFβ1 for 30 minutes. The cells were then collected for western blot analysis. To investigate the effects of endoglin knockdown on TGFβ1/Alk5 signalling and TGFβ1/Alk1 signalling pathways, phospho-Smad 2/Smad2 ratio and phospho-Smad 1,5,8/Smad 1 ratio, respectively, were calculated. Figure 4.10 demonstrates that TGFβ1 stimulation results in phosphorylation of Smad2 in both control and endoglin knockdown (*Eng-iKO*^{u}) fibroblasts (p=0.005 and p=0.001, respectively). Although following TGFβ1 stimulation mean phopho-Smad2/Smad2 ratio appears lower in the fibroblasts with endoglin knockdown, the difference is not statistically significant (p=0.247). Figure 4.11 shows that there is a reduction in phospho-Smad 1/5/8/Smad 1 ratio in endoglin depleted fibroblasts with an increase following TGFβ1 stimulation compared to control fibroblasts. However, these changes are not statistically significant. These results demonstrate that the response to TGFβ1 stimulation may be different between control and endoglin depleted fibroblasts. Any small change in Smad phosphorylation is likely to lead to larger changes in downstream gene expression and so I chose to investigate effect of TGFβ1 on gene expression of TGFβ receptors, as well as the downstream genes Id1 and Pai-1.

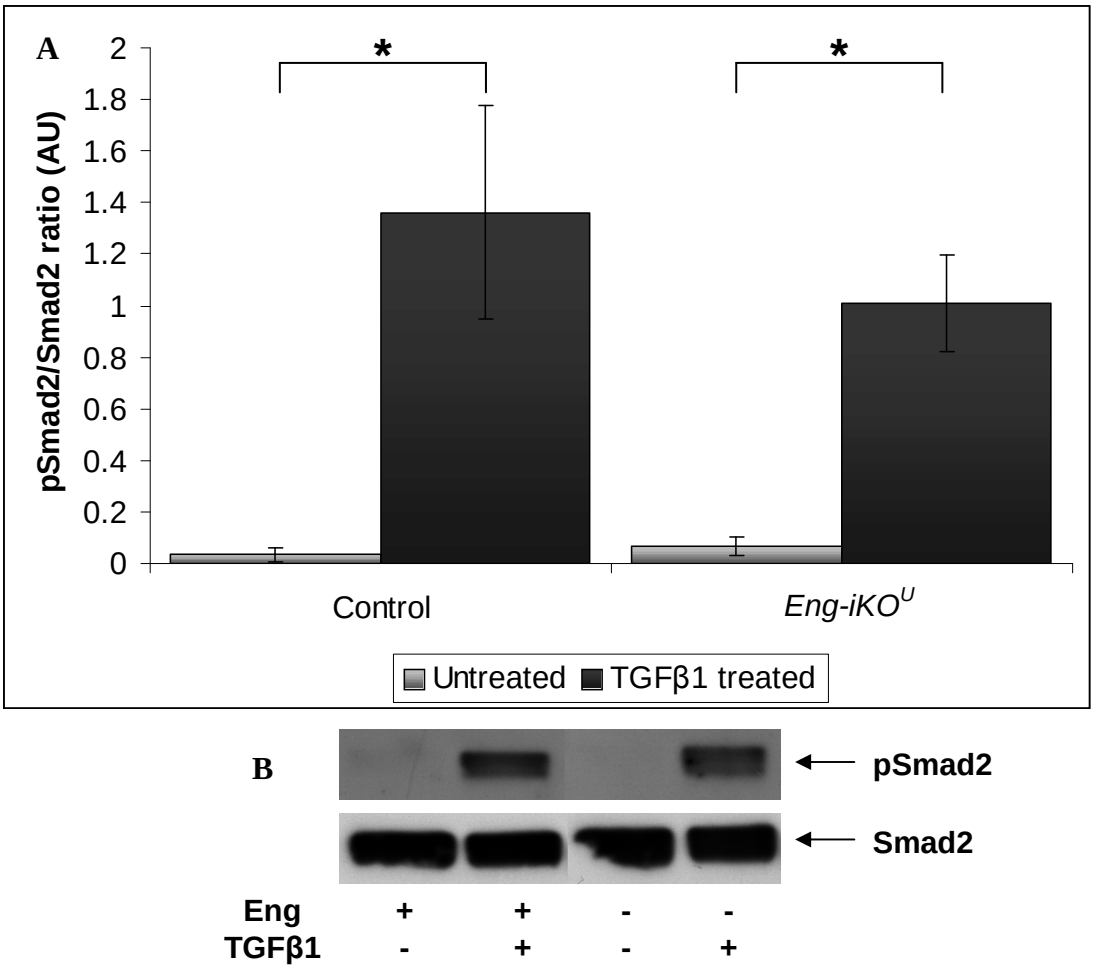

Figure 4.10 Effect of endoglin knockdown on Smad2 phosphorylation following TGFβ1 stimulation.

A. Endoglin knockdown resulted in a small, non-significant reduction in Smad2 phosphorylation in response to TGFβ1. Data from three biological replicates are presented as mean ± SD, n=3.

B. A representative western blot experiment shows TGFβ1stimulates phosphorylation of Smad2 in the absence of endoglin.

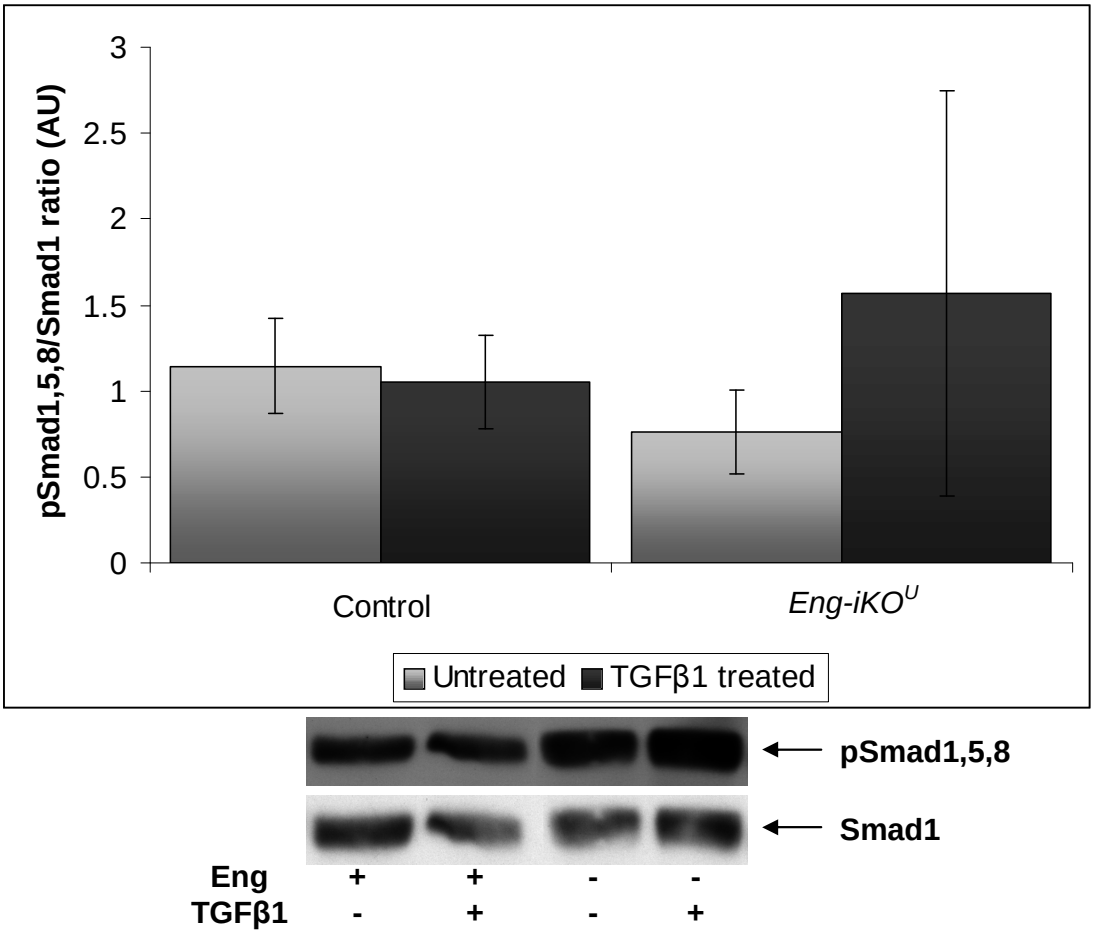

Figure 4.11 The effect of TGFβ1 stimulation on Smad1/5/8 phosphorylation in control and endoglin depleted fibroblasts.

A. Smad 1/5/8 was already phosphorylated in serum starved, unstimulated fibroblasts and was not induced by TGFβ1. Endoglin knockdown had no significant effect. Data from three biological replicates are presented as mean ± SD, n=3.

B. A representative western blot experiment shows phosphorylation of Smad1/5/8 in the absence of endoglin, with and without TGFβ1 stimulation (5ng/ml for 30 minutes).

4.2.3.3 The effect of endoglin knockdown on expression of TGFβ receptor genes and downstream signalling genes.

To investigate the effect of endoglin depletion on the expression of TGFβ receptors genes and downstream signalling genes, quantitive real time PCR (qPCR) was performed on primary cardiac fibroblasts with and without endoglin knockdown.

In these experiments all primers, except TGFβ1, were already in use in our laboratory and are summarised in table 2.7. The primers for amplifying TGFβ1 cDNA were previously published (Davidson *et al.*, 2006). The TGFβ receptor genes I investigated were the type I receptors, Alk1 and Alk5, the type II receptor (Tgfbr2) and endoglin on the basis that endoglin regulates the balance between Alk1 and Alk5 signalling (figure 1.2). To demonstrate differences in target gene activation I investigated Id1 and Id2 (inhibitor of DNA binding 1 and 2), expressed following activation of the Alk1/Smad1/5/8 pathway, and Pai-1 (plasminogen activator inhibitor 1, also known as Serpine1), expressed following Alk5/Smad2/3 activation. I also investigated any effect on transcription of TGFβ1 ligand. I used three housekeeping genes (glyceraldehyde-3-phosphate dehydrogenase (Gapdh), hypoxanthine-guanine phosphoribosyltransferase (Hprt) and β-actin) for data normalisation (see chapter 2). Table 2.7 gives details of the primers used to identify the expression of these genes and the PCR efficiency. All qPCR reactions used the SYBR green quantitative method (described in chapter 2). Figure 4.12 shows the dissociation curves for these primers used during typical qPCR reactions. This demonstrates a single melting peak for all PCR products, except for Alk5 (this will be discussed further below), confirming primer specificity. Mean PCR efficiency of each primer pair was determined from the slopes of the qPCR amplification curve using the LinReg method (table 2.7) (Ramakers *et al.*, 2003; Karlen *et al.*, 2007).

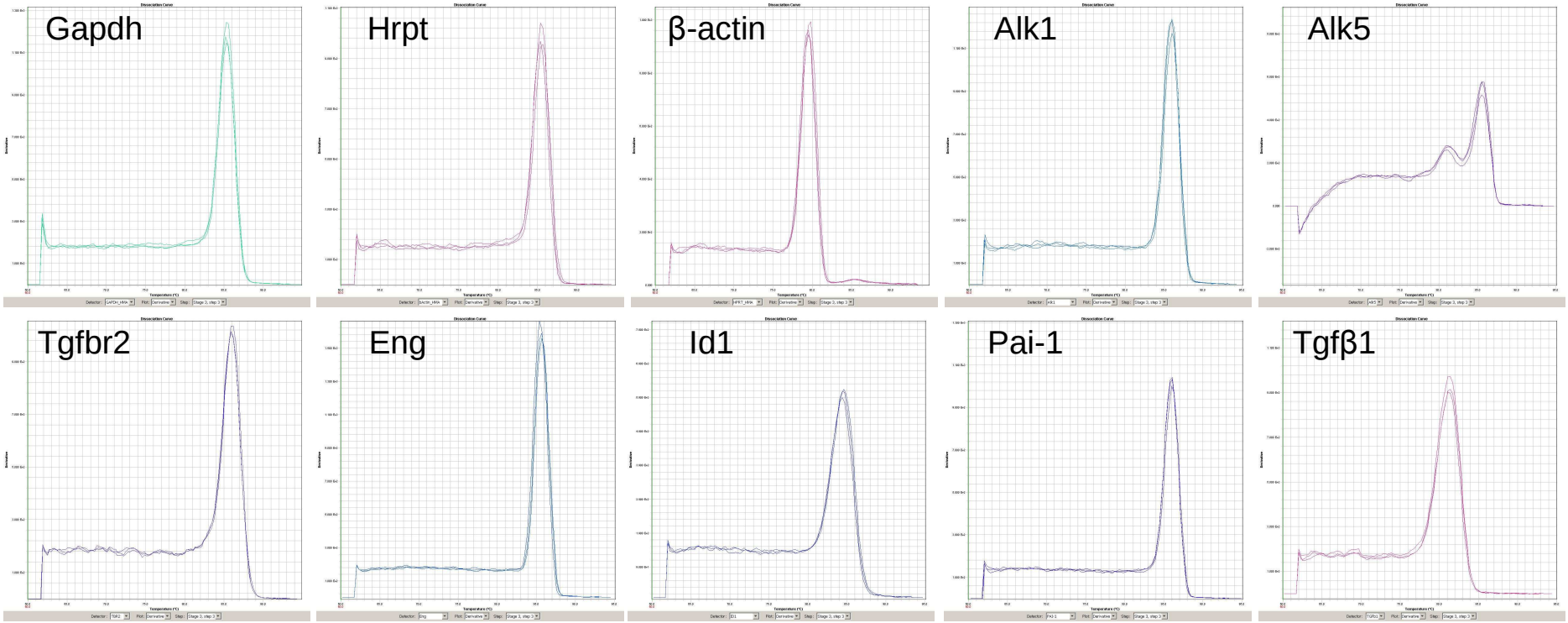

Figure 4.12 Dissociation curves of the qPCR product for each primer pair.

The single peak confirms that the primers are specific and give a single PCR product, with the exception of Alk5, which has a shape indicating more than one PCR product.

These experiments were performed with primary cardiac fibroblasts isolated from hearts of *Eng*$^{fl/fl}$ and *Eng*$^{fl/fl}$*;Rosa26-Cre*^{ERT2} mice. All cells were treated with 4-hydroxytamoxifen (1μM) at passage 1. Once they had reached confluence the fibroblasts were passaged and seeded onto 6 well plates (100,000 cells per well). They were then cultured in normal media for 24 hours. In order to assess the effect of endoglin depletion on primary cardiac fibroblasts under normal conditions, serum starvation was not used in these experiments. However, subsequent experiments assessing the effect of endoglin depletion on TGFβ1 stimulation, serum starvation was performed as for the western blot experiments above. The fibroblasts were lysed using RLT buffer (Qiagen) and stored at -80°C. Following RNA extraction and reverse transcription, as described in chapter 2, qPCR was performed using the above primers. Gene expression in endoglin depleted fibroblasts (Eng-iKO^{U}) relative to control fibroblasts was calculated using the comparative Ct method, described in chapter 2.

The relative gene expression levels are given in table 4.1. As the relative gene expression data is exponential the data was log transformed prior to graphical representation as shown in figure 4.14 and figure 4.15. As would be expected there is a significant, 14.7 fold reduction in endoglin expression ($p<0.0001$) following endoglin knockdown. There is no difference in Alk1 gene expression but there appears to be a significant, 14.7 fold increase in Alk5 expression ($p=0.001$) following endoglin knockdown. However, as mentioned above the dissociation curve for Alk5 shows the presence of 2 peaks. This indicates more than one PCR product is present but is unlikely to be due to genomic DNA contamination as the both primers span exon boundaries. Therefore, this suggests that there is primer dimer formation resulting in a false positive result.

To further clarify the effect of endoglin knock down on Alk5 gene expression I used commercially available primers (Qiagen Quantitect primers) to repeat the experiment. These primers amplified a 120bp amplicon in exons 4 and 5. The dissociation curves for these primers shows a single peak confirming specificity (figure 4.13). The qPCR results are shown in table 4.1 and demonstrate that endoglin knock down has no effect on Alk5 gene expression ($p=0.88$).

Following endoglin knockdown there is no difference in expression of Pai-1 (p=0.49) or Tgfβ1. There is a small (1.2 fold), but statistically significant, increase in Id1 expression (p=0.047) following endoglin knockdown, suggesting that the Alk1/Smad1/5/8 pathway is activated following endoglin knockdown.

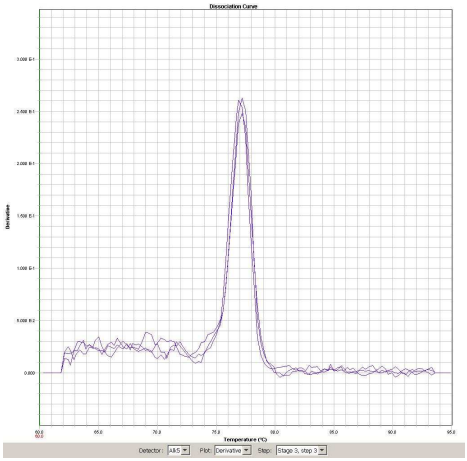

Figure 4.13 Dissociation curve for qPCR products using Qiagen Quantitect primers for Alk5. This demonstrates a single peak confirming primer specificity.

Table 4.1 Relative gene expression of TGFβ receptor and downstream signalling genes in primary cardiac fibroblasts with endoglin knockdown compared to control.
Compared to control fibroblasts, endoglin knockdown results in no difference in Alk1, Pai-1 or Tgfβ1 gene expression. As would be expected there is 14.7 fold reduction in endoglin gene expression in fibroblasts following endoglin knockdown compared to control. There is a small but significant increase (1.2 fold difference) in Id1 gene expression in fibroblasts with endoglin knockdown compared to control. Data presented a mean ± SD, n=3 biological replicates per group.

	Alk1	**Alk5 (Quantitect)**	**Endoglin**	**Id1**	**Pai-1**	**Tgfβ$_1$**
Control	1.0 ± 0.27	1.0 ± 0.26	**1.0 ± 0.03**	**1.0 ± 0.04**	1.0 ± 0.07	1.0 ± 0.05
Eng-iKO^u	1.3 ± 0.67	1.0 ± 0.39	**0.068 ± 0.03**	**1.2 ± 0.14**	1.1 ± 0.34	0.9 ± 0.34
p value	0.58	0.88	**<0.0001**	**0.047**	0.49	0.23

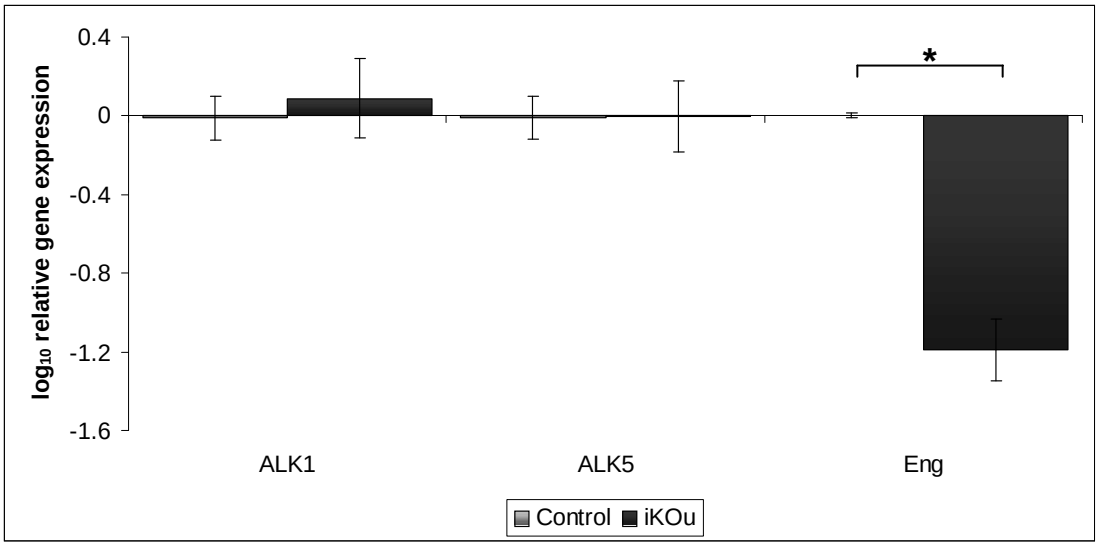

Figure 4.14 The effect of endoglin knockdown on the relative gene expression of TGFβ receptors in primary cardiac fibroblasts.

Following endoglin knockdown there is a significant (14.7 fold) decrease in endoglin expression. There is no significant difference in the expression of the type I receptors, Alk1 or Alk5. Data expressed as mean ± SD, n=3 per group, *p<0.001.

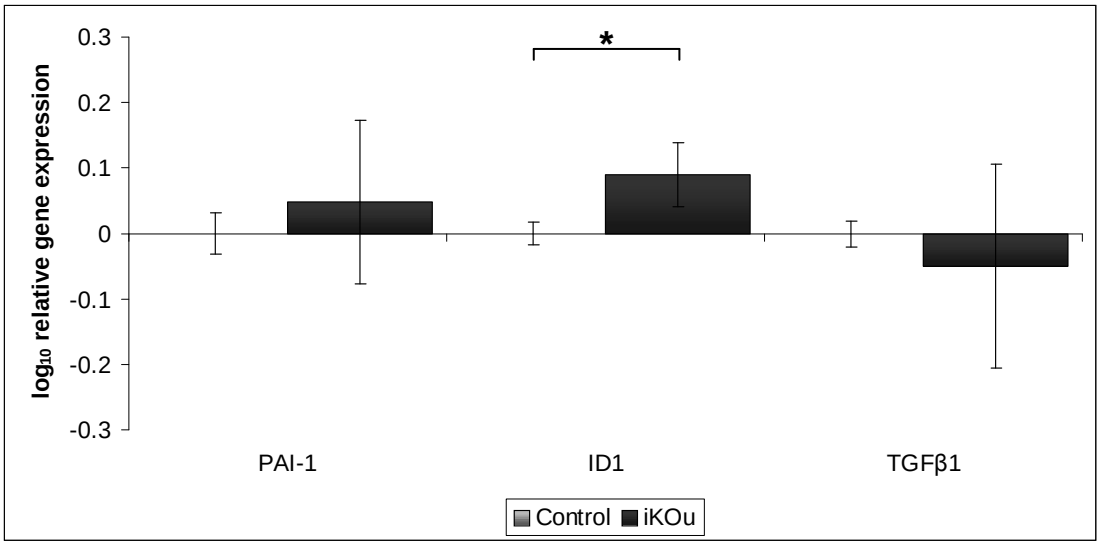

Figure 4.15 The effect of endoglin knockdown on the relative gene expression of TGFβ target genes in primary cardiac fibroblasts.

There is no significant difference in Pai-1 or TGFβ1 gene expression following endoglin knockdown. There is a small (1.2 fold) increase in Id1 expression. Data expressed as mean ± SD, n=3 biological replicates per group, *p=0.047.

4.2.3.4 The effect of endoglin knockdown on the expression of TGFβ receptors genes and downstream signalling genes in response to TGFβ1.

TGFβ1 is a major fibrogenic cytokine, and cardiac fibroblasts are primarily responsible for generating scar tissue following heart injury. I therefore investigated whether endoglin knockdown had any effect on collagen synthesis in cardiac fibroblasts following TGFβ1 stimulation. To do this, primary cardiac fibroblasts were isolated from hearts of *Eng*$^{fl/fl}$ and *Eng*$^{fl/fl}$*;Rosa26-Cre*^{ERT2} mice. All cells were treated with 4-hydroxytamoxifen (1μM) at passage 1. Once they had reached confluence the fibroblasts were passaged and seeded onto 6 well plates (100,000 cells per well). They were allowed to adhere overnight in normal media followed by serum starvation (0.2% FCS) for 24 hours prior to TGFβ1 stimulation. Fibroblasts were treated with 5ng/ml TGFβ1 or left untreated for 24 hours prior to harvest. The fibroblasts were lysed using RLT buffer (Qiagen) and stored at -80°C. Following RNA extraction and reverse transcription, as described in chapter 2, qPCR was performed using the primers in table 2.7. Gene expression in TGFβ1 treated fibroblasts relative to untreated fibroblasts, for both control and Eng-iKO^{U} fibroblasts, was calculated using the comparative Ct method as described in chapter 2 (table 4.2 and table 4.3).

In control fibroblasts (table 4.2 and figure 4.16) TGFβ1 stimulation resulted in down regulation of Alk1 (1.5 fold reduction, p=0.011) and a very small reduction in Tgfbr2 expression (1.1 fold reduction, p=0.018). In some (n=2) control fibroblast cultures there was very little change in endoglin expression in response to TGFβ1 stimulation. However, in one experiment there was an 8 fold increase in endoglin expression. As this response was not consistent between biological replicates it was not considered statistically significant, but should be monitored in future work. As expected, TGFβ1 stimulation in control fibroblasts resulted in significant up regulation of Pai-1 (2.3 fold increase, p=0.005) confirming activation of the Alk5/Smad2/3 pathway. There was also down regulation of the Alk1/Smad1/5/8 pathway with a significant down regulation of both Id1 (2.0 fold reduction, p=0.038) and Id2 (2.1 fold reduction, p=0.003). Finally, there was also a small increase in Tgfβ1 expression (1.2 fold increase, p=0.002).

Overall, TGFβ1 stimulation of fibroblasts following endoglin knockdown resulted in a similar change in gene expression to control fibroblasts. As with control fibroblasts, both Alk1 (1.5 fold reduction, $p=0.024$) and Tgfbr2 (1.2 fold reduction, $p=0.009$) were down regulated. Endoglin was up regulated following TGFβ1 stimulation (2.2 fold increase, $p=0.028$). The Alk5/Smad2/3 pathway is activated as shown by the 2.9 fold increase in Pai-1 expression ($p=0.002$) and Alk1/Smad1/5/8 pathway down regulated (3 fold reduction in Id1 expression ($p<0.0001$) and 2.3 fold reduction in Id2 expression ($p=0.004$)). Interestingly, in endoglin depleted fibroblasts, there is no increase in TGFβ1 expression following TGFβ1 stimulation ($p=0.8$), suggesting this response was endoglin dependent.

Table 4.2 Relative gene expression of TGFβ signalling pathway genes in control primary cardiac fibroblasts following TGFβ1 stimulation.

Compared to untreated fibroblasts, TGFβ1 stimulation resulted in up regulation of Pai-1 and $Tgf\beta_1$ and down regulation of Alk1, Tgfbr2 and Id1 and 2. Data expressed as mean ± SD, n=3 biological replicates per group.

	Control fibroblasts						
	Alk1	**Tgfbr2**	**Eng**	**Pai-1**	**Id1**	**Id2**	**Tgfβ1**
Untreated	1.0 ± 0.01	1.0 ± 0.002	1.0 ± 0.008	1.0 ± 0.033	1.0 ± 0.003	1.0 ± 0.001	1.0 ± 0.003
TGFβ1 treated	0.65 ± 0.14	0.89 ± 0.05	3.6 ± 4.35	2.3 ± 0.4	0.50 ± 0.3	0.47 ± 0.1	1.2 ± 0.04
p value	**0.011**	**0.018**	0.361	**0.005**	**0.038**	**0.003**	**0.002**

Table 4.3 Relative gene expression of TGFβ signalling pathway genes in endoglin depleted primary cardiac fibroblasts following TGFβ1 stimulation.

Compared to untreated fibroblasts, TGFβ1 stimulation resulted in up regulation of endoglin and Pai-1 and down regulation of Alk1, Tgfbr2 and Id1 and 2. There was no effect on Tgfβ1 expression. Data expressed as mean ± SD, n=3 biological replicates per group.

	Eng-iKO^{u} fibroblasts						
	Alk1	**Tgfbr2**	**Eng**	**Pai-1**	**Id1**	**Id2**	**Tgfβ1**
Untreated	1.0 ± 0.001	1.0 ± 0.001	1.2 ± 0.17	1.0 ± 0.06	1.0 ± 0.009	1.0 ± 0.01	1.0 ± 0.008
TGFβ1 treated	0.58 ± 0.21	0.85 ± 0.06	2.2 ± 0.48	2.9 ± 0.43	0.33 ± 0.02	0.43 ± 0.17	1.0 ± 0.12
p value	**0.024**	**0.009**	**0.028**	**0.002**	**<0.0001**	**0.004**	0.80

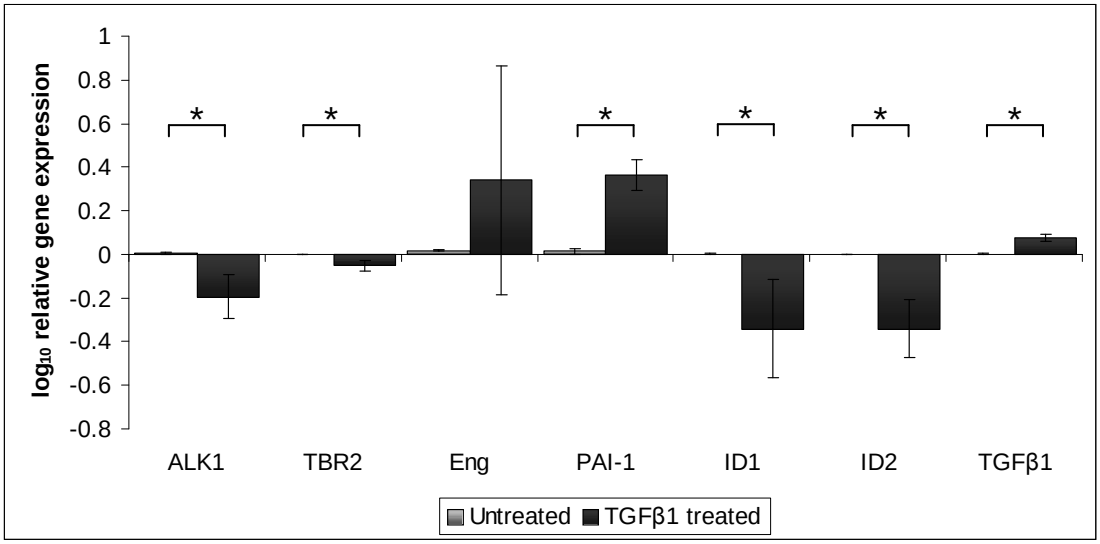

Figure 4.16 The effect of TGFβ1 stimulation on TGFβ signalling pathway gene expression in control fibroblasts.

Data expressed as mean ± SD, n=3 per group, *p<0.05

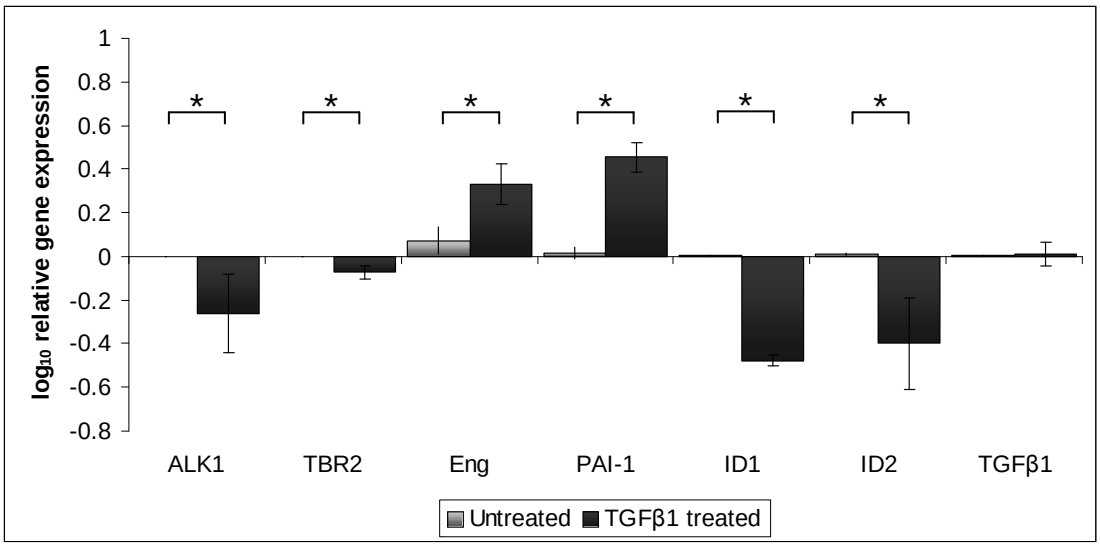

Figure 4.17 The effect of TGFβ1 stimulation on TGFβ signalling pathway gene expression in endoglin depleted fibroblasts.

Data expressed as mean ± SD, n=3 per group,*p<0.05

4.2.4 The effect of endoglin knockdown on expression of selected genes expressed in the extracellular matrix

To investigate the effect of endoglin knockdown on extracellular matrix gene expression qPCR was performed using primers to a number of genes involve in extracellular matrix remodelling (table 1.1). These were, type I collagen (Col1A1), type III collagen (Col3A1), connective tissue growth factor (Ctgf, also known as Ccn2), alpha smooth muscle actin (α-SMA, a marker of fibroblast to myofibroblast transformation), matrix metalloproteinases (Mmp) 2 and 9 and tissue inhibitors of metalloproteinases (Timp) 1 and 2. The details of the primers used in the qPCR experiments are given in table 2.7. These primers were taken from the online resource; primer bank (http://pga.mgh.harvard.edu/primerbank/), except for the primers for Ctgf which have been previously published (Davidson *et al.*, 2006). All these primers were specific as only a single peak was seen on their respective dissociation curves (figure 4.18).

4.2.4.1 The effect of endoglin knockdown on expression of extracellular matrix genes in unstimulated cells

The expression of ECM genes in control and endoglin depleted cardiac fibroblasts were compared under normal culture conditions as described in section 4.2.3.3 above. There were no significant differences in expression of these ECM genes between the control and endoglin depleted fibroblasts (table 4.4 and figure 4.19)

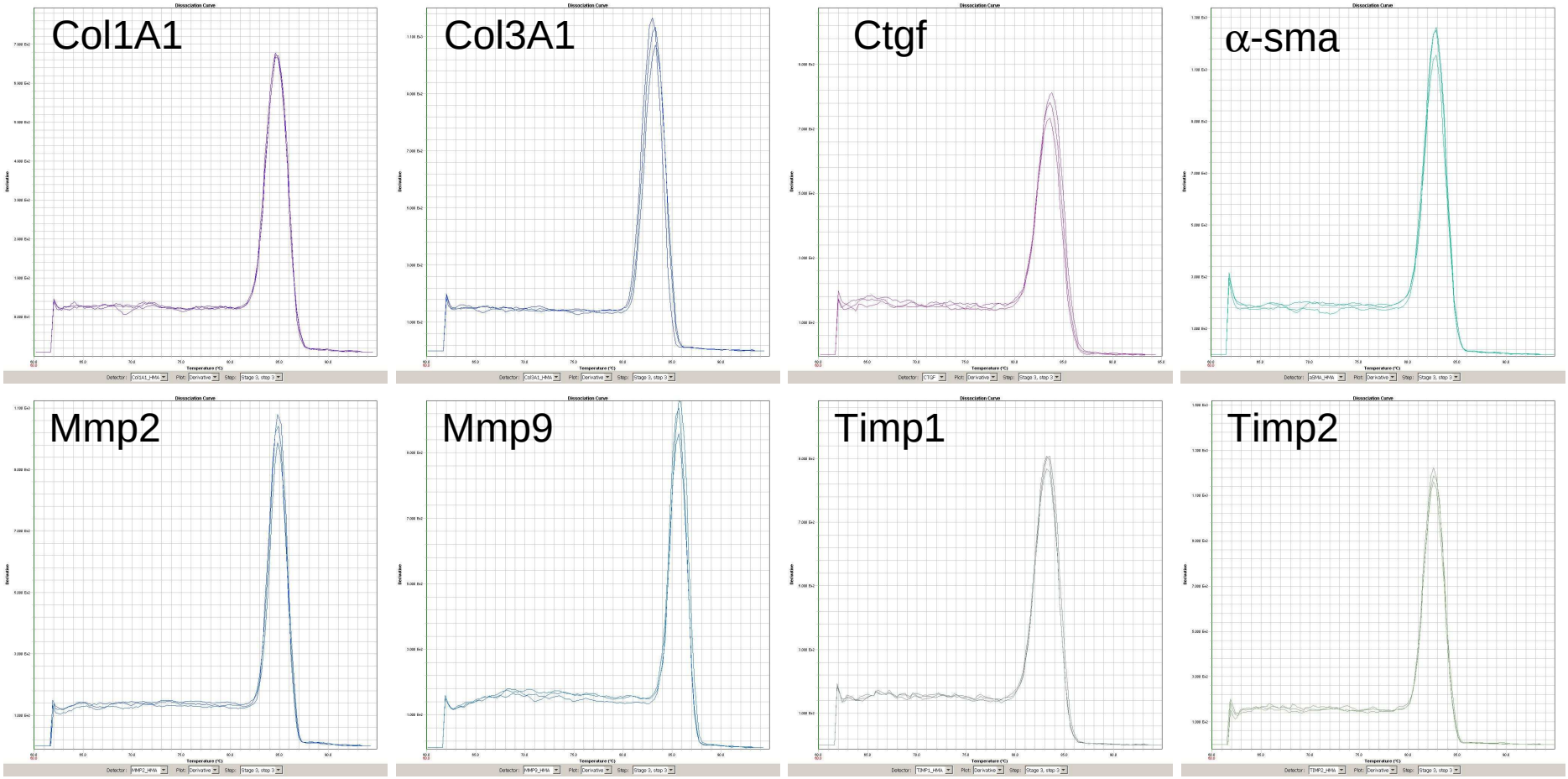

Figure 4.18 Dissociation curves of the qPCR product for each primer pair.

The single peak confirms that the primers are specific.

Table 4.4 Relative gene expression of extracellular matrix genes in primary cardiac fibroblasts with endoglin knockdown compared to control.

There was no difference in baseline expression of extracellular matrix genes in endoglin depleted fibroblasts compared to controls. Data expressed as mean ± SD, n=3 biological replicates for each group.

	Col1A1	**Col3A1**	**Ctgf**	**Mmp2**	**Mmp9**	**Timp1**	**Timp2**	**α-SMA**
Control	1.0 ± 0.06	1.0 ± 0.30	1.0 ± 0.12	1.0 ± 0.25	1.0 ± 0.63	1.0 ± 0.28	1.0 ± 0.23	1.0 ±0.11
Eng-iKO^{U}	1.0 ± 0.17	1.0 ± 0.19	0.88 ± 0.29	1.0 ± 0.067	0.79 ± 0.63	0.91 ± 0.28	0.94 ±0.30	0.89 ± 0.14
p value	0.93	0.88	0.54	0.84	0.70	0.72	0.80	0.36

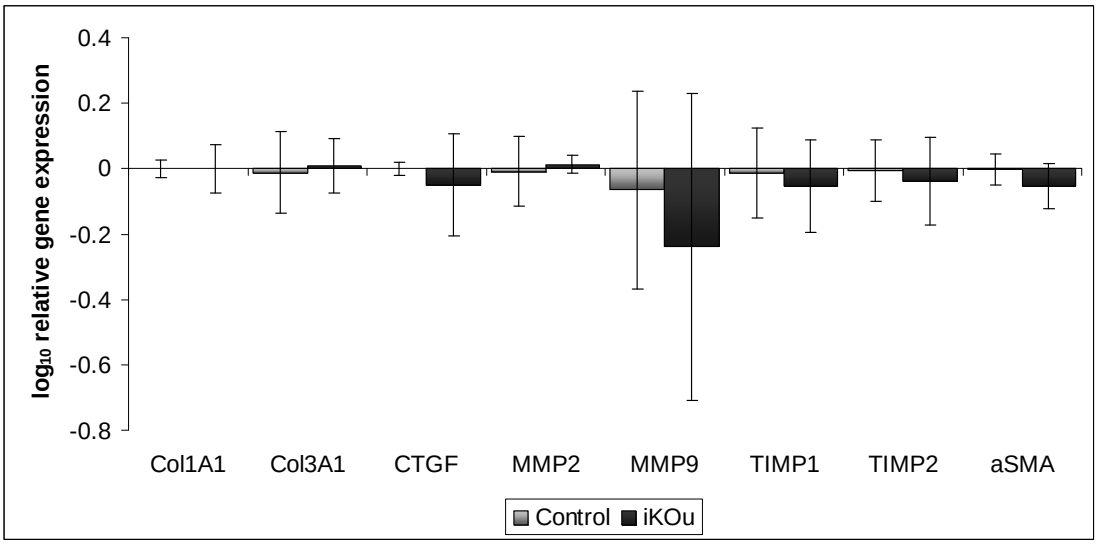

Figure 4.19 The effect of endoglin knockdown on the relative expression of extracellular matrix genes in primary cardiac fibroblasts.

There was no difference in expression of extracellular matrix genes in endoglin depleted fibroblasts compared to controls. Data expressed as mean ± SD, n=3 biological replicates for each group.

4.2.4.2 The effect of endoglin knockdown on the expression of extracellular matrix genes in response to TGFβ1.

The effect of TGFβ1 stimulation on fibroblasts with and without endoglin was examined as described in section 4.2.3.4 above.

Contrary to my expectations, collagen I expression was not increased in control fibroblasts following 24 hours of TGFβ1 stimulation (table 4.5 and figure 4.20). There was a significant down regulation of collagen III induction following TGFβ1 stimulation (2.3 fold reduction, $p=0.007$) whereas Ctgf was up regulated by 2.2 fold ($p<0.0001$) and αSMA by 2.5 fold ($p=0.025$). There was no significant change in either Mmp2 ($p=0.18$) or Mmmp9 ($p=0.13$) expression in response to TGFβ1. Timp1 gene expression was also unaffected ($p=0.29$) but Timp 2 was down regulated 1.8 fold ($p=0.023$).

TGFβ1 stimulation of endoglin depleted fibroblasts resulted in a significant down regulation of collagen III (3.2 fold reduction, $p=0.0001$) with an up regulation of both Ctgf (2.6 fold increase, $p=0.007$) and α-SMA (3.1 fold increase, $p=0.029$), similar to control fibroblasts. However, in contrast to control fibroblasts, endoglin depletion resulted in a 1.25 fold reduction in collagen I expression ($p=0.02$) and a 3.7 fold reduction in Mmp2 ($p<0.0001$) expression, following TGFβ1 stimulation. There appeared to be an increase in Mmp9 expression but this was not significant (1.64 fold increase, $p=0.065$), and was similar to the response in control fibroblasts. Timp1 expression remained unchanged ($p=0.14$) and Timp2 expression was reduced 2.8 fold ($p=0.0009$) in keeping with the response of control fibroblasts.

Overall, the results demonstrate that in contrast to control fibroblasts, endoglin knockdown results in down regulation of both type I collagen and Mmp2 gene expression in response to TGFβ1 stimulation suggesting that endoglin positively regulates their expression. Also, endoglin knockdown has little effect on the other extracellular matrix genes tested. However, changes in gene expression are dynamic and so further experiments would be needed to define the optimal conditions.

Table 4.5 Relative gene expression of extracellular matrix genes in control primary cardiac fibroblasts following TGFβ1 stimulation.

Compared to untreated fibroblasts, TGFβ1 resulted in up regulation of Ctgf and αSMA. There is down regulation of type III collagen and Timp1. There was no effect on type I collagen, Mmp2, Mmp9 and Timp2 gene expression. Data expressed as mean ± SD, n=3 biological replicates per group.

	Control fibroblasts							
	Col1A1	**Col3A1**	**Ctgf**	**Mmp2**	**Mmp9**	**Timp1**	**Timp2**	**α-SMA**
Untreated	1.0 ± 0.0004	1.0 ± 0.008	1.0 ± 0.004	1.0 ± 0.013	1.0 ± 0.036	1.0 ± 0.026	1.0 ± 0.003	1.0 ± 0.0009
TGFβ1 treated	1.0 ± 0.093	0.44 ± 0.19	2.2 ± 0.065	0.72 ± 0.32	1.6 ± 0.56	1.5 ± 0.71	0.55 ± 0.21	2.5 ± 0.73
p value	0.78	**0.007**	**<0.0001**	0.18	0.13	0.29	**0.023**	**0.025**

Table 4.6 Relative gene expression of extracellular matrix genes in endoglin depleted primary cardiac fibroblasts following TGFβ1 stimulation.

In contrast to control fibroblasts there is a significant down regulation of type I collagen and Mmp2. In keeping with control fibroblasts, TGFβ1 stimulation resulted in up regulation of Ctgf and αSMA, and down regulation of type III collagen and Timp2. There was no difference in expression of Mmp9 and Timp1. Data expressed as mean ± SD, n=3 biological replicates per group.

	Eng-iKO^{U} fibroblasts							
	Col1A1	**Col3A1**	**Ctgf**	**Mmp2**	**Mmp9**	**Timp1**	**Timp2**	**α-SMA**
Untreated	1.0 ± 0.006	1.0 ±0.046	1.0 ± 0.016	1.0 ± 0.008	1.0 ± 0.0005	1.0 ± 0.002	1.0 ± 0.033	1.0 ± 0.0005
TGFβ1 treated	0.78 ± 0.10	0.31 ± 0.063	2.6 ± 0.55	0.27 ± 0.066	1.64 ± 0.44	1.1 ± 0.14	0.36 ± 0.12	3.1 ± 1.1
p value	**0.02**	**0.0001**	**0.007**	**<0.0001**	0.065	0.14	**0.0009**	**0.029**

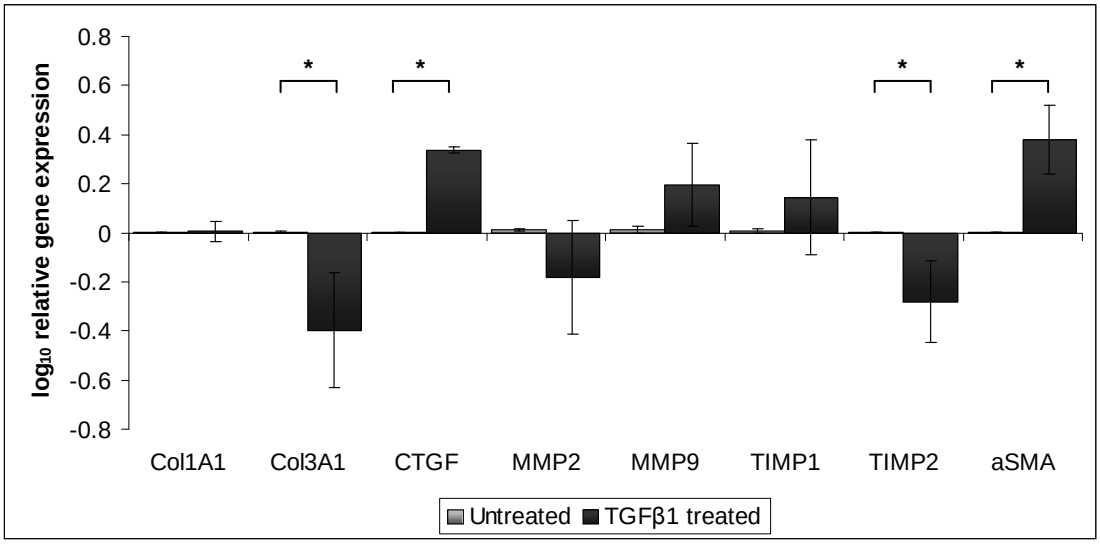

Figure 4.20 The effect of TGFβ1 stimulation on extracellular matrix gene expression in control fibroblasts.

Data expressed as mean ± SD, n=3 biological replicates per group, *p<0.05

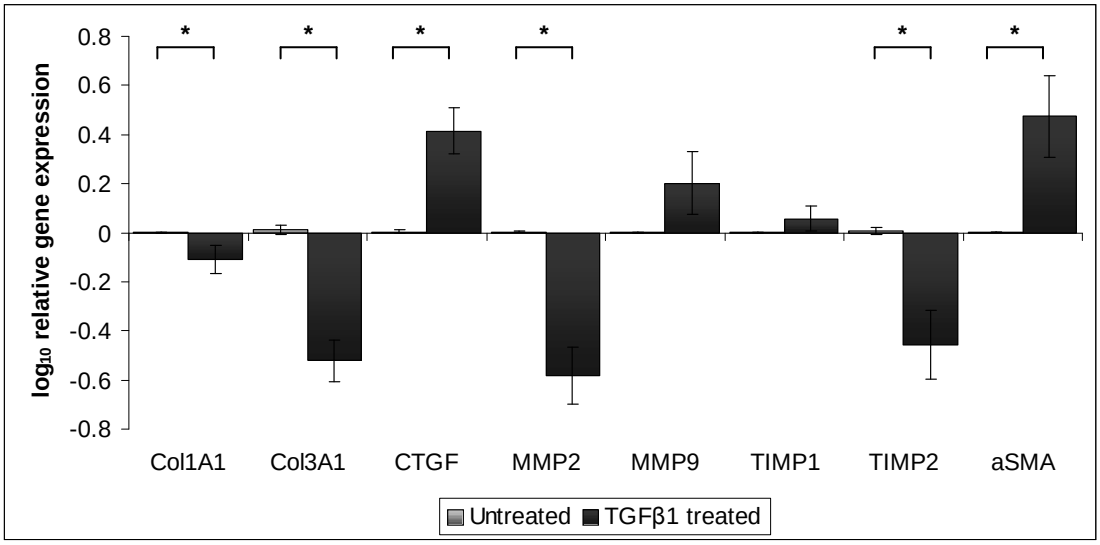

Figure 4.21 The effect of TGFβ1 stimulation on extracellular matrix gene expression in endoglin depleted fibroblasts.

Data expressed as mean ± SD, n=3 biological replicates per group, *p<0.05

4.2.4.3 TGFβ1 stimulation results in increased expression of α smooth muscle actin.

The change from fibroblast to myofibroblast is an important one during fibrosis (see chapter1) and this is associated with increased αSMA expression. Although induction of αSMA expression by TGFβ1 stimulation did not appear to be dependent on endoglin (figure 4.20 and figure 4.21), it was important to determine whether the frequency of myofibroblast differentiation was endoglin dependent. To do this, control and endoglin depleted primary cardiac fibroblast were serum starved for 24 hours followed by incubation with 5ng/ml TGFβ1 or normal media for a further 24 hours. Following this they were fixed and immunostained with an antibody to αSMA.

TGFβ1 stimulation of control primary cardiac fibroblasts resulted in an increased expression of αSMA protein (figure 4.22A and B). There was a similar increase in the expression of αSMA in endoglin depleted fibroblasts suggesting a similar level of differentiation to the myofibroblast phenotype and that this differentiation process was not endoglin dependent.

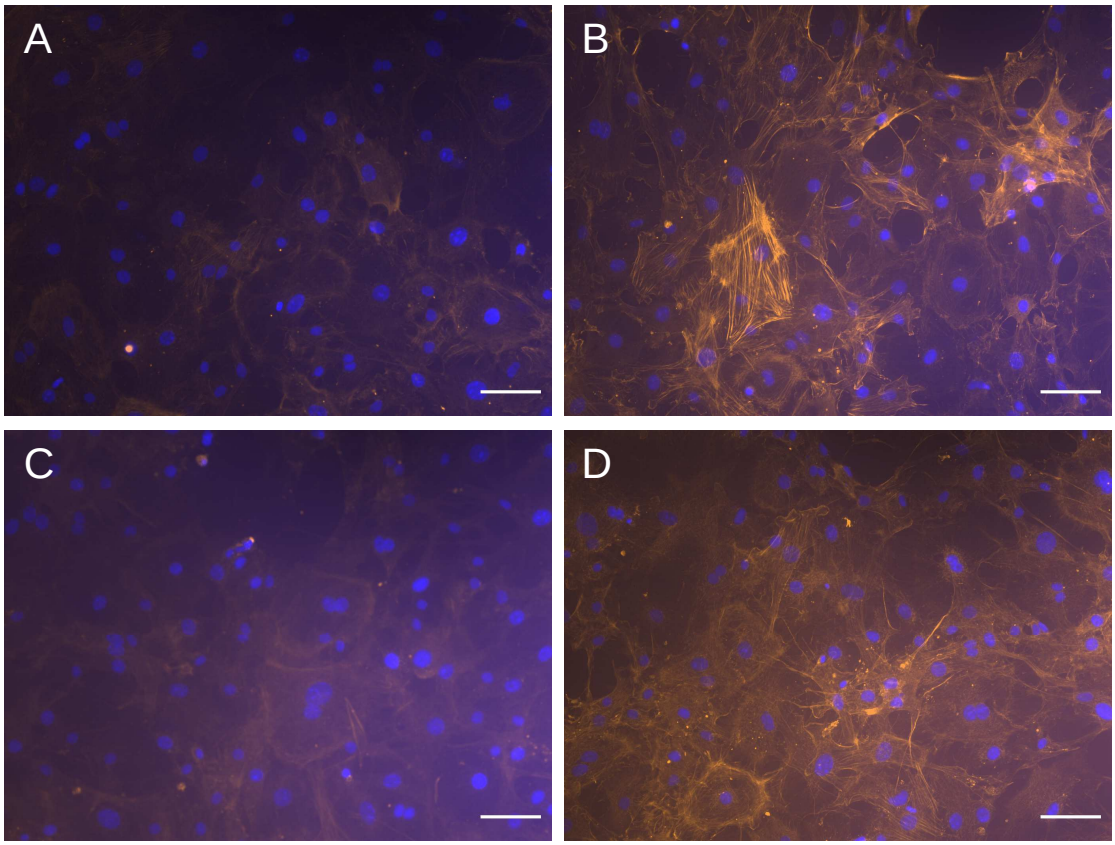

Figure 4.22 Expression of α smooth muscle actin following TGFβ1 stimulation.
Primary cardiac fibroblasts were stimulated with TGFβ1 for 24 hours. They were then immunostained with antibodies against αSMA. A and B, control primary cardiac fibroblasts with (B) and without (A) TGFβ1 stimulation. C and D, endoglin depleted primary cardiac fibroblasts with (D) and without (C) TGFβ1 stimulation. TGFβ1 stimulation results in an increased expression of αSMA in both groups. Scale bar 50μm.

4.3 Discussion

These experiments were designed to investigate the effect of endoglin knockdown on cardiac fibroblasts and their response to TGFβ1 in the context of fibrosis. Fibroblasts were readily cultured from adult mouse hearts, and were characterised by their morphological properties and by immunocytochemical analysis. With subsequent passages (greater than passage2) these cardiac fibroblasts become positive for αSMA, suggesting a shift to a myofibroblast phenotype (Gabbiani, 1998; Hinz, 2010). Cardiac fibroblasts appear to be predisposed to convert to a myofibroblast phenotype in culture. Porter et al found that fibroblasts cultured from normal human atrial explants expressed αSMA from the first passage suggesting an early activation of the myofibroblast phenotype. These cells remained positive for αSMA with subsequent passage (Porter *et al.,* 2004). However, initial immunophenotyping of rat cardiac fibroblasts demonstrated that they were negative for αSMA. It is not known if they develop a myofibroblast phenotype with subsequent passaging (K. Chen *et al.,* 2004; Shyu *et al.,* 2010). TGFβ is an important cytokine in mediating this phenotypic transformation (Eghbali *et al.,* 1991b; Leask, 2007).However, culture conditions are also important. For example, Masur and colleagues demonstrated that at low seeding density the proportion of myofibroblasts was 70 to 80% in rabbit corneal fibroblasts, whereas at high seeding density it was 5 to 10% (Masur *et al.,* 1996). In addition to seeding density the specific culture medium appears to influence this phenotypic change. Rossini et al. demonstrated that human primary cardiac fibroblasts cultured in Dulbecco's modified Eagles medium converted spontaneously to a myofibroblast phenotype but those cultured in endothelial growth medium retained a fibroblast phenotype (Rossini *et al.,* 2008). In my study, primary mouse cardiac fibroblasts were initially negative for αSMA but spontaneously developed a myofibroblast phenotype after passage two. As a consequence they likely represent a mixed fibroblast/myofibroblast population. Equally, fibroblasts and myofibroblasts are present in the healing myocardial infarct and so the presence of these two phenotypes *in vitro* may be more representative of the *in vivo* situation.

As discussed in chapter 1, endoglin is expressed in fibroblasts isolated from numerous tissues. It is also up-regulated in fibroblasts in a number of diseases where fibrosis is a feature, such as scleroderma (Leask *et al.,* 2002), Crohn's disease (Burke *et al.,* 2010)

and following myocardial infarction (van Laake *et al.*, 2006). The mouse primary cardiac fibroblasts described in this thesis were no exception- with endoglin being expressed at all passages. A number of methods have been used to regulate endoglin expression in fibroblasts. Endoglin has been targeted using antibodies specific for endoglin (K. Chen *et al.*, 2004) or small interfering (si) RNA (Burke *et al.*, 2010; Shyu *et al.*, 2010; Morris *et al.*). Endoglin overexpression studies have been performed in rat myoblasts (Obreo *et al.*, 2004), NIH3T3 and dermal fibroblasts (Leask *et al.*, 2002) and an intestinal fibroblast cell line (CCD-18Co) (Burke *et al.*, 2010) and are discussed in chapter 1. In my study I used Cre/lox technology to achieve endoglin knockdown. The floxed endoglin mouse line was developed in our laboratory (Allinson *et al.*, 2007) and has been used to investigate the role of endoglin in retinal angiogenesis (Mahmoud *et al.*, 2010) and tumour angiogenesis (Anderberg *et al.*, 2013). I have demonstrated that *Rosa26-Cre*^{ERT2} expression can be induced and endoglin efficiently depleted in primary mouse cardiac fibroblasts cultured from the *Eng*$^{fl/fl}$*;Rosa26-Cre*^{ERT2} mouse. Its use in these experiments represents a novel approach to investigate the role of endoglin in fibrosis.

The experiments described in this chapter demonstrate that TGFβ1 stimulation of control mouse primary cardiac fibroblasts results in phosphorylation of Smad2 and induction of Pai-1 expression. There was no detectable effect on Smad1/5/8 phosphorylation after 30 minutes exposure to TGFβ1, but the baseline level of Smad1/5/8 activation was already high. Nevertheless, TGFβ1 stimulation did lead to a reduction in Id1 transcription at 24 hours, indicating reduced activation of the Smad1/5/8 pathway, perhaps below the level of detection in the western blot experiments. The increase in Tgfb1 transcription following TGFβ1stimulation demonstrates autocrine induction of Tgfb1 expression. TGFβ1 stimulation also led to increased expression of Ctgf and αSMA. Interestingly there was no alteration in collagen 1 transcription in response TGFβ1 stimulation, most likely due to the activation of this pathway by serum starvation (Leicht *et al.*, 2001) and consequently it was not further activated following TGFβ1 stimulation. There was a reduction in collagen 3 and Timp2 transcription. Overall, these results are consistent with TGFβ1 signalling via the Alk5/Smad2/3 pathway in control cardiac fibroblasts, however, there was no increased expression of collagen 1 following TGFβ1 stimulation.

As expected, endoglin depleted primary cardiac fibroblasts have significantly reduced expression of endoglin, which was seen at both protein and mRNA level. There is also a small, but significant increase in Id1 transcription under normal culture conditions suggesting that endoglin may inhibit the Alk1/Smad 1/5/8 signalling pathway in normal fibroblasts. In my studies there was no difference in Alk5 expression between control and endoglin depleted cardiac fibroblasts. This differs from endothelial cells where Alk5 is reduced in endothelial cells from HHT1 patients (Fernandez *et al.*, 2005) and endoglin heterozygous mice (Lebrin *et al.*, 2004). One possible explanation for this difference is that cells may require time to undergo this adaptation. However, endoglin depletion has no effect on the expression of the majority of extracellular matrix genes examined in this chapter under the culture conditions used in this chapter.

As with control fibroblasts, TGFβ1 stimulation of endoglin depleted fibroblasts results in phosphorylation of Smad2. Again, there is no effect on Smad1/5/8 phosphorylation but similar reductions in Alk1 and Id1 expression. There is an increase in Pai-1 transcription but no increase in Tgfβ1 transcription suggesting that endoglin may be important in the autocrine regulation of Tgfβ1. Ctgf and αSMA transcription are both up regulated by TGFβ1 in endoglin deficient fibroblasts. However, unlike in control fibroblasts, collagen 1 and Mmp2 are both down regulated following TGFβ1 stimulation, suggesting that endoglin positively regulates collagen 1 and Mmp2 gene expression. There is also down regulation of collagen 3 and Timp2 gene expression. These results suggest that endoglin is involved in the autocrine regulation of Tgfβ1 and a positive regulator of collagen 1 and Mmp2 gene expression. I observed no differences between control and endoglin deplete fibroblasts in the activation of canonical TGFβ signalling pathways. This points to the possibility that endoglin is involved in regulation of the non-canonical signalling pathways such as MAP kinase (K. Chen *et al.*, 2004) or ERK 1/2 (Kapur *et al.*, 2012). Further work is needed to examine the effects of endoglin depletion on collagen protein production in response to TGFβ1 and non-canonical TGFβ signalling.

Quantative PCR (qPCR) is a widely used technique to measure gene expression (Schmittgen and Livak, 2008). However, there are a number of steps, from isolation and purification of RNA through reverse transcription PCR (to generate cDNA) to

qPCR and detection chemistry used, prior to achieving a result. All these steps need to be performed accurately as there is the possibility of error being introduced at any point. The experiments described in this thesis used SYBR green chemistry where the fluorescent dye binds to double stranded DNA (dsDNA) in the reaction mix. The advantages of this method are that it can be used to monitor the amplication of any dsDNA and so multiple genes can be investigated at relatively low cost. However, it relies on good primer design and optimisation of the PCR reaction as it can produce false positive results with binding to non specific DNA products. This was demonstrated during my experiments when quantifying Alk5 expression. The melting curve (figure 4.12) for Alk5 demonstrates 2 peaks suggesting the presence of more than one DNA product, most likely primer dimer in this case. Taqman chemistry uses a flurogenic probe which is released from the quencher dye as the target sequence is transcribed. The flurogenic probe is specific to the target sequence and different reporter dyes are available which allows amplification of more than one gene in a single reaction. Due to this specificity Taqman qPCR is more sensitive than SYBR green (Matsenko *et al.*, 2008; Cao and Shockey, 2012) which is of importance when dealing with small amounts of isolated RNA. However, it requires the synthesis of different probes for each target sequence and as a consequence the cost is greater.

The results described in this chapter have shown that the depletion of endoglin in cardiac fibroblasts potentially inhibits the autocrine regulation of TGFβ1 and reduces collagen 1 gene expression, suggesting that endoglin positively regulates extracellular matrix production. This is in keeping with other studies using rat cardiac fibroblasts and *in vivo* models of organ fibrosis. The effects of endoglin depletion *in vivo* will be investigated in the next chapter.

Chapter 5 The Effect of Endoglin on Cardiac Structure and Function.

5.1 Introduction

There is a significantly greater reduction in cardiac function following surgical LAD ligation in endoglin heterozygous mice compared to controls, possibly due to impaired neovascularisation of the infarct border zone following MI (van Laake *et al.*, 2006). However, inflammation and fibrosis also play an important role in the healing process following myocardial infarction but the role of endoglin in this process is not clearly defined. In a renal ischaemia/reperfusion injury model endoglin haploinsufficiency was protective (Docherty *et al.*, 2006) with reduced macrophage infiltration and activation in endoglin heterozygous mice. The authors concluded that it was the reduction in inflammation that resulted in this protection (Docherty *et al.*, 2006). In the irradiated mouse kidney, endoglin haploinsufficiency was also associated with reduced inflammation and a reduction in levels of the inflammatory cytokines IL-1β and IL-6 (Scharpfenecker *et al.*, 2012). The attenuation of inflammatory response in endoglin heterozygous mice is likely to explain the reduced fibrosis seen in this model (Scharpfenecker *et al.*, 2009). Although endoglin is expressed on activated macrophages (Lastres *et al.*, 1992), endothelial endoglin has been shown to be involved in the adhesion and transmigration of inflammatory cells (Elisa Rossi *et al.*, 2013). There is also impaired homing of mononuclear cells isolated from patients with HHT type 1 to infarcted myocardium in mouse models (Post *et al.*, 2010) which may be mediated through the SDF1/CXCR4 axis (Post *et al.*, 2010; K. Young *et al.*, 2012). It is unclear if the effects of endoglin in inflammation are due to direct effects on inflammatory cells, particularly macrophages, or on the adhesion and transmigration of these cells into injured tissue. It has also been demonstrated that endoglin is expressed in cardiac fibroblasts (K. Chen *et al.*, 2004; Shyu *et al.*, 2010; Kapur *et al.*, 2012), in myofibroblasts during wound healing in skin (Torsney *et al.*, 2002) and modulates fibrosis in a cardiac pressure overload model (Kapur *et al.*, 2012). All of these are important in healing following myocardial infarction but I was particularly interested in the effect of endoglin on fibrosis following myocardial infarction. I initially hypothesised that a reduction in fibrosis in the early period

following myocardial infarction resulted in a reduced tensile strength of the infarct leads to infarct expansion, as described in chapter 1, and accounted for the difference in cardiac function following MI in endoglin heterozygous mice. Whilst testing this hypothesis I discovered a novel phenotype in the *Eng-iKO*^{u} mouse, which is described in this chapter, so the focus of my studies changed during the course of my PhD. The work form this chapter has not yet been published as there are ongoing experiments to characterise this novel phenotype further.

5.2 Results

5.2.1 The expression of endoglin in normal mouse myocardium

To investigate the role of endoglin following myocardial infarction it was important to first establish its expression pattern in normal myocardium. Immunohistochemistry, using a monoclonal antibody against endoglin, was performed on 10μm cryosections, sectioned in the short axis of control (*Eng*$^{fl/fl}$) mice hearts. This demonstrated that endoglin is highly expressed in the mouse heart, particularly in the endocardium and cells surrounding cardiomyocytes but not in the cardiomyocytes themselves (figure 5.1A & B). To establish in which non-cardiomyocytes endoglin was expressed I performed co-immunofluorescence of endothelial cells (CD31), smooth muscle cells (α-smooth muscle actin (SMA)) and fibroblasts (fibroblast specific protein (Fsp1)). Figure 5.1C to E demonstrates that endoglin is co-expressed with CD31 in endothelial cells, as expected. Endoglin does not co-express with vessel associated αSMA in the vascular smooth muscle cells. Most Fsp1 positive cells do not co-localise with endoglin, but a small number do, which likely represents endothelial cells and fibroblasts in close proximity. This demonstrates that in mouse hearts, endoglin is expressed in endothelial cells but not in cardiomyocytes, smooth muscle cells or fibroblasts.

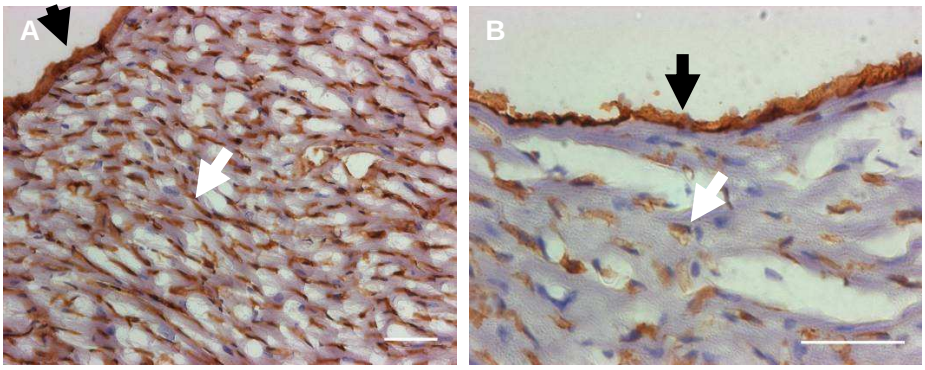

Figure 5.1 The expression pattern of endoglin in normal mouse myocardium.
10μm cryosection of mouse myocardium were cut in the short axis of the heart. **A&B**. Low and high power images of DAB stained sections demonstrating endoglin expression in the endocardium (black arrow) and non-cardiomyocyte cells in the myocardium (white arrow). Scale bar 50μm.

5.2.2 The expression of endoglin in the heart following myocardial infarction

In order to investigate the expression of endoglin within the myocardium following myocardial infarction I performed permanent coronary artery ligation of the left anterior descending artery (LAD) or sham operation on control ($Eng^{fl/fl}$) mice. Animals were euthanised 1, 3, and 5 days post infarct and the heart processed to prepare cryosections. Immunohistochemistry and immunofluorescence was performed on 10μm cryosections. Figure 5.2 shows an overview of the early changes in the infarcted myocardium. The infarcted myocardium was identified anatomically using low power to determine the anterior wall of the left ventricle which is supplied by the LAD artery. There is an infiltration of what appear to be inflammatory cells into the infarcted myocardium on day 1 post infarct (figure 5.2B & F). By day 3 post infarct the number of infiltrated cells has increased (figure 5.2C & G) and by day 5 post infarct there is heavy infiltration of cells into the infarcted myocardium, figure 5.2D & F. These changes represent the inflammatory and proliferative phases of infarct healing and were further examined using immunofluorescence microscopy.

Over the same time period (day 1 to day 5 post MI) there is a large increase in expression of endoglin within the infarcted myocardium (figure 5.3). In order to investigate which cells expressed endoglin, cryosections were co-stained with antibodies to endoglin as well as CD31 (for endothelial cells), CD11b (for macrophages), Fsp1 (for fibroblasts) and αSMA (for myofibroblasts and vascular smooth muscle cells). Figure 5.4 shows that there is an increase in endothelial cells in

the infarcted myocardium and that they all co-express endoglin and CD31. There is an increase in macrophages over time following myocardial infarction but these cells do not co-express endoglin (figure 5.5). Within the first day following infarction there are no myofibroblasts present, with only vessel associated smooth muscle staining positive for αSMA (figure 5.6A). By day 3 post infarct, myofibroblasts start to be seen but the expression of αSMA is low (figure 5.6B). There is a significant increase in myofibroblast infiltration by day 5 (figure 5.6C). At day 3 and 5 these myofibroblasts do co-localise with endoglin (figure 5.6, arrows). However, the expression of endoglin is lower in myofibroblasts than in endothelial cells. Figure 5.7 demonstrates fibroblast infiltration into the infarcted myocardium over time. However, Fsp1 expression is not co-localised with endoglin, suggesting that the endoglin becomes expressed as the phenotype changes from fibroblast to myofibroblast.

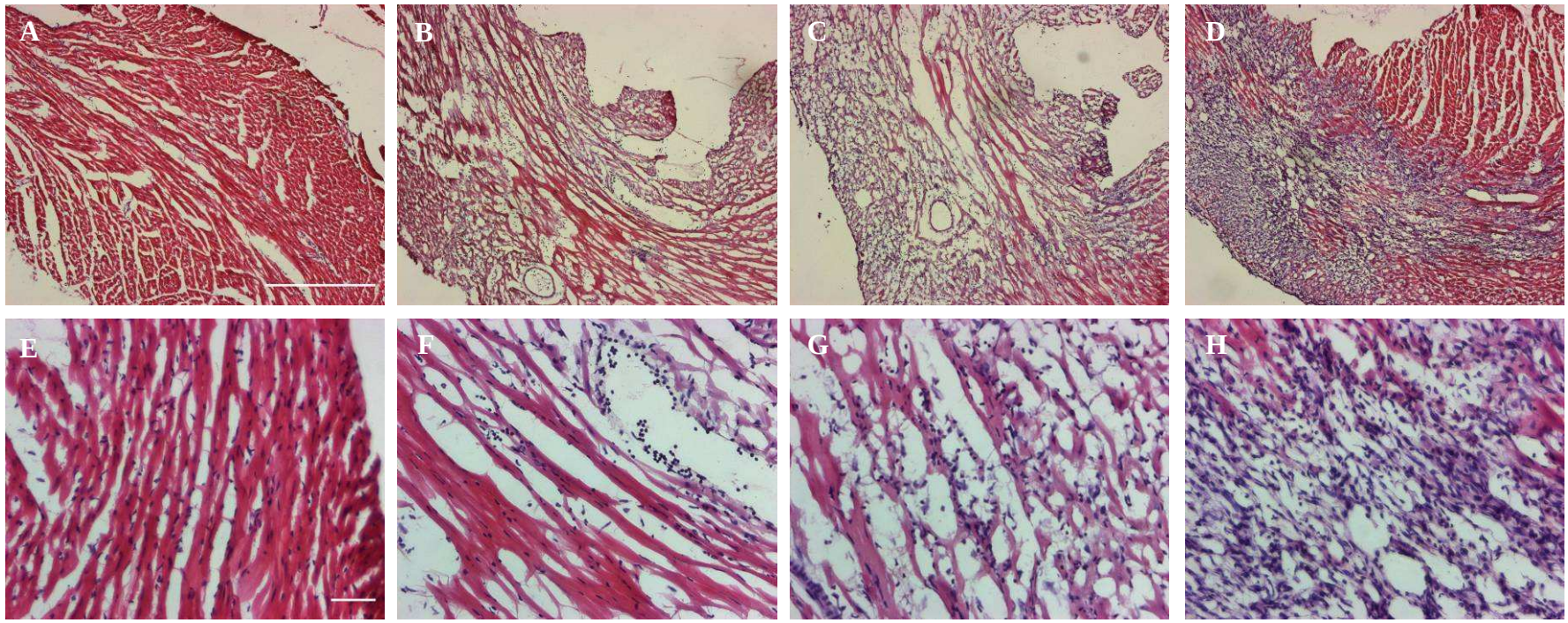

Figure 5.2 Histological changes in the myocardium following coronary artery ligation.

H&E staining at low **(A-D)** and high **(E-F)** power of the normal myocardium from control mice **(A&E)** and myocardium in the infarcted region 1 day **(B&F)** 3 days **(C&G)** and 5 days **(D&H)** following coronary artery ligation. There is infiltration of cells into the infarcted myocardium by day one (F) that increase in number at day 3 (G) a process that is more marked by day 5 (H). Scale bars: 500μm A-D and 50μm E-H.

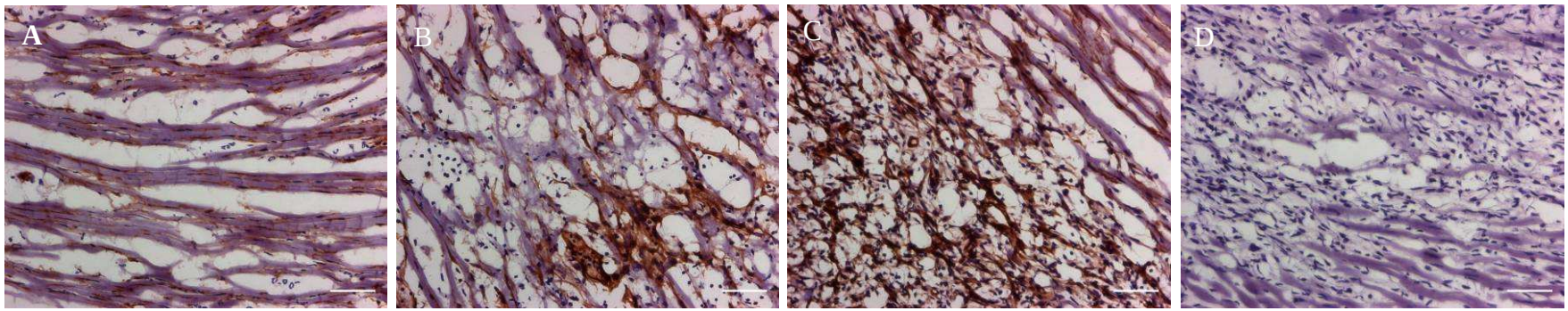

Figure 5.3 Expression of endoglin post MI.

Immunohistochemical staining with a monoclonal antibody to endoglin in the infarcted myocardium at 1 day **(A)**, 3 days **(B)** and 5 days **(C)** following coronary artery ligation shows a dramatic increase in endoglin expression (brown) . No primary control **(D)**. All sections are counter stained with haematoxylin to detect nuclei. Scale bar 50μm.

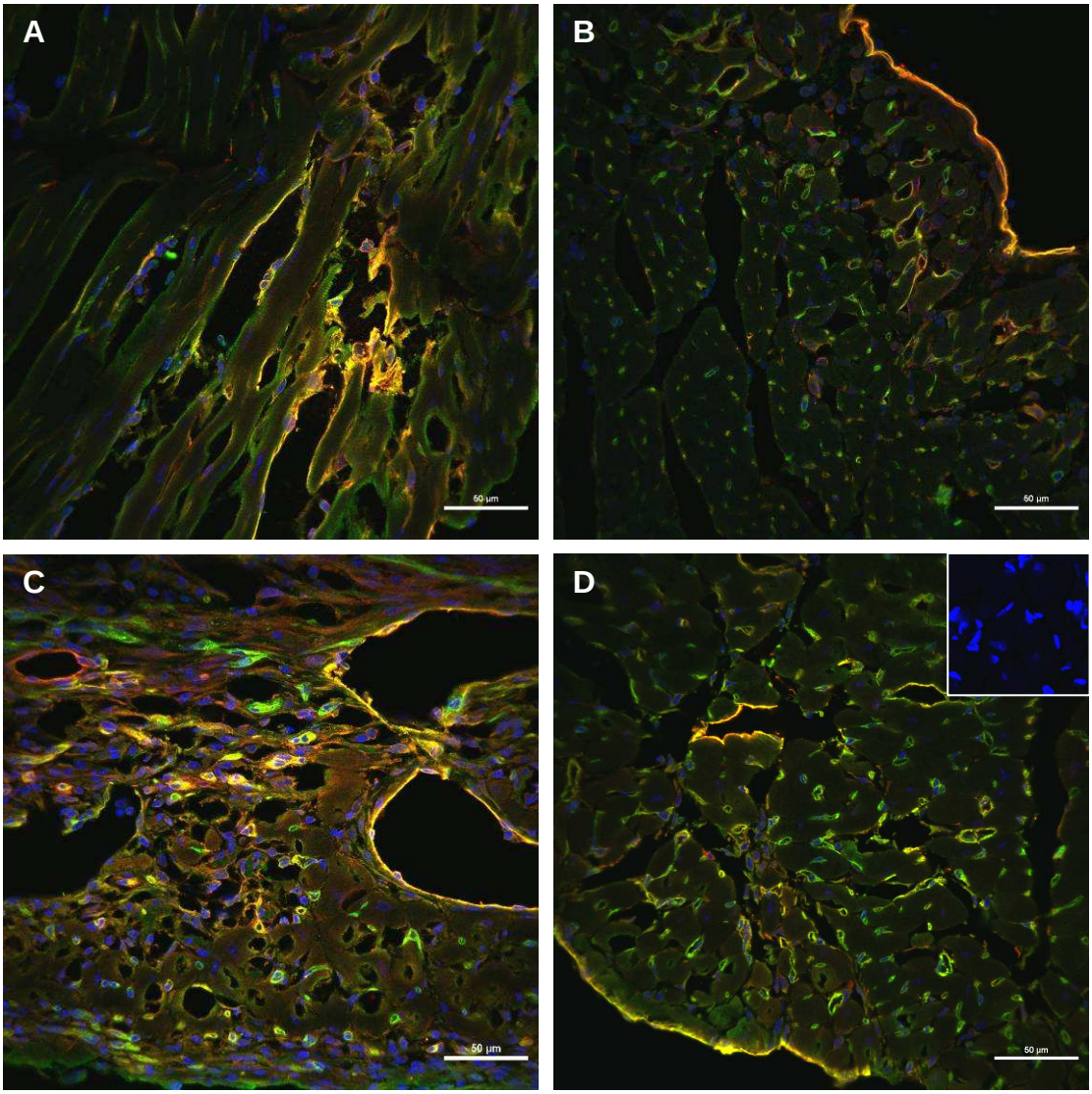

Figure 5.4 Co-immunofluorescence of endoglin (red) and CD31 (green) in the infarcted myocardium at 1 day (A) 3 days (B) and 5 days (C) following coronary artery ligation. Normal myocardium **(D)** and no primary control **(D inset)**. These images show that an infiltration and proliferation of endothelial cells in the infarct zone and they are all endoglin positive. Dapi (blue) was used to stain nuclei. Scale bar 50µm.

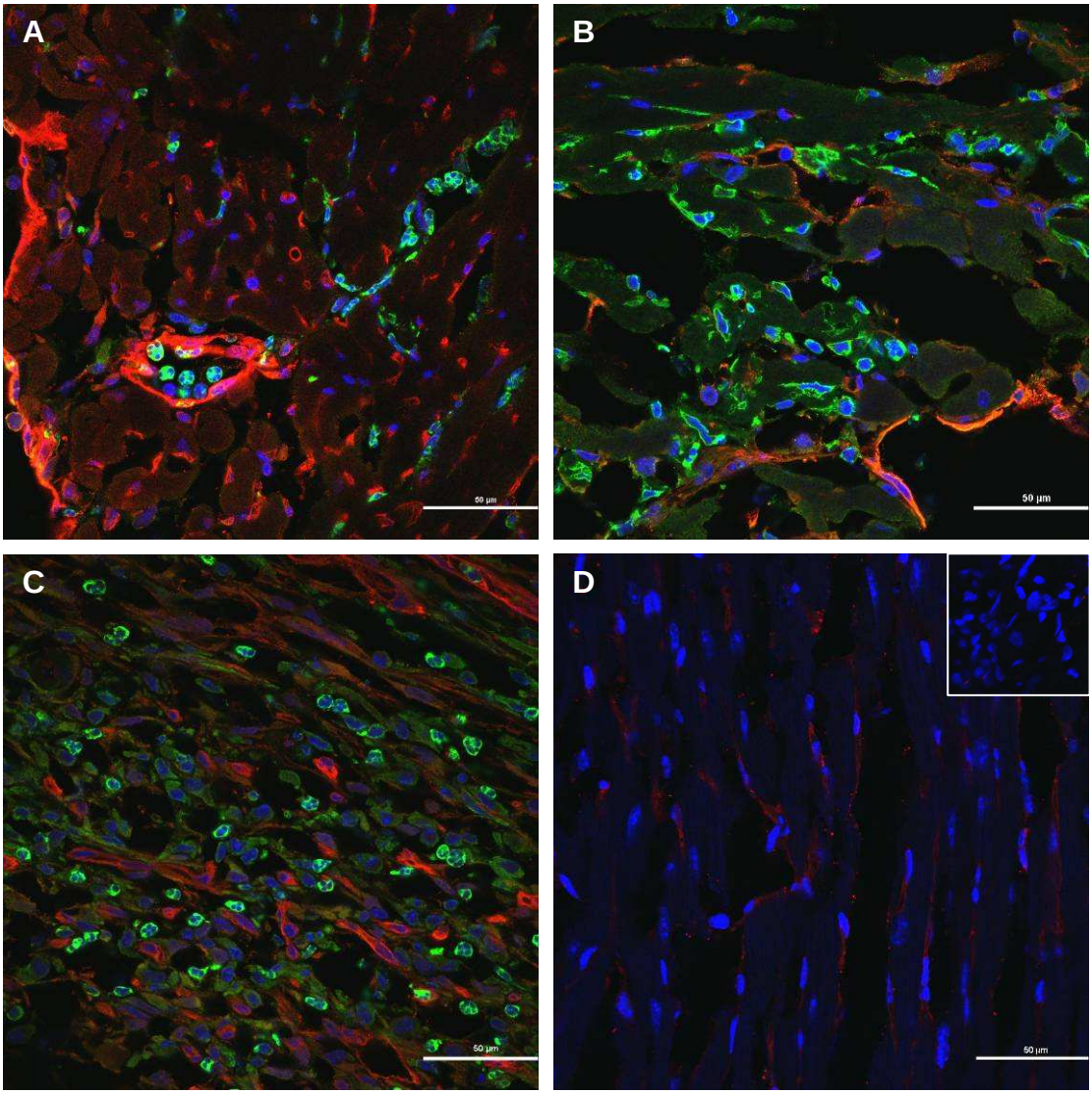

Figure 5.5 Double immunofluorescent staining of endoglin (red) and CD11b (green) in the myocardium of the infarcted myocardium at 1 day (A) 3 days (B) and 5 days (C) following coronary artery ligation.

Normal myocardium **(D)** and no primary control **(D inset)** are shown for comparison. These images show that there are an increasing number of CD11b-positive macrophages in the infarcted myocardium after day 1. The macrophages do not appear to co-express endoglin. Dapi (blue) was used to stain nuclei. Scale bar 50µm.

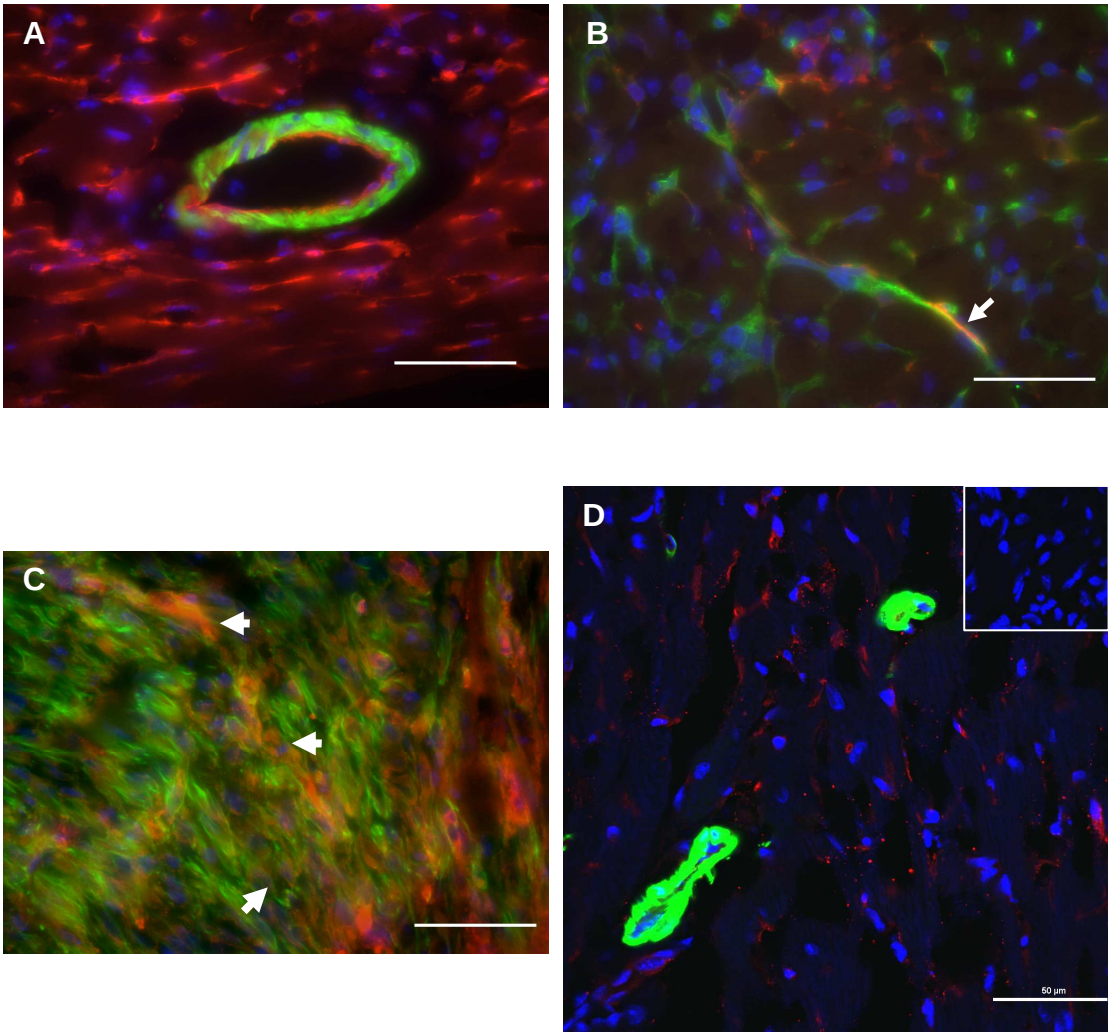

Figure 5.6 Double immunofluorescent staining of endoglin (red) and α SMA (green) in the myocardium of the infarcted myocardium at 1 day (A) 3 days (B) and 5 days (C) following coronary artery ligation.

Normal myocardium **(D)** and no primary control **(D inset)**. These images show that by day 3 there is an infiltration of αSMA positive cells, which likely represent myofibroblasts. These have significantly increased in number by day 5. Some of these cells co-express endoglin (white arrows). Dapi (blue) was used to stain nuclei. Scale bar 50µm.

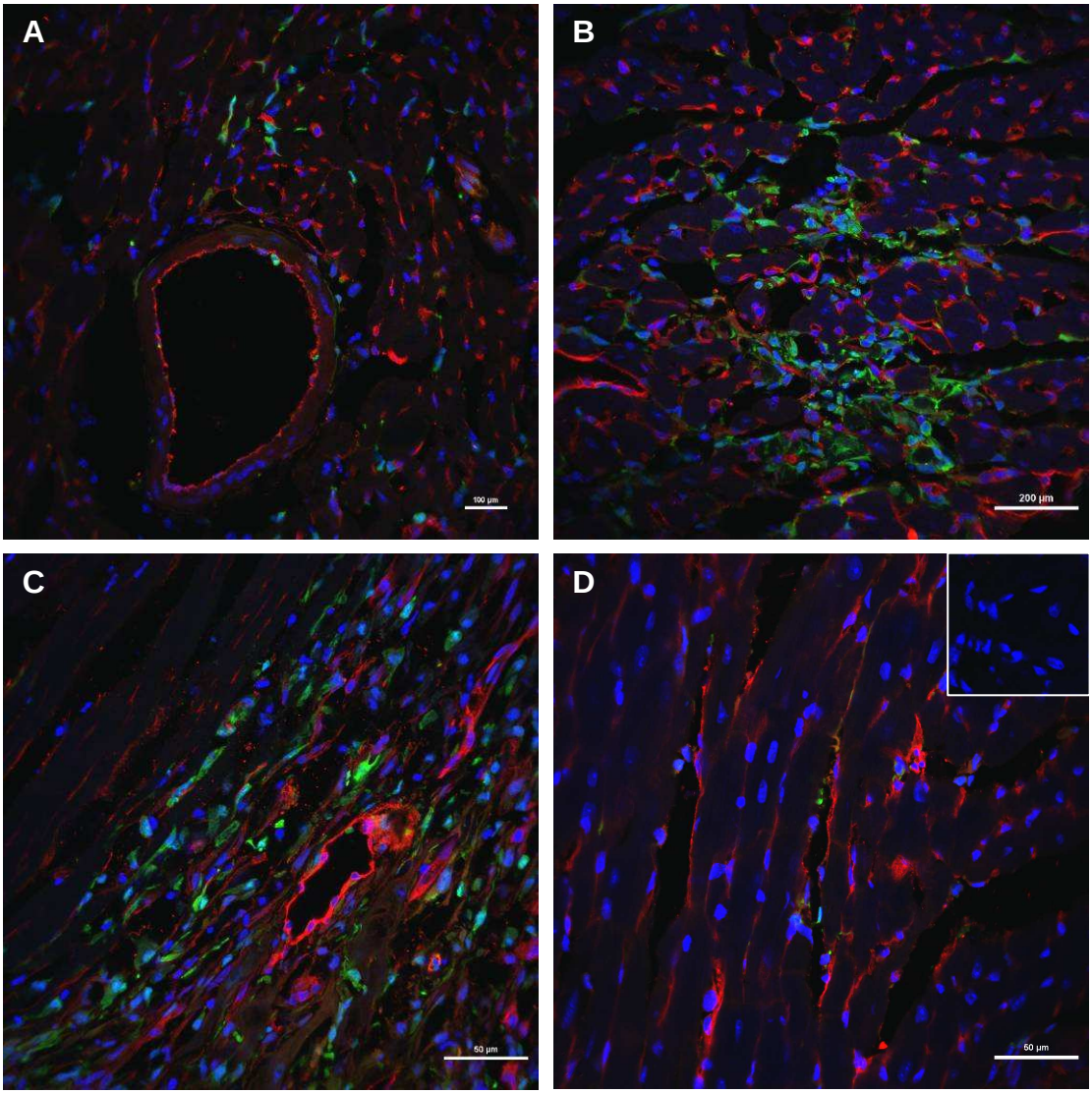

Figure 5.7 Double immunofluorescent staining of endoglin (red) and fibroblast specific protein 1 (Fsp1, green) in the myocardium of the infarcted myocardium 1 day (A) 3 days (B) and 5 days (C) following coronary artery ligation.

Normal myocardium **(D)** and no primary control **(D inset)**. These images show that there are an increased number of fibroblasts in the infarcted myocardium at days 3 and 5 compared with day 1. There is no detectable co-expression with endoglin. Dapi (blue) was used to stain nuclei. Scale bar 50µm.

5.2.3 Endoglin depletion in adult myocardium

Having demonstrated that endoglin expression is increased following myocardial infarction, in both endothelial cells and myofibroblasts, I next aimed to evaluate the role of endoglin in these cells following myocardial infarction. In order to address the role of endoglin I needed to evaluate whether endoglin can be efficiently knocked down in both these cell types in an inducible endoglin knockout mouse. As endoglin is expressed in both myofibroblasts and endothelial cells in the infarcted tissue I aimed to knock down endoglin in all cell types to test my hypothesis. For this reason I used the tamoxifen inducible *Rosa26;Cre*^{ERT2} line crossed with the *Eng*$^{fl/fl}$ line, to provide the option of ubiquitous knockdown of endoglin. To assess the expression of *Rosa26;Cre*^{ERT2} in the myocardium, *Eng*$^{fl/+}$*; Rosa26;Cre*^{ERT2}*;Rosa26R* mice (described in chapter 4) were treated with an intra-peritoneal injection of 2mg tamoxifen once a day for 5 days. Myocardial cryosections were then stained with X-gal, which demonstrated that *Rosa26;Cre*^{ERT2} is expressed in the myocardium (figure 5.8). This illustrated widespread but not absolutely ubiquitous expression and/or activation of the *Rosa26 lacZ* Cre reporter. However although known to be imperfect, the Rosa26 promoter is widely used to drive ubiquitous gene expression and was the best available mouse line for this study.

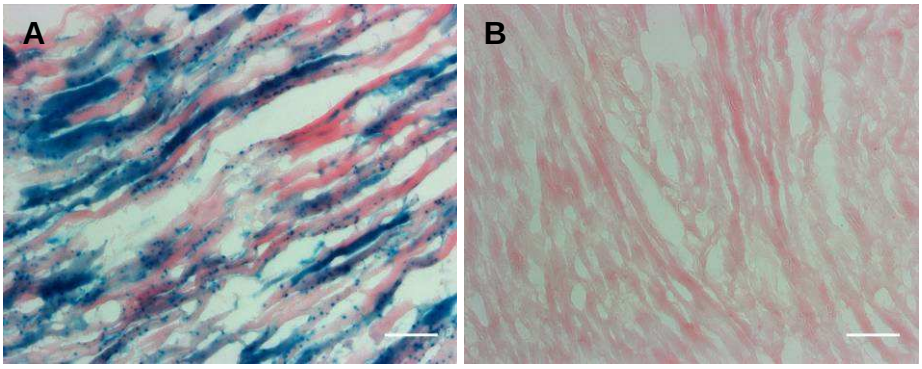

Figure 5.8 *Rosa26;Cre*^{ERT2} is expressed in the majority of myocardial cells as judged by the activation of lacZ expression (blue) in the heart tissue from *Rosa26;Cre*^{ERT2}*;Rosa26R* mice after tamoxifen treatment

(A). Control image **(B).** Scale bar 50μm.

As we did not know the optimum duration of tamoxifen treatment that would result in endoglin knockdown, the next experiment was designed to assess this. *Eng*$^{fl/fl}$*;Rosa26;Cre*^{ERT2} mice (n=3 per group) were treated with tamoxifen (ip

injection of 2mg per day) according to the following different protocols. Group 1 were treated for 3 consecutive days, group 2 were treated for 5 consecutive days and group 3 were treated for 5 consecutive days followed by 2 further 2mg tamoxifen doses on days 7 and 9. All animals were euthanised 3 days after the last dose. Untreated control animals (n=2) showed a normal pattern of endoglin expression (figure 5.9 A & B). Mice (*Eng$^{fl/fl}$;Rosa26;Cre^{ERT2}*) in group 1 showed a reduction in endoglin expression, but knockdown was not complete (figure 5.9 D-F). There is significant knockdown of endoglin after 5 days of tamoxifen treatment (group 2, figure 5.9 G-H). In group 3 there is also significant knockdown of endoglin but no greater than that seen in group 2 (figure 5.9 J-L). Surprisingly, in 2 of the mice from group 3 (both littermates) the knockdown was not as efficient (figure 5.9 J &K). Consequently in all subsequent experiments endoglin knockdown was achieved by 5 daily doses of 2mg tamoxifen.

As I proposed to assess cardiac function at 4 weeks post infarct it was important to ensure that endoglin expression did not return and remained depleted for the duration of the study. To investigate this *Eng$^{fl/fl}$;Rosa26;Cre^{ERT2}* mice were treated with tamoxifen (2mg daily for 5 days, as for group 2 above). They were then euthanised 10 weeks following the first dose of tamoxifen. Figure 5.10 demonstrates that 10 weeks following tamoxifen treatment endoglin remains depleted in the heart.

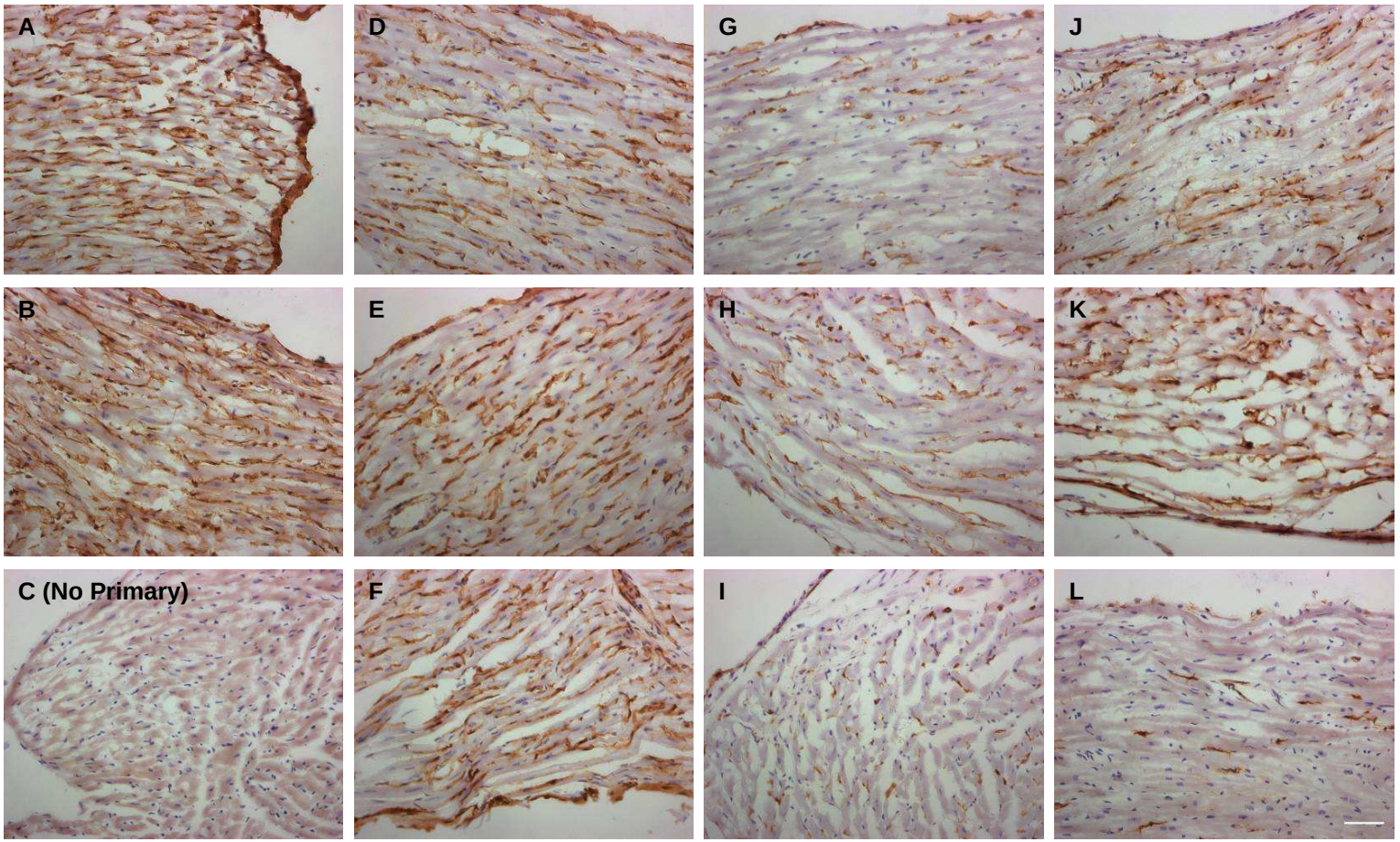

Figure 5.9 Evaluating endoglin knockdown in the *Eng$^{fl/fl}$;Rosa26;Cre^{ERT2}* mouse following Cre^{ERT2} activation with different doses of tamoxifen.

Represenative cryosections of the left ventricle of control mice **(A&B)** show normal levels of endoglin, which is only slightly reduced following the 3 dose protocol **(D-F)**, whereas there is a considerable reduction following the 5 dose protocol **(G-I)** and in some of the mice given the 7 dose protocol **(J-L). A** no primary control image demonstrates staining specificity. **(C)**. Together these images demonstrate knock down of endoglin following 5 and 7 doses of tamoxifen. Scale bar 50μm.

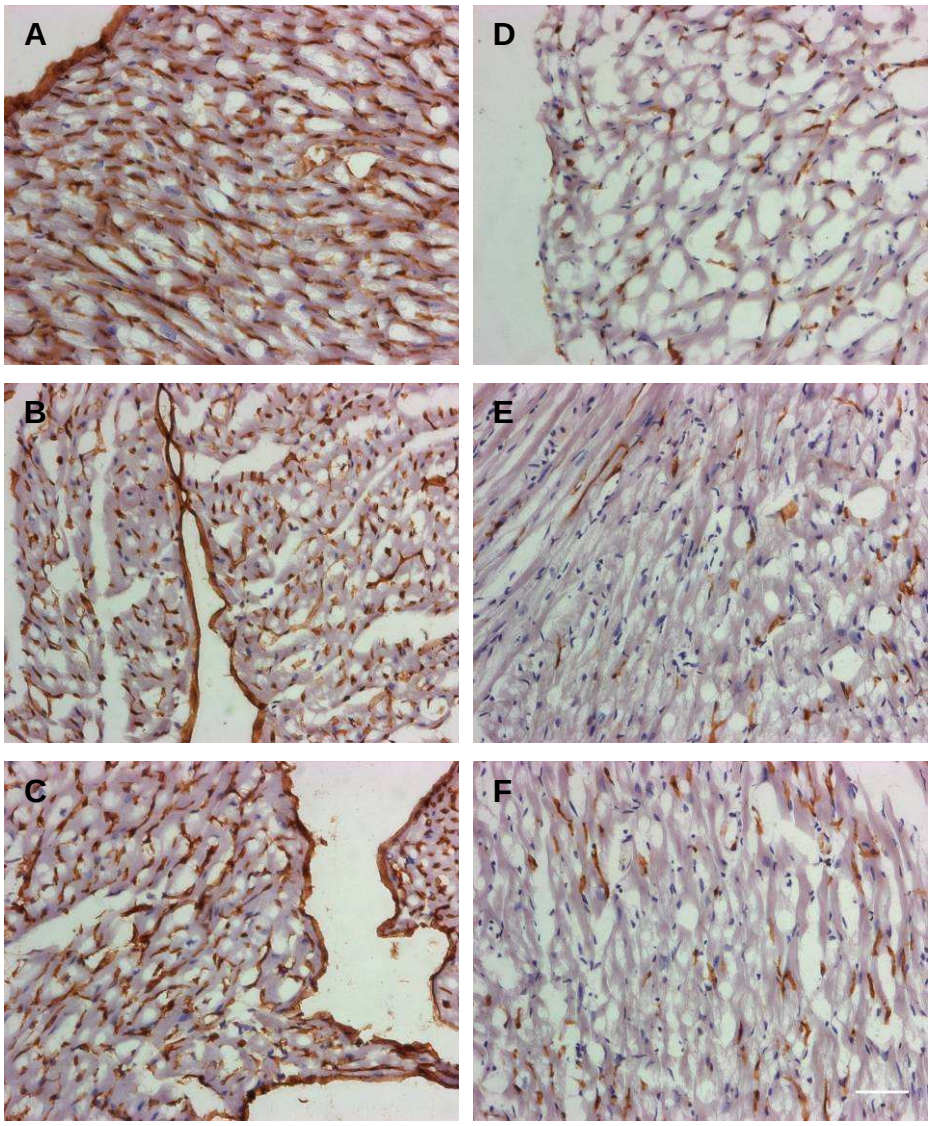

Figure 5.10 Sustained knock down of endoglin expression after 10 weeks following Cre-*ER*^{T2} activation.

Endoglin expression in *Eng*$^{fl/fl}$ control **(A-C),** and in *Eng*$^{fl/fl}$*;Rosa26;Cre*^{ERT2} mice 10 weeks following tamoxifen treatment using the 5 dose regimen**(D-F)**. This demonstrated a sustained depletion of endoglin at the10 week time point. Scale bar 50μm.

5.2.4 The effect of endoglin knockdown on cardiac function following myocardial infarction

Having established a reproducible and stable level of endoglin knockdown in the *Eng$^{fl/fl}$;Rosa26;Cre^{ERT2}* mice I proceeded to test the hypothesis that endoglin is required for efficient tissue repair following myocardial infarction. Initially a pilot group of *Eng$^{fl/fl}$;Rosa26;Cre^{ERT2}* mice were treated with tamoxifen (i.p. 2mg daily, for five days) to generate "ubiquitous" endoglin knockdown mice, from here on termed *Eng-iKO^{u}* mice. In parallel, *Eng$^{fl/fl}$* mice (termed control mice) were treated with tamoxifen in the same way and served as controls. Three days following the last dose of tamoxifen all mice underwent permanent LAD ligation or sham operation, thus giving four groups (control mice with sham operation, control mice with LAD ligation, *Eng-iKO^{u}* mice with sham operation and *Eng-iKO^{u}* mice with LAD ligation). Four weeks following MI, cardiac MRI was performed to evaluate cardiac function in vivo.

Analysis of left ventricular mass and function in the different treatment groups are given in table 5.1 and figure 5.11. The data indicate that compared to control mice following MI, *Eng-iKO^{u}* mice have greater LV mass (205.0 ± 10.6mg vs. 123.0 ± 3.6mg) and volumes (end diastolic volume 169.7 ± 3.5µl vs. 83.2 ± 3.1µl and end systolic volume 104.8 ± 3.7µl vs. 40.0 ± 2.7µl), with reduced cardiac function (ejection fraction 38.3 ± 0.9% vs. 52.1 ± 1.6%). Infarct size, as a percentage of the left ventricle, was similar in both groups (20.5 ± 0.8% vs. 18.9 ± 2.1%). These results suggest that there is greater left ventricular adverse remodelling in mice following endoglin knockdown. However, in the sham operated, Eng-iKO^{u} mouse there appeared to be a similar increase in left ventricular mass (208.1mg) and volumes (end diastolic volume 148.0µl and end systolic volume 66.8µl), but with only slightly reduced function (ejection fraction 54.9%). This led me to consider whether endoglin depletion alone, without cardiac injury, resulted in left ventricular remodelling.

Table 5.1 Analysis of MRI data to show cardiac function 4 weeks following coronary artery ligation in control and *Eng-iKO^{u}* mice.

Data expressed as mean (± SE when n>2)

	Control		***Eng-iKO^{U}***	
	Sham (n=1)	**MI (n=4)**	**Sham (n=1)**	**MI (n=2)**
Age at infarct (wks)	8.1	9.2 ± 0.3	9.7	9.3
Sex	F	2M 2F	M	2M
Weight (g)	22.6	24.6 ± 1.7	30.6	30.4
Heart rate (bpm)	420	337 ± 6.2	414	378
LV mass (mg)	108.3	123.0 ± 3.6	208.1	205.0
LV mass index (mg/g)	4.8	5.1 ± 0.3	6.8	6.8
EDV (µl)	61.9	83.2 ± 3.1	148.0	169.7
EDVI (µl/g)	2.7	3.4 ± 0.2	4.8	5.6
ESV (µl)	22.3	40.0 ± 2.7	66.8	104.8
ESVI (µl/g)	1.0	1.6 ± 0.1	2.2	3.46
SV (µl)	39.5	43.2 ± 0.9	81.2	64.9
SVI (µl/g)	1.8	1.8 ± 0.1	2.7	2.1
Ejection fraction (%)	63.9	52.1 ± 1.6	54.9	38.3
CO (ml/min)	16.61	14.6 ± 0.4	33.6	24.5
CI (ml/min/g)	0.73	0.6 ± 0.1	1.1	0.8
Infarct size (%LV)	n/a	18.9 ± 2.1	n/a	20.5

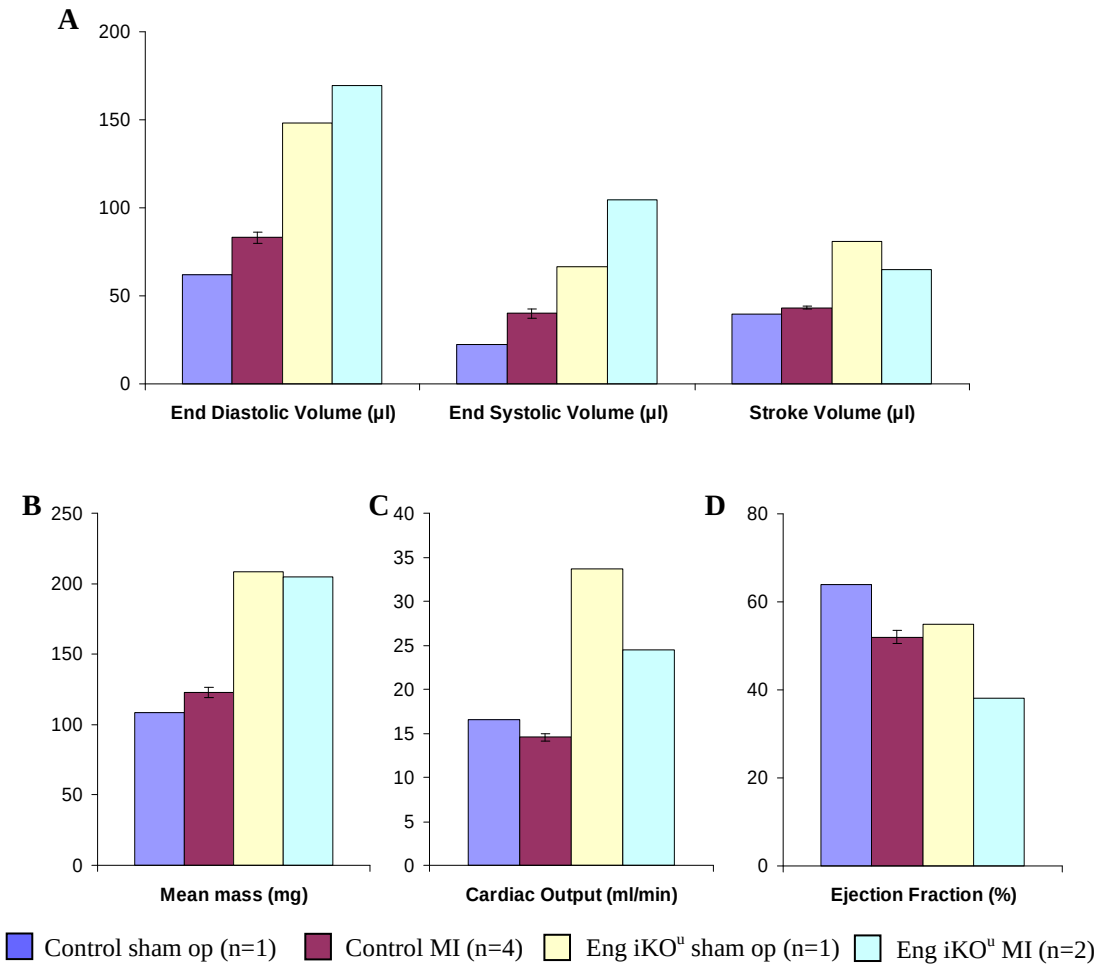

Figure 5.11 Cardiac volumes and function 4 weeks following coronary artery ligation in control and Eng-iKO^{u} mice.

Data suggests loss of endoglin alone leads to an increase in LV volume and an increase in cardiac output. Small group sizes prohibits statistical analysis.

5.2.5 Endoglin depletion results in significant ventricular remodelling

To study the effect of endoglin depletion without cardiac injury on the mouse heart, *Eng*$^{fl/fl}$;*Rosa26;Cre*^{ERT2} and control (*Eng*$^{fl/fl}$) mice were treated with tamoxifen, 2mg/day for 5 days. MRI was performed at 5 weeks following the first dose of tamoxifen. This is equivalent to the analysis time point used in the experiment described in section 5.2.4, where the timing of MRI was 4 weeks after MI, but 5 weeks after the first dose of tamoxifen.

It is clear from the MRI images (figure 5.12) and the autopsy specimens (figure 5.13) that the hearts are significantly larger in the endoglin knockdown group. MRI analysis of cardiac size and function are given in table 5.2 and shown in figure 5.14 and figure 5.15. It demonstrates that there is a significant increase in left ventricular mass (157.4 ± 12.9mg vs. 102.5 ± 13.3mg, p=0.03) and biventricular dilatation (LVEDV = 113.1 ± 8.8µl vs. 60.4 ± 2.5µl, p=0.004 and RVEDV = 93.4 ± 6.4µl vs. 52.3 ± 4.0µl, p=0.004) following endoglin knockdown. End systolic volumes were also significantly increased in the endoglin knockdown group (LVESV = 39.2 ± 4.0µl vs. 18.3 ± 0.6µl, p=0.007 and RVESV = 28.7 ± 2.6µl vs. 13.3 ± 2.3µl, p=0.009). As a result, in the endoglin knockdown group there was a significant increase in stroke volumes (LVSV = 73.9 ± 5.6µl vs. 42.1 ± 2.8µl, p=0.006 and RVSV = 64.7 ± 4.2µl vs. 39.0 ± 1.7µl, p=0.004) and consequently cardiac output (LVCO = 30.3 ± 2.8µl vs. 19.3 ± 1.6µl, p=0.03 and RVCO = 26.4 ± 1.7µl vs. 17.9 ± 1.1µl, p=0.01). However, ejection fraction was not significantly altered (LVEF = 65.5 ± 1.6% vs. 69.5 ± 2.0%, p=0.2 and RVEF = 69.4 ± 1.3% vs. 74.9 ± 2.4%, p=0.08). These differences all remained significant following indexing to body weight, with the exception of right ventricular stroke volume index and cardiac index. Interestingly the heart rate was significantly lower in the endoglin knockdown group compared to control (408 ± 8bpm vs. 458 ± 10bpm, p=0.01).

To confirm that the observed increase in left ventricular mass was secondary to myocyte hypertrophy, paraffin section from hearts of endoglin knockdown and control mice were stained with fluorescein conjugated wheat germ agglutinin, which binds carbohydrate residues on the cell membrane. Cross sectional area of the cardiomyocytes was then measured as described previously. Figure 5.16 demonstrates

that there was a significant increase in cardiomyocyte cross sectional area in the endoglin knockdown mice ($154 \pm 5.9\mu m^2$ vs. $202 \pm 5.8\mu m^2$, $p<0.0001$). This confirms that the increase in left ventricular mass was indeed due to cardiomyocyte hypertrophy.

These data demonstrate that endoglin knockdown results in biventricular remodelling even in the absence of cardiac injury. However, stroke volume and cardiac output were both increased, with no difference in ejection fraction, suggesting that cardiac function is not impaired. It is unclear from these data why this remodelling occurs. Ventricular remodelling was not seen in the endoglin heterozygous mouse in the absence of cardiac injury (van Laake *et al.*, 2006) and so perhaps suggests that there is a "dose" effect whereby these changes are only seen following >50% endoglin depletion. There are also reports of myocardial toxicity from Cre recombinase (Buerger *et al.*, 2006; Koitabashi *et al.*, 2009) and so it is important to exclude this as a possible cause of the ventricular remodelling. Finally, are these changes due to the effect of endoglin depletion within the heart or are they secondary effects from endoglin depletion in the vascular system, such as the development of arteriovenous malformations leading to a high output cardiac failure? The following experiments aim to address some of these possibilities.

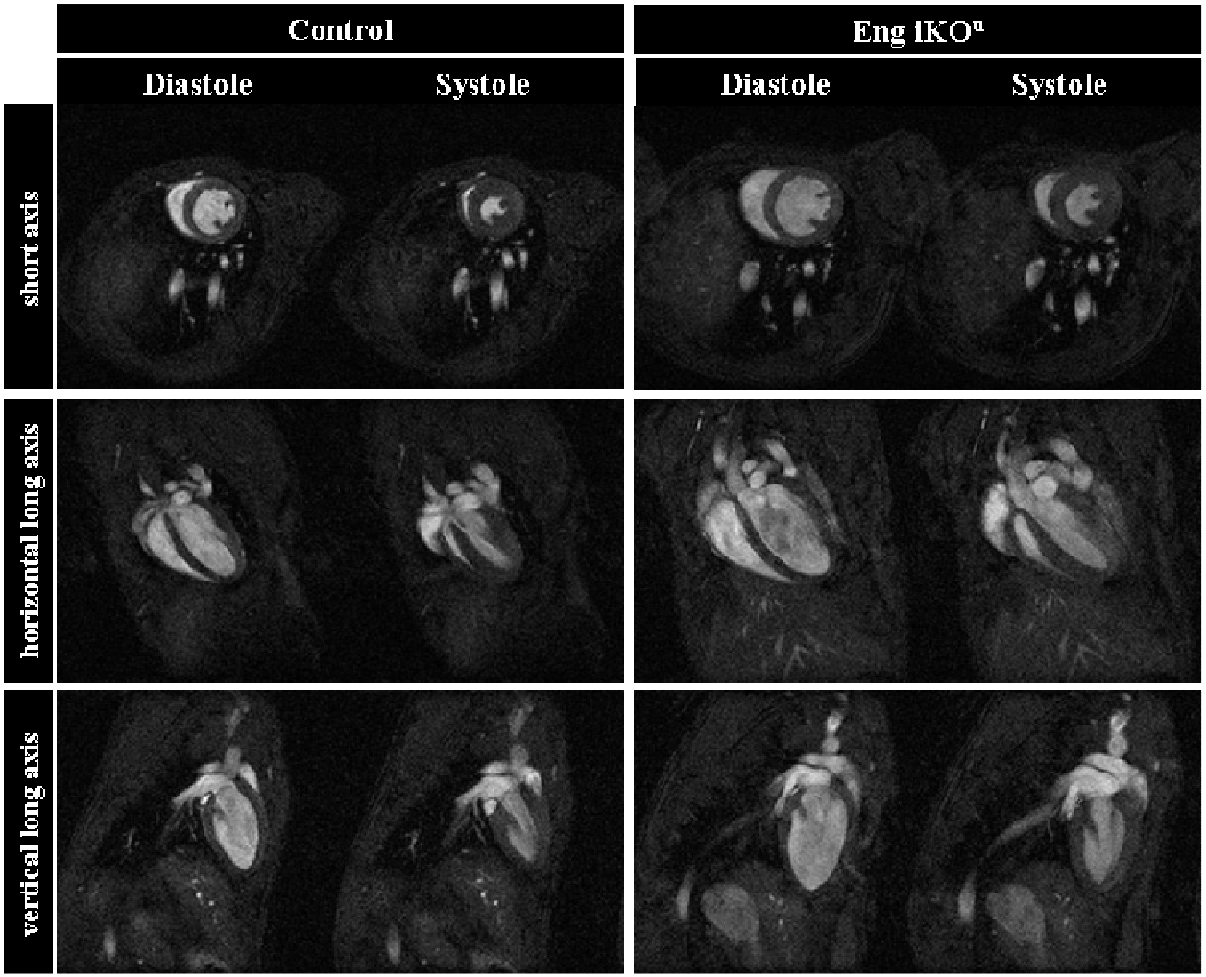

Figure 5.12 Cardiac MRI of control (*Eng*$^{fl/fl}$) and *Eng-iKO*^{u} mice.

This demonstrates significant left and right ventricular remodelling in the Eng-iKO^{u} mice 5 weeks after initiating endoglin knockdown, even in the absence of myocardial injury.

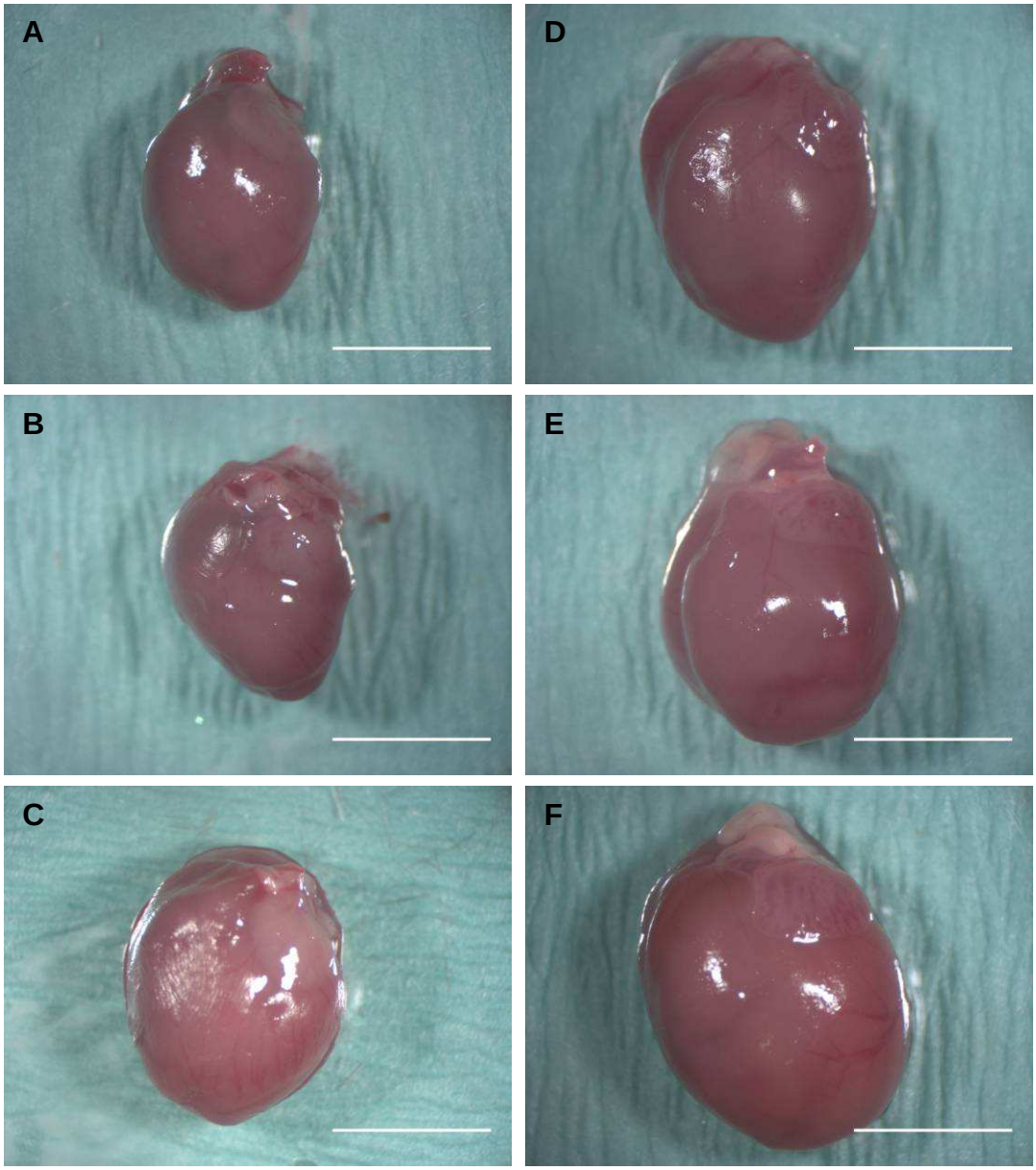

Figure 5.13 Macroscopic images of hearts from control (A-C) and endoglin iKO^{u} (D-F) adult mice.

There is an increase in heart size in Eng-iKO^{u} mice, 5 weeks after initiating depletion of endoglin. A&D, B&E and C&F are the same sex and littermates. Scale bar 5mm.

Table 5.2 Cardiac mass, volumes and function in control and Eng-iKO^{u} adult mice 5 weeks after the first tamoxifen dose.

This shows a significant change in the majority of these criteria in *Eng-iKO^{u}* mice. Data expressed as mean ± SE

	Control (n=3)	**Eng-iKO^{U} (n=4)**	**p value**
Mouse Weight (g)	24.1 ± 3.2	29.0 ± 1.6	0.2
Sex	2M 1F	3M 1F	n/a
Heart rate (bpm)	458 ± 10	408 ± 8	**0.01**
Left Ventricle			
LV mass (mg)	102.5 ± 13.3	157.4 ± 12.9	**0.03**
LV mass index (mg/g)	4.3 ± 0.1	5.4 ± 0.2	**0.004**
EDV (µl)	60.4 ± 2.5	113.1 ± 8.8	**0.004**
EDVI (µl/g)	2.6 ± 0.3	3.9 ± 0.1	**0.005**
ESV (µl)	18.3 ± 0.6	39.2 ± 4.0	**0.007**
ESVI (µl/g)	0.8 ± 0.1	1.4 ± 0.1	**0.01**
SV (µl)	42.1 ± 2.8	73.9 ± 5.6	**0.006**
SVI (µl/g)	1.8 ± 0.2	2.5 ± 0.1	**0.01**
Ejection fraction (%)	69.5 ± 2.0	65.5 ± 1.6	0.2
CO (ml/min)	19.3 ± 1.6	30.3 ± 2.8	**0.03**
CI (ml/min/g)	0.8 ± 0.1	1.0 ± 0.04	**0.05**
Right Ventricle			
EDV (µl)	52.3 ± 4.0	93.4 ± 6.4	**0.004**
EDVI (µl/g)	2.2 ± 0.1	3.2 ± 0.2	**0.02**
ESV (µl)	13.3 ± 2.3	28.7 ± 2.6	**0.009**
ESVI (µl/g)	0.6 ± 0.02	1.0 ± 0.1	**0.004**
SV (µl)	39.0 ± 1.7	64.7 ± 4.2	**0.004**
SVI (µl/g)	1.7 ± 0.1	2.3 ± 0.2	0.055
Ejection fraction (%)	74.9 ± 2.4	69.4 ± 1.3	0.08
CO (ml/min)	17.9 ± 1.1	26.4 ± 1.7	**0.01**
CI (ml/min/g)	0.8 ± 0.05	0.9 ± 0.06	0.1

.

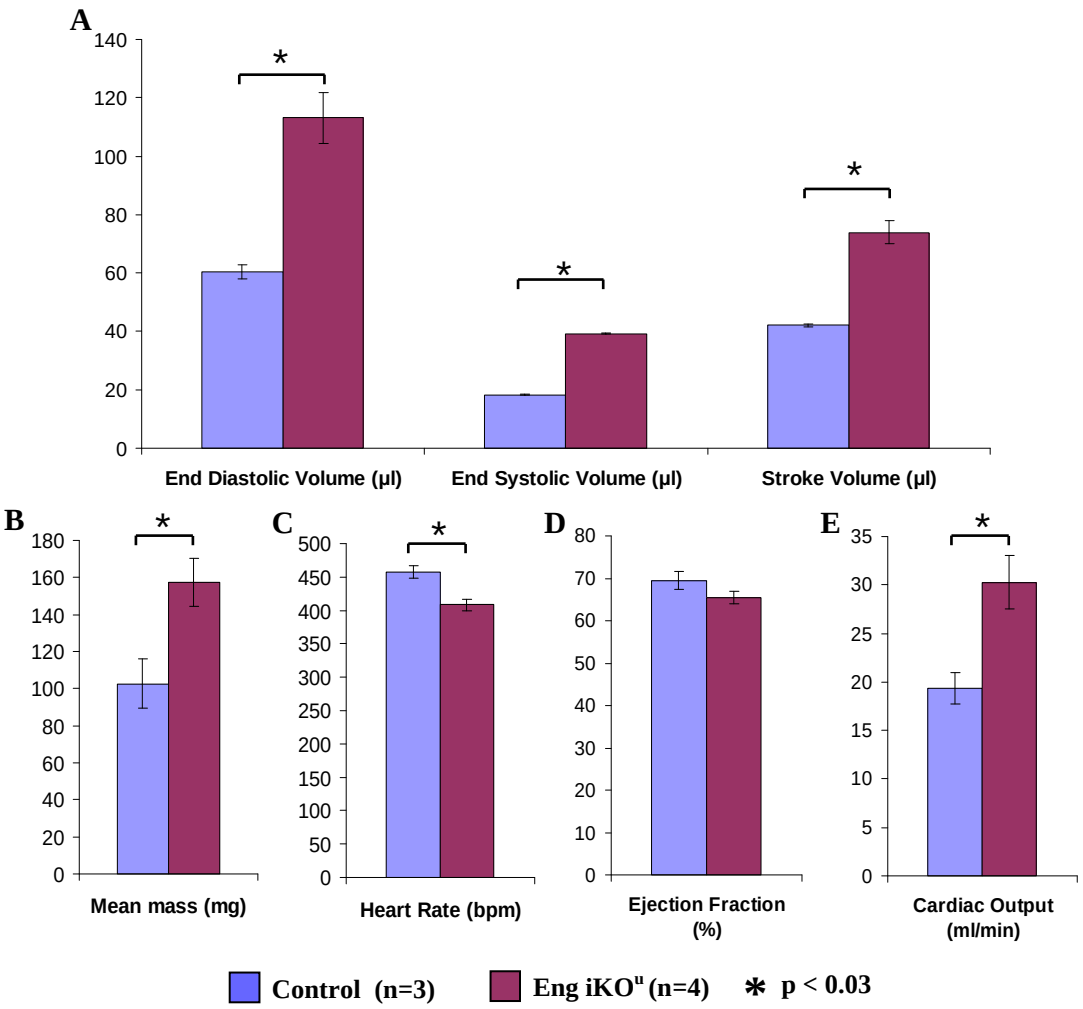

Figure 5.14 Left ventricular volumes and function in control and Eng-iKO^{u} mice.
Analysis of MRI data shows a significant increase in LV volume and LV mass and LV cardiac output, but no change in LV ejection fraction at 5 weeks following initiation of endoglin depletion. Data expressed as mean ± SE. * p<0.03

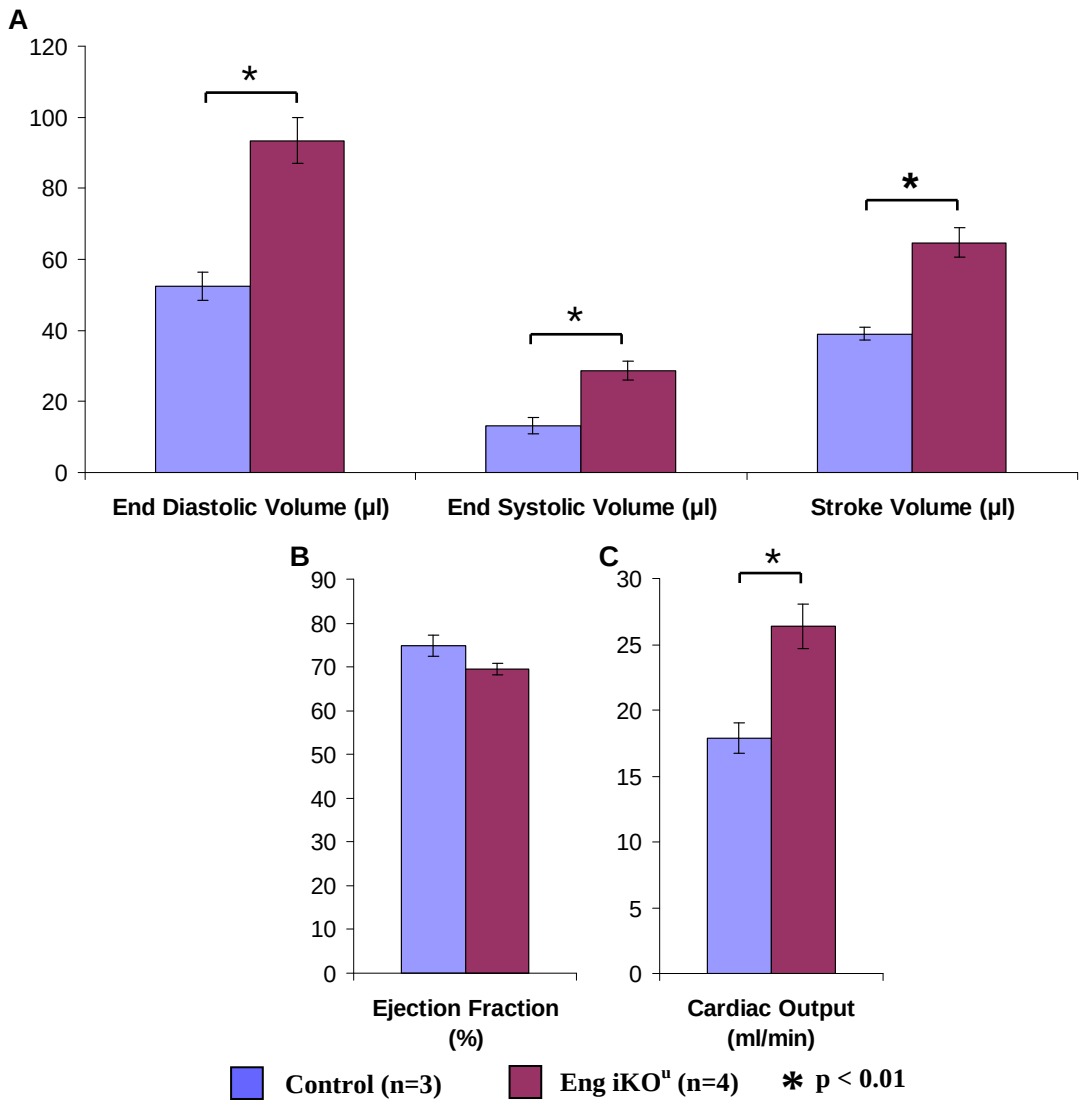

Figure 5.15 Right ventricular volumes and function in control and Eng-iKO^{u} mice.

This shows that there is a significant increase in RV volume and cardiac output, but no change in RV ejection fraction at 5 weeks following initiation of endoglin depletion. Data expressed as mean ± SE; * $p<0.01$.

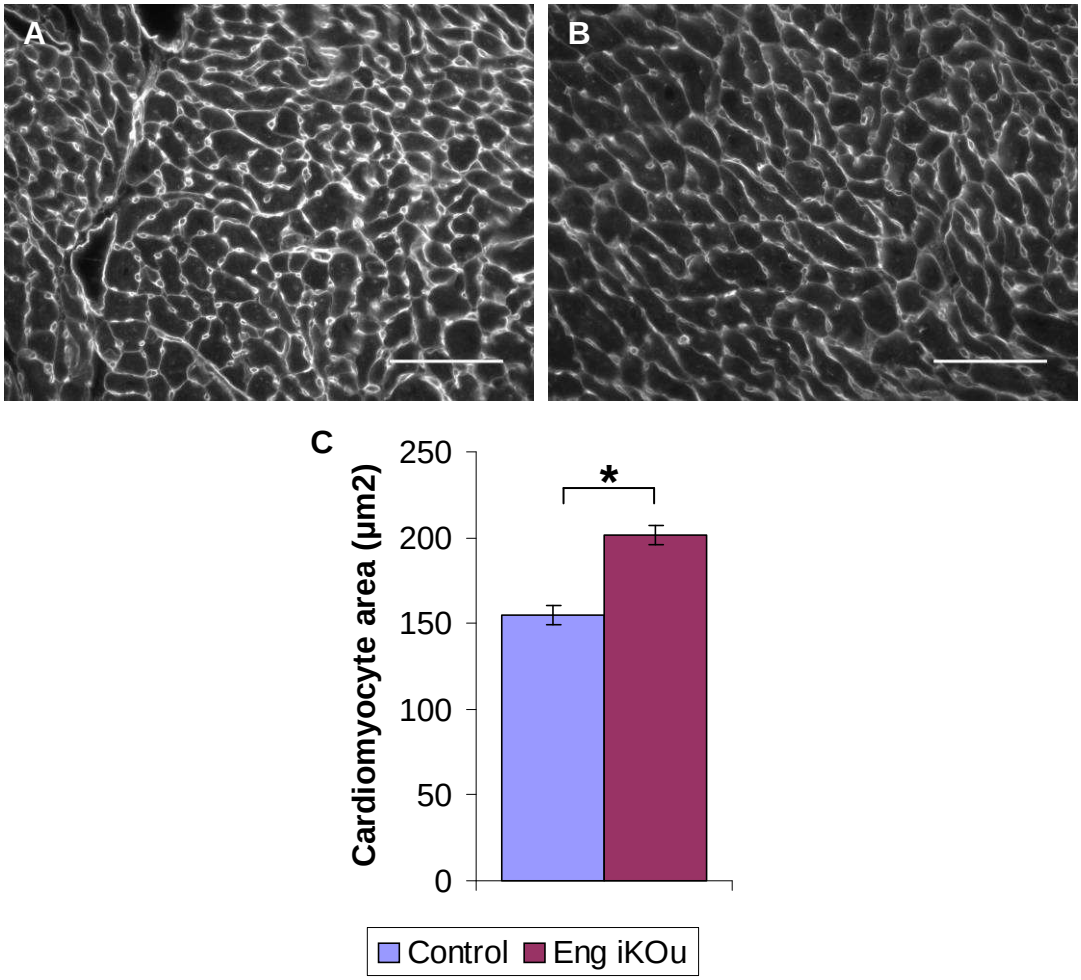

Figure 5.16 Cardiomyocyte size of control and Eng-iKO^{u} mice.

Wheat germ agglutinin staining of left ventricular cardiomyocytes of control **(A)** and Eng-iKO^{u} **(B)** mice. **C.** Analysis of average cardiomyocyte area demonstrating cardiomyocyte hypertrophy in Eng-iKO^{u} mice. Data expressed as mean ± SE; * $p<0.05$.

5.2.6 Ventricular remodelling due to depletion of endoglin is dose dependent.

It has recently been reported that Cre activation alone can affect cardiac function (Buerger *et al.*, 2006; Koitabashi *et al.*, 2009) so an experiment was designed to test whether Cre activation made any contribution to the phenotype observed in *Eng-iKO^{u}* mice. In addition, I aimed to determine whether there was an endoglin "dose" effect contributing to the cardiac phenotype seen in Eng-iKO^{u} mice. In other words whether partial endoglin expression could rescue the cardiac remodelling phenotype. To generate the mice required for these analyses *Eng$^{fl/fl}$;Rosa26;Cre^{ERT2}* mice were crossed with wild type C57Bl/6 mice to generate *Eng$^{fl/+}$;Rosa26;Cre^{ERT2}* and *Rosa26;Cre^{ERT2}* mice. The *Eng$^{fl/+}$;Rosa26;Cre^{ERT2}* mice were used to test if there was

an endoglin dose effect as only a single floxed allele is present. Heterozygosity for a null mutation in endoglin leads to a significant reduction of endoglin expression compared with wild type (Mahmoud *et al.*, 2008) but does not lead to complete loss of endoglin. Therefore tamoxifen treatment of the $Eng^{fl/+};Rosa26;Cre^{ERT2}$ line is expected to generate a mouse that is equivalent to the heterozygous $Eng^{+/-}$ mouse and to have residual endoglin expression driven by the wild type endoglin allele. $Eng^{fl/fl}$ mice were used as controls. All animals were treated with tamoxifen as described above and cardiac MRI was performed 5 weeks following the first dose.

The results are shown in table 5.3. They demonstrate that there is no difference in LV mass, volumes or function in $Eng^{fl/+};Rosa26;Cre^{ERT2}$ or $Rosa26;Cre^{ERT2}$ mice when compared to controls. The LV mass index and cardiac index is significantly lower in $Rosa26;Cre^{ERT2}$ mice compared to control mice (p=0.01 for both LV mass index and cardiac index) but there is no significant difference between control and $Eng^{fl/+};Rosa26;Cre^{ERT2}$ mice (LV mass index p= 0.07 and LV cardiac index p=0.06) or between $Eng^{fl/+};Rosa26;Cre^{ERT2}$ and $Rosa26;Cre^{ERT2}$ mice (LV mass index p=0.5 and LV cardiac index p=0.7).

These results clearly demonstrate that there is an endoglin 'dose' effect as no cardiac remodelling was seen with partial endoglin knockdown. This is consistent with the lack of reported generalised cardiac function defects in HHT1 patients, who are heterozygous for loss of function mutations in endoglin. Equally, Cre recombinase activation alone also does not result in ventricular remodelling thus excluding a direct myocardial toxicity effect of Cre activity.

Table 5.3 Cardiac mass, volumes and function calculated from MRI analysis of control (*Eng$^{fl/fl}$*), *Eng$^{fl/+}$;Rosa26;Cre^{ERT2}* and *Rosa26;Cre^{ERT2}* mice at 5 weeks following initiation of tamoxifen treatment.

	Control (n=4)	**Eng fl/+ Rosa Cre-ER^{T2} (n=6)**	**Rosa Cre-ER^{T2} (n=7)**	**p value (ANOVA)**
Weight (g)	26.5 ± 2.4	26.0 ± 1.6	29.0 ± 1.5	0.4
Heart rate (bpm)	445 ± 27	400 ± 26	417 ± 16	0.4
Sex	2M 2F	3M 3F	5M 2F	n/a
Left Ventricle				
LV mass (mg)	105 ± 6	91.1 ± 2.3	98.6 ± 3.2	0.07
LV mass index (mg/g)	4.1 ± 0.2	3.6 ± 0.2	3.4 ± 0.1	**0.02**
EDV (µl)	65.2 ± 3.2	60.0 ± 2.2	62.7 ± 1.9	0.4
EDVI (µl/g)	2.6 ± 0.2	2.4 ± 0.2	2.2 ± 0.1	0.3
ESV (µl)	21.0 ± 1.1	18.3 ± 2.0	19.3 ± 0.7	0.5
ESVI (µl/g)	0.8 ± 0.1	0.7 ± 0.1	0.7 ± 0.04	0.5
SV (µl)	44.2 ± 2.7	41.7 ± 0.6	43.4 ± 1.7	0.6
SVI (µl/g)	1.7 ± 0.1	1.6 ± 0.1	1.5 ± 0.03	0.2
EF (%)	67.7 ± 1.5	69.9 ± 2.1	69.2 ± 1.0	0.7
CO (ml/min)	19.7 ± 1.9	16.6 ± 0.9	18.2 ± 1.2	0.3
CI (ml/min/g)	0.8 ± 0.04	0.6 ± 0.03	0.6 ± 0.02	**0.03**
Right Ventricle				
EDV (µl)	51.6 ± 3.4	49.9 ± 2.2	54.9 ± 1.3	0.2
EDVI (µl/g)	2.0 ± 0.2	2.0 ± 0.2	2.2 ± 0.1	0.9
ESV (µl)	15.8 ± 1.8	13.1 ± 1.0	16.2 ± 0.9	0.1
ESVI (µl/g)	0.6 ± 0.1	0.5 ± 0.05	0.6 ± 0.03	0.4
SV (µl)	35.8 ± 1.9	36.8 ± 1.7	38.7 ± 1.0	0.6
SVI (µl/g)	1.4 ± 0.1	1.5 ± 0.1	1.4 ± 0.1	0.8
EF (%)	69.7 ± 1.7	73.8 ± 1.6	70.6 ± 1.3	0.2
CO (ml/min)	15.9 ± 0.8	14.5 ± 1.6	16.2 ± 0.9	0.3
CI (ml/min/g)	0.6 ± 0.02	0.6 ± 0.04	0.6 ± 0.02	0.4

5.2.7 Progression of ventricular remodelling following endoglin depletion

Five weeks following the first dose of tamoxifen, ubiquitous endoglin depletion in Eng-iKO^{u} mice had resulted in significant ventricular remodelling (table 5.2) but there was no significant difference in systolic function. However, it was unknown how early these ventricular remodelling changes began, nor whether the remodelling would persist, improve or deteriorate with time and whether there would be further progression to systolic dysfunction. Therefore, an experiment was designed to investigate this progression over time. A significant advantage of cardiac MRI is the ability to perform serial studies in the same mice. Therefore, *Eng-iKO*^{u} and control (*Eng*$^{fl/fl}$) mice were imaged before tamoxifen treatment and then at 1, 3, 5 and 12 weeks following the first dose of tamoxifen. The mice were all the same age (68 days) at the time of the first tamoxifen dose and all subsequent MRI scans were performed on the same day in the same order. LV mass and cardiac functional parameters were than calculated as previously described. Statistical analysis was performed using repeated measures ANOVA and *post hoc* comparisons were made using Tukey-Kramer method.

Figure 5.17 shows cardiac MRI images of both control and *Eng iKO*^{u} mice at the different time points. They show that visually there is little change in the size of the control hearts over time but in the hearts of *Eng-iKO*^{u} mice there is obvious dilatation of both the left and right ventricle as would be expected from previous studies. Importantly these changes appear to persist at 12 weeks.

Analysis of left ventriculer volume, function and mass (table 5.4 and figure 5.18) and right ventricular volume and function (table 5.5 and figure 5.19) reveal that there is no significant difference between the groups at baseline. Thus demonstrating that there is no difference in phenotype between the *Eng*$^{fl/fl}$ and *Eng*$^{fl/fl}$*;Rosa26;Cre*^{ERT2} mice prior to *Cre*^{ERT2} activation. Over the course of the study both mouse weight and mean heart rate increased over time in both groups. However, there were no significant differences between the groups over time ($p=0.5$ and $p=0.8$ respectively, repeated measures ANOVA for group by time). However, following *Cre*^{ERT2} activation, there were progressive increases in left ventricular mass as well as left and right ventricular volumes in the *Eng-iKO*^{u} mice, compared to control mice, that increased over the 12

week study period ($p<0.003$, repeated measures ANOVA for group by time). The changes in ventricular volumes resulted in significant increases in stroke volume and consequently cardiac output in *Eng-iKO*^{u} mice ($p<0.001$, repeated measures ANOVA for group by time). However, there was no significant difference in ejection fraction over this time suggesting that systolic function is preserved, despite the ventricular remodelling that has occurred.

These data confirm that, over the course of 12 weeks, ventricular remodelling occurs in *Eng-iKO*^{u} mice but not in control mice. *Post hoc* analysis of the data also reveals that in *Eng-iKO*^{u} mice there are significant differences in left ventricular mass, end diastolic volume, stroke volume and cardiac output at 3 weeks ($p<0.05$ compared to baseline measurements). This demonstrates that significant ventricular remodelling has occurred by 3 weeks post Cre activation.

Interestingly, in the *Eng-iKO*^{u} mice there is no difference in ejection fraction suggesting that systolic function is preserved in these mice. However, ejection fraction is just one measure of cardiac function and these data do not allow us to look for changes in myocardial contractility or diastolic function. Equally, cardiac output is increased suggesting that there may be changes in the wider cardiovascular system that led to the ventricular remodelling. In order to investigate some of these possibilities cardiac catheterisation of control and *Eng-iKO*^{u} mice was performed at 5 weeks following Cre induction to investigate cardiac pressure volume relationships.

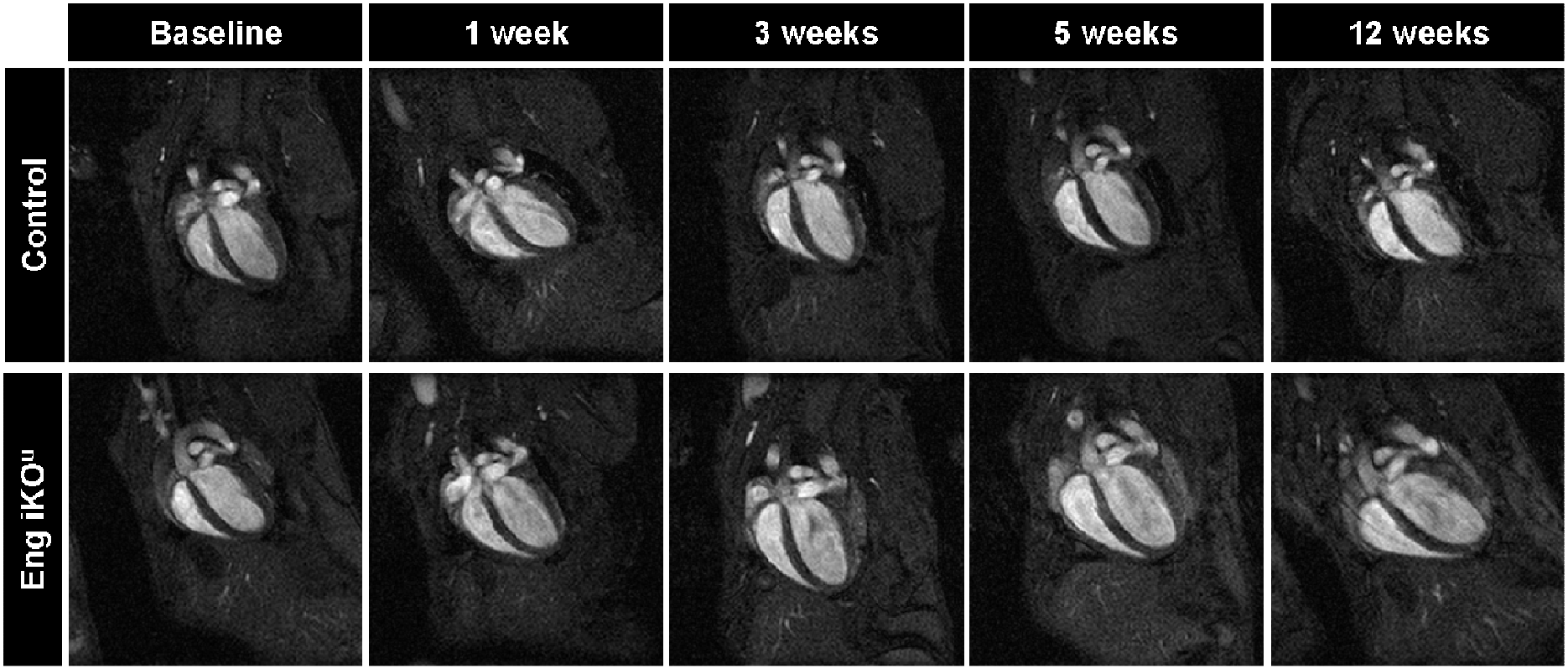

Figure 5.17 Cardiac MRI of hearts in diastole in the same control and *Eng-iKO*^{u} mice following tamoxifen treatment demonstrating increased right and left ventricular dilatation following endoglin depletion.

Table 5.4 Left ventricular volume and function in control (n=4, 2M 2F) and Eng-iKO^{u} (n=6, 3M 3F) mice over time following tamoxifen treatment.

Data analysed from MRI images and expressed as mean ± SE, p value represents repeat measures ANOVA, *=p<0.05 post hoc comparison compared to control mice at same time point using Tukey-Kramer method.

Time	**Baseline**		**1 week**		**3 weeks**		**5 weeks**		**12 weeks**		**p value**
Group	**Control**	**Eng-iKO^{U}**	**Control**	**Eng-iKO^{U}**	**Control**	**Eng-iKO^{U}**	**Control**	**Eng-KO^{U}**	**Control**	**Eng-iKO^{U}**	
Weight (g)	23.6 ± 2.2	23.4 ± 1.4	25.0 ± 2.0	24.9 ± 1.2	26.1 ± 1.8	26.6 ± 1.7	26.5 ± 2.4	27.4 ± 1.3	31.1 ± 3.6	30.2 ± 1.6	0.5
Heart rate (bpm)	408 ± 17	389 ± 14	418 ± 36	402 ± 18	469 ± 25	429 ± 11	445 ± 27	436 ± 9	442 ± 11	430 ± 21	0.8
LV mass (mg)	88.8 ± 2.6	82.4 ± 1.9	96.9 ± 8.1	88.1 ± 4.3	101.8 ± 6.1	118.6 ± 6.3	105 ± 6	129 ± 5.4*	103 ± 3.2	148 ± 5.6*	**<0.001**
LV mass index (mg/g)	3.9 ± 0.4	3.6 ± 0.3	3.9 ± 0.07	3.6 ± 0.16	3.9 ± 0.1	4.5 ± 0.1*	4.1 ± 0.2	4.7 ± 0.1*	3.4 ± 0.3	5.0 ± 0.2*	**<0.001**
LV EDV (µl)	60.6 ± 3.8	59.3 ± 1.6	62.2 ± 5.7	65.7 ± 3.0	65.6 ± 4.3	94.0 ± 6.0*	65.2 ± 3.2	106 ± 7.9*	70.8 ± 7.4	120 ± 9.9*	**<0.001**
LV EDVI (µl/g)	2.6 ± 0.2	2.6 ± 0.1	2.5 ± 0.03	2.7 ± 0.12	2.5 ± 0.1	3.6 ± 0.1*	2.6 ± 0.2	3.9 ± 0.2*	2.3 ± 0.08	4.0 ± 0.3*	**<0.001**
LV ESV (µl)	20.4 ± 2.3	20.0 ± 2.3	15.1 ± 2.6	15.9 ± 1.0	19.2 ± 2.3	26.9 ± 2.7	21.0 ± 1.1	36.3 ± 5.1	24.9 ± 4.0	45.3 ± 5.5*	**0.002**
LV ESVI (µl/g)	0.9 ± 0.05	0.9 ± 0.1	0.6 ± 0.06	0.7 ± 0.06	0.7 ± 0.05	1.0 ± 0.06*	0.8 ± 0.1	1.3 ± 0.1*	0.8 ± 0.05	1.5 ± 0.2*	**0.003**
LV SV (µl)	40.2 ± 2.5	39.3 ± 1.0	47.1 ± 3.4	49.8 ± 2.6	46.4 ± 2.2	67.0 ± 3.7*	44.2 ± 2.7	69.9 ± 2.9*	45.9 ± 3.6	75.0 ± 5.3*	**<0.001**
LV SVI (µl/g)	1.8 ± 0.2	1.7 ± 0.1	1.9 ± 0.04	2.0 ± 0.08	1.8 ± 0.09	2.5 ± 0.1*	1.7 ± 0.1	2.6 ± 0.1*	1.5 ± 0.08	2.5 ± 0.1*	**<0.001**
LV EF (%)	66.6 ± 2.8	66.5 ± 2.8	76.2 ± 2.1	75.7 ± 1.4	71.1 ± 1.7	71.7 ± 1.3	67.7 ± 1.5	66.6 ± 2.2	65.4 ± 2.3	62.9 ± 2.3	0.9
LV CO (ml/min)	16.4 ± 1.1	15.3 ± 0.7	20.0 ± 3.0	20.0 ± 1.4	21.9 ± 2.1	28.8 ± 2.0*	19.7 ± 1.9	30.6 ± 1.8*	20.4 ± 2.1	32.4 ± 3.3*	**<0.001**
LV CI (ml/min/g)	0.7 ± 0.05	0.7 ± 0.05	0.8 ± 0.06	0.8 ± 0.04	0.8 ± 0.04	1.1 ± 0.06*	0.8 ± 0.04	1.1 ± 0.05*	0.7 ± 0.03	1.1 ± 0.08*	**<0.001**

Table 5.5 Right ventricular volume and function in control (n=4) and Eng-iKO^{u} (n=6) mice over time following tamoxifen treatment.

Data analysed from MRI images and expressed as mean ± SE, p value represents repeat measures ANOVA, *=p<0.05 post hoc comparison compared to control mice at same time point using Tukey-Kramer method.

Time	**Baseline**		**1 week**		**3 weeks**		**5 weeks**		**12 weeks**		**p value**
Group	**Control**	**Eng-iKO^{U}**	**Control**	**Eng-iKO^{U}**	**Control**	**Eng-iKO^{U}**	**Control**	**Eng- iKO^{U}**	**Control**	**Eng-iKO^{U}**	
RV EDV (µl)	48.1 ± 0.8	51.9 ± 2.1	52.0 ± 4.1	57.3 ± 3.7	52.9 ± 3.6	75.6 ± 3.4*	49.9 ± 2.2	80.1 ± 3.7*	52.1 ± 4.0	97.8 ± 6.3*	**<0.001**
RV EDVI (µl/g)	2.1 ± 0.2	2.2 ± 0.1	2.1 ± 0.04	2.3 ± 0.06	2.0 ± 0.05	2.9 ± 0.05*	2.0 ± 0.2	2.9 ± 0.1*	1.7 ± 0.1	3.2 ± 0.1*	**<0.001**
RV ESV (µl)	16.3 ± 2.2	18.0 ± 2.1	12.2 ± 2.3	13.9 ± 1.8	15.0 ± 2.4	23.5 ± 2.3*	13.1 ± 1.0	31.1 ± 2.3*	18.6 ± 3.3	39.3 ± 4.1*	**<0.001**
RV ESVI (µl/g)	0.7 ± 0.04	0.8 ± 0.07	0.5 ± 0.06	0.5 ± 0.05	0.6 ± 0.06	0.9 ± 0.03*	0.5 ± 0.05	1.1 ± 0.1*	0.6 ± 0.1	1.3 ± 0.1*	**<0.001**
RV SV (µl)	31.8 ± 1.9	33.9 ± 0.7	39.8 ± 2.1	43.2 ± 2.1	37.9 ±1.7	52.1 ± 1.4*	36.8 ± 1.7	49.0 ± 1.9*	33.6 ± 1.9	58.3 ± 4.3*	**<0.001**
RV SVI (µl/g)	1.4 ± 0.2	1.5 ± 0.09	1.6 ± 0.06	1.7 ± 0.05	1.5 ±0.04	2.0 ± 0.08*	1.5 ± 0.1	1.8 ± 0.1*	1.1 ± 0.1	1.9 ± 0.1*	**<0.001**
RV EF (%)	66.2 ± 4.3	65.9 ± 2.8	77.1 ± 2.5	76.2 ± 1.6	72.1 ± 2.6	69.3 ± 1.7	73.8 ± 1.6	61.4 ± 1.6	65.1 ± 4.0	59.9 ± 2.5	0.3
RV CO (ml/min)	12.9 ± 0.4	13.2 ± 0.6	16.8 ± 2.2	17.6 ± 1.5	17.9 ± 1.7	22.3 ± 0.9*	14.5 ± 1.6	21.3 ± 0.9*	14.9 ± 1.2	25.3 ± 2.5*	**<0.001**
RV CI (ml/min/g)	0.6 ± 0.06	0.6 ± 0.05	0.7 ± 0.04	0.7 ± 0.05	0.7 ± 0.03	0.9 ± 0.04*	0.6 ± 0.04	0.8 ± 0.03*	0.5 ± 0.03	0.8 ± 0.06*	**0.003**

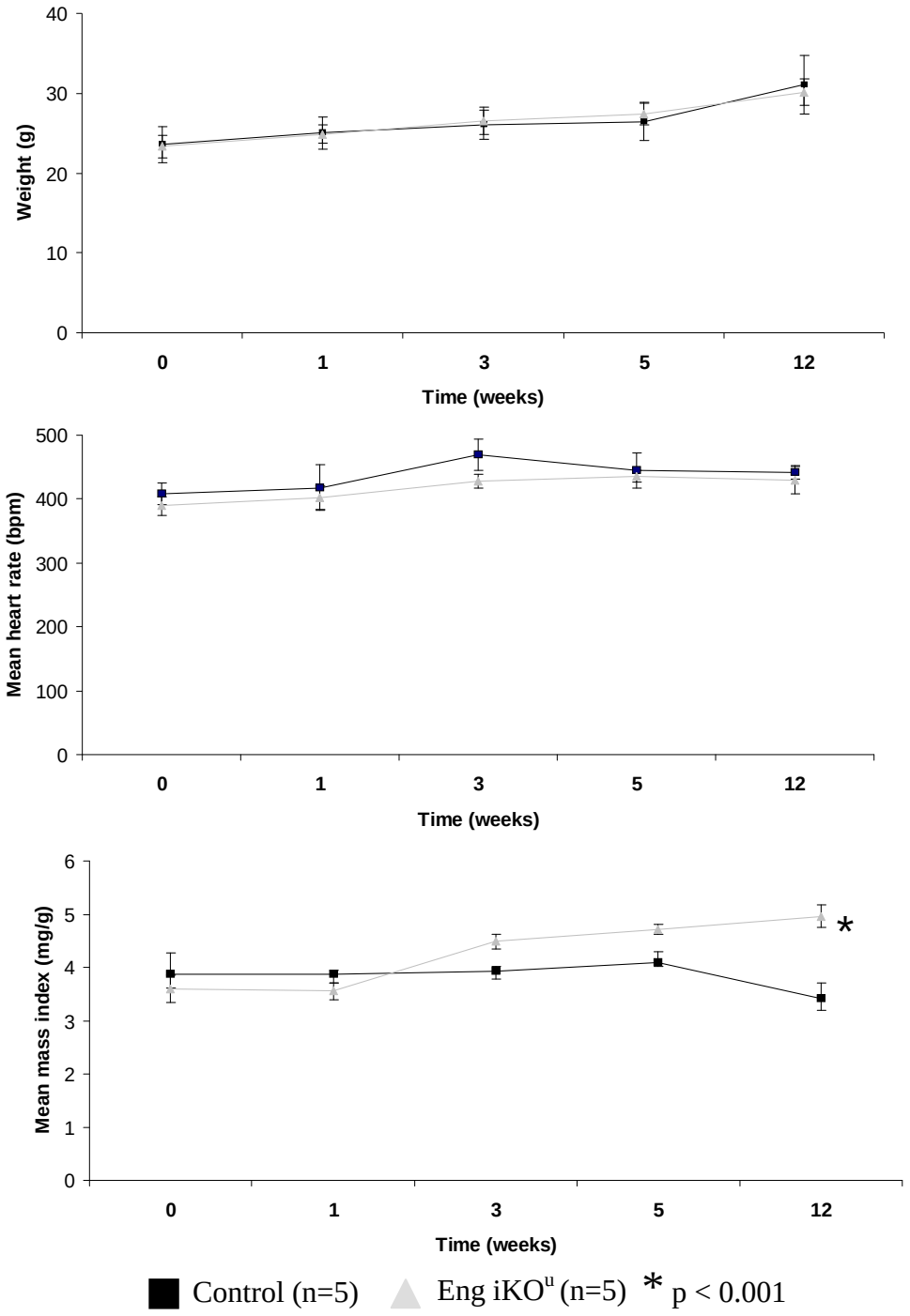
Weight (g)
40
30
20
10
0
0
1
3
5
12
Time (weeks)
Mean heart rate (bpm)
500
400
300
200
100
0
0
1
3
5
12
Time (weeks)
Mean mass index (mg/g)
6
5
4
3
2
1
0
*
0
1
3
5
12
Time (weeks)
Control (n=5)
Eng iKO^u (n=5)
* p < 0.001

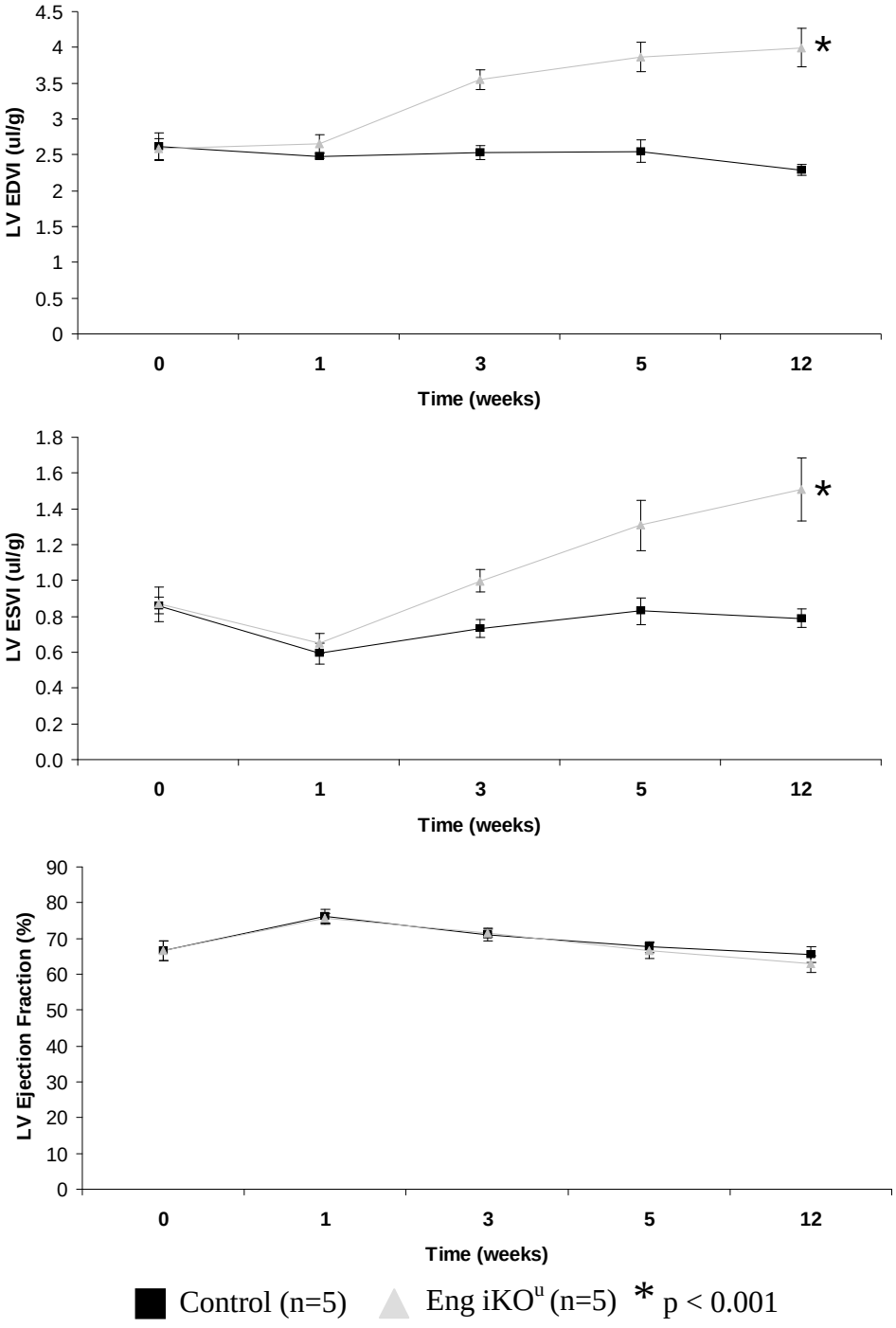

Figure 5.18 Changes in mean left ventricular mass, volume and function in control (n=4) and Eng-iKO^{u} (n=6) mice over 12 weeks following tamoxifen treatment.

Data expressed as mean ± SE.*p<0.001 repeat measures ANOVA.

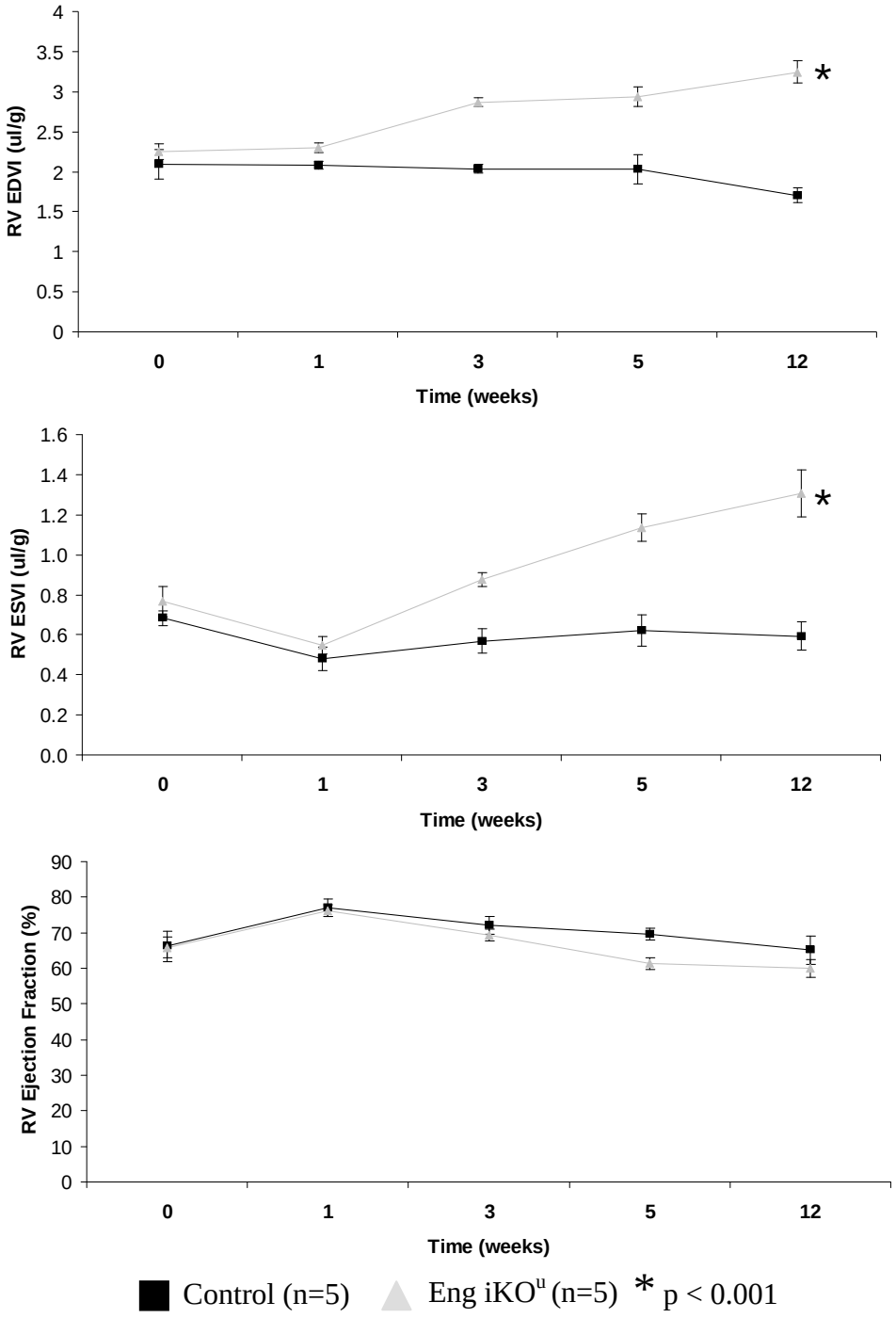

Figure 5.19 Right ventricular volume and function in control (n=4) and Eng-iKO^{u} (n=6) mice over time following tamoxifen treatment.

Data expressed as mean ± SE. *p<0.001 repeat measures ANOVA.

5.2.8 Effect of endoglin depletion on LV pressure-volume relationships.

Cardiac catheterisation using a conductance catheter allows for examination of the relationship between ventricular pressure and volumes throughout the cardiac cycle. This procedure gives information about systolic and diastolic ventricular function and can be used to obtain load independent measures of ventricular contractility. Combining these measurements with inotropic agents allows for assessment of the intact heart under basal and stress conditions. The major limitations of the procedure are the technical skills required to obtain accurate data and, in small animals, the measurements are limited to a single time point; due to its invasive nature this procedure is performed under terminal anaesthesia. As I saw no difference in ejection fraction between the control and *Eng-iKO*^{u} mice during the MRI experiments, these experiments were designed to assess if endoglin depletion resulted in more subtle effects on ventricular function. Equally it would allow assessment under basal and stress conditions and finally may give some insights into the effect of endoglin depletion on the wider cardiovascular system.

These experiments were performed using the same protocol as the initial MRI experiments. Briefly, *Eng*$^{fl/fl}$ and *Eng*$^{fl/fl}$*;Rosa26;Cre*^{ERT2} mice were treated with tamoxifen (2mg/day for 5 days). Five weeks following the first dose of tamoxifen cardiac catheterisation was performed as described in Chapter 2. Dobutamine, a positive inotrope and vasodilator, was infused at 5μg/kg/min and 10μg/kg/min to examine cardiac function under stress conditions. Analysis of the data was performed using the PVAN pressure-volume analysis software package (Millar). Details of the parameters obtained are shown in chapter 2 (table 2.2).

Analysis of the pressure volume loops obtained under basal and stress conditions are shown in table 5.6. Under basal conditions there were no significant differences in aortic or left ventricular pressures between *Eng-iKO*^{u} and control mice. However, there was a significant increase in left ventricular end systolic volume (28.7±5.9μl) in *Eng iKO*^{u} mice compared with 15.2±2.6μl in control(p=0.04) and a trend towards increased end diastolic volume (52.4±5.3μl) in *Eng iKO*^{u} mice compared with 41.1±2.5μl in control (p=0.06). These increases agree with those observed from the MRI analysis, but the volumes measured by conductance catheter were smaller than

those measured by MRI; this a recognised feature from previous studies comparing MRI and conductance catheter data and is discussed below. Unlike the MRI analysis the catheter data revealed no significant differences in stroke volume or cardiac output between *Eng-iKO*^{u} mice and controls. There was a significant difference in maximal left ventricular volume (55.5±5.4µl in *Eng-iKO*^{u} mice vs. 43.1±2.4µl in control, p=0.05) which would be consistent with an increased preload in endoglin depleted mice. However, there was no significant difference in arterial elastance (Ea) or systemic vascular resistance between the groups suggesting endoglin depletion has no effect on afterload under basal conditions. Measures of systolic and diastolic function (both load dependent and independent) did not reveal any significant differences under basal conditions confirming that endoglin depletion has no effect on cardiac function under resting conditions.

Following administration of dobutamine in control animals there was an expected increase in cardiac output, systolic function and left ventricular contractility. These effects were not seen following dobutamine administration in *Eng-iKO*^{u} mice with cardiac output, dP/dt_{max} and stroke work showing very little change. The load independent parameter dP/dt-EDV reduced with dobutamine in *Eng-iKO*^{u} mice whereas in control mice it increased. This difference following dobutamine administration was not universal across the load independent parameters. The difference between load dependent and independent parameters is likely due to the increased preload on the heart in *Eng-iKO*^{u} mice. This is also indicated by an increase LVEDV and dilated internal jugular veins (figure 5.20) in these mice. Arterial elastance (Ea), a measure of cardiac afterload, decreased in control mice following dobutamine administration at both doses. This would be expected as dobutamine is a vasodilator as well as an inotrope. However, in *Eng-iKO*^{u} mice there was no change in Ea with dobutamine. These results suggest that there may be an impairment of contractile reserve and vasomotor function, with reduced vasodilator response to dobutamine in *Eng-iKO*^{u} mice.

Table 5.6 Volumetric and haemodynamic parameters from cardiac catheter analysis of control and Eng-iKO^{u} mice 5 weeks following tamoxifen treatment.

Data expressed as mean ± SE. *p<0.05 # p=0.06.

	Baseline		**Dobutamine** 5μg/kg/min		**Dobutamine** 10μg/kg/min	
	Control n=10	***Eng iKO^{u}* n=9**	**Control n=6**	***Eng iKO^{u}* n=6**	**Control n=6**	***Eng iKO^{u}* n=6**
Sex	6M 4F	9M 1F	2M 4F	5M 1F	2M 4F	5M 1F
Aortic SBP (mmHg)	96.5 ± 3.7	93.6 ± 2.9				
Aortic DBP (mmHg)	66.7 ± 3.9	62.3 ± 2.8				
MAP (mmHg)	76.6 ± 3.8	72.7 ± 2.8				
Heart rate (bpm)	477 ± 17	438 ± 15	477 ± 14	448 ± 9.2	479 ± 14.3	452 ± 7
LV EDV (μl)	41.1 ± 2.5	**52.4±5.3#**	45.6 ± 2.9	52.7 ± 7.6	42.9 ± 1.8	52.1 ± 7.2
LV ESV (μl)	15.2 ± 2.6	**28.7±5.9***	13.0 ± 3.0	25.5 ± 8.9	10.7 ± 2.5	23.4 ± 9.0
LV SV (μl)	28.5 ± 2.0	28.6 ±2.9	35.0 ± 1.6	31.9 ± 5.2	35.4 ± 1.0	32.7 ± 5.7
CO (ml/min)	13.6 ± 1.1	12.6 ± 1.4	16.8 ± 1.2	14.4 ± 2.5	17.0 ± 0.9	14.9 ± 2.7
EF (%)	67.1 ± 4.8	53.9 ± 6.0	75.9 ± 5.1	59.5 ± 8.6	78.5 ± 4.2	61.8 ± 8.9
LV EDP (mmHg)	10.4 ± 0.9	12.5 ± 1.7	13.9 ± 1.8	11.5 ± 1.6	14.4 ±1.3	13.9 ± 1.2
LV ESP (mmHg)	91.5 ± 2.4	97.5 ± 1.9	94.8 ± 3.1	103.3±3.9	90.1 ± 3.7	93.5 ± 4.1
Stroke work (mmHg.μl)	2255 ± 218	2323 ± 250	2751 ± 279	2411 ± 386	2718 ± 200	2222 ± 365
Ea (mmHg/μl)	3.3 ± 0.19	3.7 ± 0.4	2.7 ± 0.1	3.6 ± 0.7	2.6 ± 0.1	3.5 ± 0.8
dP/dt_{max} (mmHg/s)	8179 ± 742	7516 ± 516	9697 ± 792	**7537 ± 629#**	9896 ± 596	**7603 ± 528***
dP/dt_{min} (mmHg/s)	-7069 ± 455	-6245 ± 463	-6333 ± 402	-5145 ± 500	-6022 ± 364	-4973 ± 503
Tau (ms)	11.5 ± 1.1	13.3 ± 1.1	12.9 ± 0.6	14.6 ± 1.5	12.2 ± 0.8	15.1 ±1.9
Total SVR (mmHg/ml/min)	5.7 ± 0.3	6.3 ± 0.8				
Parameters obtained after temporary preload reduction.						
PRSW (mmHg)	62.5 ± 6.4	59 ± 10.5	62.1 ± 6.9	67.1 ± 17	65.0 ± 7.8	66.1 ± 14
Ees (mmHg/μl)	2.92 ± 0.6	2.8 ± 0.4	2.4 ± 0.6	2.2 ± 0.5	2.7 ± 1.0	2.5 ± 0.8
dP/dt_{max}-EDV (mmHg/s/μl)	121.4 ± 22.8	97.4 ± 21.0	144.1 ± 19.9	**75.8 ± 16.8***	152 ± 18	**82.5 ± 15.8***

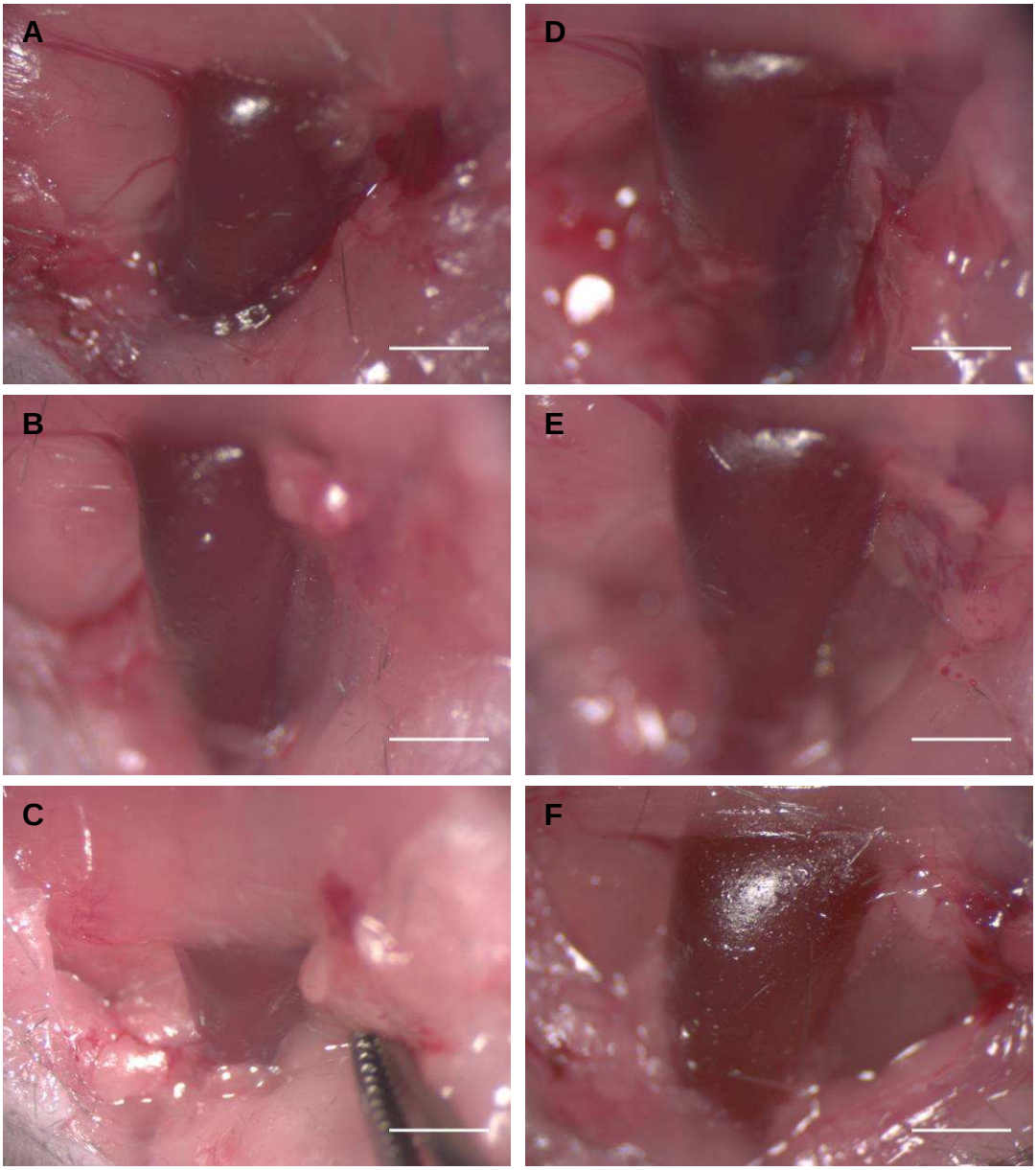

Figure 5.20 Macroscopic images of the left internal jugular vein of control (A-C, n=3) and Eng-iKO^{u} (D-F, n=3) mice.

The internal jugular vein appears larger in Eng-iKO^{u} mice suggesting elevated right heart pressures. A&D, B&E and C&F are littermates of the same gender. Scale bar 5mm.

5.2.9 Endothelial specific endoglin knockdown results in ventricular remodelling.

The MRI and cardiac catheter data both clearly show that ubiquitous endoglin knockdown in the *Eng-iKO*^{u} mice results in significant ventricular remodelling. As endoglin is expressed in a number of cell types, I wanted to determine whether the ventricular remodelling observed following ubiquitous knockdown of endoglin was partly or completely dependent on the role of endoglin in endothelial cells. To investigate this I used an endothelial specific Cre recombinase (*Cdh5(PAC)-Cre*^{ERT2}) that is well established in our lab to induce an endothelial specific endoglin knockdown (*Eng-iKO*^{e}) (Mahmoud *et al.*, 2010). As in previous experiments *Eng*$^{fl/fl}$ and *Eng*$^{fl/fl}$*;Cdh5(PAC)-Cre*^{ERT2} mice were treated with tamoxifen 2mg/day for 5 days to induce endoglin knockdown in endothelial cells. Cardiac MRI was then performed 5 weeks following the first dose of tamoxifen.

Analysis of left ventricular mass, volume and function is shown in table 5.7 and figure 5.21. There was a significant difference in the body weight between the 2 groups due to there being more male animals in the *Eng-iKO*^{e} group than the control group. Therefore it is important to use indexed measurements to account for this difference. As with the ubiquitous endoglin knockdown, endothelial specific knockdown resulted in increased left ventricular mass index (5.2 ± 0.2mg/g for *Eng-iKO*^{e} mice vs. 4.3 ± 0.1mg/g for control mice, p=0.01). Also indexed ventricular volumes, stroke volume index and cardiac index were significantly greater in the *Eng-iKO*^{e} group than controls. Interestingly, following endothelial specific endoglin knockdown there was a significant reduction in left ventricular ejection fraction in the *Eng-iKO*^{e} group (57.6 ± 3.3%) versus in the control group, (69.5 ± 2.0%, p=0.04).

These data suggest that the ventricular remodelling seen following endoglin knockdown is due to depletion of endoglin from the endothelium. Consequently, the changes seen in the heart are likely secondary to haemodynamic changes in the wider cardiovascular system.

Table 5.7 Analysis of MRI data showing cardiac mass, volumes and function in control and Eng-*iKO*^{e} mice 5 weeks after first tamoxifen dose.

Data expressed as mean ± SE.

	Control (n=3)	**Eng-iKO^{e} (n=5)**	**p value**
Sex	1M 2Fs	5M	**n/a**
Weight (g)	24.1 ± 3.2	29.7 ± 0.3	**0.05**
Heart rate (bpm)	458 ± 10	414 ± 20	0.2
Left Ventricle			
LV mass (mg)	102.5 ± 13.3	153.2 ± 4.9	**0.005**
LV mass index (mg/g)	4.3 ± 0.1	5.2 ± 0.2	**0.01**
EDV (µl)	60.4 ± 2.5	135.5 ± 12.0	**0.004**
EDVI (µl/g)	2.6 ± 0.3	4.6 ± 0.4	**0.01**
ESV (µl)	18.3 ± 0.6	59.0 ± 10.2	**0.02**
ESVI (µl/g)	0.8 ± 0.1	2.0 ± 0.3	**0.04**
SV (µl)	42.1 ± 2.8	76.6 ± 2.4	**0.0001**
SVI (µl/g)	1.8 ± 0.2	2.6 ± 0.1	**0.004**
Ejection fraction (%)	69.5 ± 2.0	57.6 ± 3.3	**0.04**
CO (ml/min)	19.3 ± 1.6	31.7 ± 1.9	**0.004**
CI (ml/min/g)	0.8 ± 0.1	1.1 ± 0.1	**0.05**

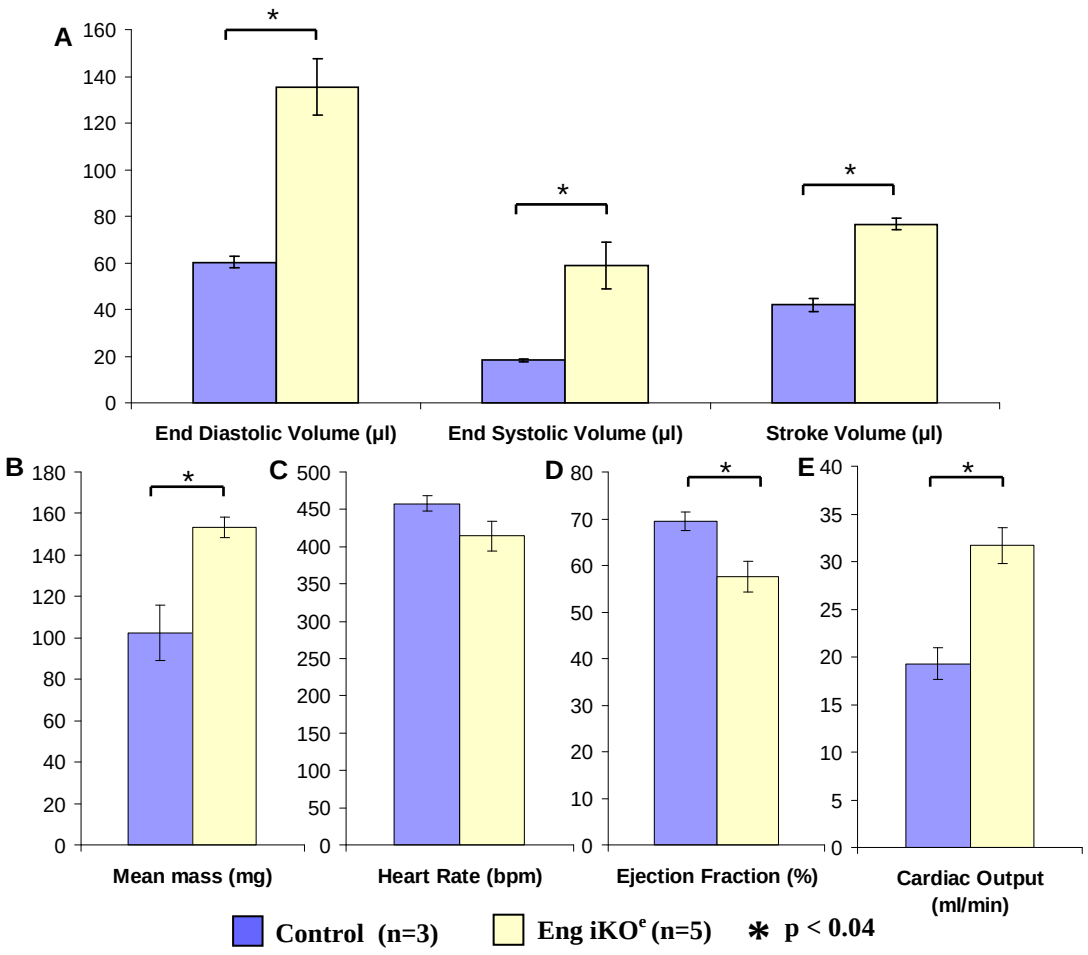

Figure 5.21 Analysis of MRI data showing cardiac mass, volumes and function in control and Eng-iKO^{e} mice 5 weeks after first tamoxifen dose.

Data expressed as mean ± SE, * = p<0.04.

5.2.10 Changes in extracellular matrix following endoglin knockdown.

In order to investigate if there were any changes in the extracellular matrix following endoglin knockdown, I performed a number of experiments to quantify collagen 1 protein expression and expression of extracellular matrix genes. Three groups of mice *Eng*$^{fl/fl}$, *Eng*$^{fl/fl}$*;Rosa26-Cre*^{ERT2} and *Eng*$^{fl/fl}$*;Cdh5(PAC)-Cre*^{ERT2} mice were treated with tamoxifen 2mg/day for 5 days, to generate control, *Eng-IKO*^{u} and *Eng-iKO*^{e} mice as previously n=3 per group). 5 weeks following the first dose of tamoxifen hearts were dissected and processed appropriately for protein or RNA quantification (using the methods described in chapter 2).

A Western blot was performed to quantify the expression of collagen 1, a major extracellular matrix protein in the heart. Quantification of this demonstrated no significant differences between the 3 groups (figure 5.22).

Quantitive real time PCR suggested that loss of endoglin may lead to increased expression of collagen 3, Ctgf, Timp1, Timp2 and Tgfβ1 with reduced expression of Mmp9 (figure 5.23). However, none of these differences were statistically significant (ANOVA) and there was considerable variation between individuals so that verification of any results would require large sample sizes. Furthermore, it is likely that any changes in extracellular matrix synthesis are related to the ventricular remodelling process rather than being a primary consequence of endoglin depletion *per se*, and that therefore any changes will be dynamic during the cardiac remodelling process. Testing this would require large sample sizes at multiple time points and was not possible within the time constraints of my PhD studies.

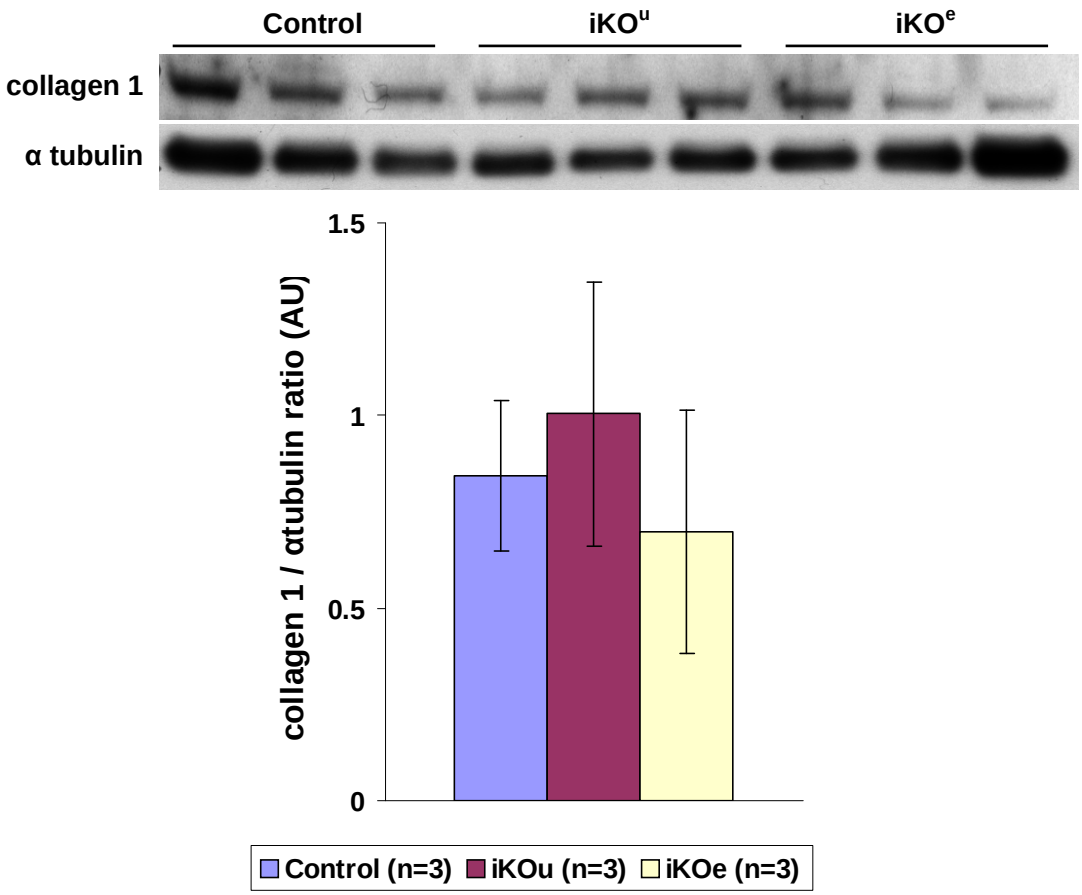

Figure 5.22 Expression of collagen 1 protein from hearts of control, Eng-iKO^{u} and Eng-iKO^{e} mice.

Western blot of cardiac protein from 3 mice of each group. Collagen I protein was detected using anti-Collagen I antibody and alpha-tubulin was used as a gel loading control. There was no significant difference between collagen I protein levels (normalised to alpha-tubulin) between the groups. Data was analysed using ANOVA.

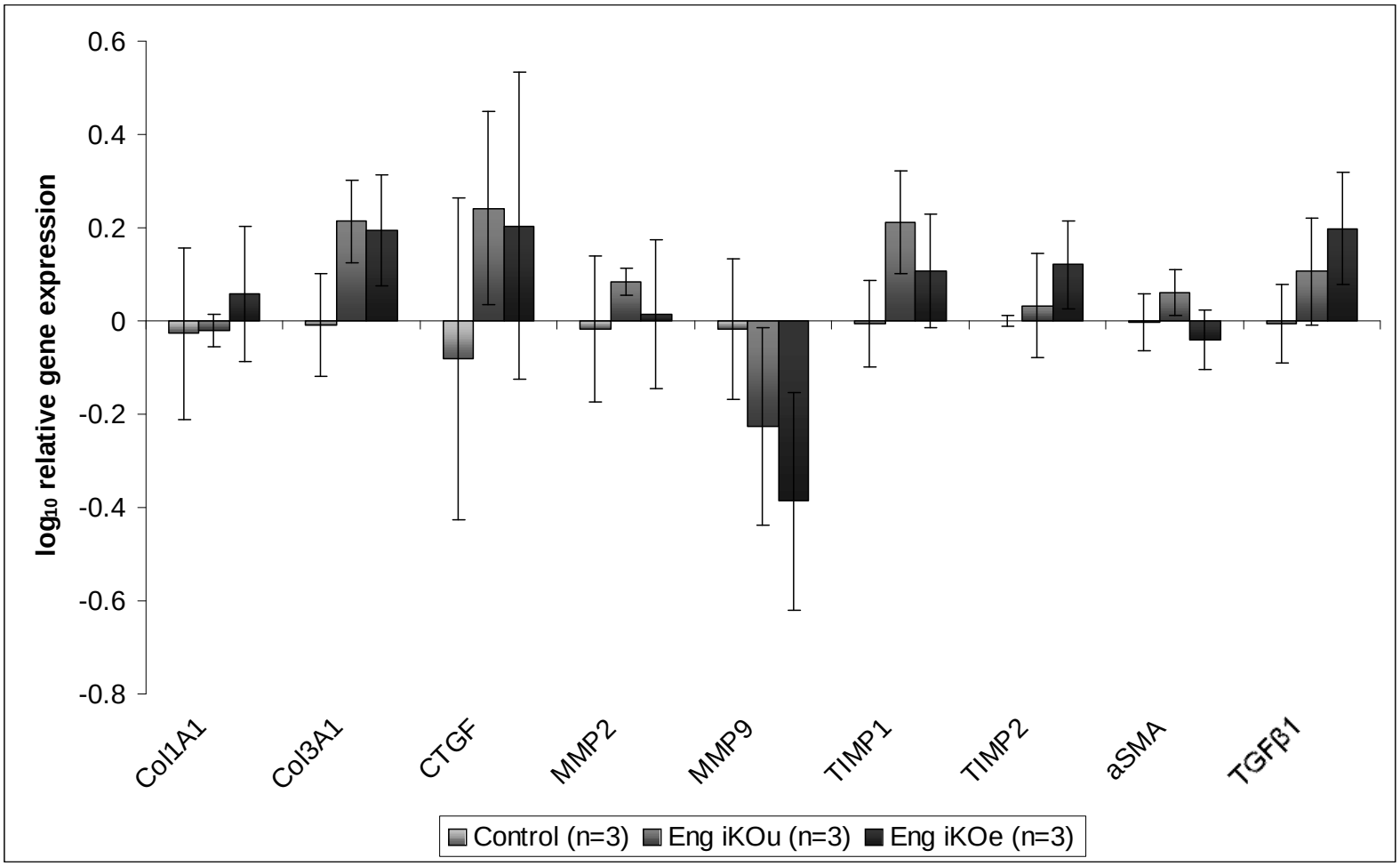

Figure 5.23 Expression of fibrosis genes from hearts of control, Eng-iKO^{u} and Eng-iKO^{e} mice.

There was no significant difference between the groups using ANOVA.

5.2.11 Endoglin depletion may result in eNOS uncoupling.

As ventricular remodelling is seen after endothelial specific endoglin depletion it is important to investigate changes in endothelial specific proteins. Endoglin has been shown to be critical for coupling of endothelial nitric oxide synthase (eNOS) activity (Jerkic *et al.*, 2004; Toporsian *et al.*, 2005). I therefore looked at the effect of losing endoglin expression on eNOS uncoupling. One approach that has been widely used to examine eNOS uncoupling is to investigate the ratio of eNOS monomer to dimer in tissues using native protein gels (i.e. proteins are separated by electrophoresis in the absence of reducing agents to preserve any dimeric forms). A high monomer/dimer ratio of eNOS protein corresponds to increased uncoupling (Cai *et al.*, 2005).

Figure 5.24 is a Western blot demonstrating eNOS expression in whole heart lysates from control, *Eng-iKO^{u}* and *Eng-iKO^{e}* mice. This suggests that there is a reduction in the dimeric form of eNOS in both Eng-iKO^{u} and Eng-iKO^{e} mice, which would be consistent with eNOS uncoupling in these mice. However, there is still a large amount of monomeric eNOS in all the samples. This could be due to the fact that eNOS is expressed in cardiomyocytes as well as endothelial cells (Balligand *et al.*, 1995). So it would be important to repeat these experiments in freshly prepared vascular endothelial cells, following endoglin knockdown, to determine whether there is endothelial specific eNOS uncoupling in *Eng-iKO^{e}* mice.

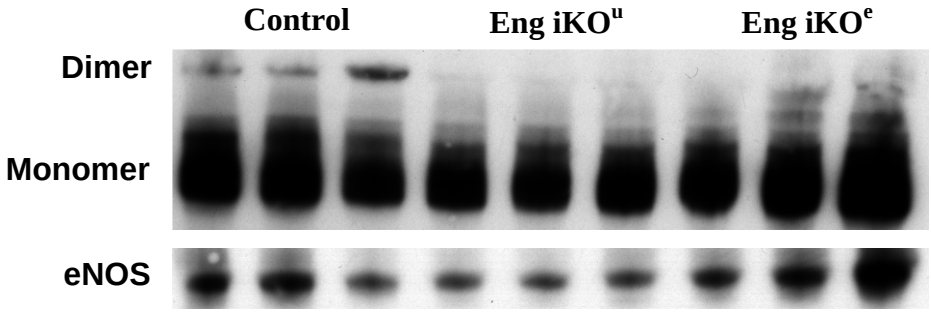

Figure 5.24 Expression of monomeric, dimeric and total eNOS protein from hearts of control, Eng-iKO^{u} and Eng-iKO^{e} mice.

This 'cold' western blot of native proteins shows the levels of dimeric and monomeric eNOS protein in whole heart extracts. The level of dimeric eNOS is reduced in both Eng-iKO^{u} and Eng-iKO^{e} mice. The lower gel shows total eNOS run under reducing conditions at normal temperatures.

5.3 Discussion

In vivo analysis of cardiac function in this chapter has shown that endoglin is essential in endothelial cells to maintain normal adult cardiovascular function. Using the inducible endoglin knockdown models, developed in our lab, I have demonstrated that endoglin is expressed in the normal mouse heart and that it can be efficiently depleted following Cre-ER^{T2} activation. The majority of endoglin protein is expressed in endothelial cells of the endocardium and blood vessels. This is consistent with previously published data demonstrating that endoglin and the endothelial cell maker, CD31, are expressed in similar patterns in the normal myocardium (van Laake *et al.*, 2006). However, this study used serial histological sections, each stained with a single antibody. In contrast, my work used co-immunofluorescence to establish that endoglin and CD31 are co-expressed in the same endothelial cells. Furthermore, previous work has not clearly established whether endoglin is co-expressed with other (non-endothelial) cell types in the normal heart. Chen et al reported that endoglin is co-expressed with fibroblasts (K. Chen *et al.*, 2004). Although their *in vitro* study is consistent with my results (chapter 4) showing endoglin expression in cardiac fibroblasts cultured *in vitro*, expression of endoglin in endogenous fibroblasts in the heart tissue was not shown. My data suggests that the level of endoglin expression is low in cardiac fibroblasts, certainly much lower than in endothelial cells. However, cardiac fibroblasts are large, flat cells that wrap around other cells within the myocardium in thin layers and so are not easily seen in tissue sections. Also, compared to other animal models where fibroblasts form the majority of cells, in the mouse heart, fibroblasts only account for around 27% of cells in the myocardium (Banerjee *et al.*, 2007). Although endoglin expression in cardiomyocytes was not specifically tested in the co-immunofluorescence experiments, immunohistochemical staining of mouse hearts for endoglin clearly show that endoglin is expressed in the cells surrounding the cardiomyocytes, but not in cardiomyocytes. Recently published data from Kapur confirm that in mouse myocardium endoglin is expressed in endothelial cells but not cardiomyocytes (Kapur *et al.*, 2012). This paper also reports endoglin expression in cultured cardiac fibroblasts.

The cellular changes within the infarcted myocardium post MI are well described (Frangogiannis *et al.*, 2002). My double immunofluorescence experiments confirmed

that there is an infiltration of inflammatory cells in the first 24 to 72 hours which is followed by proliferation of endothelial cells and fibroblasts by 5 days. There was also an increase in cells positive for αSMA between days 3 and 5 suggesting a proliferation of myofibroblasts in the injured myocardium. I have demonstrated that endoglin expression is increased in injured myocardium following infarction. This increase in expression is primarily driven by endothelial cell proliferation. However, endoglin expression was also seen in some αSMA-positive myofibroblasts infiltrating the wound by day 5. Macrophages and fibroblasts infiltrating the wound did not express endoglin.

My data is consistent with the findings of van Laake (van Laake *et al.*, 2006) who demonstrated an increase in endoglin expression in both mouse and human hearts following myocardial infarction. Tian and colleagues also demonstrated a similar increase in endoglin expression in the mouse myocardium following infarction (Tian *et al.*, 2010). In both these studies, the increased endoglin expression was thought to be confined to endothelial cells as both endoglin and CD31 showed a similar pattern of expression in serial sections. Increases in endoglin expression are seen in models of injury in other organ systems and are not isolated to endothelial cells alone. For example, in a porcine model of coronary artery injury, endoglin expression was increased and co-localised to endothelial cells, adventitial fibroblasts and those expressing αSMA, thought to be vascular smooth muscle cells (Ma *et al.*, 2000). Increased expression of endoglin has also been demonstrated in a variety of inflamed human tissues including bowel, liver, lung and skin (Torsney *et al.*, 2002). Similar to the work described in this chapter, the increased endoglin expression seen in dermal wound healing is primarily due to increases in numbers of endothelial cells, with no expression seen in macrophages or fibroblasts. However, between 4 and 10 days after injury endoglin is seen to be expressed in myofibroblasts migrating through the wound (Torsney *et al.*, 2002).

In my experiments, although endoglin was expressed in myofibroblasts following MI, it was not expressed universally in these cells. This leads to interesting hypotheses as to the source and diversity of the myofibroblasts themselves. Work by Zeisberg has demonstrated that endothelial to mesenchymal cell transition (EndMT) contributes to

myocardial fibrosis in a mouse model of cardiac pressure overload (Zeisberg *et al.*, 2007). Therefore, it is possible that those myofibroblasts expressing endoglin are endothelial cells undergoing EndMT in the injured myocardium. However, in order to demonstrate this is the case then cell lineage tracing would be needed.

In order to study the effects of endoglin depletion on the injured heart it was important to establish a knockdown model for this. Furthermore, as I had shown the endoglin was expressed in myofibroblasts and endothelial cells in the heart following myocardial infarction, I used a ubiquitous Cre to ensure knockdown in both cell types. I was able to demonstrate that the Rosa26-Cre^{ERT2} was expressed within the heart and that activation of the Cre^{ERT2} with intraperitoneal delivery of tamoxifen led to endoglin knockdown. The tamoxifen dose titration studies demonstrated that a 5 day course of tamoxifen was sufficient to do this. However, two mice in the 7 dose cohort demonstrated only partial endoglin knockdown. These mice were littermates. The reasons for this poor response are unclear but possibilities include genotyping errors, incomplete expression of the Rosa26-Cre^{ERT2} within the myocardium, dosing errors or problems with injection and absorption of tamoxifen. However, all further experiments used the 5 dose protocol and immunohistochemical analysis demonstrated a consistent knockdown even after 3 months. Also, all animals in the MRI experiments had a consistent phenotype suggesting efficient knockdown of endoglin.

In their paper van Laake and colleagues (van Laake *et al.*, 2006) demonstrated that cardiac function following myocardial infarction was significantly worse in endoglin heterozygous mice. My pilot experiment concurred with their findings with greater left ventricular adverse remodelling and worse cardiac function following myocardial infarction in *Eng-iKO^{u}* mice than controls (table 5.1). However, group numbers were too small to perform statistical analysis. Nevertheless, it was clear from these experiments that considerable ventricular remodelling occurred in the sham operated *Eng-iKO^{u}* mice. Unfortunately this finding meant that this was no longer a useful model for studying the effects of endoglin depletion on cardiac function post myocardial infarction. Instead there was a gradual ventricular remodelling, which was evident at the 3rd week following endoglin depletion. Without an earlier time point assessing cardiac function it is impossible establish if the greater remodelling and

worse function was due to the lack of endoglin in the healing infarct or secondary to further remodelling on the already infarcted heart. The fact that the infarct size was the same in both the *Eng iKO*^{u} and control groups (table 5.1) points towards the latter. There appeared to be reduced LV ejection fraction in the injured *Eng-iKO*^{u} mice compared with controls following MI (table 5.1), and this was not seen in the uninjured *Eng-iKO*^{u} or *Eng-iKO*^{e} mice (table 5.2, table 5.4 and table 5.7). There was no evidence of ventricular remodelling in the *Eng*$^{fl/+}$*;Rosa26-Cre*^{ERT2} mouse (table 5.3) suggesting that the ventricular remodelling was endoglin-dose dependent perhaps making this a better model to study the effects of endoglin depletion post myocardial infarction.

The finding that endoglin depletion leads to *de novo* ventricular remodelling in the absence of injury is novel and has not previously been described. My experiments clearly show that both left and right ventricles undergo remodelling. A note of caution must be introduced with regard to the right ventricular measurements as these were made using images orientated to the short axis of the left ventricle rather than the right ventricle. The complex geometry and the wide angle between the inflow and outflow of the right ventricle make accurate assessment of volume and function challenging (Wiesmann *et al.*, 2002). Ideally images used to quantify right ventricular volumes and function should be orientated to the short axis of the RV (Wiesmann *et al.*, 2002; Schneider *et al.*, 2006) but this would increase imaging time if performed in addition to LV images. However, the changes in RV volume and function are consistent across different experiments and so likely represent a true finding.

In *Eng iKO*^{u} mice there is an increase in left ventricular mass and myocyte hypertrophy consistent with left ventricular hypertrophy. In these mice there are significant increases in ventricular volumes, stroke volume and consequently cardiac output. Significant remodelling has occurred by 3 weeks following gene knockdown and both left and right ventricles continue to enlarge; the latest time point used in this study was 3 months. Over this time period there is no reduction in systolic function as measured by left ventricular ejection fraction. Endoglin heterozygous mice do not develop a similar phenotype (Torsney *et al.*, 2003; van Laake *et al.*, 2006). This is consistent with the fact that tamoxifen treated *Eng*$^{fl/+}$*;Rosa26-Cre*^{ERT2} mice did not undergo cardiac remodelling. This suggests that there is a “dose” effect with endoglin

depletion needing to reach a critical, low level before the phenotypic changes manifest themselves.

It has been described that expression of Cre recombinase within the myocardium can lead to toxicity (Buerger *et al.*, 2006; Koitabashi *et al.*, 2009). Buerger and colleges demonstrated that the over expression of Cre recombinase within the myocardium, particularly at high levels, resulted in the development on a dilated cardiomyopathy (Buerger *et al.*, 2006). This cardiomyopathy was not reversible but survival was improved with treatment with ACE inhibitors and beta blockers (Buerger *et al.*, 2006). However, activation of Cre recombinase within the myocardium by a tamoxifen inducible, myocardial specific Cre (MerCreMer transgenic mice) resulted in a transient cardiomyopathy (Koitabashi *et al.*, 2009). This transient cardiomyopathy was not evidence when lower doses of tamoxifen or raloxifene (another oestrogen receptor modulator). This may be due to reduced activation of Cre recombinase and hence lower toxicity or that tamoxifen may cause a transient cardiomyopathy at higher doses. However, control mice did not demonstrate any cardiac dysfunction following tamoxifen administration suggesting that tamoxifen toxicity was not the cause (Koitabashi *et al.*, 2009). There is *in* vitro evidence that tamoxifen can cause impaired myocyte contractility and calcium handling (Asp *et al.*, 2013). My experiments in mice expressing *Rosa26-Cre*^{ERT2} demonstrate that there is no evidence on myocardial toxicity from activation of Cre recombinase using this tamoxifen inducible Cre. It also suggests that there is no evidence of toxicity from tamoxifen treatment. This is supported by the time course experiment, where control animals were imaged prior to tamoxifen administration and did not demonstrate any cardiac dysfunction over the course on the experiment.

The pattern of remodelling that occurred following endoglin depletion (table 5.8) is that of high output heart failure with left and right ventricular dilatation (in both systole and diastole) with increased cardiac output and is similar to that seen in models of volume overload heart failure. One such model induces volume overload by the creation of an aortocaval fistula. In this model there are no changes in heart rate or blood pressure but evidence of left ventricular dilatation and hypertrophy. However, there is evidence of reduced cardiac function, contractility and elevated venous and left ventricular pressures (Tanaka *et al.*, 1996; Scheuermann-Freestone *et*

al., 2001). This contrasts with pressure overload following transverse aortic constriction where a reduced systolic blood pressure, ventricular hypertrophy and systolic dysfunction with LV dilatation developing later (Liao *et al.*, 2002). These are extreme forms of cardiomyopathy and so the changes seen in my experiments may just represent a milder phenotype. However, the changes of left ventricular hypertrophy, ventricular dilatation, increased stroke volume and cardiac output with preserved systolic function are not dissimilar to those seen in the hearts of athletes (Maron and Pelliccia, 2006). Endoglin depleted mice could be left for a longer period (e.g. 6 months) to monitor progression of the ventricular remodelling. Specifically this may discriminate between athlete's heart and high cardiac output heart failure.

My data was consistent with previous data showing that ventricular volumes and ejection fractions are consistently lower when measured by conductance catheters compared to MRI (Jacoby *et al.*, 2006; Nielsen *et al.*, 2007; Winter *et al.*, 2008). I did notice marked variation in data (particularly volumetric) collected using the conductance catheters and as consequence this limited the ability to discriminate between the experimental groups. My data did confirm LV dilatation in endoglin depleted mice compared to controls with no differences in resting systolic function. However, there did appear to be an impairment of contractile reserve as measures of myocardial contractility (dP/dt and the dP/dt-EDV relationship) did not increase following dobutamine administration. It is important to note that dP/dt is load dependent and so may be affected by differences in afterload induced by dobutamine, but the dP/dt-EDV relationship is load independent and so this is likely to reflect a true change. Also, there was not a reduction in afterload in endoglin deplete mice, unlike in control mice, following dobutamine (an inodilator). This change was not significant but does suggest that endoglin depletion has an effect on vasomotor function (see below). I would also have expected that total systemic resistance (TVR) should be lower in *Eng-iKO*^{u} as the mean aortic blood pressure (MAP) was the same, compared to controls, but the cardiac output (CO) is higher in these mice (TVR=MAP/CO). However, there was no significant difference.

Initial studies examining the effects of dobutamine on the human heart demonstrated approximately 50% increase in cardiac output with dobutamine administration at 8μg/kg/min, but no significant effect on heart rate (Rigaud *et al.*, 1977). Therefore,

the increase in cardiac output following dobutamine administration in my experiments, approximately 25%, is lower than would be expected. In studies involving mice the effect of dobutamine is variable. For example, Bauer and colleagues demonstrated approximately a 2 fold increase in cardiac output, when measured by conductance catheters (Bauer *et al.*, 2008; Bauer *et al.*, 2010a). However, in studies using MRI to measure cardiac function the increase in cardiac output was in the region of 20 to 25% (Wiesmann *et al.*, 2001b; Williams *et al.*, 2001). It is unclear why these differences exist but it is likely due to differences in genetic background of the mice, the choice of anaesthetic agent and experimental variables such as temperature.

The cardiac catheter data is inconclusive but this is technically a very challenging technique that requires a high level of experience to achieve good quality data. Comparing conductance catheters to cardiac MRI, Winter and colleagues demonstrated that MRI is more sensitive for detection changes post MI. They showed that in mice, following myocardial infarction, MRI had 100% sensitivity and specificity for distinguishing between mice with small infarcts (<30% of LV mass) and sham operated mice (Winter *et al.*, 2008). For conductance catheters the sensitivity was 93% and specificity was 80% (Winter *et al.*, 2008). This study also highlighted the advantages and disadvantages of these techniques. MRI is a sensitive, non-invasive technique that also allows measurement of global and regional cardiac function along with visualisation of myocardial structure and calculation of myocardial mass and infarct size. Although not used in my studies, stress cardiac MRI with dobutamine would offer an alternative, non-invasive measure of contractile reserve (Wiesmann *et al.*, 2001b; Williams *et al.*, 2001). Conductance catheters are invasive (with potential for blood loss during surgery which would affect outcomes) and are limited to single time point measurements. However, they have high temporal resolution (0.5ms) and provide sensitive, load independent measurements of systolic and diastolic function in real time. In addition, conductance catheters also provide insight into the interaction of the heart and vascular system (Winter *et al.*, 2008).

Endoglin is not expressed in cardiomyocytes in the adult heart (Kapur *et al.*, 2012) and in the uninjured heart is primarily restricted to the endothelial cells. Furthermore, I have demonstrated that the cardiac phenotype is due to the effects of endoglin depletion in endothelium as the same phenotype was seen following endothelial

specific knockdown and ubiquitous endoglin knockdown. Therefore, the phenotypic changes seen following endoglin depletion are due either to loss of endoglin function within the vasculature of the heart, or are secondary to an effect on the wider cardiovascular system.

Endoglin has been shown to be important in the regulation of vascular tone. Jerkic and colleagues demonstrated that mean arterial blood pressure is higher in endoglin heterozygous mice and that there is an attenuation of the normal dose dependent reduction in mean arterial pressure with endothelial dependent vasodilators. They also demonstrated in an isolated, perfused hind limb model, that endothelium dependent reduction in vascular resistance was impaired in these mice (Jerkic *et al.*, 2004). Levels of endothelial nitric oxide synthase (eNOS) and nitric oxide (NO) activity were reduced in endoglin heterozygous mice and Jerkic et al suggested this was the cause of the reduced effect of NO dependent vasodilatation. They hypothesise that this impairment in vasomotor control leads to AV shunting and that subsequent capillary remodelling results in AV malformations seen in HHT (Jerkic *et al.*, 2004). In contrast to this Toporsian et al. found that there was an enhanced endothelium and eNOS mediated vasodilatation in pre-constricted, isolated mesenteric arterioles from endoglin heterozygous mice. They confirmed that eNOS was reduced in endothelial cells isolated from these mice and demonstrated that this was due to a reduced plasma half life. They also demonstrated that endoglin is important in the regulation of eNOS coupling. They found that treatment of the arteries from endoglin heterozygous mice with a superoxide scavenger reversed the vasomotor abnormalities suggesting that eNOS uncoupling resulted in this impaired response and may contribute to the pathogenesis of HHT (Toporsian *et al.*, 2005). My data demonstrates that there was no reduction in cardiac afterload following dobutamine administration in *Eng-iKO*^{u} mice. This suggests an abnormal vasodilator response, but could represent either the inability to vasodilate in an already maximally vasodilated circulation, which would be more consistent with Toporsian's results, or a failure of vasodilatation, more consistent with Jerkic. I have also demonstrated that eNOS appears to be uncoupled in *Eng-iKO*^{u} mice. If this is the case then examining alterations in cardiac afterload following administration of short acting vasodilators followed by vasoconstrictors may be able to clarify the effect of endoglin depletion on vasomotor function. Also if this effect is due to eNOS uncoupling then treatment of these animals with

tetrahydrobiopterin (BH4), an essential cofactor of endothelial NO synthase, may result in a rescue of this phenotype.

These data show a novel phenotype in endoglin depleted mice and show that loss of endothelial endoglin has a major effect on both left and right ventricles of the heart (table 5.8). MRI experiments demonstrate that both ventricles are dilated by 3 weeks following endoglin knockdown and this phenotype persists for at least 3 months. Cell specific endoglin knockdown demonstrated that these changes are mediated by endoglin depletion in endothelial cells. Conductance catheters have suggested an impairment of vasomotor regulation may lead to this phenotype. It is possible that this is mediated by the effect of endoglin depletion on eNOS function in endothelial cells. However, further work is needed to establish the exact mechanisms behind this novel phenotype.

Table 5.8 Summary of the changes in left ventricular mass and systolic function following myocardial infarction and endoglin knockdown.
Eng-iKO^{u} = ubiquitous endoglin knockdown, Eng-iKO^{e} = endothelial specific endoglin knockdown, ↑ = increased, ↓ = decreased, → = no change.

	Myocardial infarction	**Eng-iKO^{u}**	**Eng-iKO^{e}**
Left ventricular mass	↑	↑	↑
Left ventricular mass index	↑	↑	↑
End diastolic volume	↑	↑	↑
End diastolic volume index	↑	↑	↑
End systolic volume	↑	↑	↑
End systolic volume index	↑	↑	↑
Stroke volume	↓	↑	↑
Stroke volume index	↓	↑	↑
Ejection fraction	↓	→	↓
Cardiac output	↓	↑	↑
Cardiac index	↓	↑	↑

Chapter 6 Discussion and future work

It is well recognised that endoglin plays an important role in vascular development and disease (Lopez-Novoa and Bernabeu, 2010). However, little is known about the role of endoglin in cardiac fibrosis. My studies have demonstrated that endoglin is expressed in cardiac myofibroblasts *in vitro*, with expression seen in endothelial cells and cardiac fibroblasts *in vivo*. This is consistent with published studies showing endoglin expression in endothelial cells (van Laake *et al.*, 2006; Kapur *et al.*, 2012), cardiac fibroblasts (K. Chen *et al.*, 2004; Shyu *et al.*, 2010; Kapur *et al.*, 2012) but not cardiomyocytes (Kapur *et al.*, 2012). The published *in vitro* studies described in section 1.6.5 demonstrate that inhibition of endoglin can attenuate collagen I secretion from rat cardiac fibroblasts suggesting that endoglin is a positive regulator of fibrogenesis. Using Cre-lox technology I was able to efficiently knock down endoglin expression in primary cardiac fibroblasts and used this novel approach to study the effects of endoglin on the fibrotic response to TGFβ1. Stimulation of mouse primary cardiac fibroblasts by TGFβ1 led to the phosphorylation of Smad2 with no effect on the phosphorylation of Smad1/5/8 confirming that TGFβ1 signals via the Smad2/3 pathway in cardiac fibroblasts (ten Dijke and Arthur, 2007). In their study, Shyu and colleagues examined the effects of TGFβ1 stimulation on Smad3 phosphorylation and confirmed that there is an increase in Smad3 phosphorylation following stimulation with TGFβ1. However, they demonstrated that TGFβ1 also signals via non-canonical pathways (Shyu *et al.*, 2010). In endoglin depleted fibroblasts pSmad2 levels were similarly increased in response to TGFβ1. However, there did appear to be an increase in Smad1/5/8 phosphorylation albeit not statistically significant. Interestingly, gene expression of Id1, a downstream target of Smad1/5/8 signalling, was marginally increased in *Eng iKO*^{u} fibroblasts compare to controls under basal conditions. There were significant reductions in collagen 1 and Mmp2 gene expression in *Eng iKO*^{u} fibroblasts suggesting that endoglin depletion may result in modification of the fibrotic response to TGFβ1. However, the response of TGFβ signalling pathway genes following stimulation with TGFβ1 was similar between control and *Eng iKO*^{u} fibroblasts.

In vitro studies using fibroblasts isolated from other organ systems give conflicting results with some suggesting endoglin is a negative regulator of fibrosis (Diez-Marques *et al.*, 2002; Leask *et al.*, 2002; Burke *et al.*, 2010; Holmes *et al.*, 2011), with other suggesting the opposite (K. Chen *et al.*, 2004; Meurer *et al.*, 2010; Shyu *et al.*, 2010; Morris *et al.*, 2011; Kapur *et al.*, 2012). The different methodologies used to investigate the effect of endoglin are likely to explain these differing responses. Those that suggest that endoglin is a positive regulator over-expressed endoglin in fibroblasts, whereas those that demonstrated negative regulation inhibited endoglin either by siRNA or endoglin specific antibodies. The over-expression studies do not take into account the possibility that soluble endoglin, which is known to antagonise TGFβ1 (Venkatesha *et al.*, 2006; Walshe *et al.*, 2009), may also be increased. This effect of over-expressing endoglin was confirmed by Kapur and colleagues who demonstrated that the over-expression of endoglin resulted in an increase in soluble endoglin in culture media and that soluble endoglin attenuated collagen 1 production in response to TGFβ1 (Kapur *et al.*, 2012). It is likely that endoglin is indeed a positive regulator of fibrogenesis and this concept is supported by *in vivo* data investigating fibrosis in endoglin heterozygous mice. In two models of renal fibrosis (radiation induced fibrosis and infarct reperfusion injury) there was reduced fibrosis in endoglin heterozygous mice compared to controls (Docherty *et al.*, 2006; Scharpfenecker *et al.*, 2009). Equally, in pressure overload heart failure there was reduced fibrosis seen in endoglin heterozygous mice (Kapur *et al.*, 2012).

The lack of any significant difference in collagen expression between endoglin replete and depleted cells may be due to the dynamic responses to TGFβ1 stimulation. Shyu demonstrated that peak expression of collagen 1 and endoglin in rat cardiac fibroblasts following TGFβ1 stimulation is at 16 hours (Shyu *et al.*, 2010). Also, growth arresting cardiac fibroblasts with serum starvation, as in my own studies, induces expression of extracellular matrix proteins (Leicht *et al.*, 2001), and so further stimulation may not produce a further response. Further studies are needed to confirm the optimal culture conditions and duration of stimulation experiments to ensure maximal responses are seen.

My studies have seen the successful introduction of pre-clinical cardiac MRI at Newcastle University and have highlighted the powerful nature of this technique. I

have demonstrated that MRI can be used in a number of models of cardiac disease and significant differences can be seen, even with small sample sizes. There are a number of methods available to measure cardiac structure and function in mice. As with any investigation there are advantages and disadvantages. The major advantage of MRI is that it provides true three dimensional images without relying on geometrical assumptions (Florentine *et al.*, 1986; Shapiro *et al.*, 1989; Ruff *et al.*, 1998). This is particularly important for studies following surgical myocardial infarction as there is significant deformation of the left ventricle as can be seen in figure 3.8 and figure 3.10. Given the accuracy and reproducibility of cardiac MRI (Ruff *et al.*, 1998) it is ideally suited to longitudinal studies. In addition to simple functional assessment, MRI is ideally suited to performing multimodal studies investigating several pathophysiological parameters at a time including, perfusion, regional function and energy metabolism (Akki *et al.*, 2013). The hardware requirements and consequently costs for MRI are greater. However, I have demonstrated that, despite the technical challenges of cardiac MRI, it is possible that the introduction of new techniques can be researcher led. Equally, I have demonstrated that it is possible to achieve moderate throughput with the acquisition of the dataset required for cardiac function assessment taking about 45 minutes and 10 animals scanned in a normal working day.

The other commonly used method for assessing cardiac structure and function are echocardiography and invasive cardiac catheterisation. Echocardiography has the advantages of being quick, so rapid throughput is achievable. However, as discussed in chapter 3 it has moderate correlation with MRI derived functional parameter but is less reproducible than MRI (Stuckey *et al.*, 2008). Consequently, more animals would be needed to provide statistical power (Stuckey *et al.*, 2008). Invasive cardiac catheter experiments provide volumetric and functional data, but not structural information. However, as discussed in chapter 5, it gives load dependent and independent measures of cardiac function with high temporal resolution. Also it allows rapid measurement of alterations to cardiac function following administration of cardio-active drugs, such as dobutamine. However, compared to MRI, it underestimates ventricular volumes and ejection fraction (Jacoby *et al.*, 2006; Winter *et al.*, 2008). Finally, its invasive nature means that longitudinal measurements are not possible.

Pragmatically the method used for measuring cardiac function depends on access and expertise of any given institution and on the information needed for any given study. However, these methods are not mutually exclusive and may give different information. Thus, a hybrid approach may give complementary data as in my studies whereby I was able to quickly establish the phenotype in a small number of mice and measure the longitudinal progression using cardiac MRI. This information was supplemented by invasive catheter data that demonstrated an impairment of contractile reserve and vasodilator response following dobutamine administration.

One of the initial aims of my research was to examine the effects of endoglin on healing and fibrosis following myocardial infarction. However, I discovered that ubiquitous knock down of endoglin in adult mice resulted in a novel phenotype with biventricular dilatation and a high cardiac output. Consequently, a ubiquitous endoglin knockdown model is not suitable to study the effects of endoglin on post myocardial infarction healing. However, one of the advantages of the Cre-lox system is its flexibility (Davey and MacLean, 2006). As a result I was able to establish that the phenotype was not due to Cre toxicity seen in other models (Buerger *et al.*, 2006; Koitabashi *et al.*, 2009), that there was a 'dose' effect, with no phenotype seen following loxP recombination of a single floxed endoglin allele and that the phenotypic changes seen were due to endoglin knock down in endothelial cells, by using an endothelial specific Cre. There are a number of methods available to investigate the role of specific genes in animal models. In my experiments we used an inducible gene knockdown technique using Cre-Lox technology, as described in sections 1.7, 4.2.2 and 5.2.3. The advantage of using this technology is that endoglin can be knocked down in a time and tissue specific manner. Equally, the mice develop normally prior to Cre induction which is important where homozygous deletion of a gene result in embryonic lethality, as with endoglin (Arthur *et al.*, 2000). There may also be adaptations to gene knockout when using global knockout models, such as in endoglin heterozygous endothelial cells where there is a down regulation of Alk5 expression (Lebrin *et al.*, 2004). Therefore, one advantage of using Cre-Lox technology is that these adaptations may not have time to develop following gene knockdown.

My studies revealed that depletion of endoglin results in biventricular dilation and a high cardiac output state which, based on the cardiac catheter data, may be progressing to cardiac failure. The catheter data also suggests that there is an impaired vasomotor response which is discussed in section 5.3. My data and that of van Laake (van Laake *et al.*, 2006) suggest that endoglin is essential for the maintenance of normal cardiac structure and function in health and disease. It is important to consider how these findings relate to previous work by Kapur et al (Kapur *et al.*, 2012) showing that a reduction in endoglin results in improved haemodynamics, reduced fibrosis and increased survival in a pressure overload model of heart failure. There are a number of possible explanations. Firstly following myocardial infarction there is a significant insult followed by inflammation and fibrosis. So it may be that impairment of the inflammatory response, particularly recruitment of mononuclear cells (Post *et al.*, 2010) results in delayed infarct healing and consequently greater adverse remodelling in endoglin heterozygous mice. However, it may also be that reduced fibrosis results in infarct expansion and more severe LV dysfunction. My studies initially aimed to address this hypothesis. Unfortunately, with the ubiquitous Cre used and subsequent effects of endoglin knockdown on the heart, there were endogenous changes to so I was unable to address this. However, my host laboratory has now acquired a collagen specific inducible Cre which may aid future studies of this hypothesis. Also, Zeisberg demonstrated that endothelial to mesenchymal transition (endMT) contributes to fibrosis in a pressure overload model (Zeisberg *et al.*, 2007) and as endoglin is predominantly expressed in endothelial cells, it would be important to investigate its role in the contribution of endMT to fibrosis in both MI and pressure overload models.

The second possibility is that in the pressure overload heart failure model it is the reduced level of endoglin and its effects on vascular function that results in beneficial effects on the myocardium. If endoglin depletion does result in vasodilatation then that could be responsible for the favourable effects. Inhibition of the renin angiotensin system results in vasodilatation. Treating mice with either angiotenisn converting enzyme inhibitors or angiotensin receptor blockers following aortic constriction results in reduce myocyte hypertrophy, improved cardiac function and reduced fibrosis.(M. A. Rossi and Peres, 1992; Rockman *et al.*, 1994; Lei Li *et al.*, 2010; Martino *et al.*, 2011; Muller *et al.*, 2012). These changes are not dissimilar to those

seen in endoglin heterozygous mice. Interestingly, soluble endoglin also reduced fibrosis but did not improve cardiac haemodynamic following aortic constriction (Kapur *et al.*, 2012), perhaps suggesting that the mechanism of action of soluble endoglin may be different to that of tissue endoglin.

With regard to the work presented in this thesis future studies will help to clarify some of these points. Specifically:

1. Further longitudinal studies following endothelial endoglin knockdown will allow us to determine if these mice eventually develop heart failure.
2. Carefully performed cardiac catheter studies investigating the response to vasodilators and vasoconstrictors may help clarify the haemodynamic effects endoglin depletion has *in vivo* on the vascular system.
3. Further studies investigating the role of eNOS in mediating the effects of endoglin knockdown and possible rescue using BH4.
4. Evaluation of vasomotor responses in *Eng-iKO^{e}* resistance arteries *ex vivo* (e.g. mesenteric artery)
5. The use of an inducible collagen 1 Cre will allow us to examine the effects of endoglin depletion on fibrosis following myocardial infarction.
6. The use of lineage tracing with *Cdh5(PAC)-Cre^{ERT2};Rosa26-floxedstopYFP* line would allow examination of the endothelial contribution to fibrosis following myocardial infarction in a manner similar to Zeisberg (Zeisberg *et al.*, 2007).

However, one of the main limitations in mouse models, including those described in this thesis, are that they use young, healthy animals which don't readily mimic human cardiovascular disease. Therefore, it may be appropriate to choose a different model, for example, the ApoE knockout or the ApoE/LDL double knockout mice which show features of atherosclerosis when fed high fat diets. Indeed endoglin is expressed in human atherosclerotic plaque (Piao and Tokunaga, 2006) and statins appear to modulate the expression of endoglin (Rathouska *et al.*, 2011). So modulating the expression of endoglin may lead to new therapies designed to prevent or slow the progression of atherosclerosis before a major cardiovascular event has occurred. In addition myocardial infarction induced by permanent LAD occlusion does not allow study of the effects of reperfusion injury and perhaps is a better model for studying

chronic heart failure. In this case an infarct reperfusion MI model (Michael *et al.*, 1995) may be better suited given the majority of patients receive reperfusion therapy following STEMI (Gavalova and Weston, 2012).

In conclusion, the work in this thesis has demonstrated that the depletion of endoglin *in vivo* results in significant ventricular remodelling with onset of a high cardiac output state. This is due to knockdown of endoglin within endothelial cells and is likely due to changes in the wider cardiovascular system rather than specific effects on the heart. I have also demonstrated the power of cardiac MRI to identify these changes and to monitor them longitudinally. It is clear that endoglin expression is increased in patients with heart failure (Kapur *et al.*, 2010; Kapur *et al.*, 2012), and that a reduction in endoglin is associated with haemodynamic benefits (Kapur *et al.*, 2012). However, the work presented in this thesis and that of van Laake (van Laake *et al.*, 2006) suggest caution as reduced endoglin can also lead to deleterious effects on the heart. So further work is needed to identify how and when modification of endoglin would be beneficial.

References

Adam, P. J., Clesham, G. J. and Weissberg, P. L. (1998) 'Expression of endoglin mRNA and protein in human vascular smooth muscle cells', *Biochem Biophys Res Commun*, 247, pp. 33 - 37.

Akki, A., Gupta, A. and Weiss, R. G. (2013) 'Magnetic resonance imaging and spectroscopy of the murine cardiovascular system', *American Journal of Physiology - Heart and Circulatory Physiology*, 304(5), pp. H633-H648.

Albinana, V., Sanz-Rodriguez, F., Recio-Poveda, L., Bernabae, C. and Botella, L. M. (2011) 'Immunosuppressor FK506 Increases Endoglin and Activin Receptor-Like Kinase 1 Expression and Modulates Transforming Growth Factor-β1 Signaling in Endothelial Cells', *Molecular Pharmacology*, 79(5), pp. 833-843.

Allender, S., Peto, V., Scarborough, P., Kaur, A. and Rayner, M. (2008) *Coronary heart disease statistics*. 2008 edn. London: British Heart Foundation.

Allinson, K. R., Carvalho, R. L. C., van den Brink, S., Mummery, C. L. and Arthur, H. M. (2007) 'Generation of a floxed allele of the mouse endoglin gene', *Genesis*, 45(6), pp. 391-395.

Amundsen, B. H., Ericsson, M., Seland, J. G., Pavlin, T., Ellingsen, O. and Brekken, C. (2011) 'A comparison of retrospectively self-gated magnetic resonance imaging and high-frequency echocardiography for characterization of left ventricular function in mice', *Laboratory Animals*, 45(1), pp. 31-37.

Anderberg, C., Cunha, S. I., Zhai, Z., Cortez, E., Pardali, E., Johnson, J. R., Franco, M., Paez-Ribes, M., Cordiner, R., Fuxe, J., Johansson, B. R., Goumans, M. J., Casanovas, O., ten Dijke, P., Arthur, H. M. and Pietras, K. (2013) 'Deficiency for endoglin in tumor vasculature weakens the endothelial barrier to metastatic dissemination', *J Exp Med*, 210(3), pp. 563-79.

Annes, J. P., Munger, J. S. and Rifkin, D. B. (2003) 'Making sense of latent TGFβ activation', *Journal Cell Science*, 116(2), pp. 217-224.

Arthur, H. M., Ure, J., Smith, A. J. H., Renforth, G., Wilson, D. I., Torsney, E., Charlton, R., Parums, D. V., Jowett, T., Marchuk, D. A., Burn, J. and Diamond, A. G. (2000) 'Endoglin, an ancillary TGF beta receptor, is required for extraembryonic angiogenesis and plays a key role in heart development', *Developmental Biology*, 217(1), pp. 42-53.

Asp, M. L., Martindale, J. J. and Metzger, J. M. (2013) 'Direct, Differential Effects of Tamoxifen, 4-Hydroxytamoxifen, and Raloxifene on Cardiac Myocyte Contractility and Calcium Handling', *PLoS One*, 8(10), p. e78768.

Balligand, J., Kobzik, L., Han, X., Kaye, D. M., Belhassen, L., O'Hara, D. S., Kelly, R. A., Smith, T. W. and Michel, T. (1995) 'Nitric Oxide-dependent Parasympathetic Signaling Is Due to Activation of Constitutive Endothelial (Type III) Nitric Oxide Synthase in Cardiac Myocytes', *Journal of Biological Chemistry*, 270(24), pp. 14582-14586.

Banerjee, I., Fuseler, J. W., Price, R. L., Borg, T. K. and Baudino, T. A. (2007) 'Determination of cell types and numbers during cardiac development in the neonatal and adult rat and mouse', *American Journal of Physiology - Heart and Circulatory Physiology*, 293(3), pp. H1883-H1891.

Banerjee, I., Yekkala, K., Borg, T. K. and Baudino, T. A. (2006) 'Dynamic Interactions between Myocytes, Fibroblasts, and Extracellular Matrix', *Annals of the New York Academy of Sciences*, 1080, pp. 76-84.

Barry, F. P., Boynton, R. E., Haynesworth, S., Murphy, J. M. and Zaia, J. (1999) 'The Monoclonal Antibody SH-2, Raised against Human Mesenchymal Stem Cells, Recognizes an Epitope on Endoglin (CD105)', *Biochemical and Biophysical Research Communications*, 265(1), pp. 134-139.

Bauer, R., Blain, A., Greally, E., Bushby, K., Lochmuller, H., Laval, S., Straub, V. and MacGowan, G. A. (2010a) 'Intolerance to beta-blockade in a mouse model of delta-sarcoglycan-deficient muscular dystrophy cardiomyopathy', *European Journal of Heart Failure*, 12(11), pp. 1163-1170.

Bauer, R., Blain, A., Greally, E., Lochmuller, H., Bushby, K., MacGowan, G. A. and Straub, V. (2010b) 'Attenuation of adverse cardiac effects in prednisolone-treated delta-sarcoglycan-deficient mice by mineralocorticoid-receptor-antagonism', *Neuromuscular Disorders*, 20(1), pp. 21-28.

Bauer, R., MacGowan, G. A., Blain, A., Bushby, K. and Straub, V. (2008) 'Steroid treatment causes deterioration of myocardial function in the delta-sarcoglycan-deficient mouse model for dilated cardiomyopathy', *Cardiovascular Research*, 79(4), pp. 652-661.

Belik, J., Jerkic, M., McIntyre, B. A. S., Pan, J., Leen, J., Yu, L. X., Henkelman, R. M., Toporsian, M. and Letarte, M. (2009) 'Age-dependent endothelial nitric oxide synthase uncoupling in pulmonary arteries of endoglin heterozygous mice', *American Journal of Physiology - Lung Cellular and Molecular Physiology*, 297(6), pp. L1170-L1178.

Bellón, T., Corbi, A., Lastres, P., Calés, C., Cebrián, M., Vera, S., Cheifetz, S., Massague, J., Letarte, M. and Bernabéu, C. (1993) 'Identification and expression of two forms of the human transforming growth factor-β-binding protein endoglin with distinct cytoplasmic regions', *European Journal of Immunology*, 23(9), pp. 2340-2345.

Blaha, M., Cermanova, M., Blaha, V., Jarolim, P., Andrys, C., Blazek, M., Maly, J., Smolej, L., Zajic, J., Masin, V., Zimova, R. and Rehacek, V. (2008) 'Elevated serum soluble endoglin (sCD105) decreased during extracorporeal elimination therapy for familial hypercholesterolemia', *Atherosclerosis*, 197(1), pp. 264-270.

Blain, A., Greally, E., Laval, S., Blamire, A., Straub, V. and MacGowan, G. A. (2013) 'Beta-blockers, left and right ventricular function, and in-vivo calcium influx in muscular dystrophy cardiomyopathy', *PLoS One*, 8(2), p. e57260.

Blanco, F. J., Grande, M. T., Langa, C., Oujo, B., Velasco, S., Rodriguez-Barbero, A., Perez-Gomez, E., Quintanilla, M., Lopez-Novoa, J. M. and Bernabeu, C. (2008) 'S-Endoglin Expression Is Induced in Senescent Endothelial Cells and Contributes to Vascular Pathology', *Circulation Research*, 103(12), pp. 1383-1392.

Bland, M. J. and Altman, D. G. (1986) 'Statistical Methods for Assessing Agreement Between Two Methods of Clinical Measurement', *The Lancet*, 327(8476), pp. 307-310.

Bland, M. J. and Altman, D. G. (1999) 'Measuring agreement in method comparison studies', *Statistical Methods in Medical Research*, 8(2), pp. 135-160.

Blanjesteijn, W. M., Creemers, E., Lutgens, E., Cleutjens, J. P. M., Daemen, M. J. A. P. and Smits, J. F. M. (2001) 'Dynamics of cardiac wound healing following myocardial infarction: observations in genetically altered mice', *Acta Physiologica Scandinavica*, 173(1), pp. 75-82.

Blann, A. D., Wang, J. M., Wilson, P. B. and Kumar, S. (1996) 'Serum levels of the TGF-beta receptor are increased in atherosclerosis', *Atherosclerosis*, 120(1-2), pp. 221-6.

Blazquez-Medela, A., Garcia-Ortiz, L., Gomez-Marcos, M., Recio-Rodriguez, J., Sanchez-Rodriguez, A., Lopez-Novoa, J. and Martinez-Salgado, C. (2010) 'Increased plasma soluble endoglin levels as an indicator of cardiovascular alterations in hypertensive and diabetic patients', *BMC Medicine*, 8(1), pp. 86-97.

Blobe, G. C., Schiemann, W. P. and Lodish, H. F. (2000) 'Mechanisms of Disease: Role of Transforming Growth Factor (beta) in Human Disease', *New England Journal of Medicine*, 342(18), pp. 1350-1358.

Braverman, I. M., Keh, A. and Jacobson, B. S. (1990) 'Ultrastructure and three-dimensional organization of the telangiectases of hereditary hemorrhagic telangiectasia', *Journal of Investigative Dermatology*, 95(4), pp. 422-7.

Brown, R. D., Ambler, S. K., Mitchell, M. D. and Long, C. S. (2005) 'The Cardiac Fibroblast: Therapeutic Target in Myocardial Remodeling and Failure', *Annual Review of Pharmacology and Toxicology*, 45(1), pp. 657-687.

Buerger, A., Rozhitskaya, O., Sherwood, M. C., Dorfman, A. L., Bisping, E., Abel, E. D., Pu, W. T., Izumo, S. and Jay, P. Y. (2006) 'Dilated Cardiomyopathy Resulting From High-Level Myocardial Expression of Cre-Recombinase', *Journal of Cardiac Failure*, 12(5), pp. 392-398.

Bujak, M. and Frangogiannis, N. G. (2007) 'The role of TGF-beta signaling in myocardial infarction and cardiac remodeling', *Cardiovascular Research*, 74(2), pp. 184-195.

Bujak, M., Ren, G., Kweon, H. J., Dobaczewski, M., Reddy, A., Taffet, G., Wang, X.-F. and Frangogiannis, N. G. (2007) 'Essential Role of Smad3 in Infarct Healing and in the Pathogenesis of Cardiac Remodeling', *Circulation*, 116(19), pp. 2127-2138.

Burke, J. P., Watson, R. W. G., Mulsow, J. J., Docherty, N. G., Coffey, J. C. and O'Connell, P. R. (2010) 'Endoglin negatively regulates transforming growth factor beta1-induced profibrotic responses in intestinal fibroblasts', *British Journal of Surgery*, 97(6), pp. 892-901.

Bushby, K., Muntoni, F. and Bourke, J. P. (2003) '107th ENMC International Workshop: the management of cardiac involvement in muscular dystrophy and myotonic dystrophy. 7th-9th June 2002, Naarden, the Netherlands', *Neuromuscular Disorders*, 13(2), pp. 166-172.

Cai, S., Khoo, J. and Channon, K. M. (2005) 'Augmented BH4 by gene transfer restores nitric oxide synthase function in hyperglycemic human endothelial cells', *Cardiovascular Research*, 65(4), pp. 823-831.

Camelliti, P., Borg, T. K. and Kohl, P. (2005) 'Structural and functional characterisation of cardiac fibroblasts', *Cardiovascular Research*, 65(1), pp. 40-51.

Cao, H. and Shockey, J. M. (2012) 'Comparison of TaqMan and SYBR Green qPCR methods for quantitative gene expression in tung tree tissues', *J Agric Food Chem*, 60(50), pp. 12296-303.

Cassidy, P. J., Schneider, J. E., Grieve, S. M., Lygate, C., Neubauer, S. and Clarke, K. (2004) 'Assessment of motion gating strategies for mouse magnetic resonance at high magnetic fields', *Journal of Magnetic Resonance Imaging*, 19(2), pp. 229-37.

Chapon, C., Herlihy, A. H. and Bhakoo, K. K. (2008) 'Assessment of myocardial infarction in mice by late gadolinium enhancement MR imaging using an inversion recovery pulse sequence at 9.4T', *Journal of Cardiovascular Magnetic Resonance*, 10(1), p. 6.

Chaves, A. A., Weinstein, D. M. and Bauer, J. A. (2001) 'Non-invasive echocardiographic studies in mice: Influence of anesthetic regimen', *Life Sciences*, 69(2), pp. 213-222.

Cheifetz, S., Bellon, T., Cales, C., Vera, S., Bernabeu, C., Massague, J. and Letarte, M. (1992) 'Endoglin is a component of the transforming growth factor-beta receptor system in human endothelial cells', *Journal of Biological Chemistry*, 267, pp. 19027 - 19030.

Chen, K., Mehta, J. L., Li, D., Joseph, L. and Joseph, J. (2004) 'Transforming growth factor beta receptor endoglin is expressed in cardiac fibroblasts and modulates profibrogenic actions of angiotensin II', *Circulation Research*, 95(12), pp. 1167-1173.

Chen, Y., Hao, Q., Kim, H., Su, H., Letarte, M., Karumanchi, S. A., Lawton, M. T., Barbaro, N. M., Yang, G. Y. and Young, W. L. (2009) 'Soluble endoglin modulates aberrant cerebral vascular remodeling', *Ann Neurol*, 66, pp. 19 - 27.

Cheng, Y., Sudarov, A., Szulc, K. U., Sgaier, S. K., Stephen, D., Turnbull, D. H. and Joyner, A. L. (2010) 'The Engrailed homeobox genes determine the different foliation patterns in the vermis and hemispheres of the mammalian cerebellum', *Development*, 137(3), pp. 519-529.

Cingolani, O. H. and Kass, D. A. (2011) 'Pressure-Volume Relation Analysis of mouse Ventricular Function', *American Journal of Physiology - Heart and Circulatory Physiology*, 301(6), pp. H2198-H2206.

Cohn, J. N., Ferrari, R. and Sharpe, N. (2000) 'Cardiac remodeling--concepts and clinical implications: a consensus paper from an international forum on cardiac remodeling', *Journal of the American College of Cardiology*, 35(3), pp. 569-582.

Conley, B. A., Smith, J. D., Guerrero-Esteo, M., Bernabeu, C. and Vary, C. P. (2000) 'Endoglin, a TGF-beta receptor-associated protein, is expressed by smooth muscle cells in human atherosclerotic plaques', *Atherosclerosis*, 153, pp. 323 - 335.

Coral-Vazquez, R., Cohn, R. D., Moore, S. A., Hill, J. A., Weiss, R. M., Davisson, R. L., Straub, V., Barresi, R., Bansal, D., Hrstka, R. F., Williamson, R. and Campbell, K. P. (1999) 'Disruption of the Sarcoglycan-Sarcospan Complex in Vascular Smooth Muscle: A Novel Mechanism for Cardiomyopathy and Muscular Dystrophy', *Cell*, 98(4), pp. 465-474.

Cranney, G. B., Lotan, C. S., Dean, L., Baxley, W., Bouchard, A. and Pohost, G. M. (1990) 'Left ventricular volume measurement using cardiac axis nuclear magnetic resonance imaging. Validation by calibrated ventricular angiography', *Circulation*, 82(1), pp. 154-163.

Cruz-Gonzalez, I., Pabón, P., Rodríguez-Barbero, A., Martín-Moreiras, J., Pericacho, M., Sánchez, P. L., Ramirez, V., Sánchez-Ledesma, M., Martín-Herrero, F., Jiménez-Candil, J., Maree, A. O., Sánchez-Rodríguez, A., Martín-Luengo, C. and López-Novoa, J. M. (2008) 'Identification of serum endoglin as a novel prognostic marker after acute myocardial infarction', *Journal of Cellular and Molecular Medicine*, 12(3), pp. 955-961.

Cudmore, M., Ahmad, S., Al-Ani, B., Fujisawa, T., Coxall, H., Chudasama, K., Devey, L. R., Wigmore, S. J., Abbas, A., Hewett, P. W. and Ahmed, A. (2007) 'Negative Regulation of Soluble Flt-1 and Soluble Endoglin Release by Heme Oxygenase-1', *Circulation*, 115(13), pp. 1789-1797.

Davey, R. A. and MacLean, H. E. (2006) 'Current and future approaches using genetically modified mice in endocrine research', *American Journal of Physiolology Endocrinology and Metabolism*, 291(3), pp. E429-E438.

Davidson, E. N. B., Vitters, E. L., Mooren, F. M., Oliver, N., van den Berg, W. B. and van der Kraan, P. M. (2006) 'Connective tissue growth factor/CCN2 overexpression in mouse synovial lining results in transient fibrosis and cartilage damage', *Arthritis & Rheumatism*, 54(5), pp. 1653-1661.

Dawson, D., Lygate, C. A., Saunders, J., Schneider, J. E., Ye, X., Hulbert, K., Noble, J. A. and Neubauer, S. (2004) 'Quantitative 3-dimensional echocardiography for accurate and rapid cardiac phenotype characterization in mice', *Circulation*, 110(12), pp. 1632-7.

Derynck, R. and Zhang, Y. E. (2003) 'Smad-dependent and Smad-independent pathways in TGF-[beta] family signalling', *Nature*, 425(6958), pp. 577-584.

Deten, A., Hölzl, A., Leicht, M., Barth, W. and Zimmer, H.-G. (2001) 'Changes in Extracellular Matrix and in Transforming Growth Factor Beta Isoforms After Coronary Artery Ligation in Rats', *Journal of Molecular and Cellular Cardiology*, 33(6), pp. 1191-1207.

Dewald, O., Ren, G., Duerr, G. D., Zoerlein, M., Klemm, C., Gersch, C., Tincey, S., Michael, L. H., Entman, M. L. and Frangogiannis, N. G. (2004) 'Of Mice and Dogs: Species-Specific Differences in the Inflammatory Response Following Myocardial Infarction', *Am J Pathol*, 164(2), pp. 665-677.

Dietmann, A., Lackner, P., Fischer, M., Broessner, G., Pfausler, B., Helbok, R., Schmutzhard, E. and Beer, R. (2012) 'Soluble Endoglin and Transforming Growth Factor-β1 and the Development of Vasospasm after Spontaneous Subarachnoid Hemorrhage: A Pilot Study', *Cerebrovascular Diseases*, 33(1), pp. 16-22.

Diez-Marques, L., Ortega-Velazquez, R., Langa, C., Rodriguez-Barbero, A., Lopez-Novoa, J. M., Lamas, S. and Bernabeu, C. (2002) 'Expression of endoglin in human mesangial cells: Modulation of extracellular matrix synthesis', *Biochimica et Biophysica Acta - Molecular Basis of Disease*, 1587(1), pp. 36-44.

Dobaczewski, M., Gonzalez-Quesada, C. and Frangogiannis, N. G. (2010) 'The extracellular matrix as a modulator of the inflammatory and reparative response following myocardial infarction', *Journal of Molecular and Cellular Cardiology*, 48(3), pp. 504-511.

Docherty, N. G., Lopez-Novoa, J. M., Arevalo, M., Duwel, A., Rodriguez-Pena, A., Perez-Barriocanal, F., Bernabeu, C. and Eleno, N. (2006) 'Endoglin regulates

renal ischaemia-reperfusion injury', *Nephrology Dialysis Transplantation*, 21(8), pp. 2106-2119.

Duff, S. E., Li, C., Garland, J. M. and Kumar, S. (2003) 'CD105 is important for angiogenesis: evidence and potential applications', *The FASEB Journal*, 17(9), pp. 984-992.

Dulce, M. C., Mostbeck, G. H., Friese, K. K., Caputo, G. R. and Higgins, C. B. (1993) 'Quantification of the left ventricular volumes and function with cine MR imaging: comparison of geometric models with three-dimensional data', *Radiology*, 188(2), pp. 371-376.

Eghbali, M., Tomek, R., Sukhatme, V. P., Woods, C. and Bhambi, B. (1991a) 'Differential effects of transforming growth factor-beta 1 and phorbol myristate acetate on cardiac fibroblasts. Regulation of fibrillar collagen mRNAs and expression of early transcription factors', *Circ Res*, 69(2), pp. 483-490.

Eghbali, M., Tomek, R., Woods, C. and Bhambi, B. (1991b) 'Cardiac fibroblasts are predisposed to convert into myocyte phenotype: specific effect of transforming growth factor beta', *Proceedings of the National Academy of Sciences of the United States of America*, 88(3), pp. 795-799.

Epstein, F. H., Yang, Z., Gilson, W. D., Berr, S. S., Kramer, C. M. and French, B. A. (2002) 'MR tagging early after myocardial infarction in mice demonstrates contractile dysfunction in adjacent and remote regions', *Magnetic Resonance in Medicine*, 48(2), pp. 399-403.

Feil, R., Wagner, J. r., Metzger, D. and Chambon, P. (1997) 'Regulation of Cre Recombinase Activity by Mutated Estrogen Receptor Ligand-Binding Domains', *Biochemical and Biophysical Research Communications*, 237(3), pp. 752-757.

Fernandez, L. A., Sanz-Rodriguez, F., Zarrabeitia, R., Perez-Molino, A., Hebbel, R. P., Nguyen, J., Bernabeu, C. and Botella, L. M. (2005) 'Blood outgrowth endothelial cells from Hereditary Haemorrhagic Telangiectasia patients reveal abnormalities compatible with vascular lesions', *Cardiovasc Res*, 68(2), pp. 235-48.

Fibrinolytic Therapy Trialists' Collaborative Group (1994) 'Indications for fibrinolytic therapy in suspected acute myocardial infarction: collaborative overview of early mortality and major morbidity results from all randomised trials of more than 1000 patients', *The Lancet*, 343(8893), pp. 311-322.

Finnson, K. W., Parker, W. L., Chi, Y., Hoemann, C. D., Goldring, M. B., Antoniou, J. and Philip, A. (2010) 'Endoglin differentially regulates TGF-β-induced Smad2/3 and Smad1/5 signalling and its expression correlates with extracellular matrix production and cellular differentiation state in human chondrocytes', *Osteoarthritis and cartilage*, 18(11), pp. 1518-1527.

Flather, M. D., Yusuf, S., Køber, L., Pfeffer, M., Hall, A., Murray, G., Torp-Pedersen, C., Ball, S., Pogue, J., Moyé, L. and Braunwald, E. (2000) 'Long-term ACE-inhibitor therapy in patients with heart failure or left-ventricular dysfunction: a systematic overview of data from individual patients', *The Lancet*, 355(9215), pp. 1575-1581.

Florentine, M. S., Grosskreutz, C. L., Chang, W., Hartnett, J. A., Dunn, V. D., Ehrhardt, J. C., Fleagle, S. R., Collins, S. M., Marcus, M. L. and Skorton, D. J. (1986) 'Measurement of left ventricular mass in vivo using gated nuclear magnetic resonance imaging', *J Am Coll Cardiol*, 8(1), pp. 107-112.

Franco, F., Dubois, S. K., Peshock, R. M. and Shohet, R. V. (1998) 'Magnetic resonance imaging accurately estimates LV mass in a transgenic mouse model of cardiac hypertrophy', *American Journal of Physiology - Heart and Circulatory Physiology*, 274(2), pp. H679-H683.

Frangogiannis, N. G. (2008) 'The immune system and cardiac repair', *Pharmacological Research*, 58(2), pp. 88-111.

Frangogiannis, N. G., Smith, C. W. and Entman, M. L. (2002) 'The inflammatory response in myocardial infarction', *Cardiovasc Res*, 53(1), pp. 31-47.

Gabbiani, G. (1998) 'Evolution and clinical implications of the myofibroblast concept', *Cardiovasc Res*, 38(3), pp. 545-548.

Gao, X., He, X., Luo, B., Peng, L., Lin, J. and Zuo, Z. (2009) 'Angiotensin II increases collagen I expression via transforming growth factor-beta1 and extracellular signal-regulated kinase in cardiac fibroblasts', *European Journal of Pharmacology*, 606(1-3), pp. 115-120.

Gardin, J. M., Siri, F. M., Kitsis, R. N., Edwards, J. G. and Leinwand, L. A. (1995) 'Echocardiographic Assessment of Left Ventricular Mass and Systolic Function in Mice', *Circ Res*, 76(5), pp. 907-914.

Gavalova, L. and Weston, C. (2012) *Myocardial Ischaemia National Audit Project: How the NHS cares for patients with heart attack. Annual Public Report April 2011 - March 2012*. Available at: www.ucl.ac.uk/nicor/audits/minap/publicreports/pdfs/2012minappublicreportv2 (Accessed: 21st June 2013).

Gersh, B. J., Stone, G. W., White, H. D. and Holmes, D. R., Jr. (2005) 'Pharmacological facilitation of primary percutaneous coronary intervention for acute myocardial infarction: is the slope of the curve the shape of the future?', *JAMA*, 293(8), pp. 979-86.

Gilson, W. D. and Kraitchman, D. L. (2007) 'Cardiac magnetic resonance imaging in small rodents using clinical 1.5 T and 3.0 T scanners', *Methods*, 43(1), pp. 35-45.

Giordano, A., Romano, S., Monaco, M., Sorrentino, A., Corcione, N., Di Pace, A. L., Ferraro, P., Nappo, G., Polimeno, M. and Romano, M. F. (2012) 'Differential effect of atorvastatin and tacrolimus on proliferation of vascular smooth muscle and endothelial cells', *American Journal of Physiology - Heart and Circulatory Physiology*, 302(1), pp. H135-H142.

Gordon, K. J. and Blobe, G. C. (2008) 'Role of transforming growth factor-[beta] superfamily signaling pathways in human disease', *Biochimica et Biophysica Acta (BBA) - Molecular Basis of Disease*, 1782(4), pp. 197-228.

Gougos, A. and Letarte, M. (1990) 'Primary structure of endoglin, an RGD-containing glycoprotein of human endothelial cells', *J. Biol. Chem.*, 265(15), pp. 8361-8364.

Goumans, M. J., Valdimarsdottir, G., Itoh, S., Rosendahl, A., Sideras, P. and ten Dijke, P. (2002) 'Balancing the activation state of the endothelium via two distinct TGF-beta type I receptors', *Embo J*, 21(7), pp. 1743-53.

Goustin, A. S., Leof, E. B., Shipley, G. D. and Moses, H. L. (1986) 'Growth Factors and Cancer', *Cancer Research*, 46(3), pp. 1015-1029.

Greally, E., Davison, B. J., Blain, A., Laval, S., Blamire, A., Straub, V. and MacGowan, G. A. (2013) 'Heterogeneous abnormalities of in-vivo left ventricular calcium influx and function in mouse models of muscular dystrophy cardiomyopathy', *J Cardiovasc Magn Reson*, 15, p. 4.

Haase, A., Frahm, J., Matthaei, D., Hanicke, W. and Merboldt, K. D. (1986) 'FLASH imaging. Rapid NMR imaging using low flip-angle pulses', *Journal of Magnetic Resonance*, 67(2), pp. 258-266.

Hao, J., Ju, H., Zhao, S., Junaid, A., Scammell-La Fleur, T. and Dixon, I. M. C. (1999) 'Elevation of Expression of Smads 2, 3, and 4, Decorin and TGF-[beta]in the Chronic Phase of Myocardial Infarct Scar Healing', *Journal of Molecular and Cellular Cardiology*, 31(3), pp. 667-678.

Hawinkels, L. J. A. C., Kuiper, P., Wiercinska, E., Verspaget, H. W., Liu, Z., Pardali, E., Sier, C. F. M. and ten Dijke, P. (2010) 'Matrix Metalloproteinase-14 (MT1-MMP) Mediated Endoglin Shedding Inhibits Tumor Angiogenesis', *Cancer Research*, 70(10), pp. 4141-4150.

Heffernan, K. S., Kuvin, J. T., Patel, A. R., Karas, R. H. and Kapur, N. K. (2011) 'Endothelial Function and Soluble Endoglin in Smokers With Heart Failure', *Clinical Cardiology*, 34(12), pp. 729-733.

Henson, R. E., Song, S. K., Pastorek, J. S., Ackerman, J. J. and Lorenz, C. H. (2000) 'Left ventricular torsion is equal in mice and humans', *Am J Physiol Heart Circ Physiol*, 278(4), pp. H1117-23.

Hinz, B. (2010) 'The myofibroblast: Paradigm for a mechanically active cell', *Journal of Biomechanics*, 43(1), pp. 146-155.

Holmes, A., Ponticos, M., Shi-wen, X., Denton, C. and Abraham, D. (2011) 'Elevated CCN2 expression in scleroderma: a putative role for the TGFbeta accessory receptors TGFbetaRIII and endoglin', *Journal of Cell Communication and Signaling*, 5(3), pp. 173-177.

Hu, T. C., Bao, W., Lenhard, S. C., Schaeffer, T. R., Yue, T., Willette, R. N. and Jucker, B. M. (2004) 'Simultaneous assessment of left-ventricular infarction size, function and tissue viability in a murine model of myocardial infarction by cardiac manganese-enhanced magnetic resonance imaging (MEMRI)', *NMR in Biomedicine*, 17(8), pp. 620-626.

Hu, T. C., Pautler, R. G., MacGowan, G. A. and Koretsky, A. P. (2001) 'Manganese-enhanced MRI of mouse heart during changes in inotropy', *Magnetic Resonance in Medicine*, 46(5), pp. 884-90.

Hutchins, G. M. and Bulkley, B. H. (1978) 'Infarct expansion versus extension: Two different complications of acute myocardial infarction', *The American journal of cardiology*, 41(7), pp. 1127-1132.

Ignotz, R. A. and Massague, J. (1986) 'Transforming growth factor-beta stimulates the expression of fibronectin and collagen and their incorporation into the extracellular matrix', *J. Biol. Chem.*, 261(9), pp. 4337-4345.

Ikemoto, T., Hojo, Y., Kondo, H., Takahashi, N., Hirose, M., Nishimura, Y., Katsuki, T., Shimada, K. and Kario, K. (2012) 'Plasma endoglin as a marker to predict cardiovascular events in patients with chronic coronary artery diseases', *Heart and Vessels*, 27(4), pp. 344-351.

Ikeuchi, M., Tsutsui, H., Shiomi, T., Matsusaka, H., Matsushima, S., Wen, J., Kubota, T. and Takeshita, A. (2004) 'Inhibition of TGF-{beta} signaling exacerbates early cardiac dysfunction but prevents late remodeling after infarction', *Cardiovasc Res*, 64(3), pp. 526-535.

Jacoby, C., Molojavyi, A., Flogel, U., Merx, M. W., Ding, Z. and Schrader, J. (2006) 'Direct comparison of magnetic resonance imaging and conductance

microcatheter in the evaluation of left ventricular function in mice.[see comment]', *Basic Research in Cardiology*, 101(1), pp. 87-95.

Jerkic, M., Rivas-Elena, J. V., Prieto, M., Carron, R., Sanz-Rodriguez, F., Perez-Barriocanal, F., Rodriguez-Barbero, A., Bernabeu, C. and Lopez-Novoa, J. M. (2004) 'Endoglin regulates nitric oxide dependent vasodilatation', *FASEB J*, 18, pp. 609 - 611.

Johnson, K. (2008) 'Introduction to rodent cardiac imaging', *ILAR Journal*, 49(1), pp. 27-34.

Jorgensen, L. H., Blain, A., Greally, E., Laval, S. H., Blamire, A. M., Davison, B. J., Brinkmeier, H., MacGowan, G. A., Schroder, H. D., Bushby, K., Straub, V. and Lochmuller, H. (2011) 'Long-term blocking of calcium channels in mdx mice results in differential effects on heart and skeletal muscle', *Am J Pathol*, 178(1), pp. 273-83.

Jugdutt, B. I. (2003) 'Ventricular Remodeling After Infarction and the Extracellular Collagen Matrix: When Is Enough Enough?', *Circulation*, 108(11), pp. 1395-1403.

Kapur, N. K., Heffernan, K. S., Yunis, A. A., Parpos, P., Kiernan, M. S., Sahasrabudhe, N. A., Kimmelstiel, C. D., Kass, D. A., Karas, R. H. and Mendelsohn, M. E. (2010) 'Usefulness of Soluble Endoglin as a Noninvasive Measure of Left Ventricular Filling Pressure in Heart Failure', *The American journal of cardiology*, 106(12), pp. 1770-1776.

Kapur, N. K., Wilson, S., Yunis, A. A., Qiao, X., Mackey, E., Paruchuri, V., Baker, C., Aronovitz, M. J., Karumanchi, S. A., Letarte, M., Kass, D. A., Mendelsohn, M. E. and Karas, R. H. (2012) 'Reduced Endoglin Activity Limits Cardiac Fibrosis and Improves Survival in Heart Failure', *Circulation*, 125(22), pp. 2728-2738.

Karlen, Y., McNair, A., Perseguers, S., Mazza, C. and Mermod, N. (2007) 'Statistical significance of quantitative PCR', *BMC Bioinformatics*, 8(1), p. 131.

Keeley, E. C., Boura, J. A. and Grines, C. L. (2003) 'Primary angioplasty versus intravenous thrombolytic therapy for acute myocardial infarction: a quantitative review of 23 randomised trials', *The Lancet*, 361(9351), pp. 13-20.

Keeley, E. C. and Hillis, L. D. (2007) 'Primary PCI for Myocardial Infarction with ST-Segment Elevation', *N Engl J Med*, 356(1), pp. 47-54.

Kober, F., Iltis, I., Cozzone, P. J. and Bernard, M. (2004) 'Cine-MRI assessment of cardiac function in mice anesthetized with ketamine/xylazine and isoflurane', *Magma*, 17(3-6), pp. 157-61.

Kohl, P., Camelliti, P., Burton, F. L. and Smith, G. L. (2005) 'Electrical coupling of fibroblasts and myocytes: relevance for cardiac propagation', *Journal of Electrocardiology*, 38(4, Supplement 1), pp. 45-50.

Koitabashi, N., Bedja, D., Zaiman, A. L., Pinto, Y. M., Zhang, M., Gabrielson, K. L., Takimoto, E. and Kass, D. A. (2009) 'Avoidance of Transient Cardiomyopathy in Cardiomyocyte-Targeted Tamoxifen-Induced MerCreMer Gene Deletion Models', *Circ Res*, 105(1), pp. 12-15.

Krenning, G., Zeisberg, E. M. and Kalluri, R. (2010) 'The origin of fibroblasts and mechanism of cardiac fibrosis', *J Cell Physiol*, 225(3), pp. 631-7.

Kubota, T., McTiernan, C. F., Frye, C. S., Slawson, S. E., Lemster, B. H., Koretsky, A. P., Demetris, A. J. and Feldman, A. M. (1997) 'Dilated Cardiomyopathy in Transgenic Mice With Cardiac-Specific Overexpression of Tumor Necrosis Factor-α', *Circulation Research*, 81(4), pp. 627-635.

Lastres, P., Bellon, T., Cabanas, C., Sanchez-Madrid, F., Acevedo, A., Gougos, A., Letarte, M. and Bernabeu, C. (1992) 'Regulated expression on human macrophages of endoglin, an Arg-Gly-Asp-containing surface antigen', *Eur J Immunol*, 22(2), pp. 393-7.

Lastres, P., Letamendia, A., Zhang, H., Rius, C., Almendro, N., Raab, U., Lopez, L. A., Langa, C., Fabra, A., Letarte, M. and Bernabeu, C. (1996) 'Endoglin modulates cellular responses to TGF-beta 1', *J. Cell Biol.*, 133(5), pp. 1109-1121.

Leask, A. (2007) 'TGFbeta, cardiac fibroblasts, and the fibrotic response', *Cardiovasc Res*, 74(2), pp. 207-212.

Leask, A. (2010) 'Potential Therapeutic Targets for Cardiac Fibrosis', *Circulation Research*, 106(11), pp. 1675-1680.

Leask, A., Abraham, D. J., Finlay, D. R., Holmes, A., Pennington, D., Shi-Wen, X., Chen, Y., Venstrom, K., Dou, X., Ponticos, M., Black, C., Jackman, J. K., Findell, P. R. and Connolly, M. K. (2002) 'Dysregulation of transforming growth factor β signaling in scleroderma: Overexpression of endoglin in cutaneous scleroderma fibroblasts', *Arthritis & Rheumatism*, 46(7), pp. 1857-1865.

Lebrin, F., Goumans, M.-J., Jonker, L., Carvalho, R. L. C., Valdimarsdottir, G., Thorikay, M., Mummery, C., Arthur, H. M. and Dijke, P. t. (2004) 'Endoglin promotes endothelial cell proliferation and TGF-[beta]/ALK1 signal transduction', *Embo J*, 23(20), pp. 4018-4028.

Lefer, A. M., Ma, X. L., Weyrich, A. S. and Scalia, R. (1993) 'Mechanism of the cardioprotective effect of transforming growth factor beta 1 in feline myocardial ischemia and reperfusion', *Proceedings of the National Academy of Sciences of the United States of America*, 90(3), pp. 1018-1022.

Lefer, A. M., Tsao, P., Aoki, N. and Palladino, M. A., Jr. (1990) 'Mediation of cardioprotection by transforming growth factor-beta', *Science*, 249(4964), pp. 61-64.

Leicht, M., Briest, W., Holzl, A. and Zimmer, H.-G. (2001) 'Serum depletion induces cell loss of rat cardiac fibroblasts and increased expression of extracellular matrix proteins in surviving cells', *Cardiovasc Res*, 52(3), pp. 429-437.

Li, L., Zhou, N., Gong, H., Wu, J., Lin, L., Komuro, I., Ge, J. and Zou, Y. (2010) 'Comparison of angiotensin II type 1-receptor blockers to regress pressure overload-induced cardiac hypertrophy in mice', *Hypertens Res*, 33(12), pp. 1289-1297.

Li, P., Wang, D., Lucas, J., Oparil, S., Xing, D., Cao, X., Novak, L., Renfrow, M. B. and Chen, Y.-F. (2008) 'Atrial Natriuretic Peptide Inhibits Transforming Growth Factor Î²â€“Induced Smad Signaling and Myofibroblast Transformation in Mouse Cardiac Fibroblasts', *Circulation Research*, 102(2), pp. 185-192.

Li, X., van der Meer, J. J., van der Loos, C. M., Ploegmakers, H. J. P., de Boer, O. J., de Winter, R. J. and van der Wal, A. C. (2012) 'Microvascular endoglin (CD105) expression correlates with tissue markers for atherosclerotic plaque vulnerability in an ageing population with multivessel coronary artery disease', *Histopathology*, 61(1), pp. 88-97.

Liao, Y., Ishikura, F., Beppu, S., Asakura, M., Takashima, S., Asanuma, H., Sanada, S., Kim, J., Ogita, H., Kuzuya, T., Node, K., Kitakaze, M. and Hori, M. (2002) 'Echocardiographic assessment of LV hypertrophy and function in aortic-banded mice: necropsy validation', *American Journal of Physiology - Heart and Circulatory Physiology*, 282(5), pp. H1703-H1708.

Liu, W., Ashford, M. W., Chen, J., Watkins, M. P., Williams, T. A., Wickline, S. A. and Yu, X. (2006) 'MR tagging demonstrates quantitative differences in regional ventricular wall motion in mice, rats, and men', *American Journal of Physiology - Heart & Circulatory Physiology*, 291(5), pp. H2515-21.

López-Casillas, F., Cheifetz, S., Doody, J., Andres, J. L., Lane, W. S. and Massague, J. (1991) 'Structure and expression of the membrane proteoglycan betaglycan, a component of the TGF-β receptor system', *Cell*, 67(4), pp. 785-795.

Lopez-Novoa, J. M. and Bernabeu, C. (2010) 'The physiological role of endoglin in the cardiovascular system', *Am J Physiol Heart Circ Physiol*, 299(4), pp. H959-74.

Ma, X., Labinaz, M., Goldstein, J., Miller, H., Keon, W. J., Letarte, M. and O'Brien, E. (2000) 'Endoglin Is Overexpressed After Arterial Injury and Is Required for Transforming Growth Factor-{beta}-Induced Inhibition of Smooth Muscle Cell Migration', *Arterioscler Thromb Vasc Biol*, 20(12), pp. 2546-2552.

Mahmoud, M., Allinson, K. R., Zhai, Z., Oakenfull, R., Ghandi, P., Adams, R. H., Fruttiger, M. and Arthur, H. M. (2010) 'Pathogenesis of arteriovenous malformations in the absence of endoglin', *Circ Res*, 106(8), pp. 1425 - 1433.

Mahmoud, M., Borthwick, G. M., Hislop, A. A. and Arthur, H. M. (2008) 'Endoglin and activin receptor-like-kinase 1 are co-expressed in the distal vessels of the lung: implications for two familial vascular dysplasias, HHT and PAH', *Lab Invest*, 89(1), pp. 15-25.

Mahmoud, M., Upton, P. D. and Arthur, H. M. (2011) 'Angiogenesis regulation by TGFbeta signalling: clues from an inherited vascular disease', *Biochem Soc Trans*, 39(6), pp. 1659-66.

Manning, W. J., Wei, J. Y., Katz, S. E., Litwin, S. E. and Douglas, P. S. (1994) 'In vivo assessment of LV mass in mice using high-frequency cardiac ultrasound: necropsy validation', *Am J Physiol Heart Circ Physiol*, 266(4), pp. H1672-1675.

Maron, B. J. and Pelliccia, A. (2006) 'The Heart of Trained Athletes: Cardiac Remodeling and the Risks of Sports, Including Sudden Death', *Circulation*, 114(15), pp. 1633-1644.

Martino, T. A., Tata, N., Simpson, J. A., Vanderlaan, R., Dawood, F., Kabir, M. G., Khaper, N., Cifelli, C., Podobed, P., Liu, P. P., Husain, M., Heximer, S., Backx, P. H. and Sole, M. J. (2011) 'The primary benefits of angiotensin-converting enzyme inhibition on cardiac remodeling occur during sleep time in murine pressure overload hypertrophy', *J Am Coll Cardiol*, 57(20), pp. 2020-8.

Masur, S. K., Dewal, H. S., Dinh, T. T., Erenburg, I. and Petridou, S. (1996) 'Myofibroblasts differentiate from fibroblasts when plated at low density', *Proceedings of the National Academy of Sciences*, 93(9), pp. 4219-4223.

Matsenko, N. U., Rijikova, V. S. and Kovalenko, S. P. (2008) 'Comparison of SYBR Green I and TaqMan real-time PCR formats for the analysis of her2 gene dose in human breast tumors', *Bull Exp Biol Med*, 145(2), pp. 240-4.

McAllister, K. A., Grogg, K. M., Johnson, D. W., Gallione, C. J., Baldwin, M. A., Jackson, C. E., Helmbold, E. A., Markel, D. S., McKinnon, W. C., Murrell, J.

and et al. (1994) 'Endoglin, a TGF-beta binding protein of endothelial cells, is the gene for hereditary haemorrhagic telangiectasia type 1', *Nat Genet*, 8(4), pp. 345-51.

McKay, R. G., Pfeffer, M. A., Pasternak, R. C., Markis, J. E., Come, P. C., Nakao, S., Alderman, J. D., Ferguson, J. J., Safian, R. D. and Grossman, W. (1986) 'Left ventricular remodeling after myocardial infarction: a corollary to infarct expansion', *Circulation*, 74(4), pp. 693-702.

Messina, E., De Angelis, L., Frati, G., Morrone, S., Chimenti, S., Fiordaliso, F., Salio, M., Battaglia, M., Latronico, M. V. G., Coletta, M., Vivarelli, E., Frati, L., Cossu, G. and Giacomello, A. (2004) 'Isolation and Expansion of Adult Cardiac Stem Cells From Human and Murine Heart', *Circ Res*, 95(9), pp. 911-921.

Meurer, S. K., Tihaa, L., Borkham-Kamphorst, E. and Weiskirchen, R. (2010) 'Expression and functional analysis of endoglin in isolated liver cells and its involvement in fibrogenic Smad signalling', *Cellular Signalling*, 23(4), pp. 683-699.

Michael, L. H., Entman, M. L., Hartley, C. J., Youker, K. A., Zhu, J., Hall, S. R., Hawkins, H. K., Berens, K. and Ballantyne, C. M. (1995) 'Myocardial ischemia and reperfusion: a murine model', *Am J Physiol Heart Circ Physiol*, 269(6), pp. H2147-2154.

Mitchell, G. F., Lamas, G. A., Vaughan, D. E. and Pfeffer, M. A. (1992) 'Left ventricular remodeling in the year after first anterior myocardial infarction: a quantitative analysis of contractile segment lengths and ventricular shape', *J Am Coll Cardiol*, 19(6), pp. 1136-1144.

Morris, E., Chrobak, I., Bujor, A., Hant, F., Mummery, C., ten Dijke, P. and Trojanowska, M. (2011) 'Endoglin promotes TGF-β/Smad1 signaling in scleroderma fibroblasts', *Journal of Cellular Physiology*, 226(12), pp. 3340-3348.

Mosmann, T. (1983) 'Rapid colorimetric assay for cellular growth and survival: Application to proliferation and cytotoxicity assays', *Journal of Immunological Methods*, 65(1-2), pp. 55-63.

Muller, P., Kazakov, A., Semenov, A., Jagoda, P., Friedrich, E. B., Bohm, M. and Laufs, U. (2012) 'Ramipril and Telmisartan Exhibit Differential Effects in Cardiac Pressure Overload-Induced Hypertrophy Without an Additional Benefit of the Combination of Both Drugs', *Journal of Cardiovascular Pharmacology and Therapeutics*, 18(1), pp. 87-93.

Murry, C. E., Jennings, R. B. and Reimer, K. A. (1986) 'Preconditioning with ischemia: a delay of lethal cell injury in ischemic myocardium', *Circulation*, 74(5), pp. 1124-36.

Nachtigal, P., Pospisilova, N., Vecerova, L., Micuda, S., Brcakova, E., Pospechova, K. and Semecky, V. (2009) 'Atorvastatin Increases Endoglin, SMAD2, Phosphorylated SMAD2/3 and eNOS Expression in ApoE/LDLR Double Knockout Mice', *Journal of Atherosclerosis and Thrombosis*, 16(3), pp. 265-274.

Nahrendorf, M., Streif, J. U., Hiller, K.-H., Hu, K., Nordbeck, P., Ritter, O., Sosnovik, D., Bauer, L., Neubauer, S., Jakob, P. M., Ertl, G., Spindler, M. and Bauer, W. R. (2006) 'Multimodal functional cardiac MRI in creatine kinase-deficient mice reveals subtle abnormalities in myocardial perfusion and mechanics', *Am J Physiol Heart Circ Physiol*, 290(6), pp. H2516-2521.

Nielsen, J. M. l., Kristiansen, S. B., Ringgaard, S., Nielsen, T. T., Flyvbjerg, A., Redington, A. N. and Batker, H. E. (2007) 'Left ventricular volume measurement in mice by conductance catheter: evaluation and optimization of calibration', *American Journal of Physiology - Heart and Circulatory Physiology*, 293(1), pp. H534-H540.

Nonaka, I. (1998) 'Animal models of muscular dystrophies', *Laboratory Animal Science*, 48(1), pp. 8-17.

Obreo, J., Diez-Marques, L., Lamas, S., Duwell, A., Eleno, N., Bernabeu, C., Pandiella, A., Lopez-Novoa, J. M. and Rodriguez-Barbero, A. (2004) 'Endoglin

expression regulates basal and TGF-β1-induced extracellular matrix synthesis in cultured L6E9 myoblasts', *Cellular Physiology and Biochemistry*, 14(4-6), pp. 301-310.

Okada, H., Takemura, G., Kosai, K.-i., Li, Y., Takahashi, T., Esaki, M., Yuge, K., Miyata, S., Maruyama, R., Mikami, A., Minatoguchi, S., Fujiwara, T. and Fujiwara, H. (2005) 'Postinfarction Gene Therapy Against Transforming Growth Factor-{beta} Signal Modulates Infarct Tissue Dynamics and Attenuates Left Ventricular Remodeling and Heart Failure', *Circulation*, 111(19), pp. 2430-2437.

Opie, L. H., Commerford, P. J., Gersh, B. J. and Pfeffer, M. A. (2006) 'Controversies in ventricular remodelling', *The Lancet*, 367(9507), pp. 356-367.

Pacher, P., Nagayama, T., Mukhopadhyay, P., Batkai, S. and Kass, D. A. (2008) 'Measurement of cardiac function using pressure-volume conductance catheter technique in mice and rats', *Nat. Protocols*, 3(9), pp. 1422-1434.

Packer, M., Coats, A. J. S., Fowler, M. B., Katus, H. A., Krum, H., Mohacsi, P., Rouleau, J. L., Tendera, M., Castaigne, A., Roecker, E. B., Schultz, M. K., Staiger, C., Curtin, E. L., DeMets, D. L. and the Carvedilol Prospective Randomized Cumulative Survival Study, G. (2001) 'Effect of Carvedilol on Survival in Severe Chronic Heart Failure', *N Engl J Med*, 344(22), pp. 1651-1658.

Pedro, L., Teresa, B., Carlos, C., Francisco, S.-M., Agustin, A., Anne, G., Michelle, L. and Carmelo, B. (1992) 'Regulated expression on human macrophages of endoglin, an Arg-Gly-Asp-containing surface antigen', *European Journal of Immunology*, 22(2), pp. 393-397.

Pfeffer, J. M., Pfeffer, M. A., Fletcher, P. J. and Braunwald, E. (1991) 'Progressive ventricular remodeling in rat with myocardial infarction', *Am J Physiol Heart Circ Physiol*, 260(5), pp. H1406-1414.

Pfeffer, M. A. and Braunwald, E. (1990) 'Ventricular remodeling after myocardial infarction. Experimental observations and clinical implications', *Circulation*, 81(4), pp. 1161-1172.

Piao, M. and Tokunaga, O. (2006) 'Significant Expression of Endoglin (CD105), TGFbeta-1 and TGFbetaR-2 in the Atherosclerotic Aorta: An Immunohistological Study', *Journal of Atherosclerosis and Thrombosis*, 13(2), pp. 82-89.

Pitt, B., Remme, W., Zannad, F., Neaton, J., Martinez, F., Roniker, B., Bittman, R., Hurley, S., Kleiman, J., Gatlin, M., the Eplerenone Post-Acute Myocardial Infarction Heart Failure, E. and Survival Study, I. (2003) 'Eplerenone, a Selective Aldosterone Blocker, in Patients with Left Ventricular Dysfunction after Myocardial Infarction', *N Engl J Med*, 348(14), pp. 1309-1321.

Politano, L., Nigro, V., Passamano, L., Petretta, V., Comi, L. I., Papparella, S., Nigro, G., Rambaldi, P. F., Raia, P., Pini, A., Mora, M., Giugliano, M. A. M., Esposito, M. G. and Nigro, G. (2001) 'Evaluation of cardiac and respiratory involvement in sarcoglycanopathies', *Neuromuscular Disorders*, 11(2), pp. 178-185.

Porter, K. E. and Turner, N. A. (2009) 'Cardiac fibroblasts: At the heart of myocardial remodeling', *Pharmacology & Therapeutics*, 123(2), pp. 255-278.

Porter, K. E., Turner, N. A., O'Regan, D. J., Balmforth, A. J. and Ball, S. G. (2004) 'Simvastatin reduces human atrial myofibroblast proliferation independently of cholesterol lowering via inhibition of RhoA', *Cardiovascular Research*, 61(4), pp. 745-755.

Post, S., Smits, A. M., van den Broek, A. J., Sluijter, J. P. G., Hoefer, I. E., Janssen, B. J., Snijder, R. J., Mager, J. J., Pasterkamp, G., Mummery, C. L., Doevendans, P. A. and Goumans, M.-J. (2010) 'Impaired recruitment of HHT-1 mononuclear cells to the ischaemic heart is due to an altered CXCR4/CD26 balance', *Cardiovasc Res*, 85(3), pp. 494-502.

Protti, A., Sirker, A., Shah, A. M. and Botnar, R. (2010) 'Late gadolinium enhancement of acute myocardial infarction in mice at 7T: cine-FLASH versus inversion recovery', *J Magn Reson Imaging*, 32(4), pp. 878-86.

Ramakers, C., Ruijter, J. M., Deprez, R. H. L. and Moorman, A. F. M. (2003) 'Assumption-free analysis of quantitative real-time polymerase chain reaction (PCR) data', *Neuroscience Letters*, 339(1), pp. 62-66.

Rathouska, J., Vecerova, L., Strasky, Z., Slanarova, M., Brcakova, E., Mullerova, Z., Andrys, C., Micuda, S. and Nachtigal, P. (2011) 'Endoglin as a possible marker of atorvastatin treatment benefit in atherosclerosis', *Pharmacological Research*, 64(1), pp. 53-59.

Reimer, K. A. and Jennings, R. B. (1979) 'The "wavefront phenomenon" of myocardial ischemic cell death. II. Transmural progression of necrosis within the framework of ischemic bed size (myocardium at risk) and collateral flow', *Lab Invest*, 40(6), pp. 633-44.

Rigaud, M., Boschat, J., Rocha, P., Ferreira, A., Bardet, J. and Bourdarias, J. P. (1977) 'Comparative haemodynamic effects of dobutamine and isoproterenol in man', *Intensive Care Med*, 3(2), pp. 57-62.

Rockman, H. A., Wachhorst, S. P., Mao, L. and Ross, J., Jr. (1994) 'ANG II receptor blockade prevents ventricular hypertrophy and ANF gene expression with pressure overload in mice', *Am J Physiol*, 266(6 Pt 2), pp. H2468-75.

Ross, A. J., Yang, Z., Berr, S. S., Gilson, W. D., Petersen, W. C., Oshinski, J. N. and French, B. A. (2002) 'Serial MRI evaluation of cardiac structure and function in mice after reperfused myocardial infarction', *Magnetic Resonance in Medicine*, 47(6), pp. 1158-68.

Rossi, E., Sanz-Rodriguez, F., Eleno, N., Dawell, A., Blanco, F. J., Langa, C., Botella, L. M., Cabaras, C., Lopez-Novoa, J. M. and Bernabeu, C. (2013) 'Endothelial endoglin is involved in inflammation: role in leukocyte adhesion and transmigration', *Blood*, 121(2), pp. 403-415.

Rossi, M. A. and Peres, L. C. (1992) 'Effect of captopril on the prevention and regression of myocardial cell hypertrophy and interstitial fibrosis in pressure overload cardiac hypertrophy', *Am Heart J*, 124(3), pp. 700-9.

Rossini, A., Zacheo, A., Mocini, D., Totta, P., Facchiano, A., Castoldi, R., Sordini, P., Pompilio, G., Abeni, D., Capogrossi, M. C. and Germani, A. (2008) 'HMGB1-stimulated human primary cardiac fibroblasts exert a paracrine action on human and murine cardiac stem cells', *Journal of Molecular and Cellular Cardiology*, 44(4), pp. 683-693.

Roth, D. M., Swaney, J. S., Dalton, N. D., Gilpin, E. A. and Ross, J., Jr. (2002) 'Impact of anesthesia on cardiac function during echocardiography in mice', *Am J Physiol Heart Circ Physiol*, 282(6), pp. H2134-2140.

Ruff, J., Wiesmann, F., Hiller, K. H., Voll, S., von Kienlin, M., Bauer, W. R., Rommel, E., Neubauer, S. and Haase, A. (1998) 'Magnetic resonance microimaging for noninvasive quantification of myocardial function and mass in the mouse', *Magnetic Resonance in Medicine*, 40(1), pp. 43-8.

Scharpfenecker, M., Floot, B., Russell, N. S. and Stewart, F. A. (2012) 'The TGF-β co-receptor endoglin regulates macrophage infiltration and cytokine production in the irradiated mouse kidney', *Radiotherapy and oncology : journal of the European Society for Therapeutic Radiology and Oncology*, 105(3), pp. 313-320.

Scharpfenecker, M., Floot, B., Russell, N. S., ten Dijke, P. and Stewart, F. A. (2009) 'Endoglin haploinsufficiency reduces radiation-induced fibrosis and telangiectasia formation in mouse kidneys', *Radiotherapy and Oncology*, 92(3), pp. 484-491.

Scheuermann-Freestone, M., Freestone, N. S., Langenickel, T., Hahnel, K., Dietz, R. and Willenbrock, R. (2001) 'A new model of congestive heart failure in the mouse due to chronic volume overload', *European Journal of Heart Failure*, 3(5), pp. 535-543.

Schmierer, B. and Hill, C. S. (2007) 'TGF[beta]-SMAD signal transduction: molecular specificity and functional flexibility', *Nat Rev Mol Cell Biol*, 8(12), pp. 970-982.

Schmittgen, T. D. and Livak, K. J. (2008) 'Analyzing real-time PCR data by the comparative C(T) method', *Nat Protoc*, 3(6), pp. 1101-8.

Schneider, J. E., Cassidy, P. J., Lygate, C., Tyler, D. J., Wiesmann, F., Grieve, S. M., Hulbert, K., Clarke, K. and Neubauer, S. (2003) 'Fast, high-resolution in vivo cine magnetic resonance imaging in normal and failing mouse hearts on a vertical 11.7 T system', *Journal of Magnetic Resonance Imaging*, 18(6), pp. 691-701.

Schneider, J. E., Wiesmann, F., Lygate, C. A. and Neubauer, S. (2006) 'How to Perform an Accurate Assessment of Cardiac Function in Mice using High-Resolution Magnetic Resonance Imaging', *Journal of Cardiovascular Magnetic Resonance*, 8(5), pp. 693 - 701.

Sechtem, U., Pflugfelder, P. W., Gould, R. G., Cassidy, M. M. and Higgins, C. B. (1987) 'Measurement of right and left ventricular volumes in healthy individuals with cine MR imaging', *Radiology*, 163(3), pp. 697-702.

Shapiro, E. P., Rogers, W. J., Beyar, R., Soulen, R. L., Zerhouni, E. A., Lima, J. A. and Weiss, J. L. (1989) 'Determination of left ventricular mass by magnetic resonance imaging in hearts deformed by acute infarction', *Circulation*, 79(3), pp. 706-711.

Sharma, V., Bell, R. M. and Yellon, D. M. (2012) 'Targeting reperfusion injury in acute myocardial infarction: a review of reperfusion injury pharmacotherapy', *Expert Opin Pharmacother*, 13(8), pp. 1153-75.

Shi, Y. and Massagué, J. (2003) 'Mechanisms of TGF-[beta] Signaling from Cell Membrane to the Nucleus', *Cell*, 113(6), pp. 685-700.

Shyu, K. G., Wang, B. W., Chen, W. J., Kuan, P. and Hung, C. R. (2010) 'Mechanism of the inhibitory effect of atorvastatin on endoglin expression induced by transforming growth factor-1 in cultured cardiac fibroblasts', *European Journal of Heart Failure*, 12(3), pp. 219-226.

Siri, F. M., Jelicks, L. A., Leinwand, L. A. and Gardin, J. M. (1997) 'Gated magnetic resonance imaging of normal and hypertrophied murine hearts', *American Journal of Physiology*, 272(5 Pt 2), pp. H2394-402.

Smart, N., Bollini, S., Dube, K. N., Vieira, J. M., Zhou, B., Davidson, S., Yellon, D., Riegler, J., Price, A. N., Lythgoe, M. F., Pu, W. T. and Riley, P. R. (2011) 'De novo cardiomyocytes from within the activated adult heart after injury', *Nature*, 474(7353), pp. 640-644.

Smith, R. R., Barile, L., Cho, H. C., Leppo, M. K., Hare, J. M., Messina, E., Giacomello, A., Abraham, M. R. and Marban, E. (2007) 'Regenerative Potential of Cardiosphere-Derived Cells Expanded From Percutaneous Endomyocardial Biopsy Specimens', *Circulation*, 115(7), pp. 896-908.

Soriano, P. (1999) 'Generalized lacZ expression with the ROSA26 Cre reporter strain', *Nat Genet*, 21(1), pp. 70-71.

Souders, C. A., Bowers, S. L. K. and Baudino, T. A. (2009) 'Cardiac Fibroblast', *Circulation Research*, 105(12), pp. 1164-1176.

Strasky, Z., Vecerova, L., Rathouska, J., Slanarova, M., Brcakova, E., Kudlackova, Z., Andrys, C., Micuda, S. and Nachtigal, P. (2011) 'Cholesterol effects on endoglin and its downstream pathways in ApoE/LDLR double knockout mice', *Circulation Journal*, 75(7), pp. 1747-1755.

Stuckey, D. J., Carr, C. A., Tyler, D. J. and Clarke, K. (2008) 'Cine-MRI versus two-dimensional echocardiography to measure in vivo left ventricular function in rat heart', *NMR in Biomedicine*, 21(7), pp. 765-772.

Sun, Y., Zhang, J. Q., Zhang, J. and Ramires, F. J. A. (1998) 'Angiotensin II, Transforming Growth Factor-[beta]1and Repair in the Infarcted Heart', *Journal of Molecular and Cellular Cardiology*, 30(8), pp. 1559-1569.

Tanaka, N., Dalton, N., Mao, L., Rockman, H. A., Peterson, K. L., Gottshall, K. R., Hunter, J. J., Chien, K. R. and Ross, J. (1996) 'Transthoracic Echocardiography in Models of Cardiac Disease in the Mouse', *Circulation*, 94(5), pp. 1109-1117.

ten Dijke, P. and Arthur, H. (2007) 'Extracellular control of TGFbeta signalling in vascular development and disease', *Nature Reviews: Molecular Cell Biology*, 8(11), p. 857.

ten Dijke, P., Goumans, M.-J. and Pardali, P. (2008) 'Endoglin in angiogenesis and vascular diseases', *Angiogenesis*, 11(1), pp. 79-89.

Tian, F., Zhou, A.-X., Smits, A. M., Larsson, E., Goumans, M.-J., Heldin, C.-H., Borén, J. and Akyürek, L. M. (2010) 'Endothelial cells are activated during hypoxia via endoglin/ALK-1/SMAD1/5 signaling in vivo and in vitro', *Biochemical and Biophysical Research Communications*, 392(3), pp. 283-288.

Toporsian, M., Gros, R., Kabir, M. G., Vera, S., Govindaraju, K., Eidelman, D. H., Husain, M. and Letarte, M. (2005) 'A role for endoglin in coupling eNOS activity and regulating vascular tone revealed in hereditary hemorrhagic telangiectasia', *Circ Res*, 96, pp. 684 - 692.

Torsney, E., Charlton, R., Diamond, A. G., Burn, J., Soames, J. V. and Arthur, H. M. (2003) 'Mouse Model for Hereditary Hemorrhagic Telangiectasia Has a Generalized Vascular Abnormality', *Circulation*, 107(12), pp. 1653-1657.

Torsney, E., Charlton, R., Parums, D., Collis, M. and Arthur, H. M. (2002) 'Inducible expression of human endoglin during inflammation and wound healing in vivo', *Inflammation Research*, 51(9), pp. 464-470.

Tsang, A., Hausenloy, D. J. and Yellon, D. M. (2005) 'Myocardial postconditioning: reperfusion injury revisited', *Am J Physiol Heart Circ Physiol*, 289(1), pp. H2-7.

van Laake, L. W., van den Driesche, S., Post, S., Feijen, A., Jansen, M. A., Driessens, M. H., Mager, J. J., Snijder, R. J., Westermann, C. J. J., Doevendans, P. A., van Echteld, C. J. A., ten Dijke, P., Arthur, H. M., Goumans, M.-J., Lebrin, F. and Mummery, C. L. (2006) 'Endoglin Has a Crucial Role in Blood Cell-Mediated Vascular Repair', *Circulation*, 114(21), pp. 2288-2297.

Vanhoutte, D., Schellings, M., Pinto, Y. and Heymans, S. (2006) 'Relevance of matrix metalloproteinases and their inhibitors after myocardial infarction: A temporal and spatial window', *Cardiovasc Res*, 69(3), pp. 604-613.

Vecerova, L., Strasky, Z., Rathouska, J., Slanarova, M., Brcakova, E., Micuda, S. and Nachtigal, P. (2012) 'Activation of TGF-beta; Receptors and Smad Proteins by

Atorvastatin is Related to Reduced Atherogenesis in ApoE/LDLR Double Knockout Mice', *Journal of Atherosclerosis and Thrombosis*, 19(2), pp. 115-126.

Velasco, S., Alvarez-Munoz, P., Pericacho, M., Dijke, P. t., Bernabeu, C., Lopez-Novoa, J. M. and Rodriguez-Barbero, A. (2008) 'L- and S-endoglin differentially modulate TGFβ1 signaling mediated by ALK1 and ALK5 in L6E9 myoblasts', *Journal of Cell Science*, 121(6), pp. 913-919.

Venkatesha, S., Toporsian, M., Lam, C., Hanai, J., Mammoto, T., Kim, Y. M., Bdolah, Y., Lim, K. H., Yuan, H. T., Libermann, T. A., Stillman, I. E., Roberts, D., D'Amore, P. A., Epstein, F. H., Sellke, F. W., Romero, R., Sukhatme, V. P., Letarte, M. and Karumanchi, S. A. (2006) 'Soluble endoglin contributes to the pathogenesis of preeclampsia', *Nat Med*, 2, pp. 642 - 649.

Waghorn, B., Edwards, T., Yang, Y., Chuang, K.-H., Yanasak, N. and Hu, T. C. C. (2008) 'Monitoring dynamic alterations in calcium homeostasis by T1-weighted and T1-mapping cardiac manganese-enhanced MRI in a murine myocardial infarction model', *NMR in Biomedicine*, 21(10), pp. 1102-1111.

Walshe, T. E., Saint-Geniez, M., Maharaj, A. S., Sekiyama, E., Maldonado, A. E. and D'Amore, P. A. (2009) 'TGF-beta is required for vascular barrier function, endothelial survival and homeostasis of the adult microvasculature', *PLoS One*, 4(4), p. e5149.

Wansapura, J. P., Millay, D. P., Dunn, R. S., Molkentin, J. D. and Benson, D. W. (2011) 'Magnetic resonance imaging assessment of cardiac dysfunction in [delta]-sarcoglycan null mice', *Neuromuscular Disorders*, 21(1), pp. 68-73.

Weber, K. T. (2004) 'Fibrosis in hypertensive heart disease: focus on cardiac fibroblasts', *Journal of Hypertension*, 22(1), pp. 47-50.

Weisman, H. F., Bush, D. E., Mannisi, J. A., Weisfeldt, M. L. and Healy, B. (1988) 'Cellular mechanisms of myocardial infarct expansion', *Circulation*, 78(1), pp. 186-201.

Westbrook, C., Kaut Roth, C. and Talbot, J. (2005) *MRI in Practice*. Third edn. Oxford, UK: Blackwell Publishing.

White, H. D., Norris, R. M., Brown, M. A., Brandt, P. W., Whitlock, R. M. and Wild, C. J. (1987) 'Left ventricular end-systolic volume as the major determinant of survival after recovery from myocardial infarction', *Circulation*, 76(1), pp. 44-51.

Wiesmann, F., Frydrychowicz, A., Rautenberg, J., Illinger, R., Rommel, E., Haase, A. and Neubauer, S. (2002) 'Analysis of right ventricular function in healthy mice and a murine model of heart failure by in vivo MRI', *American Journal of Physiology - Heart & Circulatory Physiology*, 283(3), pp. H1065-71.

Wiesmann, F., Neubauer, S., Haase, A. and Hein, L. (2001a) 'Can we use vertical bore magnetic resonance scanners for murine cardiovascular phenotype characterization? Influence of upright body position on left ventricular hemodynamics in mice', *Journal of Cardiovascular Magnetic Resonance*, 3(4), pp. 311-5.

Wiesmann, F., Ruff, J., Engelhardt, S., Hein, L., Dienesch, C., Leupold, A., Illinger, R., Frydrychowicz, A., Hiller, K. H., Rommel, E., Haase, A., Lohse, M. J. and Neubauer, S. (2001b) 'Dobutamine-stress magnetic resonance microimaging in mice : acute changes of cardiac geometry and function in normal and failing murine hearts.[see comment]', *Circulation Research*, 88(6), pp. 563-9.

Willems, I. E., Havenith, M. G., De Mey, J. G. and Daemen, M. J. (1994) 'The alpha-smooth muscle actin-positive cells in healing human myocardial scars', *Am J Pathol*, 145(4), pp. 868-875.

Williams, S. P., Gerber, H. P., Giordano, F. J., Peale, F. V., Jr., Bernstein, L. J., Bunting, S., Chien, K. R., Ferrara, N. and van Bruggen, N. (2001) 'Dobutamine stress cine-MRI of cardiac function in the hearts of adult cardiomyocyte-specific VEGF knockout mice', *Journal of Magnetic Resonance Imaging*, 14(4), pp. 374-82.

Winter, E. M., Grauss, R. W., Atsma, D. E., Hogers, B., Poelmann, R. E., Van Der Geest, R. J., Tschöpe, C., Schalij, M. J., Gittenberger-de Groot, A. C. and Steendijk, P. (2008) 'Left ventricular function in the post-infarct failing mouse

heart by magnetic resonance imaging and conductance catheter: a comparative analysis', *Acta Physiologica*, 194(2), pp. 111-122.

Yang, Z., Berr, S. S., Gilson, W. D., Toufektsian, M. C. and French, B. A. (2004) 'Simultaneous evaluation of infarct size and cardiac function in intact mice by contrast-enhanced cardiac magnetic resonance imaging reveals contractile dysfunction in noninfarcted regions early after myocardial infarction', *Circulation*, 109, pp. 1161 - 1167.

Young, A. A., French, B. A., Yang, Z., Cowan, B. R., Gilson, W. D., Berr, S. S., Kramer, C. M. and Epstein, F. H. (2006) 'Reperfused myocardial infarction in mice: 3D mapping of late gadolinium enhancement and strain', *Journal of Cardiovascular Magnetic Resonance*, 8(5), pp. 685-92.

Young, K., Conley, B., Romero, D., Tweedie, E., O'Neill, C., Pinz, I., Brogan, L., Lindner, V., Liaw, L. and Vary, C. P. (2012) 'BMP9 regulates endoglin-dependent chemokine responses in endothelial cells', *Blood*, 120(20), pp. 4263-73.

Yu, C.-M., Tipoe, G. L., Wing-Hon Lai, K. and Lau, C.-P. (2001) 'Effects of combination of angiotensin-converting enzyme inhibitor and angiotensin receptor antagonist on inflammatory cellular infiltration and myocardial interstitial fibrosis after acute myocardial infarction', *J Am Coll Cardiol*, 38(4), pp. 1207-1215.

Zeisberg, E. M., Tarnavski, O., Zeisberg, M., Dorfman, A. L., McMullen, J. R., Gustafsson, E., Chandraker, A., Yuan, X., Pu, W. T., Roberts, A. B., Neilson, E. G., Sayegh, M. H., Izumo, S. and Kalluri, R. (2007) 'Endothelial-to-mesenchymal transition contributes to cardiac fibrosis', *Nat Med*, 13(8), pp. 952-961.

Zhong, J., Liu, W. and Yu, X. (2008) 'Characterization of three-dimensional myocardial deformation in the mouse heart: an MR tagging study', *Journal of Magnetic Resonance Imaging*, 27(6), pp. 1263-70.